RECEIVED
LAWRENCE
RADIATION LABORATORY

APR 1 1975

LIBRARY AND
DOCUMENTS SECTION

LBL-3675
c.1

2nd High Energy Heavy Ion Summer Study

July 15–26,1974

at the

Lawrence Berkeley Laboratory

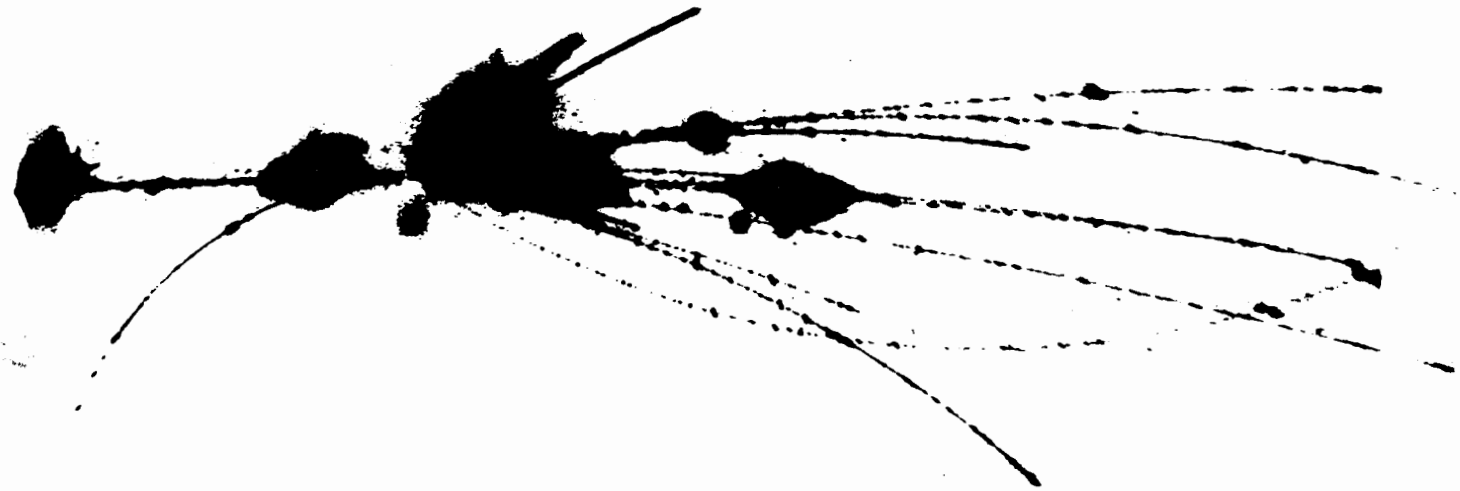

For Reference

Not to be taken from this room

LBL-3675
c.1

HIGH ENERGY HEAVY ION SUMMER STUDY PARTICIPANTS

ANDERSON, L. (LBL)
ARENS, R. (Goddard Space Ctr.--NASA)
BAUMGARDT, H. (Univ. of Frankfurt)
BERMAN, B. (LLL)
BJORKEN, J. (SLAC)
BLAKE, J. (Aerospace Corp.)
BLOCKI, J. (LBL)
BOCK, R. (G.S.I.)
BOER, J. (Univ. of Munich)
BOWEN, T. (Univ. of Arizona)
BRADY, F. (UC Davis)
CARTWRIGHT, B. (UC Berkeley)
CHAMBERLAIN, O. (LBL)
CHANG, G. (UC Riverside)
CHAPLINE, G. (LLL)
CHINTALAPUDI, S. (LBL)
CHU, H. (LBL)
CHU, S. (LBL)
CLARK, D. (LBL)
CLARKE, K. (LBL)
CORK, B. (LBL)
CREBBIN, K. (LBL)
DAVIS, B. (LBL)
DEBROSSE, C. (LBL)
EGGERS, R. (LBL)
EBERHARD, P. (LBL)
FESSENDEN, P. (Stanford Univ.)
FRAENKEL, Z (Weizman Inst.)
FREIER, P. (Univ. of Minnesota)
GOLDHABER, A. (State Univ. of NY, Stony Brook)
GORN, W. (UC Riverside)
GRAF, H. (LBL)
GREINER, D (LBL/Univ. of Cal. Space Sciences)
GRUNDER, H. (LBL)
GYULASSYI, M. (LBL)
HASHIMOTO, O (Univ. of Tokyo)
HEARN, W. (LBL)
HECKMAN, H. (LBL)
HENDRIE, D. (LBL)
HILF, E. (LBL)
HOLLEY, W. (LBL)
HYDE, E. (LBL)
IGO, G. (UCLA)
IJU, J (UC Riverside)
JAROS, J. (LBL)
JENKINS, T. (LBL)
JOHNSON, R. (LBL)
KAPLAN, S. (LBL)
KATCOFF, S. (BNL)
KEEFE, D. (LBL)
KELLER, R. (BNL)
KERMAN, A. (Mass. Inst. of Tech.)
KIERNAN, G. (UC Riverside)
KING, N. (UC Davis)
KOPLIK, J (LBL)
KRAPPE, H (Hahn-Meitner Inst., Berlin)
LEPORE, J. (LBL)
LIU, F. (State Univ. of Cal., San Bernadino)
LOFGREN, E. (LBL)
LU, J. (UC Riverside)
MALIK, B (Indiana University)
MARKOWITZ, S. (LBL)
MARSHALEK, E. (Notre Dame)
MASSMANN, H. (LBL)
MOSKOWSKI, S (UCLA)
MEYER TER VEN, J. (LBL)
MOHR, P. (LBL)

INTRODUCTION

In the last few years a small number of conventional proton accelerators (Berkeley, Dubna, PPA, Saclay) have accelerated light heavy-ions (d,α,C,N,O,...) to energies in the range of a few hundred to several GeV/nucleon. The availability of multi-GeV/nucleon heavy-ion beams provides new virgin territory for experimental and theoretical studies of nuclear matter. These studies by necessity cross the boundaries that have tended to separate the various physical sciences.

Investigations of nucleus-nucleus collisions at high energies like those available at the Bevalac Facility at Berkeley will provide information that is useful to particle physics, nuclear physics and chemistry, astro-physics, and biology and medicine. With this in mind, a High Energy Heavy Ion Study program was held in the Summer of 1973. This first meeting consisted of a series of very informal talks held over a period of two weeks between interested physicists and chemists at the Lawrence Berkeley Laboratory and a group of invited speakers. These discussions centered on reviewing existing experimental data and current theoretical techniques on nucleus-nucleus collisions. This approach was useful for the first study because most of the participants were relatively unfamiliar with this new area of heavy-ion research. No formal proceedings of this study was published, although review notes were put together by several of the invited speakers.

With an additional year of both experimental and theoretical work on nucleus-nucleus collisions at Bevalac energies, it was felt that a somewhat more formal summer program should be undertaken. The Second High Energy Heavy Ion Summer Program was held from July 15-26, 1974 at Berkeley and was jointly sponsored by the Lawrence Berkeley Laboratory and the Bevalac Users' Association. The purpose of this second program was to investigate those areas of atomic, nuclear, particle, and astro-physics that could be studied with beams of relativistic nuclei. Because the majority of the study was devoted to the theoretical treatment of the subject of nucleus-nucleus collisions, the first day was given to a review of existing data, primarily from recent Berkeley experiments. However, none of the experimental review talks was written up for the proceedings. The invited talks which appear here are essentially in the order that they were given, except for some shifting to put similar material together. It is hoped that these proceedings will stimulate others into thinking about the problems of nuclear collisions at high energies.

It goes without saying, but should be presented for all to see that the smooth operation of the Summer Study could not have been attained without the help of Anita Sando and Kathy Williams who with great relish and efficiency did all of the busy work which helps make such an undertaking a success.

Lee S. Schroeder

Lee S. Schroeder
Editor

MONARD, J. (LBL)
MORETTO, L. (LBL)
MOULTON, J. (LBL)
MURPHY, D. (LBL)
MYERS, D. (LBL)
NAGAMINE, K. (Univ. of Tokyo)
NAGAMIYA, S. (Univ. of Tokyo)
NAGARAJAN, M. (LBL)
NITSCHKE, M. (LBL)
OH, Y. (UC Riverside)
ORTH, C. (LBL)
OTTO, R. (LBL)
OZAWA, J. (UC Riverside)
PEREZ-MENDEZ, V. (LBL)
POE, R. (UC Riverside)
POSKANZER, A. (LBL)
PRICE, B. (UC Berkeley)
PUGH, H. (Univ. of Maryland)
RAISBECK, G. (Orsay)
RANDRUP, J. (LBL)
RAO, G. (LBL)
RASMUSSEN, J. (LBL)
RAUSCHER, E. (LBL)
REALE, A. (Frascati)
REDLICH, M. (LBL)
REINHARD, S. (LBL)
RICHARDSON, M.(LBL)
RIDDELL, R. (LBL)
SCHAEFFER, R. (Saclay)
SCHNEIDER, W. (LBL)
SCHROEDER, L. (LBL)
SCHWE, H. (East Stroudsburg State College)
SCOTT, D. (LBL)
SEGRE, E. (LBL)
SELOVE, F. (Univ. of Pennsylvania)
SESSLER, A. (LBL)
SEXTRO, R. (LBL)
SHIHAB, A. (LBL)
SIMON, R. (LBL)
SMOTT, G. (UC Berkeley)
SOH, K. (Cornell)
SPINKA, H. (UCLA)
STAPP, H. (LBL)
STEINER, H. (LBL)
STERNA, L. (LBL)
STOCK, R. (Univ. of Marbourg)
STRANG, R. (UCLA)
SVENTEK, J. (LBL)
SWIATECK, W. (LBL)
TAISTO, R. (Univ. of Helinski)
TELLER, E. (LLL)
TERRIEN, Y. (LBL)
THOMPSON, S. (LBL)
TRURAN, J. (Univ. of Illinois)
TSANG, C. (LBL)
UCHIYAMA, F. (LBL)
VARY, J. (BNL)
VINAYA, J. (Old Dominion Univ., VA)
WANG, W. (LBL)
WEDELL, J. (Naval Research Lab)
WHITE, M. (Princeton)
WHITTEN, C. (UCLA)
WIEGAND, C. (LBL)
WELCH, G. (LBL)
WEISS, M. (LLL)
WISS, J. (LBL)
ZAJEC, E. (LBL)
ZEBELMAN, A. (LBL)
ZINGHER, A. (LBL)

NUCLEAR SHOCK WAVES IN RELATIVISTIC HEAVY ION COLLISIONS*

Werner Scheid, Jürgen Hofmann, and Walter Greiner**

Institut für Theoretische Physik der Johann Wolfang Goethe-Universität Frankfurt am Main, Germany

I. Introduction

The possibility of compressed nuclear matter in the overlap volume of two colliding nuclei has been discussed in recent papers [1]. At very low relative energy between the ions the nucleon orbitals have time to rearrange. In this case the process is, therefore, adiabatic. At higher energy this rearrangement cannot fully develop, so that an energy-dependent hard core potential between the nuclei results. The so called sudden potential occurs in that particular limiting case where the two nuclei keep their individual identity, which results in a double density region within the overlap volume. The shallow energy-dependent potentials observed in the collision of light nuclei by the Yale-group[2], can be understood as intermediate cases between the adiabatic and sudden limits [1]. This picture was successful in explaining the surprising quasimolecular nuclear structures observed up to 60 MeV above the Coulomb barrier of the ^{12}C-^{12}C and ^{16}O-^{16}O-systems[25].Various model calculations for global compression helped to deepen our insight into the connection between adiabatic and sudden potentials. We refer to the literature [3] . In order to investigate the local density compression effect in a nucleus- nucleus collision more appropriately, and to prevent the extensive solution

---

* Work supported by the Bundesministerium für Forschung und Technologie and by the Gesellschaft für Schwerionenforschung (GSI).

** Invited speaker at the Symposium on Physics with Relativistic Heavy Ions at LBL, Berkeley, Calif., July 1974.

of complete hydrodynamic equations of colliding drops of nuclear matter, we have constructed a simple phenomenological model. Its density distributions are described in Fig. 1. Only central collisions are considered so far. The zone of high density between the two equal nuclei is assumed to be of an ellipsoidal shape. Within this ellipsoid and also within the rest nuclei, separated by r, the densities are assumed to be homogeneous; namely ϱ_1 and ϱ_0 respectively. The radius R of the two equal individual nuclei is assumed constant during the collision process. Thus the model has three degrees of freedom:

1) r, describing the relative motion of the two nuclear centers.
2) The semi-axis a of the compression ellipsoid describing decompression along the direction of the colliding nuclei.
3) The semi-axis b of the compression ellipsoid, describing the flux of nuclear matter perpendicular to the collision axis.

Of course, instead of a and b one could choose one of the axis (either a or b) only and the density ϱ_1 as the other degree of freedom, because the total amount of nuclear matter within the geometrical configuration of Fig. 1 is to be conserved.

The dynamical process will develop along the following steps: The ellipsoidal zone contains compressed matter, i.e. $\varrho_1 \geq \varrho_0$, which tends to expand. At the same time matter from the uncompressed volume will continue to flow into the ellipsoid. Depending on the relative velocity $\dot{r}$, the density ϱ_1 will further increase (more compression) or decrease (decompression). Our calculations show that for small relative velocities, i.e. $\dot{r} < c_s$ (c_s is the

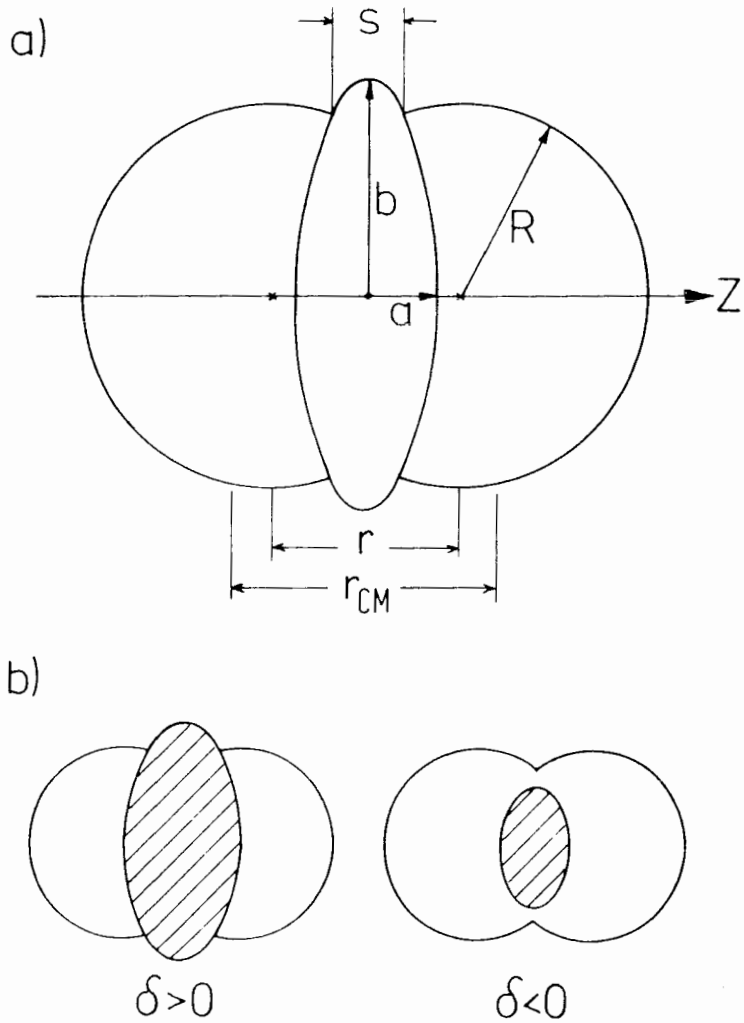

Fig. 1: The basic features of the model constructed for the investigation of compression in general, and shock waves in particular.

velocity of first sound) the ellipsoid will expand along the collision axis (Fig. 1), while for high relative velocities ($\dot{r} > c_s$) the matter will flow out perpendicular to the collision axis.

In order to keep the model as simple as possible, we will make certain assumptions on the kinetic and potential energy, establish the Lagrangian and derive from that the equations of motion for r, a and b.

In the second part of our investigation we generalize the model in two very important steps. Firstly the temperature T is introduced as a fourth degree of freedom. It will be most important to find T as a function of ϱ. The second generalization concerns the introduction of the density ϱ_{N^*} of <u>excited nucleons</u>, which may decay into pions

$$N^* \longrightarrow N + \pi$$

This will allow the calculation of pion production due to the ordinary individual nucleon-nucleon collisions, which do occur in the compressed volume. The process has to be carefully distinguished from a second one, which we called <u>pionization of nuclear matter:</u> Due to the <u>highly compressed shock wave</u> in the overlapping volume the pionic field can for very large nucleonsnumbers become overcritical in analogy to the overcritical spinor fields studied earlier [4] . We will speculate about the pionization process at the end of this investigation.

II. Compression of Nuclear Matter - Validity of Hydrodynamics

What does compression of nuclear matter mean? We all know that the nuclear low-energy spectra (lack of compressional 0^+-states)

and the saturation density of nuclei indicate that nuclei are nearly incompressible. The phonomenological phrase "compression" comprises two effects, namely

1) The nucleon-nucleon potential is repulsive at short distances (Fig. 2). This soft core becomes "active" as the internucleon distance is becoming smaller

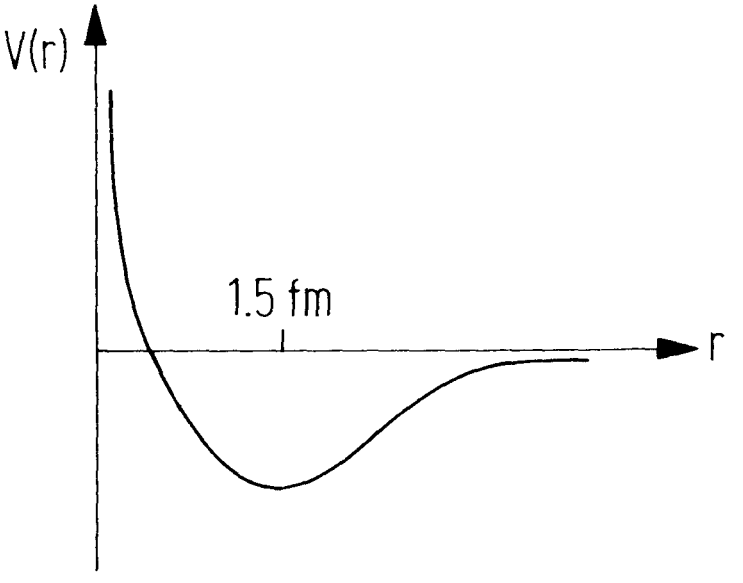

Fig. 2: Nucleon-Nucleon force as a function of internucleon distance r

2) The Pauli-principle requires the occupation of energetically higher orbitals as the nuclear density is increased. This is very nicely illustrated in Fig. 3, which shows the single particle schemes of the nuclear Two-Center Shell Model for two cases: a) for the sudden potential (keeping the individual radii R of the approaching nuclei constant) and b) for the adiabatic potential (incorporating volume conservation of the shell model equipotentials and thus no compression). These shell model schemes lead straightforwardly - after proper re-

normalization on the Extended Liquid Drop Model (ELDM) - to the sudden and adiabatic potentials between complex nuclei as shown in Fig. 4 (for more details see refs. 1 and 3 and further literature given there).

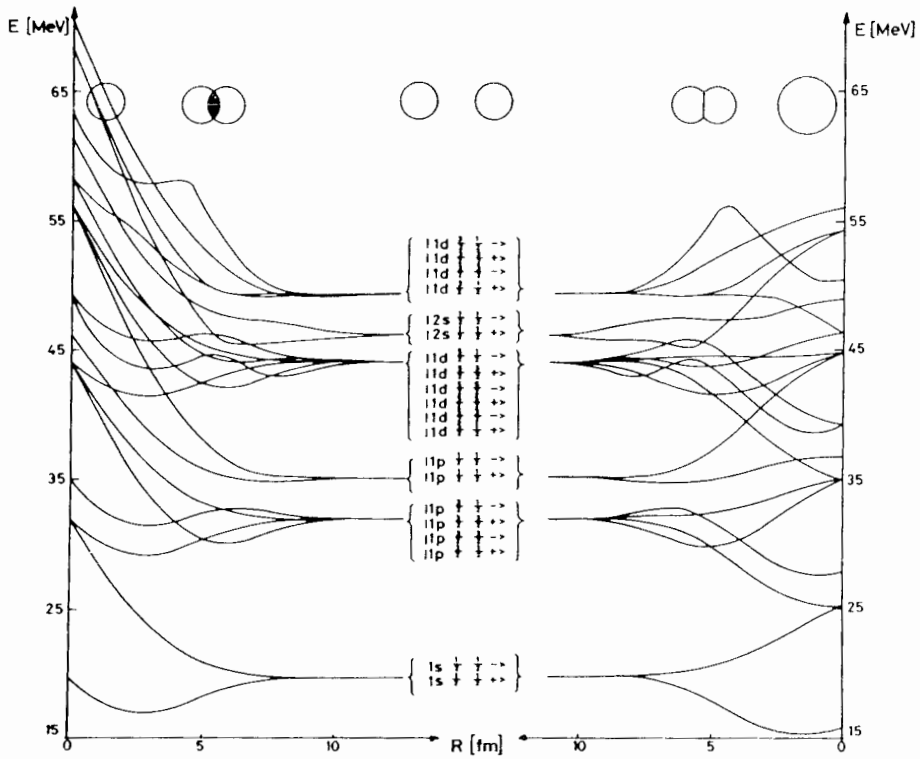

a) b)

Fig. 3: The Two-Center-Shell-Model Level Diagram of the ^{16}O-^{16}O-system a) for sudden compression and b) for the adiabatic non-compressed case. The rise of the sudden levels to higher energies with decreasing nuclear distance is clearly seen.

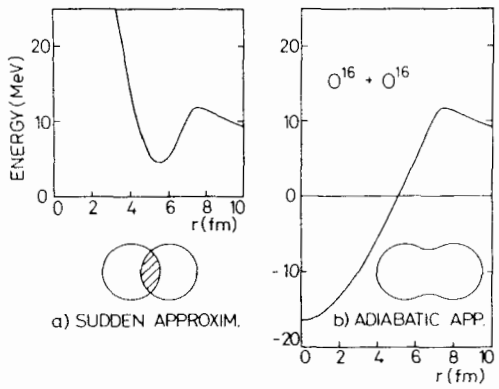

Fig.4: a) sudden and b) adiabatic nucleus-nucleus potential for the ^{16}O-^{16}O system.

The effect of the Pauli principle can most easily be studied within the non-interacting Fermi gas, where the Fermi momentum is given by

$$k_f = \left(\frac{3\pi^2}{2}\right)^{1/3} \rho^{1/3} \tag{1}$$

which again reflects the connection between excitation energy and density:

$$\frac{(\hbar k_f)^2}{2M} \sim \rho^{2/3} \tag{2}$$

A few definitions and conventions are now appropriately reminded to: Suppose the energy per nucleon in nuclear matter, E/A, is known as a function of the density, i.e. $\frac{E}{A} = \frac{E(\rho)}{A}$. Then the pressure p is given by

$$p = -\frac{\partial E}{\partial V} \tag{3}$$

and the compressibility κ is defined as

$$\frac{1}{\kappa} = -V\frac{\partial p}{\partial V} = V\frac{\partial^2 E}{\partial V^2} \tag{4}$$

It measures the change of pressure with the change of volume. Introducing the quantity $C = \frac{1}{\kappa \varrho_o} = \varrho_o^2 \frac{d^2 E/A}{d\varrho_o^2}$, where $\varrho_o = \frac{A}{V}$ is the nuclear equilibrium density for which $\frac{\partial(E/A)}{\partial \varrho_o} = 0$, one easily obtains the compression constant of the equilibrium density ϱ_o for a spherical nucleus with radius R_o :

$$K = 9C = R_o^2 \frac{d^2 E/A}{d R_o^2} \tag{5}$$

From nuclear matter calculations one expects $K \approx 100 - 300$ MeV, and a functional form of E/A as shown in Fig. 5.

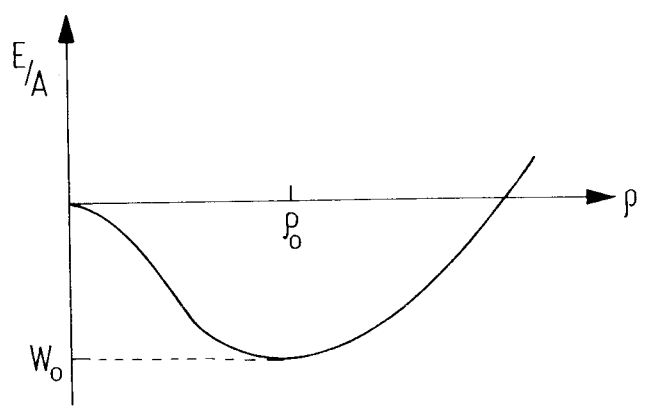

Fig. 5: Schematic functional dependence of the binding energy per nucleon, $\frac{E}{A}(\varrho)$, on the density ϱ . ϱ_o is the equilibrium density of nuclear matter, W_o is the binding energy per nucleon at equilibrium.

In order to get a feeling for the typical quantities we are dealing with in our investigation, let us estimate the velocity of first sound C_s (compression sound - contrary to second sound, which is an isospin wave, see Fig. 6) and compare it with the relative ion velocity v_r .

The latter is obtained for two equal nuclei with masses A·M and with the CM-energy E_{CM} by:

$\frac{AM}{4} \quad v_r^2 = E_{CM}$, where M is the nucleon mass, while the former is given with (5) by $C_s = \sqrt{\frac{K}{9M}} = \sqrt{\frac{C}{M}}$ yielding

$$\frac{V_r}{C_s} = 6\sqrt{\frac{E_{CM}}{A\ K}} \qquad (6)$$

With E_{CM} = 30 MeV, A = 16, K = 150 MeV one finds

$$\frac{V_r}{C_s} \approx 0.67 \ .$$

Clearly, local density compression can be expected as soon as $v_{r_2} \approx C_s$ which obviously happens at $E_{CM}/A \approx$ 8 MeV/nucleon.

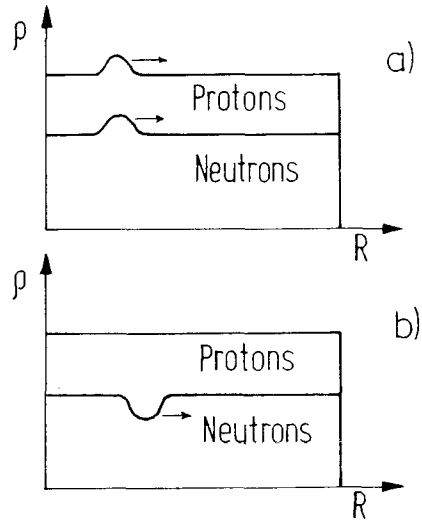

Fig. 6: a) schematic model for first sound, which manifests itself in the travelling of a T = 0 disturbance of the total density.

b) schematic model for second sound, which characterizes the travelling of a relative proton-neutron deadmixture (T=1 giant resonances) <u>without</u> change of total density.
The arrows shall indicate the direction of the travelling of the disturbance.

We also mention that for high relative energies between the nuclei the Pauli principle plays no role anymore for the compression effect. The reason is that the areas of states occupied by the nucleons in the two nuclei are far separated in the phase space due to the relative momentum, i.e. they are non-overlapping, and thus the antisymmetrization of the wave function becomes unimportant. This has been investigated very nicely by

Fließbach [5] , who finds, that e.g. for O^{16}-O^{16} collisions at 800 MeV the antisymmetrization between both nuclei can be neglected. His results are illustrated in Fig.7.

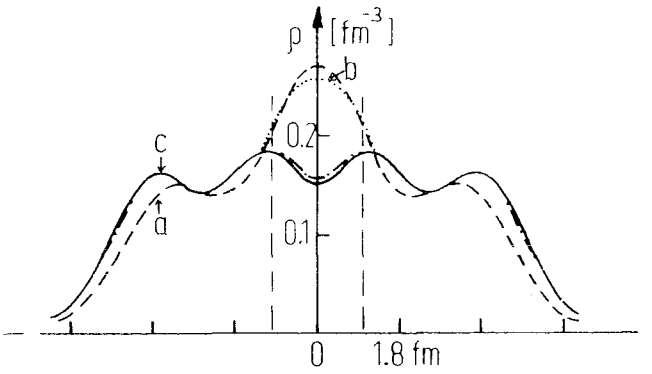

Fig.7: a) O^{16}-O^{16} density distribution according to $\rho_{O^{16}} + \rho_{O^{16}}$, where simply the two undistorted densities are added; this means no antisymmetrization. The distance between the individual centers is 3.6 fm. The compression is noticed.

b) density of the same system at the same nucleus-nucleus distance, but at 800 MeV relative energy with antisymmetrization. No significant change to the former case is noticed.

c) the same as in b) but for zero relative energy. The compression has disappeared.

A few words are also necessary on the validity of the hydrodynamic picture in nucleus-nucleus collisions. Such classical concepts as "fluid, gas, temperature" etc. are only valid if the mean free path of the nucleons is small compared to the dimensions of the system. In other words, hydrodynamics is valid if sufficient collisions inside the nuclear volume can happen, so that an equilibrization takes place.

There seems to occur a puzzle: The validity of the nuclear shell model is established beyond any doubt. It is based on the independent quasiparticle motion in a common potential. Hence the mean free path of a shell model nucleon is large compared to nuclear dimension. How is this possible even though strong internucleon forces are acting? One reason is that the particles moving in a shell model potential are really quasiparticles, i.e. "dressed" nucleons. Another reason is, that in low energy regimes, where the shell model holds, the Pauli principle does only allow scattering near the Fermi surface, where indeed nucleons are most intensely interacting. This is different, if the shell model potential changes as a whole in the sense of the Two Center Shell Model [6] used in fission and heavy ion collisions. Then also the deeply bound shells have to deform, i.e. all the nucleons in these shells have to "scatter" into the new shells while the nucleus changes its shape. This is the reason, why the average behaviour in fission and heavy ion collisions can be based on the liquid drop model (Strutinsky-renormalization). If the excitation energy is high enough, the situation becomes similar as for giant resonances (20 MeV) [7], and the liquid drop model has again some validity.

The situation becomes ideal in high energetic heavy ion collisions, where the nucleons of the individual nuclei have high relative momentum so that the Pauli principle becomes unimportant, as discussed above. The nucleons of both nuclei can now scatter on each other and the mean free path will be given by

$$\lambda = \frac{1}{\sigma \varrho} \tag{7}$$

where now one can use - because of the neglection of the Pauli principle - the free nucleon-nucleon cross section for σ , i.e. $\sigma \simeq 30$ mb= 3 fm^2.

With $\varrho_o = 0.17 \frac{1}{fm^3}$ we thus find

$$\lambda = \frac{1}{3 \cdot 0.17} \frac{\varrho_o}{\varrho} \text{ fm} \simeq 2 \frac{\varrho_o}{\varrho} \text{ fm} \tag{8}$$

which yields $\lambda = 2, 1, 0.5$ fm for $\varrho = \varrho_o, 2\varrho_o, 4\varrho_o$ respectively. Therefore hydrodynamics should be better the higher matter is compressed in the collisions.

III. Analogy of Relativistic Ion-Ion Collisions with the Collision of Stars in Galaxies

The collision of stars in galaxies has some instructive features, which may guide us to some extent in our investigation of relativistic heavy ion collisions. In our own galaxy the collision of stars is extremely rare. In recent years, however, one assumes that some very energetic processes occurring in very distant galaxies can be related to the collision of stars: Galaxies with strong radio sources have intensely luminating point centers, where the density of stars must be very high. In such regions collisions between stars should occur. Various hypotheses (Wotjer, Gold, Spitzer, Saslow [8]) assume that star collisions furnish the main source of energy, which is irradiated again by radio sources. It turns out that in such collisions the stars are dissolving, if the velocity is high enough. Colgate [8] shows that also stars of relatively low masses may slowly collide, and - through successive collisions - amalgamate high mass compounds (50 $M_\odot$), which again may collide with each other towards the center of the galaxy with higher velocities leading to the above described process, i.e. high energy star-star collision with annihilation of the stars.

The hydrodynamical equations for a star-star collision (gases with gravitation) have been solved by Cameron and Seidl [8] in computer calculations. Their results are illustrated in Figs. 8a - 8d and Figs. 9a - 9d. The former shows the equi-density distribution in the process, Fig.8b indicates initial "molecular" contact while Fig.8c shows the matter outflow perpendicular to the collision axis, which had been expected similarly for heavy ion collisions by Scheid and Greiner [9] . Fig. 8d shows the emerging shock wave along the direction of the collision. The dark zones indicate amalgamated matter. Figs. 9a-9d show the velocity field in the same collision. It can be noticed that it is practically irrotational except for the shock front.

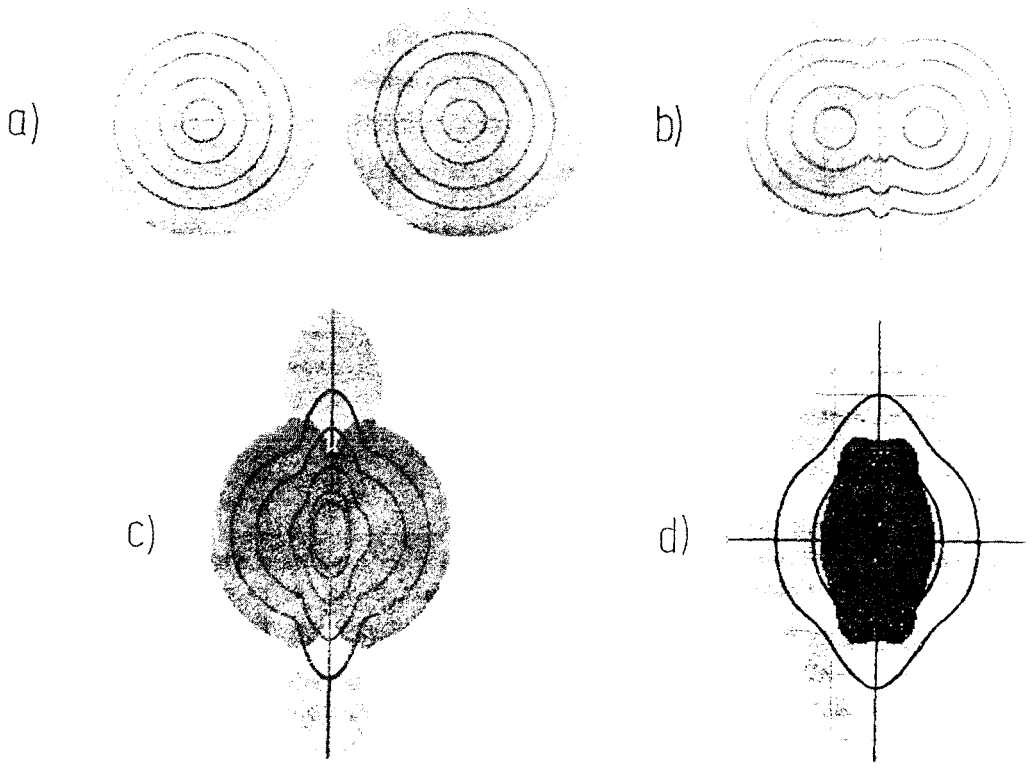

Fig. 8: Density distribution in a star-star collision with 1 $M_\odot$ and a relative velocity of 1000 km/sec. $\rho/\rho_{central}$ = 0.5, 0.1, 0.01, 0.001 are the densities along the equidensity lines.

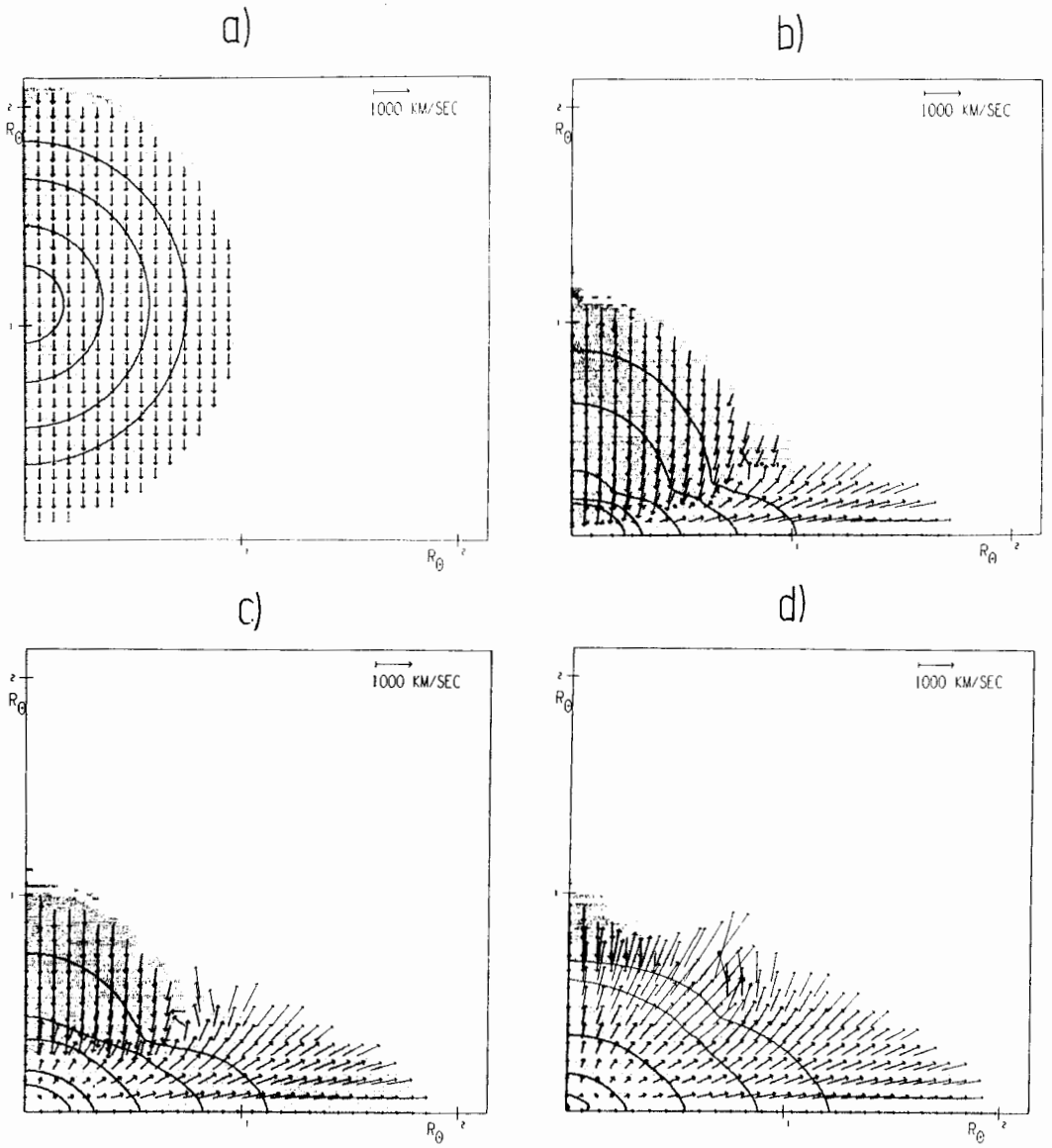

Fig. 9 Sequence of the velocity fields in the same star-star collision. The arrows indicate the velocity of the mass elements. The shock front occurs where the velocity field is (nearly) reversed. Outside the shock front the velocity field is practically irrotational again.

Fig. 9a corresponds to Fig. 8a ; Fig. 9b corresponds to Fig. 8c.

IV. Model for Local Density Increase in Nucleus-Nucleus Collisions

The possibility of compression of nuclear matter in nucleus-nucleus collisions is one of the most interesting aspects of heavy-ion physics. It has been discussed earlier in connection with the sudden nucleus-nucleus potentials [1, 9] and their energy dependence [10], which seems to confirm the experimentally deduced heavy-ion potentials of the Yale group [2]. These earlier considerations are valid as long as the relative heavy-ion velocity v_r does not exceed the velocity of first sound in nuclear matter C_s; i.e., for $v_r < C_s$. Here the first sound is an isospin T=0 compression wave while the second sound describes an isospin T=1 wave where a proton-neutron separation travels in constant nuclear matter density $\rho_o = \rho_p + \rho_n$ (see Fig. 6).

In order to study local compression effects for the cases $v_r > C_s$ in head-on nucleus collisions, we propose the following very simplified model: [10a] We restrict ourselves to two identical nuclei whose volume is divided into three parts (see Fig. 1 a)), namely an ellipsoid with axes a and b sandwiched between two cut-off spheres with radius R and relative distance r. The system will clearly be rotationally symmetric around the z axis, connecting the centers of the two spheres and of the ellipsoid. The nuclear matter is assumed to be homogeneously distributed over the different volumes. Compression ($\rho > \rho_o$) should only occur in the ellipsoidal region. The four coordinates a, b, r, and R define the geometry of the system. We choose, however, R=const in the collision so that we are dealing with three degrees of freedom only. This approximation is rather inessential for the results, but simplifies the theoretical considerations considerably.

If the density in the cut-off spheres is the equilibrium density ρ_o, the density in the ellipsoidal region follows from matter conservations as

$$\rho_1 = \rho_0 \left[(R^3/ab^2)(1+\alpha)^2(1-\tfrac{1}{2}\alpha) + (1-\beta)^2(1+\tfrac{1}{2}\beta) \right] \quad , \tag{9}$$

where $\alpha = (s-r)/2R$ and $\beta = s/2a$ with s the distance between the intersection points of the two spheres with the ellipsoid (see Fig. 1a) The various types of shapes shown in Fig. 1 b) are possible, depending on the relative size of the ellipsoid and the spheres; they can be characterized by the quantity

$$\delta = b^2 - R^2 + (\tfrac{1}{2}r)^2 \tag{10}$$

We will later exclude the case $\delta < 0$, because it corresponds to an ellipsoid with compressed matter embedded completely within the two spheres, which is unphysical. The distance s is given by

$$s = \frac{r}{\epsilon}\left[\left(1 + \frac{4\epsilon\delta}{r^2}\right)^{1/2} - 1\right] \tag{11}$$

for $\delta > 0$, where $\epsilon = b^2/a^2 - 1$, and $s \equiv 0$ for $\delta < 0$.

Because the solution of the full hydrodynamical problem is too complicated, we make the following approximation for the calculation of the kinetic energy $E = \frac{1}{2}M\int \rho\, v^2 d\tau$: (I) The velocity field of the matter in the cut-off spheres is homogeneous and equal to the velocity of the respective centers, i.e.

$$\vec{v} = \pm \tfrac{1}{2}\dot{r}\, \vec{e}_z . \tag{12}$$

(II) The velocity field in the ellipsoid is irrotational and can thus be derived from a potential through the equations

$$\vec{v} = \operatorname{grad} \varphi \quad ,$$

$$\Delta\varphi = - \rho_1^{-1}\, \partial\rho_1/\partial t \quad . \tag{13}$$

These assumptions are in agreement with the results for star-star collisions discussed earlier (see fig. 9).
The boundary condition $v = b$ and $\vec{v} \cdot \vec{e}_z = 0$ along the circle $z = 0$, $x^2+y^2=b^2$ gives for the solution of (13)

$$\vec{v} = \frac{\dot{b}}{b}(x\vec{e}_x + y\vec{e}_y) - \left(\frac{1}{\rho_1}\frac{\partial\rho_1}{\partial t} + \frac{2\dot{b}}{b}\right) z\, \vec{e}_z \ , \tag{14}$$

which allows with (12) the calculation of the kinetic energy in the form

$$E_{kin} = 1/2\ M\int \varrho\, v^2 d\tau = \frac{1}{2} \sum_{i,k} m_{ik}\dot{q}_i\dot{q}_k \quad , \tag{15}$$

where $q_i = \{r,a,b\}$.

If the Coulomb energy is disregarded, the potential energy is given by the compression energy [12]and the heat energy of the Fermi gas [11] in the ellipsoidal region, i.e.

$$E_{pot} = \int W\varrho\ d\tau = W\ (\varrho_1)\varrho_1\ \frac{4}{3}\pi ab^2 \tag{16}$$

with the energy density per nucleon

$$W(\varrho) = (C/2\varrho_o\varrho)\ (\varrho-\varrho_o)^2+\frac{1}{2}\beta T^2\varrho^{-2/3} \quad ,$$

T being the temperature in the compressed region. The expression $W(\varrho)$ used here is approximative in two ways. The first term is an expansion of $\frac{E}{A}(\varrho)$,shown in Fig.5 around ϱ_o: For large densities the correct functional $\frac{E}{A}(\varrho)$ should be used supplemented by the Coulomb energy per nucleon. The second term is the excitation energy per particle of a Fermi gas expanded for small temperatures. For higher temperatures one has to include higher terms in T as well [13] . The presently used formula is valid for nuclear excitations ΔE for which

$$\Delta E = k_B T < k_B T_{Fermi} = 30\text{-}40\ \text{MeV} \equiv E_{Fermi}$$

To avoid unphysical shapes with $\delta<0$, a potential of constraints $\frac{1}{2}V_o\delta^2$ is added for $\delta<0$ to the potential energy. It forces the system to shapes with $\delta>0$. The strength V_o has negligible influence on the results.

Since we have introduced regions of different densities ϱ_1 and ϱ_o, the following boundary conditions along the surface between

ρ_1 and ρ_0 have to hold [14].

$$[M\rho U] = 0, \quad [\rho U M\,\vec{v} + p\,\vec{n}] = 0 \tag{17}$$
$$[\rho U(\ M/2\vec{v}^2 + W) + p\,\vec{v}\cdot\vec{n}] = 0\ ,$$

The brackets $[f]$ denote the jump of the quantity f across the surface, i.e., $[f] = f_1 - f_2$; $\vec{n}$ is the unit vector on the surface, and $U = \vec{v}\cdot\vec{n} - G$ where G is the speed of advance of the surface. In our special case we may illustrate the situation as in Fig.10. According to ordinary hydrodynamics the fluxes of mass, momentum and energy must be

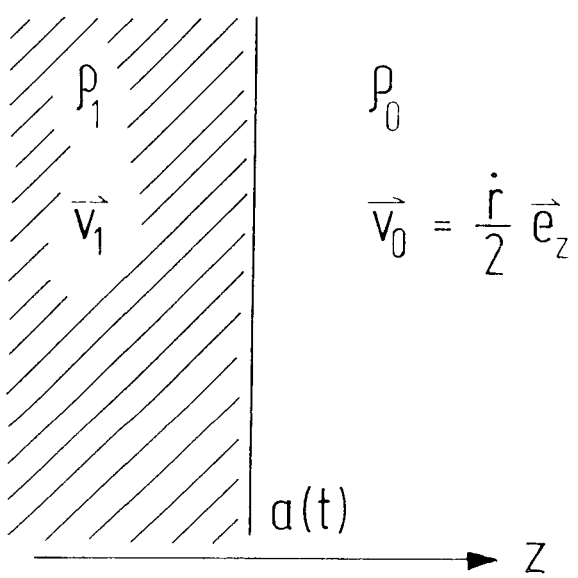

Fig. 10: Illustration of the boundary situation at the end point of the semi-axis a of the ellipsoid.

continuous at the boundary surface. Transforming to a coordinate system moving with the velocity of the boundary surface one gets by (17)

from continuity of mass flow $\varrho_1(v_1-\dot{a})=\varrho_o(v_o-\dot{a})$

from continuity of momentum flow $M\varrho_1(v_1-\dot{a})(v_1-\dot{a})+p_1=M\varrho_o(v_o-\dot{a})(v_o-\dot{a})+p_o$

from continuity of energy flow $(\frac{M}{2}(v_1-\dot{a})^2+W_1)\varrho_1(v_1-\dot{a})+p_1(v_1-\dot{a}) =$ (18)

$=(\frac{M}{2}(v_o-\dot{a})^2+W_o)\varrho_o(v_o-\dot{a})+p_o(v_o-\dot{a})$

After some manipulations, these equations lead to the following relations (Hugoniot (1887), Rankine (1870)):

$$(p_1+p_o)\left(\frac{1}{\varrho_o}-\frac{1}{\varrho_1}\right) = 2\ (W_1-W_o) \tag{19}$$

The pressure p is related to the density of the potential energy according to

$$p = \varrho^2 \left.\frac{dW}{d\varrho}\right|_{\text{const entropy}} = \frac{C}{2\varrho_o}(\varrho^2-\varrho_o^2)+\frac{\beta}{3}T^2\varrho^{1/3} \tag{20}$$

From Eqs. (18) follows that

$$\beta T^2\varrho^{1/3} = \frac{3}{8}\frac{C}{\varrho_o}(\varrho_1-\varrho_o)^2\ \frac{\varrho_1/\varrho_o-1}{1-\varrho_1/4\varrho_o}\ , \tag{20a}$$

which shows that the temperature becomes very high near the pole $\varrho_1 = 4\varrho_o$. This pole depends on the ansatz for the functional W as function of ϱ and T. Because the velocity field is already given as a function of the coordinates a, b, and r, the above Eqs. (18) connect the velocities $\dot{a}$, $\dot{b}$, and $\dot{r}$. For simplicity we only fulfill these equations at the points $z = \pm a$, $x = y = 0$ and obtain

$$\dot{a} = c_s \left[\frac{1}{2} \frac{\rho_1}{\rho_o} \left(1 + \frac{\rho_1}{\rho_o} + \frac{(\rho_1/\rho_o - 1)^2}{4 - \rho_1/\rho_o} \right) \right]^{1/2} + \frac{\dot{r}}{2} , \tag{21}$$

where $c_s = (C/M)^{1/2}$ is the velocity of first sound, with the nucleon mass M. This indicates that the coordinate a is not an independent degree of freedom in this model. For $\rho_1 = \rho_o$ and $\dot{r} = 0$, a is obviously moving with the velocity of sound c_s. Since $\dot{r}$ is negative, $\dot{a}$ can also be negative for $\rho_1 = \rho_o$ and $c_s < \left| \frac{\dot{r}}{2} \right|$. In this case the motion of the residual nucleus is pushing the overlap zone towards higher density.

The total energy of the system,

$$E = \frac{1}{2} \sum_{i,k} m_{ik} \dot{q}_i \dot{q}_k + E_{pot} , \tag{22}$$

has to be constant in time, i.e. dE/dt=0. The solutions of (22) have to fulfill the additional condition (21), which serves as an equation of motion. Introducing the momenta $p_k = \sum_i m_{ki} \dot{q}_i$, the three equations of motion to be solved are

$$\begin{aligned} &\partial E/\partial q_3 + \dot{p}_3 = 0, \\ &(\partial E/\partial q_1 + \dot{p}_1)\dot{q}_1 + (\partial E/\partial q_2 + \dot{p}_2)\dot{q}_2 = 0, \\ &d\psi/dt = 0 \end{aligned} \tag{23}$$

with (Eqs. (21))

$$\psi = \frac{\dot{q}_1}{2} - \dot{q}_2 + c_s \left[\frac{1}{2} \frac{\rho_1}{\rho_o} \left(1 + \frac{\rho_1}{\rho_o} + \frac{(\rho_1/\rho_o - 1)^2}{4 - \rho_1/\rho_o} \right) \right]^{1/2} = 0 \tag{24}$$

The calculations are carried out for ^{16}O-^{16}O scattering. The two parameters of the model are chosen as $C = \frac{100}{9}$MeV, which corresponds to a compressibility constant K = 100 MeV, and $\rho_o = 0.138$ fm^{-3}

(see Ref. 9). Restricting ourselves first for simplicity, to the case that ρ does not deviate too much from ρ_o, we disregard the temperature dependence (see eqs. (20 and (20a)).

. The initial compression $\rho_1 = 2\rho_o$ in the surface zone does not influence the results, as can be seen from $\rho_1(t)$ in Fig.11. The initial conditions for all other coordinates a, r, and $\dot{a}$ are determined by Eqs. (9), (21), and (22).

Figure 11 shows the results for the time dependence of r, a, t, $r_{c.m.}$, and ρ_1. Here $r_{c.m.}$ means the distance between centers of mass of the two halves of the nuclear system (see Fig. 1(a)). Clearly, the model can only be used as long as $\frac{1}{2}r+R>a$ is fulfilled. Obviously the radius a(t) increases with nearly constant velocity, in contrast to b(t) which increases faster for higher energies. This means that matter is pushed outwards perpendicular to the relative motion of the two nuclei. Note that for small energies the density ρ_1 is first decreasing rapidly and then again increasing slowly at larger times. The fast decrease in the beginning is the adjustment of the compressed nuclear density from the initial condition $\rho_1 = 2\rho_o$ to the final density. Therefore the results are independent of the initial conditions. The motion along the direction of the collision axis proceeds always with the same velocity, namely the velocity of first sound, c_s.

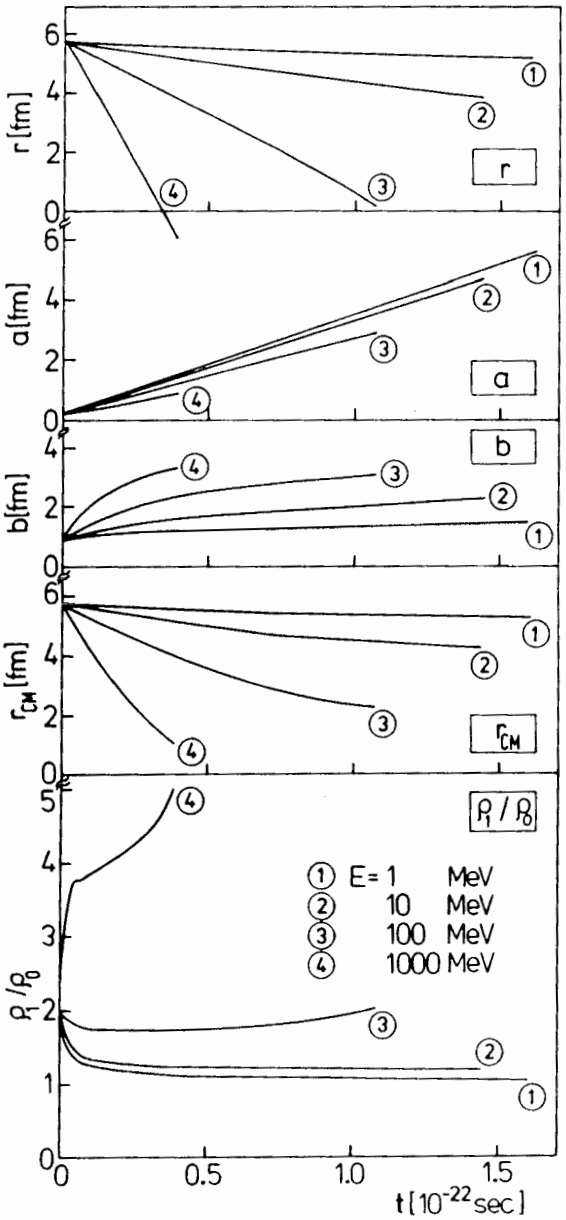

Fig. 11: Parameters r, a, b, $r_{c.m.}$, and ρ_1/ρ_o as a function of time for energies $E_{c.m.}$ = 1, 10, 100, and 1000 MeV. The results in this figure are obtained for zero temperature (T=0).

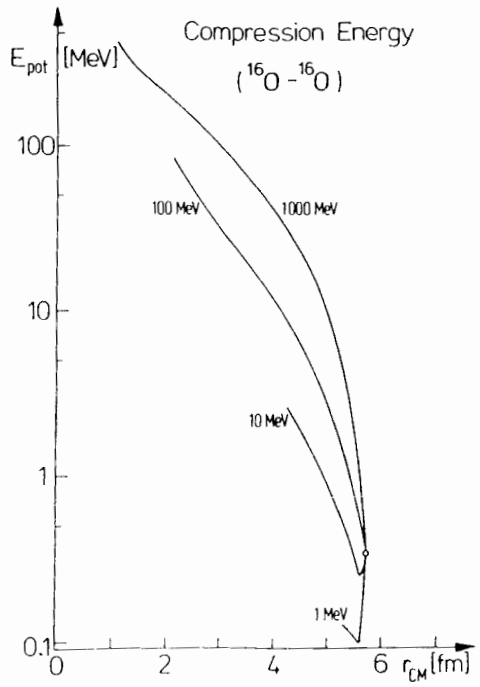

Fig. 12: Potential energy as a function of the center-of mass distance. It is strongly energy-dependent and shows a strong soft core, particularly for high energies.

Already for a bombarding energy of $E_{c.m.}$ = 100 MeV, which corresponds to a laboratory energy of E_{lab}/A = 12.5 MeV/nucleon of the ^{16}O projectile, a density compression of $\rho_1/\rho_o=2$ results. This indicates a nuclear matter shock wave, which becomes even more pronounced ($\rho_1 > \rho_o$) for very high nucleus-nucleus energies ($\geq$ 100 MeV/nucleon). In this latter case it is necessary to investigate the relativistic hydrodynamics [15]. Figure 12 shows the potential energy, which is stored in the compressed matter of the ellipsoid, as a function of $r_{c.m.}$. It obviously leads to a strong energy-dependent soft-core potential. The soft core reaches the magnitude of a few MeV for O^{16} ions of 10 MeV to several hundred MeV for O^{16} ions of 1000 MeV.

It seems worthwhile at this point to recall the results of Müller, Scheid and Greiner [10] on the dynamical interplay between compressional and adiabatic degrees of freedom. This particular model is based on the sudden and adiabatic extremes of the Two Center Shell Model. The dynamical variables are illustrated in Fig. 13. Its total Lagrangian is - for central collisions - of the

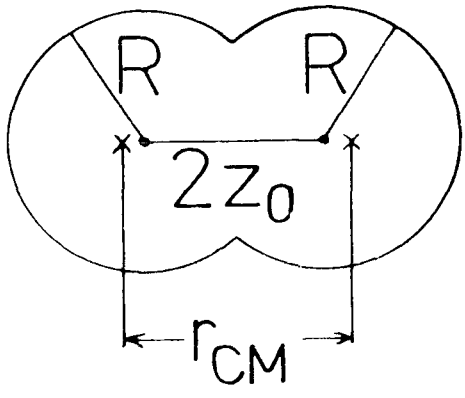

Fig. 13 The basic dynamical variables of the Two Center Shell Model. If the radius R of the individual nuclei adjusts to the lowest energy at every distance Z_o i.e. $R=R_{ad}(Z_o)$ one obtains the adiabatic limit, otherwise compression occurs.

form

$$L = \frac{1}{2} b_{zz} \dot{z}_o^2 + b_{zR} \dot{R} \dot{z}_o + \frac{1}{2} b_{RR} \dot{R}^2 - V(z_o,R) \tag{25}$$

where the potential $V(z_o,R)$ is conveniently expanded around the adiabatic one $V_{ad}(z_o) \equiv V(z_o, R_{ad})$ with $(\partial V/\partial R)_{R=Rad} = 0$

$$V(z_o,R) = V_{ad}(z_o) + \frac{1}{2} k(z_o)(R-R_{ad}(z_o))^2; \; k(z_o) = \left(\frac{\partial^2 V}{\partial R^2}\right)_{R=R_{ad}} \tag{26}$$

The second term obviously describes the <u>compression potential</u>. The compression constant K (Eq.(5) is related the "compression curvature" $k(z_o=0)$ via the relation

$$K = \left(R^2 \frac{\partial^2 (V(0,R)/A)}{\partial R^2}\right)_{R=R_{ad}} = R_{ad}^2 \frac{k(z_o=0)}{A} \tag{27}$$

The masses $b_{ik}(z_o,R)$ in (25) have been calculated within the irrotational flow model and also within the TCSM [16]. They are shown in Fig. 14.

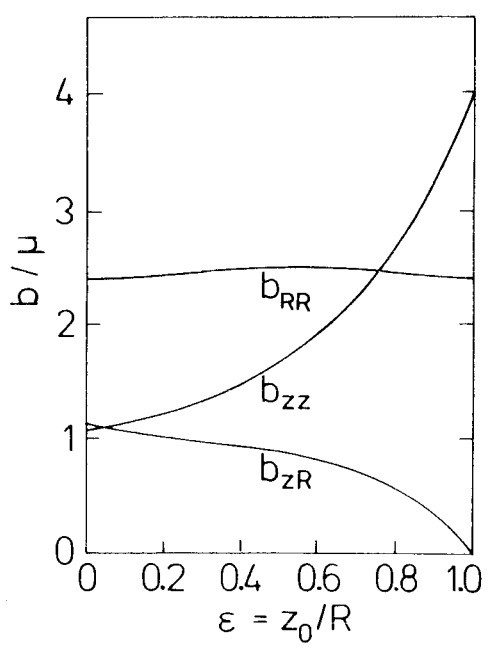

Fig. 14: The masses $b_{ik}(r)$ as obtained from the irrotational velocity field; the asymptotic reduced mass is denoted by μ.

The classical equations of motion (Lagrangian equations) following from the Lagrangian (25) are then solved. After eliminating the compression degree of freedom and requiring a constant reduced mass, μ, for the motion of the distance r_{CM} of the two centers of mass (see Fig. 13 , one obtains an effective energy dependent potential $V=E-\frac{1}{2}\mu\dot{r}^2_{CM}$ as shown in Fig.15b. It shows an energy dependent soft core and is even for low energies substantially different from the adiabatic potential.

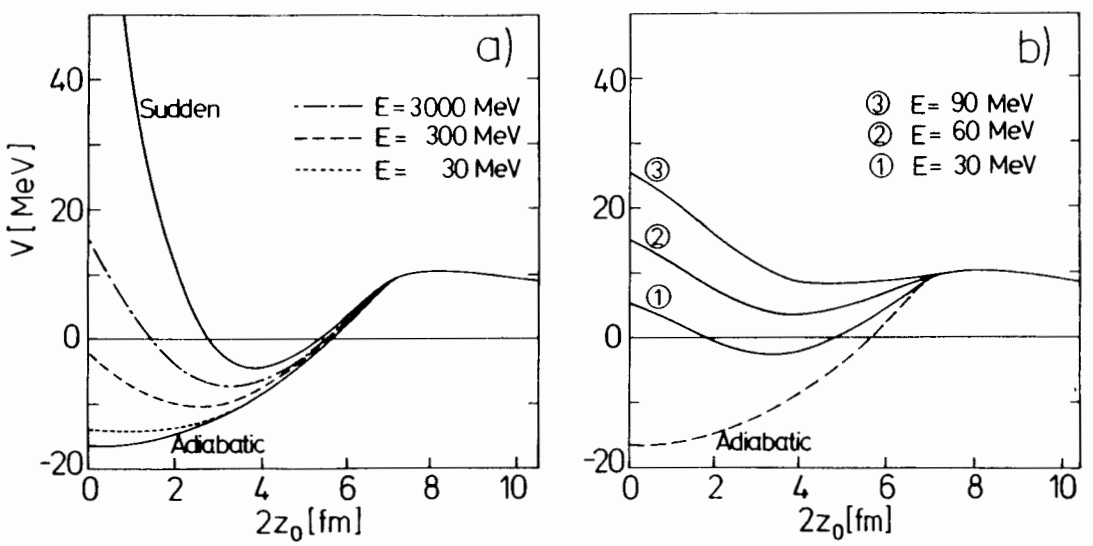

Fig. 15: The compression effect on the potential as function of the bombarding energy for the $^{16}O-^{16}O$ scattering

a) for various bombarding energies the potential energy of the compression mode is added to the adiabatic potential. The adiabatic and sudden potential are the limiting curves for slow and fast processes.

b) The kinetic and potential energy of the compression mode is added to the adiabatic potential according to $V=E-\frac{1}{2}\mu\dot{r}^2_{CM}$.

As shown in Fig. 15a these deviations from adiabaticity come only to a very minor extent from the actual compression in the system (i.e. from the compressional potential of (26)). They arise from the elimination of the compressional kinetic terms in eq. (25) (the terms containing $\dot{R}$). In other words, at these rather low relative energies nuclear matter is not compressed, but it requires the readjustment of the radii R as a function of time and this in turn absorbs a great amount of relative energy. Hence this kinetic expansion energy (proportional to $\dot{R}$) will not be available in the relative degree of freedom; thus leading to a strongly non-adiabatic potential. The deviations from adiabaticity increase with relative energy, as expected. This mechanism seems to be very essential for fusion processes, because it is the main source of friction (internal nuclear excitation).

The time dependence of the various degrees of freedom of the model of Fig. 13 is illustrated in Fig. 16 for the case, that two ^{16}O-nuclei scatter in a head-on collision with a bombarding energy of 300 MeV. One notices the excitation of the compressional degree of freedom.

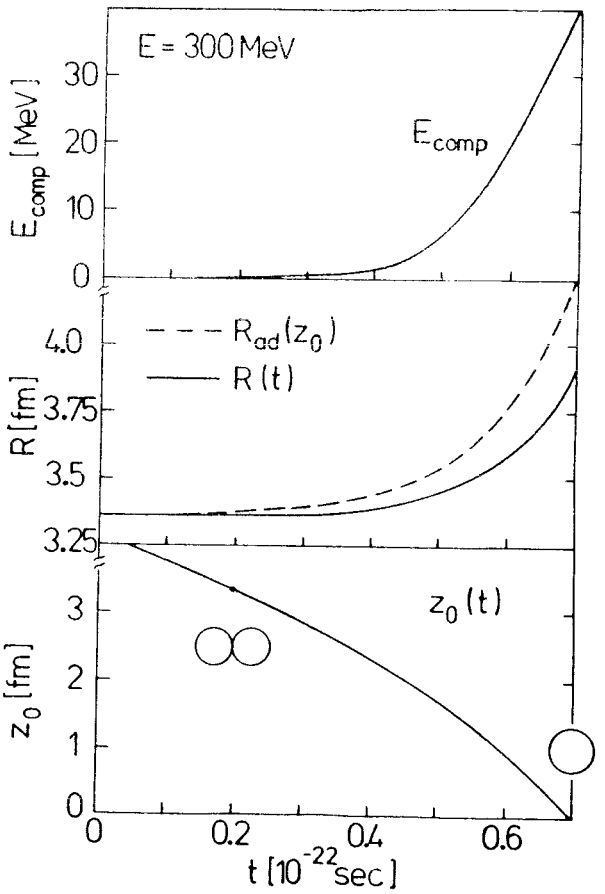

Fig. 16: Time dependence of the two-center distance z_o, the radius R and the potential and kinetic compression energy E_{comp} at a bombarding energy of E_{CM} = 300 MeV for the ^{16}O-^{16}O scattering.

We learn from this investigation and from similar ones on the study of the time dependence of nucleus-nucleus deformation reactions [17] that the entrance and exit part of the relative motion are quite different from each other. In our case the entrance orbital motion is characterized by the shock wave and therefore by the local compression effect close to the sudden approximation while the exit orbit is closer to the adiabatic limit: One can say at least that compression effects play in the exit a less dominant role.

We turn now to calculations with the model of Fig.1 which contain the internal excitation of nuclear matter in terms of heat, as we described it in our formalism by the temperature term (see eq. (16)). The results, analogue to those of Fig. 11, are presented in Fig. 17. In these calculations the initial condition had been chosen $\frac{\rho_1}{\rho_0} = 1.2$. As can be noticed, already a colliding energy of 100 MeV, the density increase in the compression zone is $\rho_1 = 1.7\rho_0$, while at 1000 MeV the compressed density can only reach $\rho_1 \sim 3\rho_0$. Again, for low energies the shock wave propagates along the collision axis (a increases) while at high energies the matter flows perpendicular to this direction (i.e. b(t) increases fastly, a(t) is practically constant). Fig. 17 c presents the <u>potential energy per nucleon</u> in the ellipsoidal region and the contribution of thermal excitation to it. Fig. 17b shows that at very high collision energy the relative amount on potential compression and thermal energy is relatively small (10% of the collision energy) while at energies which correspond to the first sound velocity a relatively large amount of internal and compression energy is observed (70% of the collision energy).

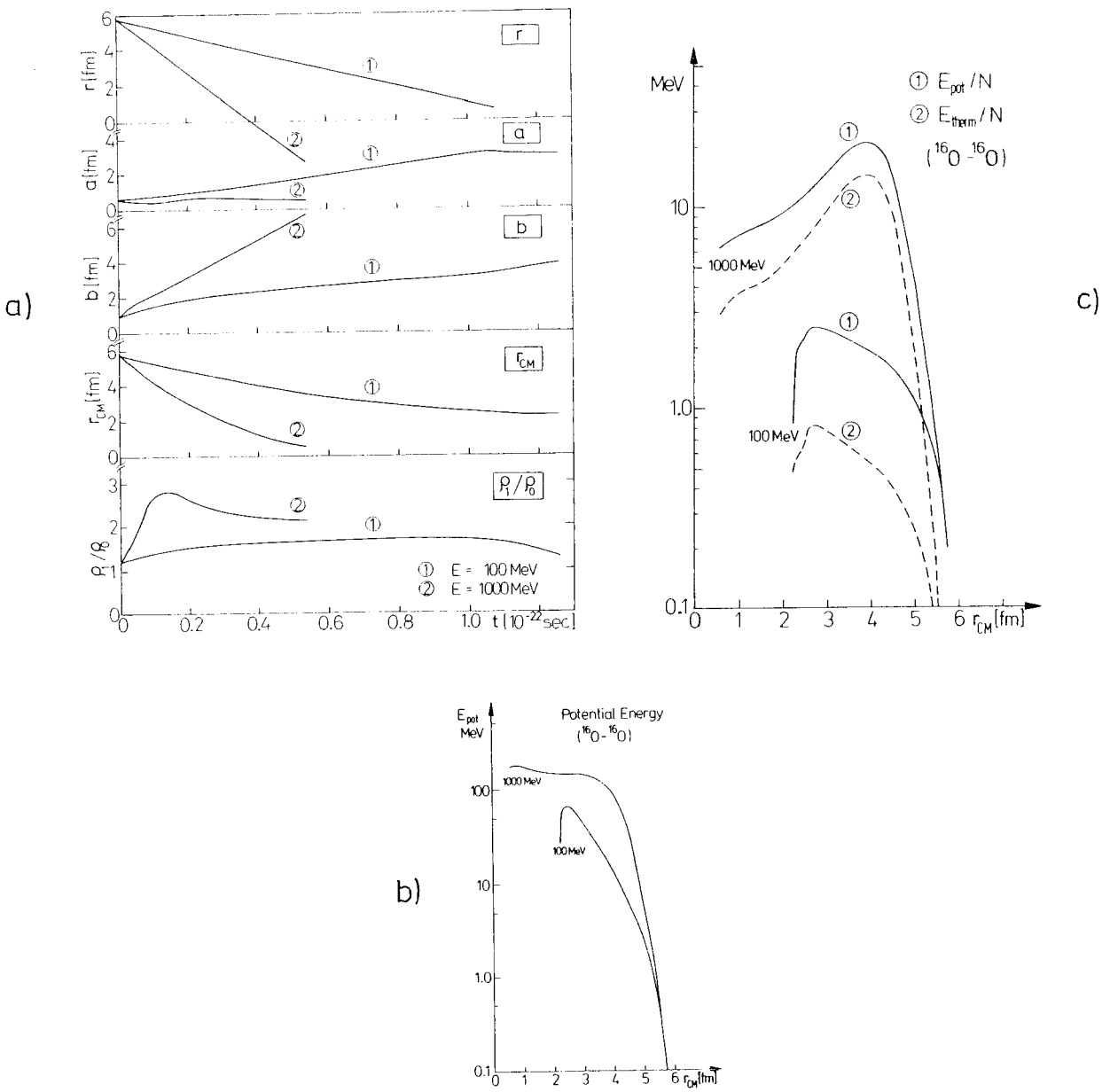

Fig. 17 a) The time dependence of the geometrical parameters of the compression zone and the compression density therein.

17 b) The potential energy as function of the center of mass distance.

17 c) The dependence of the potential compression energy per nucleon. The dashed curves show the contribution from thermal energy.

According to this discussion it seems obvious that the compression effects should show up in the strongly energy dependent nucleus-nucleus potentials with soft or hard cores, which can be deduced from elastic and inelastic scattering excitation function. These cores in the potential have three causes:

a) compression effects

b) internal excitation (here treated as temperature)

c) coordinate dependent collective masses and the associated mass flow in the collision.

Of course, the pronounced occurrence of the shock wave along the direction of collision at lower energies and perpendicular to it at higher energies should be observable in the angular distribution of the reaction products relative to the beam axis. We turn now to another important possible application of the shock waves concerning pion production and pionization of matter.

V. Temperature Pions and Pionization of Supercritical Matter

We have seen in the last section that a strong internal excitation described as thermal process can be expected in the compression zone of heavy ions (hot nuclear matter). The quantitative results of the collision process demonstrated in Figs. 11 and 17, indicate that nuclear matter will be strongly compressed only about $2 \cdot 10^{-23}$ sec. On the other hand the cross section for meson production at relevant energies is of the order of 10-30 mb. Taking $\varrho_1 \approx 3\varrho_0$, this yields an equilibration time for the excitation of mesonic degrees of freedom, of the order of 6×10^{-24} sec.[18] Therefore one can expect, that

during the collision in the zones of hot matter (compression zone) ordinary meson production should take place. With "ordinary" we mean here, that the production of mesons is due to individual nucleon-nucleon collisions in the compressed volume, where the relative kinetic energy between nucleons, N, is high enough to allow the excitation of excited nucleons, N^*, which may decay again in sequence into ordinary nucleons, N, and a pion, i.e.

$$N^* \longrightarrow N + \pi$$

This process has been discussed by Chapline et.al.[18] . It should be distinguished from another, much more fundamental process, which we call pionization of matter, and which has to be seen in analogy to the electron-positron vacuum and its decay in overcritical fields [4]. We shall first discuss the former process within our model-theory for heavy ion collisions and then turn towards the latter, which is anyway not very well worked out theoretically at the present time.

V. A. Temperature Pions

If the density of ordinary nucleons in their groundstates is denoted by ϱ_N, the density of excited nucleons ϱ_{N^*} will be given at a temperature T of the nuclear matter by

$$\varrho_{N^*} = 4 \exp\left(\frac{-E_\Delta}{k_B T}\right) \varrho_N \tag{29}$$

where $E_\Delta = E_{N^*} - E_N = (1236-938)$ MeV ~ 300 MeV and $k_B T$ is the thermal excitation energy. These excited nucleonic matter will only occur in the compression zone of our model (see Fig.1) In the other zones we have $\varrho = \varrho_o$, and excited matter should be extremely small - though not zero [19]. The total density in the compression volume

is therefore

$$\rho_1 = \rho_N + \rho_{N^*} \tag{30}$$

which gives with (29)

$$\rho_N = \frac{1}{1+4e^{-\frac{E_\Delta}{k_B T}}} \rho \equiv \alpha \rho_1 \tag{31}$$

and

$$\rho_{N^*} = \gamma \rho_1 \text{ with } \quad \gamma = 1 - \alpha \quad .$$

We are dealing now with a <u>two-phase system,</u> for which the equations of motion are again established via a Lagrange function

$$L = E_{kin} - E_{pot} \tag{32}$$

The kinetic energy in the compression zone is simply

$$E^1_{kin} = \frac{1}{2} \bar{M} \rho 1 \int v^2 \, d\tau \tag{33}$$

with $\bar{M} = M_N \alpha + M_{N^*} \gamma$ and M_N, M_{N^*} being the masses of the N and N^* respectively. Here we assumed that the N and N^* have the same velocity field, which is good in zero's order, but needs improvement.

The potential energy is given in the compression zone by:

$$E_{pot} = \int W_N \rho_N \, d\tau + \int W_{N^*} \rho_{N^*} \, d\tau \tag{34}$$

where

$$W_N = \frac{C}{2\rho_0 \rho_1} (\rho_1 - \rho_0)^2 + \frac{\beta_N}{2} T^2 \rho_N^{-2/3}$$

and

$$W_{N^*} = \frac{C}{2\rho_0 \rho_1} (\rho_1 - \rho_0)^2 + \frac{\beta_{N^*}}{2} T^2 \rho_{N^*}^{-2/3} + E_\Delta \tag{35}$$

are the energy densities for the N- and N^* matter respectively. Again for simplification it is assumed here that the compression energy depends only on the total density ρ_1. The constants

β_N and β_{N*} are given as $\beta_N = (\frac{\pi}{3})^{2/3} \frac{M_N k_B^2}{\hbar^2}$, $\beta_{N*} = (\frac{2\pi}{3})^{2/3} \frac{M_{N*} k_B^2}{\hbar^2}$ [11].

Eq. (34) can be written, by using eqs. (31) and (35), as

$$E_{pot} = \int (W_N \alpha + W_{N*} \gamma) \varrho_1 d\tau = \int W \varrho_1 d\tau \tag{36}$$

where

$$W = \frac{C}{2\varrho_1 \varrho_o} (\varrho_1 - \varrho_o)^2 + \frac{T^2}{2} \varrho_1^{-2/3} (\beta_N \alpha^{1/3} + \beta_{N*} \gamma^{1/3}) + E_\Delta \gamma \tag{37}$$

The entropy becomes

$$S = \int T \varrho_1^{1/3} B \, d\tau \qquad \text{with } B = \beta_N \alpha^{1/3} + \beta_{N*} \gamma^{1/3} \tag{38}$$

This allows to calculate the pressure

$$p = \varrho^2 \left. \frac{dW}{d\varrho} \right|_{S = \text{const}} \tag{39}$$

which gives

$$p = \frac{C}{2\varrho_o} (\varrho^2 - \varrho_o^2) + \frac{1}{3} f(T) \, T^2 \varrho^{1/3} - g(T) \, T \varrho \tag{40}$$

where for $T = 0$ $f(T) \equiv \beta_N$ and $g(T) \equiv 0$. Otherwise the $f(T)$ and $g(T)$ are functions of T.

It is important now to obtain the temperature T as a function of the density, which is achieved via the shock equations. This deserves, however, some more details: We consider the shock front $a(t)$ using the notation shown in Fig. 18a.

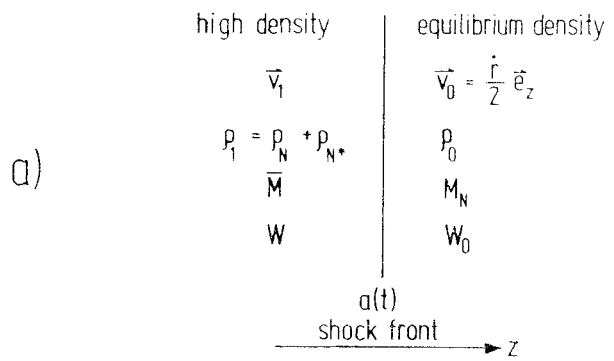

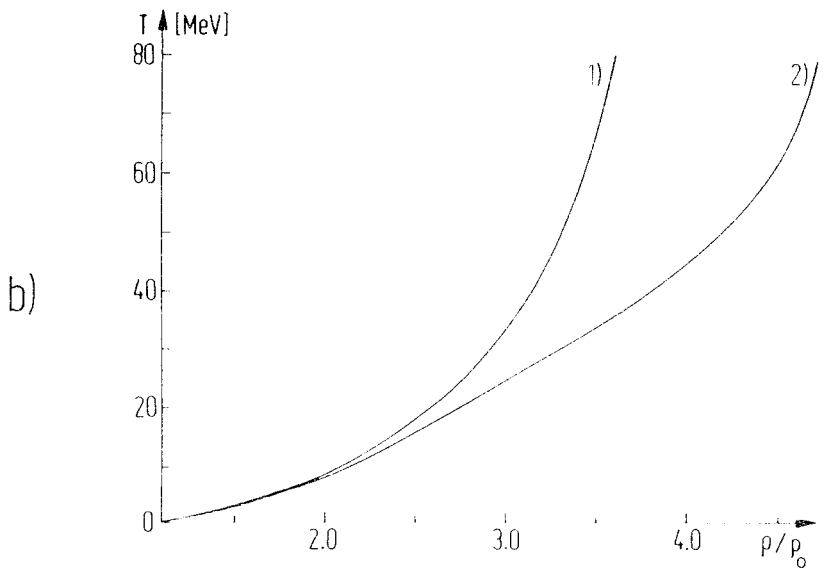

Fig. 18 a) The definition of various quantities occurring on both sides of the shock front(see also Fig. 10).

18 b) Temperature T as function of the density ρ in the compression zone for the case of no N^*-nuclei (eq. (20a), curve 1) and for the case that N^*-nuclei are formed (eq.(45), curve 2) .

Via the substitutions $\mathcal{U}_1 = v_1 - \dot{a}$, $\mathcal{U}_o = v_o - \dot{a}$ one can transform to a coordinate system at rest at the shock front and obtains the following shock equations:

1) baryon conservation:

$$\rho_1 \mathcal{U}_1 = \rho_o \mathcal{U}_o \quad \text{with } \rho_1 = \rho_N + \rho_{N^*} \tag{41}$$

2) momentum conservation:

$$\mathcal{U}_1 (M_N \alpha \rho_1 \mathcal{U}_1 + M_{N^*} \gamma \rho_1 \mathcal{U}_1) + p_1 = \\ = M_N \rho_o \mathcal{U}_o^2 + p_o \tag{42}$$

which can also be written as

$$\bar{M} \mathcal{U}_1^2 \rho_1 + p_1 = M_N \mathcal{U}_o^2 \rho_o + p_o$$

3) energy conservation:

$$\rho_1 \mathcal{U}_1 \left(\frac{\bar{M}}{2} \mathcal{U}_1^2 + W_1\right) + p_1 \mathcal{U}_1 = \\ = \rho_o \mathcal{U}_o \left(\frac{M_N}{2} \mathcal{U}_o^2 + W_o\right) + p_o \mathcal{U}_o \tag{43}$$

It is noteworthy that the first equation (41) replaces the mass flow equation $[M\rho\mathcal{U}] = 0$ (eq.17) Only the number of baryons is conserved along the shock front. These shock eqs. (41)-(45) may be brought to a more convenient form. With the abbreviation $\rho_1 \mathcal{U}_1 = \rho_o \mathcal{U}_o \equiv r$ one obtains for the eq. (42):

$$\bar{M} \frac{r^2}{\rho_1} + p_1 = M_N \frac{r^2}{\rho_o} + p_o \tag{44}$$

or

$$r^2 = \frac{p_o - p_1}{\frac{\bar{M}}{\rho_1} - \frac{M_N}{\rho_o}}$$

With that, eq. (43) becomes

$$r\left(\frac{\bar{M}}{2}\,\frac{r^2}{\varrho_1} + W_1\right) + \frac{p_1 r}{\varrho_1} = r\left(\frac{M_N}{2}\,\frac{r^2}{\varrho_o} + W_o\right) + \frac{p_o r}{\varrho_o}$$

$$\text{or } \left(\frac{\bar{M}}{\varrho_1^{\,2}} - \frac{M_N}{\varrho_o^{\,2}}\right) r^2 = 2\left(\frac{p_o}{\varrho_o} - \frac{p_1}{\varrho_1}\right) + 2\,(W_o - W_1)$$

or with (44)

$$(p_o+p_1)\left(\frac{1}{\varrho_1} - \frac{1}{\varrho_o}\right) + (p_o-p_1)\,\frac{M_N-\bar{M}}{\varrho_o\bar{M} - \varrho_1 M_N} =$$

$$= 2\,(W_o - W_1) \qquad (45)$$

which is the appropriately modified equation of Rankine (see eq. (19)). Indeed, the second term on the lefthand side of (45) vanishes for $M_N=\bar{M}$.

From $r^2 = (v_o-\dot{a})^2\varrho_o^{\,2} = \dfrac{p_o-p_1}{\frac{\bar{M}}{\varrho_1} - \frac{M_N}{\varrho_o}}$ one can solve for a and obtains the analogue to the former eq.(21) for the velocity $\dot{a}$ of the shock front

$$\dot{a} = V_o + \sqrt{(p_1-p_o)\,/\,\left(\varrho_o M_N - \frac{\varrho_o^{\,2}\bar{M}}{\varrho_1}\right)} \qquad (46)$$

$$= \frac{\dot{r}}{2} + c_s\sqrt{\frac{p_1/C}{\varrho_o\left(1 - \frac{\bar{M}}{M_N}\,\frac{\varrho_o}{\varrho_1}\right)}}$$

because $V_o = \dot{r}/2$, $p_o=0$, $c_s=\sqrt{C/M_N}$

Here $C \approx \frac{100}{9}$ MeV is the compression constant and c_s the velocity of first sound. For $T = \dot{r} = 0$ one obtains $\dot{a} = c_s$, i.e. the shock front travels then with the velocity of sound. Eq.(45) allows the calculation of the temperature as a function of the density. Since, however, this equation is of the form $T = T(\varrho,T)$, one has to use

an iteration procedure for the solution. With that one can then determine the potential and kinetic energies and the corresponding equations of motion. In Fig. 18b $T = (\rho_1/\rho_o)$ is drawn.

It is noticed, however, that there occur still some inconsistencies in the present formulation. In this highly relativistic problem one should use relativistic hydrodynamics and thermodynamics [15]. Also, eqs. (41)-(43) have in this sense to be replaced by the relativistically covariant eqs.

$$\frac{\partial T_i^k}{\partial x^k} = 0 \tag{47}$$

where T_i^k is the appropriate energy momentum tensor. The calculations are presently also extended to the case of the relativistic collision of a small resp. medium sized nucleus with a heavy one. In this case a Mach-cone develops within the heavy target. For the example studied here, for the case of equal nuclei, this Mach-cone occurs in both target and projectile, which manifests itself in the compression ellipsoid of Fig. 1. We will report in a separate paper on this generalization of the present theory and its results [15].

V. B. Pionization of Matter

We shall discuss now some fundamental, though very speculative ideas, which can be subject to experimental verification through the shock waves occurring in heavy ion collisions. The idea of supercritical fields and the decay (instability) of the vacuum into a charged vacuum was first discussed several years ago in connection with very strong Coulomb field occurring in the intermediate superheavy molecules in heavy ion collisions [4]. The electron-positron-vacuum becomes instable if $Z > Z_{cr} \approx 170$ [4]. This phenomenon is very

intimately connected with the single particle level scheme of the Dirac field and its most essential features can be understood this way. Such supercritical fields might now also occur for e.g. the Klein-Gordon field; either due to electromagnetic or to strong interaction of the pions with an external source[x] (superheavy intermediate molecule at close distances - shock wave densities). For point nuclei, the Klein-Gordon equation becomes overcritical due to the Coulomb field at $Z_c = \frac{\alpha}{2} \approx 69$; for extended nuclei this value is shifted to about at $Z_c \sim 1300$. From this, the importance of compression is already obvious.

For charged pions we study ($\hbar = c = 1$) the equation

$$(E - V(r))^2 \phi(r) = (p^2 + m^2) \phi(r) \tag{48}$$

where $\phi(r)$ is a complex scalar function and $V(r)$ is the potential energy of a negatively charged pion of mass m in the field of a fixed extended charge distribution. Eq.(48) can also be written in a Schrödinger-type form as

$$\epsilon_{eff} \phi = \frac{p^2}{2m} \phi + V_{eff} \phi \tag{48a}$$

where

$$\epsilon_{eff} = E' \left(1 + \frac{E'}{2m}\right)$$

$$V_{eff} = V \left(1 + \frac{E'}{m} - \frac{V}{2m}\right) \tag{48b}$$

$$E = E' + m$$

This will be useful later on.

---

[x] We consider here the nucleus only as an external source and neglect its own degrees of freedom. This should be a good approximation as long as the pion field is not too intense.

The strong interactions show up in additional terms which we best summarize by writing down the total Lagrangian for the nucleon-meson fields

$$
\begin{aligned}
L = \bar{\psi}(i\not{\partial} - M_o)\psi \; &+ \frac{1}{2}\left[\left(\frac{\partial\phi}{\partial x_\mu}\right)\cdot\left(\frac{\partial\phi}{\partial x^\mu}\right) - m^2\,\phi\cdot\phi\right] \\
&- i\, g_o[\bar{\psi}\gamma_5\vec{\tau}\psi]\cdot\phi - i\, g_o'[\bar{\psi}\gamma_5\vec{\tau}\psi]^2\phi^2 + \ldots \\
&+ \frac{f}{\mu}(\bar{\psi}\gamma_5\gamma_\mu\vec{\tau}\psi)\cdot\frac{\partial\phi}{\partial x_\mu} \\
&+ (g\bar{\psi}\psi + g'(\bar{\psi}\psi)^2)\,((\phi\cdot\phi)^2 + \ldots) \qquad (49) \\
&+ \lambda_3\,\phi^3 + \lambda_4\,\phi^4 + \ldots
\end{aligned}
$$

The main coupling discussed in literature is the one proportional to g_o. The term proportional to f is unpopular because it leads to a theory divergent in perturbation theory, even after mass and coupling constant renormalization. The term proportional to g would describe a higher order coupling of pions to nucleons.

The last two terms proportional to λ_3 and λ_4 are nonlinear (selfinteraction) terms of the pion field. The latter terms were discussed recently by Migdal [20] and by Lee [21]. One practically knows nothing about the last four terms in eq. (49) and very little about the standard term proportional to g_o. We will therefore restrict ourselves here to a qualitative discussion of phenomena which might be anticipated in very strong fields and speculate about the consequences of possible combinations of the terms denoted in eq.(49) We mention that the coupling to the electromagnetic field is

achieved via minimal coupling; i.e. the replacement $p_\mu \to p_\mu - \frac{e}{c} A_\mu$.

In order to be as clear as possible let us restrict to the case of simple central Coulomb potential for the π^--field as denoted in eq. (48); understand in this case the new physical phenomena and mention then the effect of the strong interaction terms. Introducing the Feshbach-Villars-representation [22]

$$\phi = \begin{pmatrix} \psi \\ (E-V)\psi \end{pmatrix} \tag{50}$$

the solutions of eq.(48) are found [23] to divide into two subsets ϕ_p and ϕ_n (p and n denote "positive" and "negative" respectively) characterized as follows

$$\begin{aligned} \int \phi_p^+ \tau_1 \phi_p &= 1 , \qquad E_p - \langle V \rangle_p > 0 \\ \int \phi_n^+ \tau_1 \phi_n &= -1 , \qquad E_n - \langle V \rangle_n < 0 \end{aligned} \tag{51}$$

where $\langle V \rangle = \frac{\int \psi^* V \psi}{\int \psi^* \psi}$. Clearly, if this classification becomes invalid, there should occur an eigenvalue for which the inequalities (51) become equalities. This indeed happens for strong fields, i.e. in our case as Z becomes very large. Because of physical reasons it is necessary to consider together the solutions for both negative and positive pions ($\pi^\mp$) . The situation is illustrated schematically in Fig. 19. For a Coulomb potential of an extended nucleus, the curve marked E_- represents in its solid part the lowest bound state of the π_- . Two special values of Z are to be noted: For $Z > Z_o$ there emerges from the negative energy continuum a new

bound state branch (dashed) which meets the Branch E_- at a point of vertical tengency, $Z = Z_c$. For $Z > Z_c$ there is simply no bound state solution corresponding to this branch. The curve marked E_+ is a reflection of E_- with respect to the abscissa $E = 0$ and represents a solution branch for π_+. This reflects the general property of the K·G. field of eq. (48), namely

$$\psi(r,E,e) = \psi(r,-E,-e) \tag{52}$$

It shows, that if branch E_- occurs for π_-, branch E_+ occurs for π_+. This is the <u>charge conjugation symmetry</u>. Considering now the

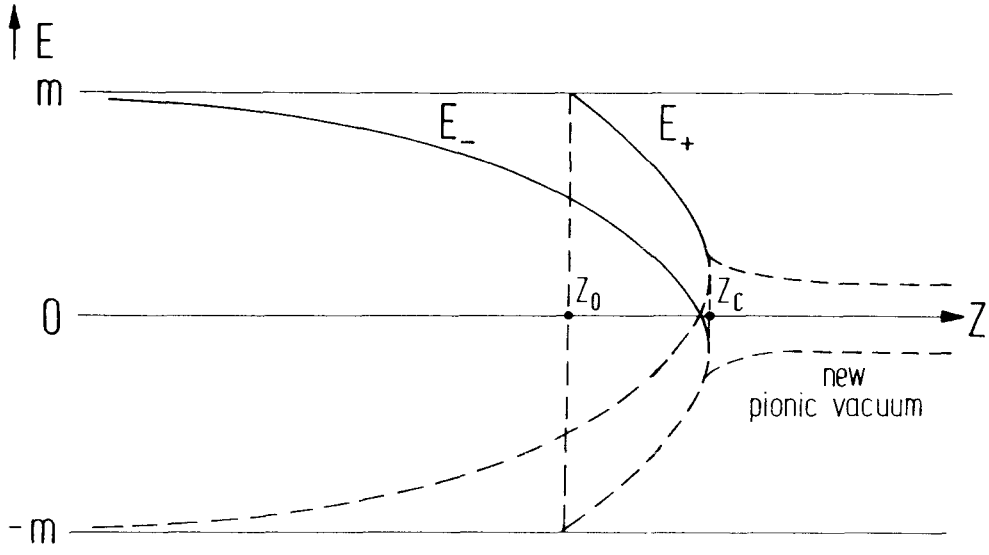

Fig. 19: Representation of the lowest bound state of a negative pion in a Coulomb field of a superheavy nucleus (E_-). Strong interactions are neglected. The energy for a positive pion is related to that by charge conjugation (E_+)

equation for π_+ near zero binding energy ($E' \approx 0$). It then follows from (48b) if - as must be in this case - the charge sign is changed

$$V_{eff}(\pi_+ , E' \sim 0) = |V(r)| - \frac{V^2}{2m} \tag{53}$$

Thus, for large enough Z the second term will dominate; even in the field of a positively charged nucleus. This is represented by the solid part of the E_+-curve. We thus understand from eqs.(52) and (53) the basic qualitative features of the Klein-Gordon solutions. One establishes easily that the solid branches of Fig. 19 have positive norm in the sense of eq.(51) and the dashed ones negative norm. The joining point has therefore always $E = \langle V \rangle$ and therefore - by replacing $V \rightarrow \lambda V$ - one gets from eq. (48)

$$\langle (E - \lambda V)^2 \rangle = \langle p^2 \rangle + m^2 \tag{54}$$

the derivative of which with respect to λ (at $\lambda = 1$) becomes due to repeated use of eq. (48)

$$(E - \langle V \rangle) \frac{dE}{d\lambda} = \langle EV \rangle - \langle V^2 \rangle \tag{55}$$

Since at the point $\langle V \rangle = E$ the right hand side of (55) will in general not vanish, such points must have $\frac{dE}{d\lambda} = \infty$, i.e. the joining points of the solid and dashed parts in Fig. 19 have vertical tangency.

We denote these points by $E_- = -m$ and $E_+ = +m$ respectively. One thus sees, field theoretically speaking, that one could produce at this point an infinite number of $\pi_- - \pi_+$ - pairs without energy (or very little energy). This will even more be true for π^0 -mesons (they only have strong interactions, of course) which are their own antiparticles. Obviously, this apparent instability has great analogy with the instable electron-positron vacuum in overcritical fields [4] and, in fact, signals the change (decay, breakdown) of the pionic vacuum.

For ordinary pions one estimates $Z_c \sim 1300$ [23]. If there would be a pion with the mass of the electron Z_c would be reduced by an order of magnitude. This is true for Coulomb forces. The overcritical fields for pions may, however, also be created by nuclear forces.

At $Z = Z_c$ the vacuum state is obviously no more unique, but degenerates with an infinite number of other states containing various numbers of $\pi_\pm$ -pairs of energy $m - m = 0$. If one considers, as usual, pions as real elementary bosons, an infinite number of $\pi^+ - \pi^-$-pairs and π_0's can be produced without energy. It should clearly be recognized, that these are all in bound states. Contrary to the electron-positron field, the antiparticle (positron for the spinor field) does not have a continuum wave function to "travel" out of the critical volume. Instead a kind of dipole-layer between π^- (sitting in an orbit closer to the origin) and π^+ (sitting in an orbit further out) is produced and also a cloud of neutral π^0's . We call this process <u>pionization of matter.</u>

The mutual interaction between pions (Coulomb, strong repulsion) can stop this process. It can also be stopped by the Pauli-principle, if the pions are not elementary particles, but build up by e.g. quark-antiquark pairs. Then - in analogy to e.g. α- particles in orbitals within O^{16}-nuclei - only a finite number of pions can be brought into one orbital and the process of pionization will quickly stop. If this does not occur, however, one can either expect complete pionization, i.e. a pionic drop, in which practically all energy is transformed into pionic matter (the baryon number is of course conserved); or one can expect partly pionized matter, depending on the pion-pion interaction (the terms of higher powers than ϕ^2 in the Lagrangian (49)).

The strong nucleon-pion interaction will be mediated by terms proportional to g_o and g in eq. (49). Such terms are particularly strong when the nuclear density is high, since they are proportional to $\bar{\psi}\psi$ of the nucleon field. Therefore the shock waves described in this article seem to be of absolute necessity for studying these eventually occurring new forms of matter.

The critical mass has not yet been determined exactly, since it depends on the coupling constants g_o and g, but is expected to be above $A \sim 300$. Similarly as the diving of the electron levels [4] can be enhanced strongly and occur earlier as the nuclei are more point-like (compressed), the compression of nuclear matter, will have similar effects on the overcritical pionic states.

Now, if the pionic self-interaction (terms proportional to λ_3 and λ_4 in eq. (49)) is such that either case a) or case b) of Fig. 20 occur, the pionized matter could stabilize a new

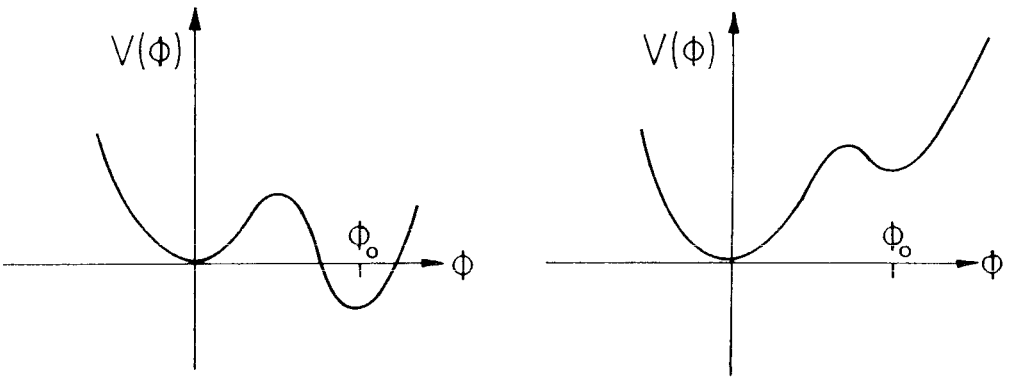

Fig. 20: Two of many possibilities for pion-pion interaction

quasistable (case b) or absolutely stable (case a) pionic vacua ϕ_o. We believe that case a) has to be ruled out, because it would be more stable than our nucleonic matter and we should most likely have come across pionic matter already. Thus, it seems, that we are left with case b) for speculation. If we could produce such pionic matter, we could expect very heavy stable (or quasi-stable)elements. In fact, if, say $A \sim 300$ would, for example, be the critical value for A, all higher values of A should also lead to pionic matter. Since the pions are energyless ($E \simeq 0$),

the masses of such nuclei are proportional to their nuclear masses (A) except for the pionic binding. The potential could look as schematically depicted in Fig. 21. Maybe we discover new very heavy "elementary" particles this way.

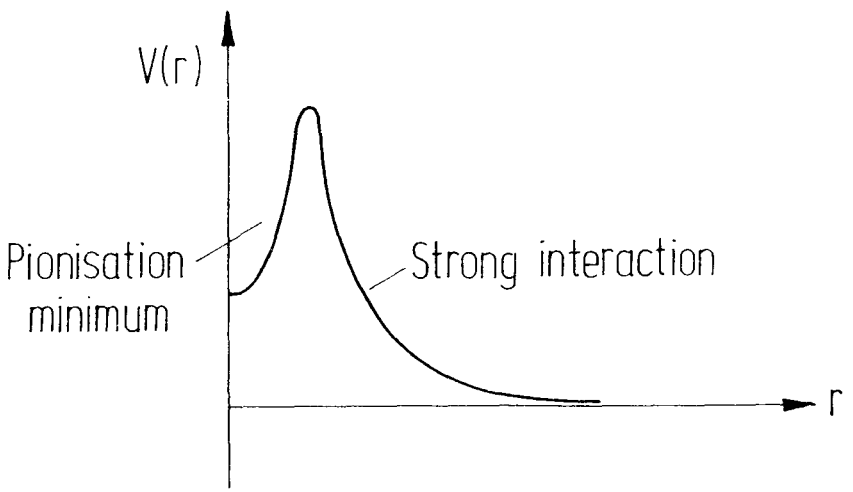

Fig. 21: Schematic figure of an effective nucleus-nucleus potential for relativistically colliding nuclei

The density of such nuclei can again be rather normal, i.e. not far from ρ_o, but their nuclear properties (spectra, deformation, shell model) are expected very different from ordinary nuclei. They can still be classified by their total charge Z, but are otherwise difficult (except for the nuclear properties mentioned and for their large mass) to recognize. The fission of such a pionic drop is expected to take place through a break-up into many fragments, because it has to take place over the "compression barrier", which needs very much energy.

These are speculations which should only be understood as such. Due to our lack of knowledge about the pion-nucleon Lagrangian, we do not claim, at this stage of the game, that such super-nuclei exist. The fun is, that they could.

We acknowledge stimulating discussions with Prof. M.S. Weiss (Livermore) during his stay as a visiting professor in June 1974 at the University of Frankfurt. He drew our attention to the inclusion of the temperature pions into our model (see ref.[18]). We are also grateful to Prof. R. Bock (GSI) and Prof. R. Stock for their interest and valuable discussions.

References:

[1] See for a review: W. Greiner and W. Scheid, J.de Physique 32 (1971) C6-91

[2] D.A. Bromley, J.A. Kuehner and E. Almqvist, Phys.Rev.Lett. 4 (1960)365; R.H. Siemssen, J.V. Maher, A. Weidinger and D.A. Bromley, Phys. Rev. Lett 19 (1967)369, and 20 (1968) 175;

J.V. Maher, M.W. Sachs,R.H. Siemssen, A. Weidinger, D.A. Bromley, Phys. Rev. 188 (1969)1665;

See also for review: A. Gobbi, Proceedings of the Symposium on Heavy Ion Scattering, Argonne Nat. Lab., 1971, Report No. ANL-7837, p. 63;

[3] W. Scheid, H.J. Fink, and H. Müller, Nuclear Molecular Structure in Heavy Ion Scattering in "Symposium on Four Nucleon Correlations and Alpha Rotator Structure", Marburg 1972, ed. R.Stock;

H. Müller, Diploma Thesis, Inst. f. Theoretische Physik der Johann Wolfgang Goethe-Universität Frankfurt/Main (1972).

[4] B. Müller, H. Peitz, J. Rafelski, and W. Greiner , Phys. Rev. Lett. 28 No.19 (1972)1235

B. Müller, J. Rafelski, and W. Greiner, Zeitschr.f.Physik 257 (1972)62 and 257 (1972)183;

J. Rafelski, B. Müller, and W. Greiner, Nucl.Phys.B68(1974)585

J. Rafelski and A. Klein, Proc. of the Int. Conf. on Reactions between Complex Nuclei, Nashville, Tenn.,June 1974, ed. by R. Robinson and J. Hamilton, North Holl.Publ.Comp.

[5] T. Fließbach, Zeitschr.f.Physik 238(1970)329; 242(1971)287; 247(1971)117; Nucl.Phys. A194(1972)625

[6] see e.g. J. Maruhn and W. Greiner, Zeitschr.f.Physik 251 (1972)431 and further references therein.

[7] For the dynamic collective model of giant resonances, which is the modern version of the Goldhaber-Teller resp. Steinwedel-Jensen model see J.M. Eisenberg and W. Greiner, Nuclear Models, North Holl.Publ.Comp., Amsterdam (1970);

[8] see e.g. F.Seidl, A. Cameron, Astrophys. and Space Science 15 (1972) 44-128.

[9] W. Scheid, R. Ligensa, and W. Greiner, Phys.Rev.Lett 21 (1968)1479, see also [7]

[10] H. Müller, W. Scheid, and W. Greiner, to be published, H. Müller, diploma thesis, Inst. f. Theor. Physik der Johann Wolfgang Goethe-Universität Frankfurt am Main (1972).

[10a] W.Scheid,H.Müller,and W.Greiner, Phys.Rev.Letters 32(1974)741

[11] L.D. Landau and E.M. Lifshitz, Statistical Physics (Pergamon, London 1958);

[12] J.D. Walecka, Phys. Rev. 126 (1962)653;
K. Woeste, Z.Physik 133 (1952)370
H.A. Bethe, Ann.Rev. Nucl.Sci. 21 (1971)93;

[13] Such work is presently at progress by J. Hofmann, Inst. f. Theoretische Physik der Universität Frankfurt/Main. The general problem is treated within relativistic hydrodynamics.

[14] J. Serrin, Handbuch der Physik, edited by S. Flügge (Springer, Berlin, 1959) Vol. 8, Part I, p. 125;

[15] For relativistic hydrodynamics in connection with relativistic heavy ion collisions, see work of J. Hofmann et al.

[16] H.J. Fink, Dissertation, Inst.f.Theor. Physik der Univ. Frankfurt/Main (1973);
H.J. Fink, W. Scheid, and W. Greiner, Contribution to the Internat. Conf. on Reactions between Complex Nuclei, Nashville, Renn., June 1974 (Proceedings ed. by R. Robinson and J. Hamilton, North Holland Publ.Comp.)

[17] H. Holm, W. Scheid, and W. Greiner, Phys.Lett.Vol 29B Nr.8(1969) see also Eisenberg-Greiner: Nuclear Models, North Holland Publ.Comp. Amsterdem (1970)

[18] G.F. Chapline, M.H. Johnson, E. Teller, and M.S. Weiss, Phys.Rev. D 8 (1973)4302

[19] H. Arenhövel and H.J. Weber, Nucl.Phys. Vol.91 Nr. 1 (1967)

[20] A.B. Migdal, Nucl.Phys. A210(1973)421

[21] T.D. Lee and G.C. Wich, Phys.Ref.D. Vol.9 (1974)2291

[22] H. Feshbach and F. Villars, Rev.Mod.Phys.30 (1958)24

[23] A. Klein and J. Rafelski, Contr. at Orbis Scientiae, Center for Theoretical Studies of the Univ.of Miami(Jan 7-12, 1974).

[24] The possibility of Mach-cones within nuclear matter emerged in discussions with Prof. D.A. Bromley, Yale University, during the spring semester 1974; see e.g. D.A. Bromley: The Physics of Complex Nuclear Interactions, Proc. of the Int.Conf. on the Interaction with Complex Nuclei, Nashville, Tennessee, June 1974 (North Holl. Publ.Comp.).

[25] B. Fink, C. Toepffer, Phys. Lett. 4513(1973)411

HIGHLY EXCITED NUCLEAR MATTER*

George F. Chapline

Lawrence Livermore Laboratory
University of California/Livermore, California

Table of Contents

Introduction 52

Hot Nuclear Matter 53

Shock Compression of Nuclear Matter 55

Diagnosis of Compression 57

Possibilities of Abnormal Nuclear States 60

Pion Lasers 61

Applications to Astrophysics - Neutron Stars 61

Applications to Astrophysics - Early Universe 63

Appendix, Comment on the validity of hydrodynamics 66

*Work was performed under the auspices of the U.S. Atomic Energy Commission

Introduction

In this lecture I will talk about a type of collision that will happen in only a very small fraction of the collision events produced with the Bevalac, if at all. Nevertheless, these collisions may lead to spectacular effects and be of great value in furthering our understanding of nuclear matter. The type of collision I refer to is the "head-on" collision between heavy nuclei in which there is considerable momentum exchange between the projectile and target nuclei. If the initial kinetic energy of the projectile nucleus is in the range 1-2GeV per nucleon then a large transfer of momentum between projectile and target could lead to energy densities in the center of mass system which are much larger than anything produced heretofore in the laboratory. It is this opportunity for studying matter in an entirely new regime of density and temperature that makes the search for head-on collisions very worthwhile.

If we consider the collision of identical nuclei where the incident nucelus has a laboratory kinetic energy per nucleon T then the internal energy per baryon in the center of mass system is

$$\varepsilon = Mc^2\left[\left(1 + \frac{T}{2Mc^2}\right)^{\frac{1}{2}} - 1\right] \tag{1}$$

For T = 2GeV/n we have $\varepsilon \approx 400$MeV. In the case of large momentum transfer between incident and target nucleus one would expect that for a brief moment a very hot gas of baryons would be formed in which the excess center

of mass energy appears as thermal energy. If we assume that this hot baryon gas can be described as an ideal gas of nucleus then the temperature Θ of this hot gas will be given by

$$\varepsilon = 3\Theta + Mc^2 \left(\frac{K_1(Mc^2/\Theta)}{K_2(Mc^2/\Theta)} - 1 \right) \tag{2}$$

This relation differs from the familiar expression $\varepsilon = \frac{3}{2}\Theta$ because the nucleons must be treated relativistically. In the ultrarelativistic limit one would have $\varepsilon = 3\Theta$. In the neighborhood of T = 2GeV eq. (2) gives $\varepsilon \approx 2\Theta$. The temperature as a function of T is shown in Figure 1 for the case of an idea gas of nucleons and for the case where excited states of the nucleon are taken into account (Chapline, Johnson, Teller, and Weiss, 1974).

Hot Nuclear Matter

At temperatures in excess of 100MeV mesons will be copiously produced. The rate of meson production in a proton gas as a function of temperature is shown in Fig. 2. This curve is calculated by averaging the experimental total cross-section for meson production with relativistic Maxwell-Boltzmann distributions for the colliding protons. The number of mesons produced does not, of course, keep increasing because one will soon reach a state of thermodynamic equilibrium. This state of thermodynamic equilibrium will be reached in heavy ion collisions if the decay time for the highly excited material in the center of mass system exceeds the equilibration time for meson degrees of freedom. In the "hydrodynamic" approximation the decay time of the highly excited material is approximately $.2R/c_s$ where R is the

radius of the excited material and c_s is the speed of sound in the highly excited material. The .2 factor simply accounts for the fact that half the mass lies within .2R of the surface. If we compare this decay time with the equilibration time, $(n\bar{\varepsilon}v)^{-1}$, and assume $R = 1.1A^{1/3}$ fermi we find that the decay time exceeds the equilibration time if

$$A^{1/3} \gtrsim 4$$

Thus, collisions of nuclei with $A \gtrsim 64$ could lead to states which are in thermodynamic equilibrium with respect to meson emission and absorption.

If one assumes that the mesons are present as an ideal gas of pions then one finds that for a baryon density equal to twice normal nuclear density the equilibrium pion density is $.11(\text{fermi})^{-3}$ for T = 2GeV/n. This corresponds to about one pion for every three nucleons in the highly excited state. Of course, at nuclear densities above that of normal nuclei it is not a very good approximation to treat the pions present as being free because of their interactions with the nucleons. At twice normal nuclear density pions with energies inside the $\Delta(1236)$ resonance will spend about 90% of their time "resonating" with the nucleons. Thus, it might not be too bad an approximation to assume that the highly excited nuclear matter can be described as a gas of necleons and excited nucleons.

The thermodynamic properties of a gas of nucelons and excited nucleons will be determined by the spectrum of excited nucleon states. According to the statistical bootstrap theory this spectrum has the form (Hamer and Frautschi 1972)

$$\rho(m) = cm^{-3} e^{m/\Theta_o} \tag{4}$$

where $\Theta_o \approx 175$MeV. In the region of baryon masses m where a thorough search for resonant states has been carried out, it is found that the density of states does increase rapidly with mass and could be fit with an expression of form (4). The temperature of an ideal gas of nucleons and excited nucelons, assuming that the spectrum of nucleon states has the form given in eq. (4), is shown as the solid line in Fig. 1. Because of the factor e^{m/Θ_o} in eq. (4) the temperature of such a gas can never exceed Θ_o. That is, as was first suggested by Hagedorn (1970), nuclear matter in thermodynamic equilibrium has a maximum temperature. Since the non-equilibrium temperature (dashed line) at T = 2GeV/n is considerably higher than Θ_o measurement of the equilibrium temperature, perhaps by measuring the A dependence of the temperature, could provide a test of Hagedorn's hypothesis.

Shock Compression of Nuclear Matter

Since nuclei coming together at relativisitic velocities are moving faster than the speed of sound in nuclear matter one would expect on the basis of classical hydrodynamics that shock waves would appear where the nuclei interpenetrated. The question of when this picture applies to collisions of nuclei is discussed in the Appendix. Here we will merely assume the hydrodynamic picture does apply and that the nuclear matter in the colliding nuclei is compressed as a result of passing through a shock wave.

The compression in a relativistic shock wave is given by (Johnson and McKee 1969):

$$\frac{n}{n_o} = \gamma\left(1 + \beta^2 \frac{e}{P}\right) \tag{5}$$

where β is the velocity of the unshocked material in the frame of the shocked material, $\gamma = (1-\beta^2)^{-\frac{1}{2}}$, e is the proper energy density of the shocked material, and P is the pressure of the shocked material. In the case of identical nuclei $\gamma = (1 + T/2Mc^2)^{\frac{1}{2}}$ and $e = n(Mc^2+\varepsilon)$ where ε is given in Eq. (1). Thus we have

$$\frac{n}{n_o} = \left(1 + \frac{T}{2Mc^2}\right)^{\frac{1}{2}} + \frac{nT}{2P} \tag{6}$$

for the shock compression produced by a nucleus with kinetic energy per nucleon T. The actural compression will depend on how the pressure P in compressed nuclear matter depends on density. If we neglect the interactions between baryons then $P = n\theta$ and therefore

$$\frac{n}{n_o} = \left(1 + \frac{T}{2Mc^2}\right)^{\frac{1}{2}} + \frac{T}{2\theta} \quad . \tag{7}$$

As an example, if the compressed nuclear matter is treated as an ideal gas of nucleons then one obtains the compressions shown in curve (b) of Fig. 3. It can be seen that one might expect to produce nucleon densities as high as $6\ n_o$, i.e. $\sim 10^{39} cm^{-3}$, with the Bevalac (T = 2 GeV/n).

The actual densities produced in nuclear shock waves may be higher or lower than for an ideal nucleon gas because of the effects of meson production and nucleon-nucleon interactions. Meson production tends to lower the temperature and therefore increase the compression, as can be seen from Eq. (7). If one uses the bootstrap density of states, Eq. 4, and neglects the interaction between baryons then one obtains the compression vs. T curve shown as curve (a) in Fig. 3. It can be seen that if baryon-baryon interactions were negligible

one would expect to reach a density $n \approx 10\ n_o$ at T = 2 GeV/n. Of course, at densities much above normal nuclear density one does not expect that baryon-baryon interactions can be neglected. The conventional picture of nuclear forces assumes that there is a strong short range repulsion between nucleons due to ω-meson exchange. Since the ω-meson couples to the baryon number this short range repulsion would be independent of the state of internal excitation of the nucleon and therefore would lead to a lower compression than indicated by curve (a). A lower bound or the compression can be obtained by assuming that the pressure $P = n\varepsilon$. The equation of state holds when the inter-nucleon separation is smaller than the range of a strong repulsive interaction (Zeldovich, 1962). It has the property that the speed of sound, i.e. $(c^2 dP/d\varepsilon)^{\frac{1}{2}}$, approaches the speed of light when the density increases to where $\varepsilon >> Mc^2$. It one substitutes $P = n\varepsilon$ into Eq. (6) and uses Eq. (1) one obtains curve (c) in Fig. 3. The actual shock compression in nuclear matter will lie somewhere between curves (a) and (c) of Fig. 3.

Diagnosis of Compression

Figure 3 shows that different possible assumptions about the equation of state of compressed nuclear matter can lead to quite different values of the shock compression even at T = 2 GeV/n. It is evident that a measurement of the shock compression in relativisitic collisions of heavy nuclei could provide useful clues as to the nature of compressed nuclear matter. One possible indication of the compression produced in nuclear collisions would be the number of pions produced. The production of pions tends to lower the pressure and therefore increase the compression.

A rigorous statement of this effect can be arrived at by making use of the virial theorem:

$$P = n\theta - \frac{1}{6} n^2 \int_0^\infty r \frac{d\phi}{dr} g(r) 4\pi r^2 dr \tag{8}$$

where $\phi(r)$ is the nucleon-nucleon potential and $g(r)$ is the pair correlation function in nuclear matter. We are using the non-relativistic form of the virial theorem since relativistic effects will not be of great importance in the temperature regime we are considering. If we integrate the right hand side of Eq. (8) by parts we obtain

$$P = n(\theta+\varepsilon_{int}) + \frac{1}{6} n^2 \int_0^\infty \phi\, g'(r) 4\pi r^3 dr \tag{9}$$

where $\varepsilon_{int} = \frac{n}{2}\int_0^\infty \phi g(r) 4\pi r^2 dr$. The quantity ε_{int} is the interaction energy per nucleon due to the nucleon-nucleon potential. If we assume that the potential is positive and repulsive, then the second term of Eq. (9) will be positive and therefore, we have

$$P \geq n(\theta+\varepsilon_{int}) \quad . \tag{10}$$

The equality will approximately hold when the repulsive potential is "soft", i.e. when the logarithmic derivative of $g(r)$ is small. Combining Eqs. (10) and (6) gives

$$\frac{n}{n_o} \leq \left(1 + \frac{T}{2Mc^2}\right)^{\frac{1}{2}} + \frac{T}{2(\theta+\varepsilon_{int})} \quad . \tag{11}$$

If we assume that the repulsive potential acting between baryons is independent of the state of internal excitation, as is the case for the potential due to

ω-meson exchange, then the energy per baryon can be written

$$\varepsilon = (\bar{m}(\theta) - M)c^2 + \frac{3}{2}\theta + \varepsilon_{int} \tag{12}$$

where $\bar{m}$ is the average baryon mass and ε_{int} is independent of $\bar{m}$. We assume here that the temperature θ is low enough so that the non-relativistic approximation, $3\theta/2$, for the thermal energy can be used. If we use the bootstrap density of states, Eq. (4), to calculate $\bar{m}(\theta)$ then Eqs. (11) and (12) imply a relation between $\bar{m}(\theta)$ and n/n_o like that shown in Fig. 4. The upper limit on the compression (solid line) holds when the repulsive potential is "soft" while the lower limit, $2\gamma + 1$, holds when the repulsive potential is "hard". It can be seen that if few pions are present in the compressed nuclear matter then the compression was near the minimum, while if many pions are present the compression can be either large or near the minimum depending on whether the repulsive potential is "soft" or "hard". Of course, as the nuclear matter expands from the compressed state it will cool leading to a reduction in the number of pions present. It is to be noted, however, that the temperature will not drop very fast if the repulsive potential is weak since the variation of temperature with volume will be determined by the ratio P/c_v where c_v is the specific heat. Since the pressure P is small for a weak soft potential the "frozen out" temperature would not differ greatly from the temperature in the compressed state. Thus measurement of the number of pions produced in the collision should give some indication whether nuclear matter is easily compressed or not.

Possibilities of Abnormal Nuclear States

In the previous discussion we have pictured compressed nuclear matter as consisting of nucleons and excited nucleous repelling each other by a repulsive potential. This is the conventional picture of compressed nuclear matter, but one should also consider the possibility that high energy collisions of nuclei could lead to abnormal states of nuclear matter. Here are a few of the possibilities:

1) The nucleon-nucleon potential might have an attractive region inside the repulsive core, e.g. due to f_1 exchange. This might lead to stable or metastable collapsed nuclei, i.e. systems with baryon number $A > 1$ and with radii much smaller than normal nuclei (Bodmer 1971).

2) If the size of excited nucleons permitted metastable nuclei containing excited nucleons might be formed. For example, one can fit 16 Δ's into the 1S orbital without violating the Pauli principle and therefore there exists the possibility of a metastable system containing 16 Δ's, analogous to an α-particle, but several times denser (Chapline and Weiss, 1973).

3) The question of whether the bootstrap density of states, eg. 3, applies to baryons in highly compressed nuclear matter is open. One possibility is that superbaryons exist, i.e. baryons with $A > 1$ and size comparable to a nucleon and for which the bootstrap density of excited states applies (Carlitz, Frantschi, and Nahm, 1973).

4) Metastable dense states of nuclei could exist where the binding is due to a non-vanishing scalar field (Lee and Wick, 1974).

Pion Lasers

If it turns out that excited baryon states can exist at densities higher than normal nuclear density then the rapid expansion of the compressed nuclear matter could lead to non-equilibrium states in which population inversions existed. This effect would be most pronounced in the lightest nuclei for which equilibrium with respect to excited nucleon states and also high compressions (see Appendix) can be established, since for these nuclei the drop of density with time will be most rapid. The existence of population inversions in the expanding nuclear matter will lead to stimulated emission of pions if the population inversion density N^* satisfies:

$$N^* \gg \frac{6\pi}{\lambda^2} \frac{1}{R_c} \tag{13}$$

where R_c is the radius of the compressed nuclear matter and λ is the pion Compton wavelength. That N^* must be large compared to the right hand side rather merely greater results from the fact that the pion laser would be operating without mirrors. Condition (13) suggests that stimulated emission of low energy (λ<200 MeV/c) pions might be possible if the compressed density were 6x normal nuclear density. In fact, as Professor Teller pointed out in his talk, stimulated emission of pions may even be stronger than expected because of the possibility of double pion emission.

Applications to Astrophysics - Neutron Stars

We have seen that crude measurements of the properties of nuclear matter at densities above normal nuclear density might be made by observing head-on collisions of heavy nuclei. One area where measurements of the equation of state of dense nuclear matter should prove useful is the theory of neutron stars. Although the results on collisions of nuclei would not

be directly applicable to neutron stars because nuclei contain protons as well as neutrons, it might be possible to produce nucleon densities with the Bevalac which are comparable to the maximum nucleon densities in neutron stars. Thus experiments with the Bevalac may lead to a much better understanding of the internal structure of neutron stars. Two problems in particular which might be clarified are the maximum mass of neutron stars and the question of whether neutron stars have a solid core.

The maximum mass of neutron stars is determined by the behavior of the speed of sound in dense neutron matter (Nauenberg and Chapline, 1973). If one assumes that the equation of state of neutron matter is known up to some density n_r and that the speed of sound in neutron matter at higher densities does not exceed the speed of light, then it is possible to derive an upper limit for the mass of a neutron star (Nauenberg and Chapline loc. cit.). If the density n_r is the density of nucleons in normal nuclei then this upper limit on the maximum mass is about 3 $M_\odot$. If the reference density n_r is 10^{39} cm^{-3}, i.e. $\sim$6x normal nuclear density, then the upper limit on the neutron star mass will be about 2 $M_\odot$. Thus, whereas ordinary nuclear physics only allows one to infer that neutron stars cannot be more massive than about 3 $M_\odot$, experiments with the Bevalac should go a long way towards defining the actual maximum mass of neutron stars, which is expected to be between 1.5 and 2.0 $M_\odot$.

Experiments with the Bevalac may also clarify the question of whether neutron stars have a solid core. The solidification pressure of neutron matter depends on the "hardness" of the short range repulsive potential between nucleons. If the repulsive potential rises steeply, as it does

between atoms, then neutron matter would solidify at densities only slightly above normal nuclear density (Anderson and Palmer, 1971). On the other hand, a relatively soft potential, such as that due to vector meson exchange, would lead to solidification only at densities $\gtrsim$ 10x normal nuclear density (Pandharipande, 1972). Some estimates of the steepness of the rise of the repulsive potential with decreasing nucleon separation might be obtained by measuring the change in pion yield in head on collisions with energy. The "frozen out" temperatures of the pions may also be useful in this repsect (see Sec. IV). It might be thought that expeirments with the Bevalac would not be relevant to the question of the solidification of neutron matter because the nuclear matter in the head on collisions would be very hot. However, as a general rule experiments on shock compressed matter give information on cold compressed matter at even higher densities due to the fact the smaller interparticle separations are being sampled in the hot matter.

Applications to Astrophysics - The Early Universe

At times earlier than 10^{-4} seconds the temperature of the universe exceeded 100 MeV. At times earlier than 10^{-8} seconds the average baryon density in the universe exceeded that in nuclei. Thus while existing proton accelerators should be adequate to elucidate the physics of the universe in the period 10^{-8} sec $< t < 10^{-4}$ sec, only the Bevalac will be capable of studying directly conditions during the epoch $t < 10^{-8}$ seconds. Some of the problems that may be elucidated by experiments with the Bevalac are the origin of the cosmic black-body radiation, the origin of galaxies, and the existence of primordial black holes.

Measurements of the temperature of the cosmic black-body radiation together with estimates of the present day average baryon density in the universe yield a value for the entropy per baryon which is quite high. This suggests that strongly dissipative processes were important at some time in the early history of the universe. Since the entropy per baryon is a free parameter in cosmological models it is necessary to understand these dissipate processes in detail in order to explain the cosmic black-body radiation. It is quite possible, however, that understanding of these dissipative processes will have to await a better understanding of dense nuclear matter. For example, Zeldovich (1973) has pointed out that damping of relatively small magnitude density fluctuations in initially cold nuclear matter could account for the observed entropy if very dense nuclear matter obeys the equation of state $p = e$. Another possibility (Carlitz, Frautschi, and Nahm, 1973) is that non-equilibrium decay of superbaryons is responsible for the black-body radiation.

One particularly interesting consequence of assuming that the statistical bootstrap spectrum of excited states applies to baryons in dense nuclear matter is that large spontaneous density fluctuations would occur (Carlitz, 1972). Carlitz, Frautschi, and Nahm (1973) have suggested that these large density fluctuations in dense nuclear matter are responsible for observed structures such as galaxies and clusters of galaxies. A difficulty with this suggestion is that structure on scales larger than clusters of galaxies would tend to be washed out, which contradicts recent observations of Peebles (1974).

Another possible consequence of large density fluctuations in dense nuclear matter is that large numbers of black holes might be formed in the early universe. The existence of large numbers of small ($M \ll M_{\odot}$) black holes in the universe would resolve some current cosmological puzzles (Chapline, to be published) and might even be of economic importance. Of course, it should be kept in mind that formation of small black holes would take place at densities orders of magnitude higher than could be produced with the Bevalac. Nevertheless, any evidence from the Bevalac bearing on the question of whether the statistical bootstrap density of states applies at densities above normal nuclear densities would be valuable in assessing the plausibility of large density fluctuations in very dense nuclear matter.

Appendix

Use of the shock condition, Eq. (5), to find the compression of nuclear matter resulting from the head-on collision of heavy ions assumes that hydrodynamic equations apply. However, it is by no means obvious that the hydrodynamic approximation applies to the collision of objects containing as few particles as nuclei. In order to verify that an equation such as the shock condition, Eq. (5), applies to a given situation one must solve the Boltzmann equation. In plane geometry, one finds that it takes about 3 mean free paths to form a shock wave if the differential scattering cross-section is isotropic. For forward peaked differential cross-sections it would take more than 3 mean free paths to form a shock wave, the exact number depending on how sharply forward peaked the differential cross-section. At 2 GeV/n the differential cross-section for nucleon-nucleon scattering is so strongly peaked forward that there could be almost no hope of forming nuclear shock waves in ion-ion collisions. However, the nucleon-nucleon collisions are inelastic; the nucleons losing several hundred MeV at each collision. In the collision of two uranium nuclei, each nucleus would be $\sim$7 mean free paths across so that most nucleons would be down to several hundred MeV before the two nuclei had gone completely thru each other. At several hundred MeV per nucleon lab energy the differential cross-section is nearly isotropic and therefore one would expect to get considerable momentum exchange between two uranium nuclei even at 2 GeV/n It seems likely however, that strong momentum exchange and the formation of shock waves is only possible in heavy nuclei, even at lower energies. Thus one can probably not use hydrodynamic equations to describe the collision of light nuclei, as was done by Scheid, Müller, and Greiner (1974). To find out what actually happens in head-on collisions of nuclei it will be necessary to solve the relativistic two-dimensional Boltzmann equation.

References

Anderson, P. W. and Plamer, R. G., 1971, Nature 231, 145.

Bodmer, A., 1971, Phys. Rev. D4, 1601.

Carlitz, R., 1972, Phys. Rev. D5, 3231.

Carlitz, R., Frautschi, S., and Nahm, W., 1973, Astron. and Astrophys. 26, 171.

Chapline, G., Johnson, M., Teller, E. and Weiss, M., 1973, Phys. Rev. D8, 4302.

Chapline, G. and Weiss, M., 1973, Bull. Am. Phys. Soc. 18, 18.

Dahlbacka, G. H., Chapline, G. and Weaver, T. A., 1974, Nature 250, 36.

Hagedorn, R., 1970, Astron, and Astrophys. 5, 184.

Hamer, C. and Frautschi, S., 1971, Phys. Rev. D4, 2125.

Johnson, M. H. and McKee, C. F., 1971, Phys. Rev. D3, 858.

Lee, T. D. and Wick, G. C., 1974, Phys. Rev. D9, 2291.

Nauenberg, M. and Chapline, G., 1973, Astrophys. J. 179, 277.

Pandharipande, V. R., 1972, proceedings of the Sixth Texas Symposium on Relativistic Astrophysics (New York).

Peebles, P. J. E., 1974, Astrophys. J. 189, L51.

Scheid, W., Muller, H. and Greiner, W., 1974, Phys. Rev. Letts., 32, 741.

Zeldovich, Ya. B., 1962, Zh. Eksp. Teor. Fiz. 41, 1609 [English translation Sov. Phys. JETP 14, 1143].

Zeldovich, Ya. B, 1973, Zh. Eksp. Teor. Fiz. 64, 58 [English translation Sov. Phys. JETP 37, 33].

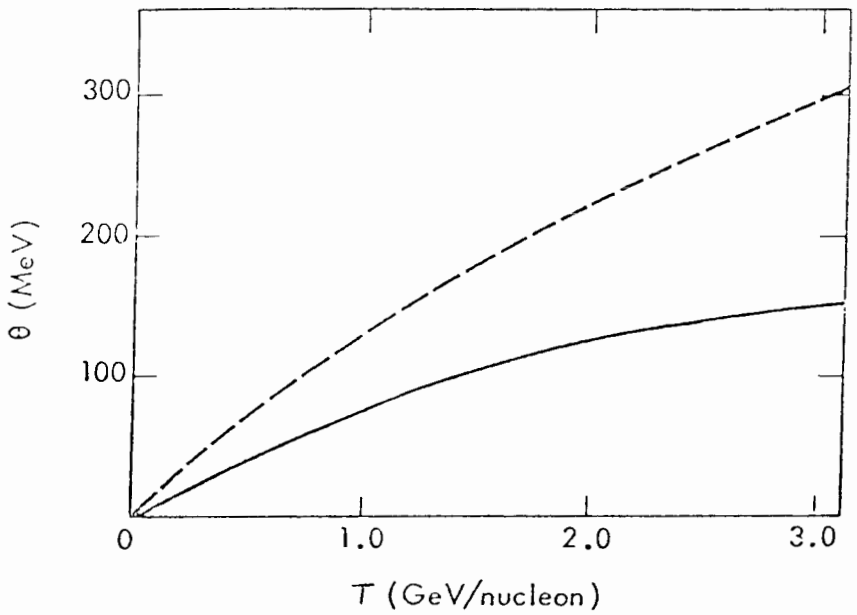

Figure 1 Nuclear temperature resulting from the head-on collision of a nucleus with laboratory kinetic energy per nucleon T with an identical stationary nucleus. The dashed curve assumes that the hot nuclear matter can be described as an ideal gas of nucleons. The solid curve is for an ideal gas of N's and N*'s where the N* mass spectrum has the form given Eq. 4.

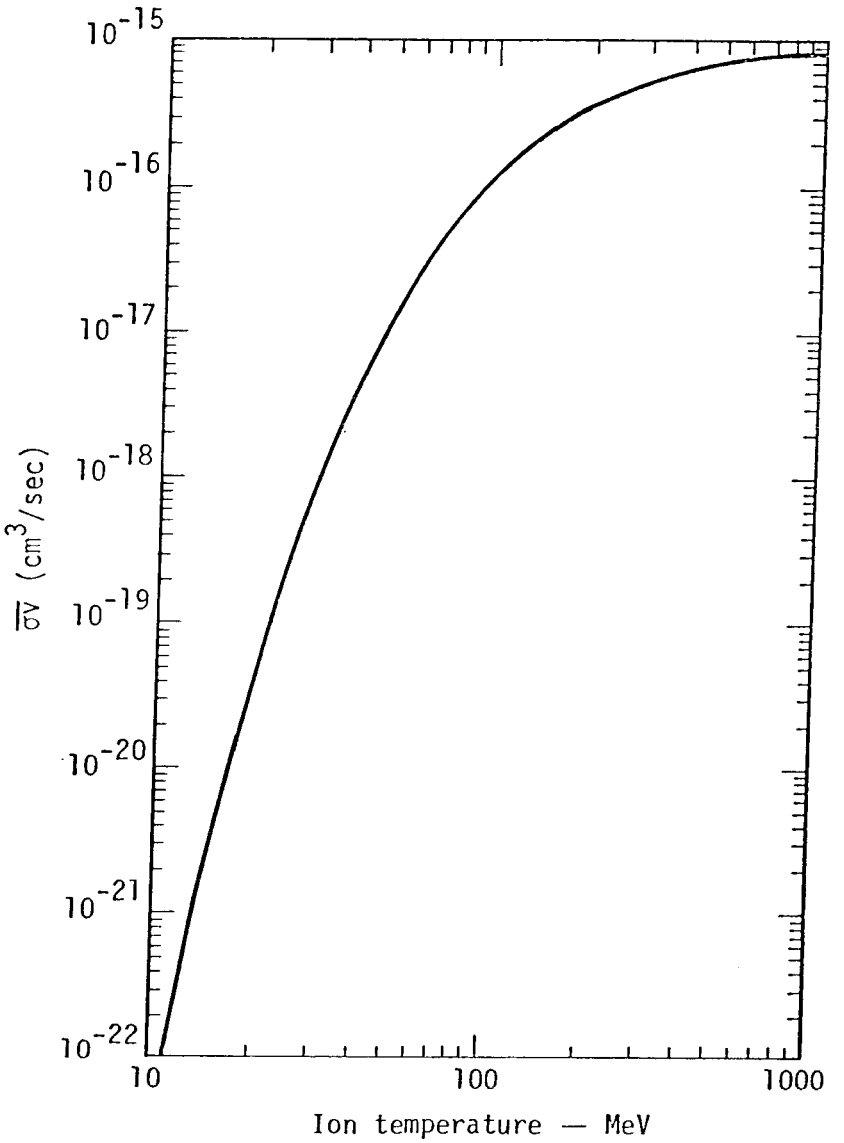

Figure 2 Thermal average rate for pion production in a hot nucleon gas, calculated using the experimental total pion production cross-section, σ, and relativistic Maxwell-Boltzmann distributions for the nucleons (Dahlbacka, Chapline, and Weaver, 1974).

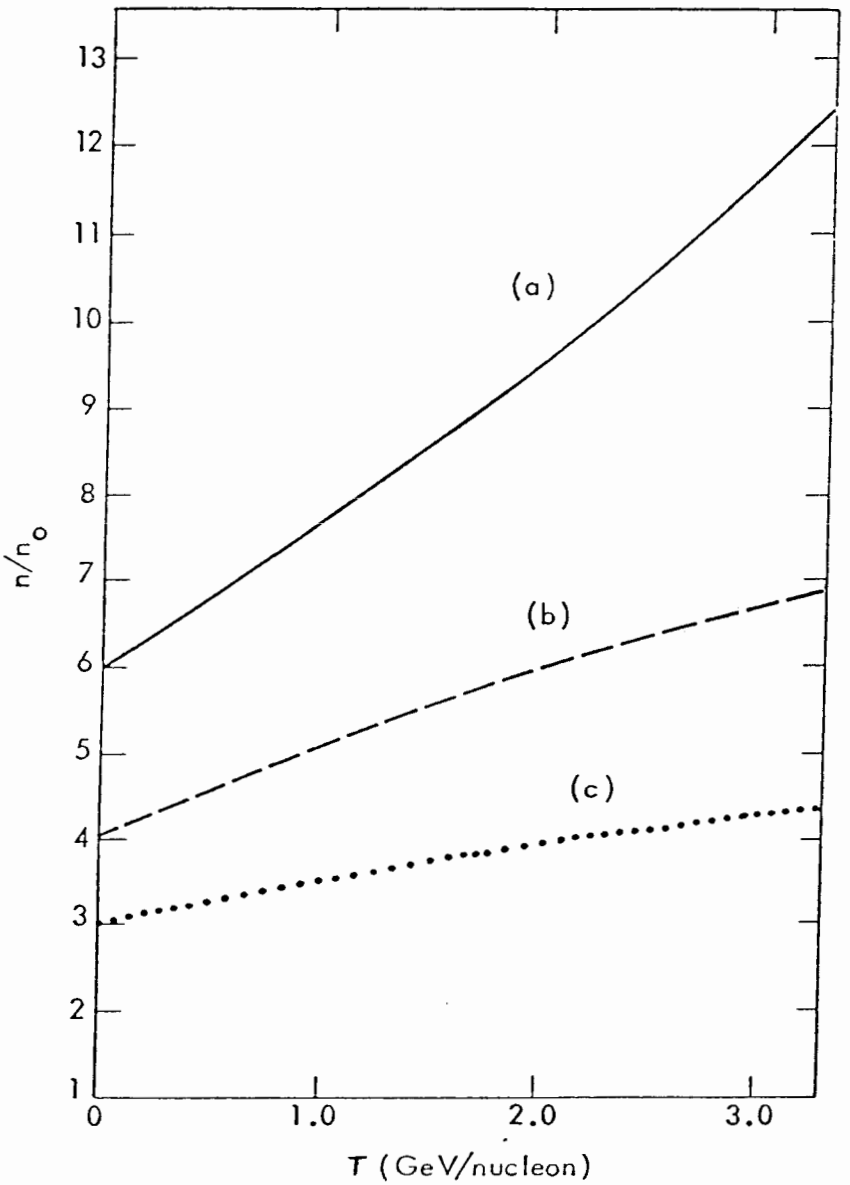

Figure 3 Nuclear shock compression that would result from the head-on collision of a heavy nucleus with laboratory kinetic energy per nucleon T with an identical stationary nucleus. Curve a (solid line) assumes that the compressed nuclear matter can be described as an ideal gas of N's and N*'s. Curve b (dashed line) assumes that the compressed nuclear matter can be described as an ideal gas of nucleons alone. Curve c (dotted line) assumes that the pressure of compressed nuclear matter is given by $P = e - nMc^2$.

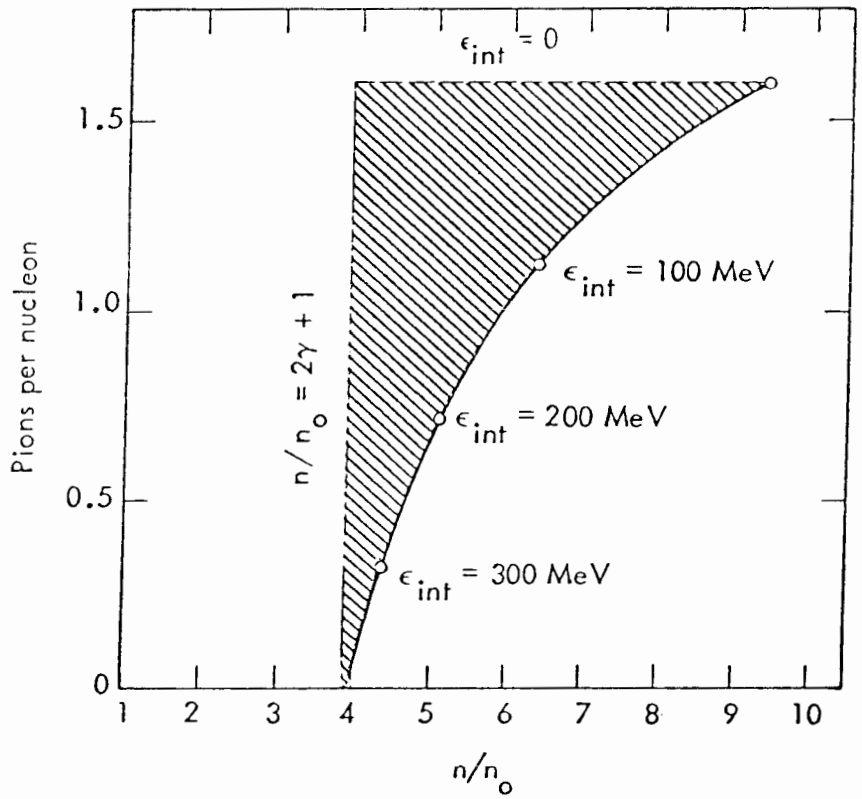

Figure 4 Number of pions per nucleon in compressed state as a function of the shock compression. It is assumed that the compressed nuclear matter can be represented as a gas of N's and N*'s and that N's and N*'s all have identical interactions. The solid line corresponds to a very "soft" repulsive interaction and the dashed line corresponds to a "hard sphere" repulsive interaction. We have chosen T = 2 GeV/nucleon.

FIELD THEORY METHODS FOR FINITE NUCLEAR SYSTEMS AND THE POSSIBILITY OF DENSITY ISOMERISM*

A. K. Kerman

and

L. Dudley Miller

Laboratory for Nuclear Science and Department of Physics
Massachusetts Institute of Technology
Cambridge, Massachusetts

*This work is supported in part through funds provided by The Atomic Energy Commission under Contract AT(11-1)-3069

Presented at the Relativistic Heavy Ion Summer Study, Berkeley, July, 1974

Center for Theoretical Physics Publication #449

I. INTRODUCTION

Since the original suggestion of Yukawa,[1] the idea that nuclei can be understood through some version of a relativistic meson field theory has been a continually recurring theme in theoretical nuclear physics. For the two-body problem successful boson exchange models have been obtained using the low mass resonances (π,ω,ρ) with coupling constants in agreement with experimental elementary particle values as long as either a scalar-isoscalar resonance[2] or a strong two-pion exchange[3] effect in the scalar-isoscalar channel is also included in the model. The scalar component is an important element in all these models since it provides an attraction at intermediate range in all channels of the nucleon-nucleon system.

Insofar as the many-body problem is concerned, it has been shown, at least in relativistic Hartree approximation, that an appropriate combination of scalar and vector mesons interacting with nucleons can reproduce the energy per particle and fermi momentum of the ground state of infinite nuclear matter,[4] or the binding energy, RMS charge radii, and single particle separation energies of the ground states of finite spherical nuclei.[5]

Recently T. D. Lee and G. C. Wick[6] have suggested that, since a scalar meson field theory needs a lagrangian density with cubic and quartic terms in the meson field in order to

be renormalizable, any renormalizable model of nucleons interacting with scalar mesons may have multiple solutions. On the basis of the σ-model[7] which incorporates these nonlinearities in a particular way, they predict the possible existence of abnormal nuclei whose particle densities may be only slightly greater than those of normal nuclei, yet whose per particle binding energies may be significantly greater than normal nuclei. They also predict the possibility of abnormal vacuum excitations, or regions in space where the vacuum expectation value of the scalar meson field operator is significantly different than is expected for the normal vacuum. These predictions are based upon approximate solutions to the Hartree approximation of the model field theory. They apply to very large systems where volume effects may be assumed to dominate over surface effects.

It is the purpose of this work to investigate certain of these predictions in a more detailed way. First a derivation of the relativistic Hartree equations for infinite or finite systems is presented. This derivation is a relativistic generalization of previous work on the Hartree-Fock approximation in the nonrelativistic theory.[8] Then the Hartree approximation of the σ-model field theory is solved exactly for the case of infinite nuclear matter and the results are compared to the approximate results of Lee and Wick.[6] This comparison leads us

to conclude that the nonlinearities of the σ-model are important not only for nuclear matter in the density region corresponding to the abnormal state but also in the region corresponding to normal nuclear densities. The importance of the nonlinearities is such that one cannot obtain a stable minimum in the saturation curve corresponding to the energy and density of normal nuclear matter by introducing a repulsive vector meson exchange interaction. One can obtain a stable minimum corresponding to normal nuclear matter parameters if one uses the phenomenological hard core interaction discussed by Lee and Wick.[6] The value of the hard core radius at which this is possible is unphysically large. At this value of the hard core radius, the energy of the abnormal solution is moved up to 28 MeV rather than the 130 MeV predicted by Lee and Wick and the barrier height separating the normal and abnormal solutions is less than an MeV.

The equations appropriate for an iterative solution of the Hartree approximation of a finite system are also presented. Attempts to solve these equations for the ^{40}Ca system have so far met with instabilities in the iteration procedure. These instabilities are discussed and speculations are made regarding the possible properties of the final converged solutions of the Hartree approximation to finite systems.

II. GENERAL METHOD

The method is presented for the especially simple case of fermions interacting with a scalar Boson field, but it should be applicable to any form of coupling. We start with the field operator equations of motion for the fermion field $\Psi(x)$ and the scalar field $\phi(x)$ (x is space-time)

$$\left(\frac{\gamma^\mu \partial_\mu}{i} + m\right) \psi(x) = -g\, \psi(x)\, \phi(x), \qquad (\text{II}-1)$$

$$-\partial^\mu \partial_\mu \phi(x) = g\, \bar{\psi}(x)\, \psi(x) + U'(\phi(x)), \qquad (\text{II}-2)$$

where $U'[\phi(x)]$ is a polynomial in $\phi(x)$ (possibly including the infinite counter terms necessary for renormalization).

Since we are interested in finite systems, we will show how our method works in general. The limit for infinite matter will be taken later. We look for the ground state of an even number of fermions with a given mass W and linear momentum $\vec{P}$. Thus we have a four vector $P \equiv (\vec{P}, \sqrt{P^2 + W^2})$. The fermion operator $\Psi(x)$ acting on our state $|P\rangle$ will produce a set of "hole" states labelled by a total momentum $\vec{p}$ and mass ω (ω may turn out to be a continuum). Thus we will be interested in a set of matrix elements

$$\langle p | \omega(x) | P \rangle \equiv \Psi(p, P)\, e^{i(P-p)x}$$

The matrix element of Eq. (II-1) leads to

$$\{ \gamma^\mu (P-p)_\mu + m \}\, \Psi = -g \langle p | \psi(0)\, \phi(0) | P \rangle. \qquad (\text{II}-3)$$

The Hartree (or classical field) approximation consists of

approximating the right hand side of Eq. (II-3) by terms in the complete set which have the same mass as P, i.e. W. Then

$$\{\gamma^\mu (P-p)_\mu + m\}\, \Psi(p,P) \cong -g \int d^3\vec{p}\,'\, \Psi(p,P')\, \langle P'|\phi(0)|P\rangle. \quad (II-4)$$

This is the Hartree equation for the "single hole" wave function $\Psi(p,P)$ and it depends only on the "form factor" of the state W, i.e. $\langle P'|\phi(0)|P\rangle$.

This form factor will be discussed below but first we examine the limit of this equation for very heavy systems. In this limit the masses ω and W are so large that we can say

$$P_0 \equiv \sqrt{\vec{P}^2 + W^2} \simeq W \quad ; \quad p_0 = \sqrt{\vec{p}^2 + \omega^2} \simeq \omega.$$

Then

$$\langle P'|\phi(0)|P\rangle \simeq \Phi\left((\vec{P}'-\vec{P})^2\right). \quad (II-5)$$

As a result of this we see that $\{(E \equiv W-\omega)\}$

$$\Psi(p,P) \simeq \Psi_E((\vec{P}-\vec{p})) \quad (II-6)$$

and the equation is $\{q_\mu = (\vec{P}-\vec{p}, E)\}$

$$(\gamma^\mu q_\mu + m)\, \Psi_E(\vec{q}) \simeq -g \int d^3q'\, \Psi_E(\vec{q}\,')\, \Phi(\vec{q}\,'-\vec{q}). \quad (II-7)$$

In coordinate space this becomes

$$\{\vec{\gamma}\cdot\frac{\nabla}{i} + m + g\,\Phi(\vec{r})\}\, \Psi_E(\vec{r}) = \gamma^0 E\, \Psi_E(\vec{r}). \quad (II-8)$$

For infinite matter, where $\Phi(r)$ is a constant, Φ, we have the usual free solutions with momentum labels $\vec{k}$

$$E = \pm \sqrt{\vec{k}^2 + (m+g\Phi)^2} \,. \qquad (\text{II}-9)$$

Having truncated Eq. (II-1) by the lowest mass state, we now go to Eq. (II-2) for the meson field and try the same approximation there. Only the term $U'(\phi)$ need be discussed because the others require no truncation. Since $U'(\phi)$ is a polynomial in ϕ we truncate each complete set with the lowest mass again*. This leads to the equation

$$(P'-P)^2\, \Phi((P'-P)^2) = g \langle P' | \bar{\psi}(0)\psi(0) | P \rangle + U'[\Phi((P'-P)^2)] . \qquad (\text{II}-10)$$

The first term on the right hand side is the scalar density form factor for $|P\rangle$ and U' is understood to be integrated on intermediate three momenta. For example the term in $\phi^2(x)$ leads to

$$\int \Phi((P-P'')^2)\, d^3P''\, \Phi((P''-P)^2) \,, \quad \text{etc.}$$

Once again the limit of large W leads to a simplification in that everything becomes only a function of three-momentum differences. Then the equation in coordinate space becomes

$$\nabla^2 \Phi(\vec{r}) = g\, \rho_s(\vec{r}) + U'(\Phi(\vec{r})) \,; \qquad (\text{II}-11)$$

$$\rho_s(\vec{r}) = \sum_E \bar{\Psi}_E(\vec{r})\, \Psi_E(\vec{r}) \,. \qquad (\text{II}-12)$$

* One can do more complicated things like carrying matrix elements of $\phi^2(o)$ and looking for an equation for $\langle P' | U(x)U(y) | P \rangle$ which will then require its own appropriate truncation. We do not discuss these possibilities here.

Equations (II-8), (II-11) and (II-12) are the self-consistent Hartree equations for our many nucleon problems provided we give a prescription for the normalization of the "single hole" wave functions $\Psi_E(\vec{r})$. These are spinor solutions of the Dirac equation (II-8) so the label E should be understood to represent not just the energy but also the other quantum numbers associated with these solutions. If we ignore the problem of vacuum polarization we will take N of the positive energy solutions to be normalized to unity and all the rest will be taken to be zero. The problem is then fully specified and the N nucleon system can be solved by the usual iteration procedures. Using the same truncation approximation as above for consistency, we can then calculate the mass W from the hamiltonian density

$$\mathcal{H}(x) = \frac{1}{2}\dot{\phi}^2(x) + \frac{1}{2}(\nabla\phi(x))^2 + \bar{\psi}(x)\left\{\vec{\gamma}\cdot\frac{\nabla}{i} + (m+g\,\phi(x))\right\}\psi(x) + \mathcal{U}(\phi(x)). \quad (\text{II}-13)$$

This implies taking the matrix element limit

$$\lim_{P'\to P}\left\{\frac{\langle P'|\int d^3x\,\mathcal{H}(x)|P\rangle}{\langle P'|P\rangle}\right\} = \langle P|\mathcal{H}(0)|P\rangle. \quad (\text{II}-14)$$

When this matrix element is evaluated with the same truncations as above, we see that the term in $\dot{\phi}^2$ vanishes as W^{-1}. Again in the limit for large W we obtain the Fourier transformed result independent of $\vec{P}$.

$$W = \int d^3r\left\{\sum_E \bar{\Psi}_E(\vec{r})\,E\,\Psi_E(\vec{r}) + \frac{1}{2}(\nabla\Phi(\vec{r}))^2 + \mathcal{U}(\Phi(\vec{r}))\right\}. \quad (\text{II}-15)$$

If we wish the result for W not large, we must examine the equations consistently in higher orders of W^{-1}.

There are several remarks to be made before going on to the specifics of the "σ-model":

(i) One could apply the same technique to the nucleon itself, but then a careful examination of the terms in W^{-1} would have to be considered.

(ii) We have only presented the case which is conventionally called the Hartree approximation. In order to see the exchange terms which were introduced by Fock, one must actually solve Eq. (II-2) formally for $\phi(x)$ and introduce it into Eq. (II-1). Then the conventional truncation leading to the Hartree-Fock or the Hartree-Fock Bogoliubov forms of Eq. (II-8) can readily be obtained.

(iii) In addition, the consideration of more than the ground state of the system will lead to what was called the Generalized Hartree Fock approximation in Ref. (8). The linearization of these equations lead to an equation for collective excitations as usual.

(iv) We have not discussed the problems associated with vacuum polarization and renormalization. These present themselves when one considers including the infinite sea of negative energy states in the sum on E of Eqs. (II-12), (II-15). A consistent Hartree-Fock theory would imply using all of these states with norm on Ψ_E of unity. When this is done we obtain the usual infinities which must be balanced by counter terms in the Lagrangian. This can easily be done for the infinite system in the Hartree approximation and leads to terms in the energy which go like $\Phi^4 \ln \Phi$.

(v) As is the usual situation in self consistent calculations, the average field $\Phi(r)$ need not satisfy any symmetry conditions since it represents the intrinsic field of the system. If it

becomes deformed or violates parity, this will imply specific types of collective motion. In addition, solutions with very different forms of Φ will represent different possible types of states of the system and could lead to various forms of Isomerism analagous to the shape isomers often discussed in nuclear physics. For example the abnormal nuclear matter of Lee and Wick for the infinite system implies a sort of density isomerism in the finite systems. Whether or not the σ-model as discussed below is really relevant to the finite nucleus problem, it does indicate that the possibility of density isomers as excited states of normal nuclei is real, and machines like the Bevalac should be searching for them. Their lifetime to decay into normal nuclei is completely analagous to the fission lifetime problem and all the usual methods may be taken over.

(vi) Finally, we remark on the general philosophy one might consider in connection with these methods of obtaining approximations for finite systems in field theory. What they do is to short circuit the usual path to many body theory through boson exchange potentials and the two body problem. This does not mean that two body information is not important. This input will have to be used in deciding on which "phenomenological" meson fields to use and also in determining some of the masses and coupling constants. The advantage would seem to be that we have a natural vehicle for considering many body effects as well as relativistic effects without a great increase in complexity.

III. σ-MODEL

The σ-model is a renormalizable model of pions and scalar isoscalar mesons interacting with nucleons via the lagrangian density

$$\mathcal{L}(x) = -\bar{\psi}(x)\left[\gamma^{\mu}\partial_{\mu} + m\right]\psi(x) - g\,\bar{\psi}(x)\psi(x)\phi(x)$$
$$-ig\,\bar{\psi}(x)\gamma_5\vec{\tau}\psi(x)\cdot\vec{\pi}(x) - \frac{1}{2}\left[-\partial_{\mu}\vec{\pi}(x)\cdot\partial^{\mu}\vec{\pi}(x) + \mu_{\pi}^2\vec{\pi}^2(x)\right]$$
$$-\frac{1}{2}\left[-\partial_{\mu}\phi(x)\partial^{\mu}\phi(x) + \mu_{\sigma}^2\phi^2(x)\right] - \left[\frac{\mu_{\sigma}^2-\mu_{\pi}^2}{2}\right]\frac{g}{m}\phi(x)\left(\phi^2(x)+\vec{\pi}^2(x)\right)$$
$$-\left[\frac{\mu_{\sigma}^2-\mu_{\pi}^2}{8}\right]\left(\frac{g}{m}\right)^2\left(\phi^2(x)+\vec{\pi}^2(x)\right)^2. \qquad (\text{III}-1)$$

The symbols $\psi(x)$, $\vec{\pi}(x)$, and $\phi(x)$ represent the nucleon, pion, and scalar meson fields respectively, while m, μ_{π}, and μ_{σ} represent the corresponding masses. The coupling constant g applies to both the NNπ and NNφ vertices. The form of the σ-model has been chosen in which the vacuum expectation value of the scalar field $\phi(x)$ is zero. Note that in obtaining this lagrangian from the more conventional form (in which the vacuum expectation value of the scalar field is responsible for the nucleon mass) terms linear in the scalar field $\phi(x)$ have been dropped. These terms are of no consequence to the approximate solutions discussed here.

While any such scalar field theory is renormalizable provided there are $\phi^3(x)$ and $\phi^4(x)$ terms in the lagrangian density,

the σ-model is of special interest since one can derive from it the conditions of CVC and PCAC upon the weak vector and axial vector currents. The model has enjoyed some success in describing the processes of π-π and π-N scattering as well.

Following Lee and Wick,[6] the pion field $\vec{\pi}(x)$ is taken to be zero in all the calculations presented here. This is consistent with the Hartree approximation since the expectation value of any pseudoscalar field with respect to a system with spherical symmetry must vanish. For simplicity the pion mass is also taken to be zero. Removing this latter restriction would not qualitatively influence any of the conclusions reached in this work.

Under these restrictions, one can derive from Eq. (III-1) the equations of motion for the nucleon and scalar meson field operators.

$$i\frac{\partial}{\partial x^0}\psi(x) = \left\{\vec{\alpha}\cdot\frac{\nabla}{i} + \gamma^0[m + g\phi(x)]\right\}\psi(x) \qquad \text{(III - 2)}$$

and,

$$(-\partial_0^2 + \nabla^2 - \mu_\sigma^2)\phi(x) = g\,\bar{\psi}(x)\psi(x) + \frac{3}{2}\mu_\sigma^2\left(\frac{g}{m}\right)\phi^2(x)$$

$$+ \frac{1}{2}\mu_\sigma^2\left(\frac{g}{m}\right)^2\phi^3(x). \qquad \text{(III - 3)}$$

Similarly the Hamiltonian density can be obtained

$$\mathcal{H}(x) = \psi^+(x)\left[\vec{\alpha}\cdot\frac{\nabla}{i} + \beta m\right]\psi(x) + g\,\bar{\psi}(x)\psi(x)\phi(x)$$

$$+ \frac{1}{2}\left\{(\partial_0\phi(x))^2 + (\nabla\phi(x))^2 + \mu_\sigma^2\phi^2(x)\right\}$$

$$+ \frac{1}{2}\mu_\sigma^2 \left(\frac{g}{m}\right) \phi^3(x) + \frac{1}{8}\mu_\sigma^2 \left(\frac{g}{m}\right)^2 \phi^4(x). \qquad \text{(III-4)}$$

One can now take matrix elements of Eqs. (III-2)-(III-4) with respect to many-body states and perform Fourier transforms as discussed in the previous section and obtain the equations appropriate to a relativistic Hartree solution of this model field theory:

$$(\nabla^2 - \mu_\sigma^2)\Phi(\vec{r}) = g\,\rho_s(\vec{r}) + \frac{3}{2}\mu_\sigma^2\left(\frac{g}{m}\right)\Phi^2(\vec{r}) + \frac{\mu_\sigma^2}{2}\left(\frac{g}{m}\right)^2 \Phi^3(\vec{r}), \qquad \text{(III-5)}$$

$$\{\vec{\alpha}\cdot\frac{\nabla}{i} + \beta[m + g\,\Phi(\vec{r})]\}\,\Psi_i(\vec{r}) = E_i\,\Psi_i(\vec{r}), \qquad \text{(III-6)}$$

and:

$$E = \sum_i E_i + \frac{1}{2}\int [(\nabla\Phi(\vec{r}))^2 + \mu_\sigma^2\,\Phi^2(\vec{r})]\,d^3r$$
$$+ \frac{1}{2}\mu_\sigma^2\left(\frac{g}{m}\right)\int \Phi^3(\vec{r})\,d^3r + \frac{1}{8}\mu_\sigma^2\left(\frac{g}{m}\right)^2\int \Phi^4(\vec{r})\,d^3r. \qquad \text{(III-7)}$$

Note that $\Phi(\vec{r})$ and $\Psi_j(\vec{r})$ are three dimensional Fourier transforms of the momentum space amplitudes for removing a meson or a nucleon (with quantum numbers i) respectively from the many-body system. The single particle eigenvalue E_i represents the energy required to remove the single nucleon in state i from the many-body system. Note that the density occurring on the RHS of Eq. (III-5) is the scalar density,

$$\rho_s(\vec{r}) = \sum_i \bar{\Psi}_i(\vec{r})\,\Psi_i(\vec{r}) \qquad \text{(III-8)}$$

and not the baryon density:

$$\rho_B(\vec{r}) = \sum_i \Phi_i^\dagger(\vec{r})\, \Phi_i(\vec{r}). \qquad (\text{III} - 9)$$

The no recoil approximations and intermediate state truncations which are necessary to allow these simple interpretations are explicitly given in Section II.

IV. INFINITE NUCLEAR MATTER

The prediction of abnormal states of nuclei by Lee and Wick[6] is based upon approximations to the Hartree solution of the σ-model for infinite nuclear matter. In uniform, zero temperature, balanced nuclear matter of baryon density

$$\rho_B = \frac{2}{3\pi^2} k_f^3 \qquad \text{(IV - 1)}$$

the meson field equation of motion becomes,

$$\Phi = -\frac{g}{\mu_\sigma^2}\rho_s(\Phi) - \frac{3}{2}\left(\frac{g}{m}\right)\Phi^2 - \frac{1}{2}\left(\frac{g}{m}\right)^2\Phi^3, \qquad \text{(IV - 2)}$$

where the scalar density ρ_s depends upon Φ through the relation:[4]

$$\rho_s = \frac{4}{(2\pi)^3}\int_0^{k_f} \frac{m + g\Phi}{[k^2 + (m+g\Phi)^2]^{1/2}}\, d^3k. \qquad \text{(IV - 3)}$$

Lee and Wick[6] argue that at normal nuclear density and below the nonlinear terms of Eq. (IV-2) are not important and that the linearized Eq. (IV-2) and Eq. (IV-3) may be solved to obtain self-consistent values of ρ_s and Φ. They note, however, that the value $\Phi = -m/g$, which leads to $\rho_s = 0$ in Eq. (IV-3), also satisfies Eq. (IV-2) when $\rho_s = 0$. This is a new solution which would not have existed without the nonlinear terms. Note that this large scalar potential exactly cancels the mass term in the nucleon equation of motion (Eq. (III-6)).

Of course it is well known that a scalar interaction alone can't produce the correct saturation properties of normal nuclear matter, so Lee and Wick[6] introduced a repulsive hard

sphere interaction as well. By choosing a hard sphere radius of .56 fm and a σ mass of 1150 MeV, they obtained the normal saturation properties ($E/A = -16$ MeV, $k_f = 1.36$) for their linearized normal solution of nuclear matter. The scalar coupling constant g^2 was already determined to be 15 from the π-N interaction. They could just as well have obtained the necessary repulsion through introduction of a vector isoscalar meson (ω) of appropriate strength.[4,5] Using these parameters, they find minima in the abnormal saturation curve corresponding to per particle binding energies of 475 MeV and 130 MeV depending on whether the repulsion was chosen to be a soft core or a truly infinite core. The densities at which these abnormal states occurred correspond respectively to 6.3 and 2.4 times the density of normal nuclear matter.

Exact self-consistent solutions of Eqs. (IV-2) and (IV-3) are now presented for both the normal and abnormal states. Defining the dimensionless scalar potential $X_s = g\Phi/m$, and evaluating the integral in Eq. (IV-3),[4] one obtains:

$$\frac{1}{2} X_s^3 + \frac{3}{2} X_s^2 + X_s = -\frac{g^2}{\mu_\sigma^2} \frac{4}{\pi} k_f^2 (1 + X_s) \left\{ (1 + a^2)^{1/2} - \frac{a^2}{2} \ln \left[\frac{(1 + a^2)^{1/2} + 1}{(1 + a^2)^{1/2} - 1} \right] \right\}, \qquad (\text{IV} - 4)$$

where

$$a = \frac{m}{k_f} (1 + X_s). \qquad (\text{IV} - 5)$$

In Fig. 1 a method of graphical solution of Eq. (IV-4) is presented. The solid line is the cubic function appearing on the LHS of the meson equation of motion. The dashed curves are plots of the RHS of Eq. (IV-4) for various values of the Fermi momentum k_f. The parameter determined by Lee and Wick ($g^2/\mu_\sigma^2 = .441$) is used in this graph. The values of X_s at which the solid and dashed curves cross are the self-consistent solutions for a particular value of k_f. Note that at low density ($k_f = .5\ fm^{-1}$ for example) there is the normal solution near $X_s = 0$, the abnormal solution at $X_s = -1$, and yet a third solution near $X_s = -2$. As the density increases ($k_f = 1\ fm^{-1}$ for example) there appear two more solutions near $X_s = -1$ due to the fact that the magnitude of the slope of the dashed curve has become greater than the magnitude of the slope of the solid curve at $X_s = -1$. As the density increases further ($k_f = 1.3\ fm^{-1}$) the two extra solutions (b and d) move away from the point $X_s = -1$ toward the normal solution (a) near $X_s = 0$ and the solution (e) near $X_s = -2$. As the density increases further, the pairs of solutions a and b and d and e become degenerate and disappear so that at $k_f = 1.5\ fm^{-1}$ and beyond there exists only the abnormal solution c at $X_s = -1$.

Once all the self-consistent solutions of Eq. (IV-4) are

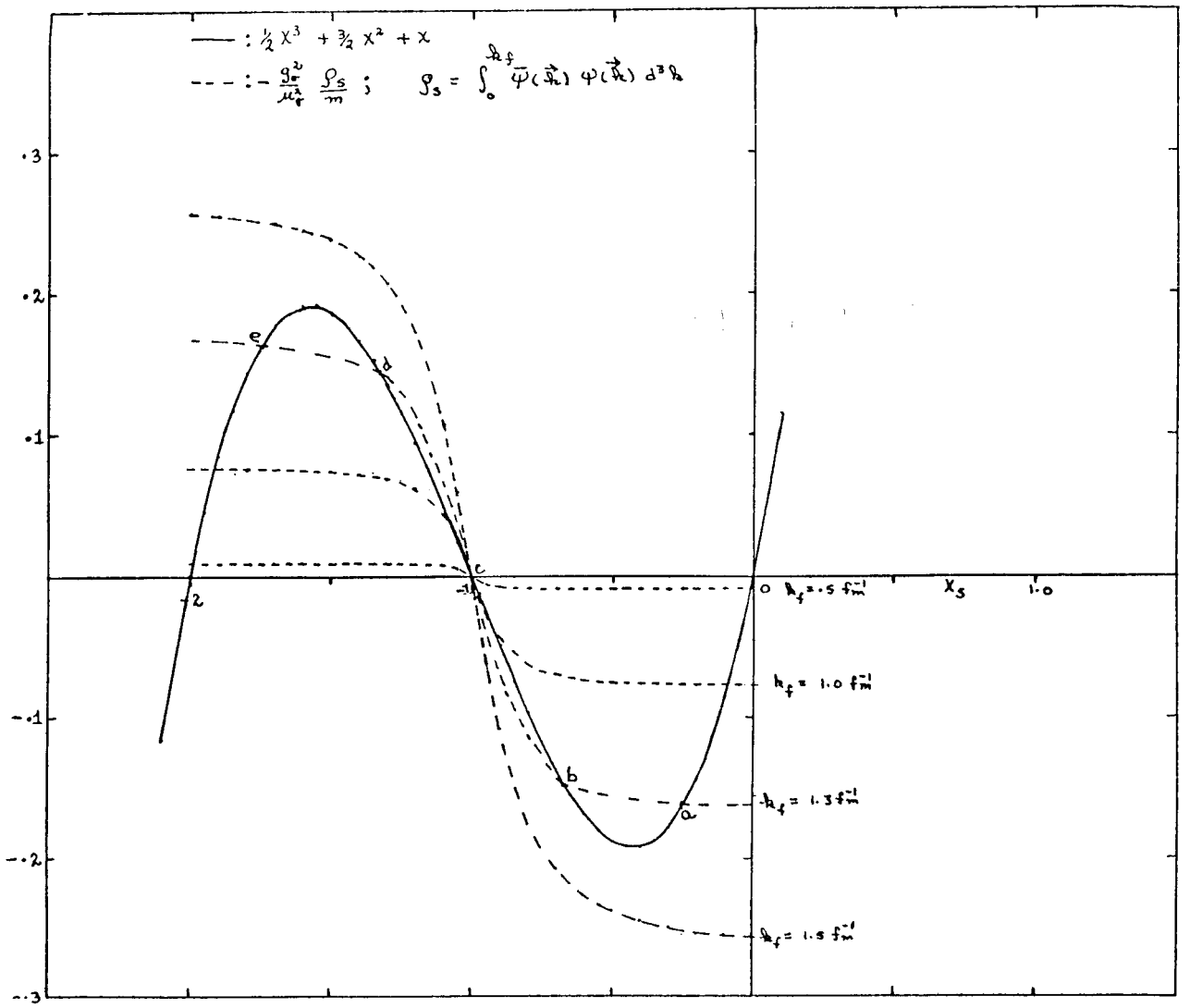
—— : ½ x³ + ³⁄₂ x² + x
- - - : − g²/μ²_π ρ_s/m ; ρ_s = ∫₀^{k_f} φ̄(k⃗) φ(k⃗) d³k
.3
.2
.1
-.1
-.2
-.3
-2
-1
0
1.0
x_s
k_f = .5 fm⁻¹
k_f = 1.0 fm⁻¹
k_f = 1.3 fm⁻¹
k_f = 1.5 fm⁻¹
a
b
c
d
e

Fig. 1

determined for each value of k_f, one can calculate the nuclear matter saturation curve (energy per particle versus k_f) for each solution. The expression for the binding energy per particle as a function of k_f and the self-consistent solution X_s may be easily derived:[4]

$$E/A = \frac{3}{8} k_f \left\{ (1+a^2)^{3/2} + (1+a^2)^{1/2} - \frac{a^4}{2} \ln\left[\frac{(1+a^2)^{1/2}+1}{(1+a^2)^{1/2}-1}\right] \right\}$$

$$+ \frac{3\pi}{8} \frac{\mu^2 \sigma}{g^2} \frac{\pi^2}{k_f^3} \left(\frac{1}{2} X_s^2 + \frac{1}{2} X_s^3 + \frac{1}{8} X_s^4 \right) - m . \qquad (\text{IV}-6)$$

Eq. (IV-6) differs from the result obtained in Ref. (4) only by the X_s^3 and X_s^4 terms present on the RHS.

In Fig. 2 the saturation curves for all the solutions presented in Fig. 1 are shown. To facilitate the identification each curve is labeled by the letter (a,b,c,d, and e) which was used to designate the self-consistent points on the $k_f = 1.3\ \text{fm}^{-1}$ curve of Fig. 1. Note that there is complete degeneracy between the curves a and e and between the curves b and d, so that there are never more than three energetically different solutions in any region of k_f. Also shown in Fig. 2 is the normal solution in which the nonlinearities are ignored (dashed cruve) and the normal solution in which a nonrelativistic effective mass approximation is further imposed (dot-dashed curve). This latter curve corresponds to the normal solution obtained by Lee and Wick.[6]

From Fig. 2 it is clear that the effective mass approximation

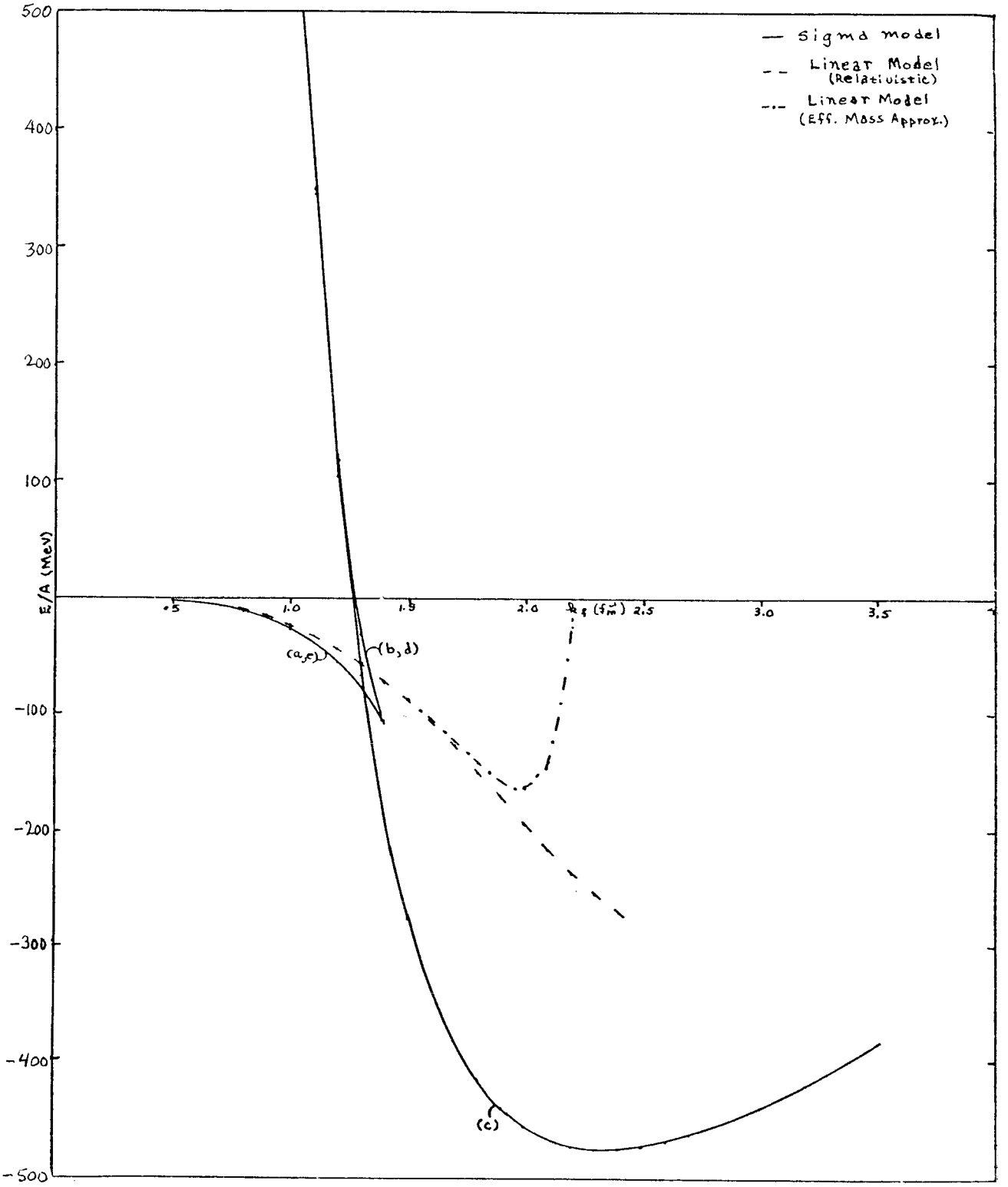
500
400
300
200
100
E/A (MeV)
-100
-200
-300
-400
-500
.5
1.0
1.5
2.0
k_f (fm^{-1}) 2.5
3.0
3.5
(a,f)
(b,d)
(c)
— Sigma model
-- Linear Model (Relativistic)
-.- Linear Model (Eff. Mass Approx.)

Fig. 2

is quite good in the region of normal nuclear density, but that ignoring the nonlinear terms has led to a substantial error in this region. Especially striking is the fact that the normal solution does not even exist beyond $k_f = 1.4\ fm^{-1}$ in the exact calculation. One also notes that the abnormal solution (c) becomes the energetically preferred solution near normal nuclear density so that there is no stable point on the overall saturation curve corresponding to normal nuclear matter. If one considers the three dimensional plot of energy per particle versus k_f and $x_s = g\Phi/m$, there is only one minimum and this is the abnormal solution.

In Fig. 3 a saturation curve is shown in which a vector meson with the parameter $g_v^2/\mu_v^2 = .426$ has been added to the σ-model result. This parameter was chosen so that the minimum point on the normal curve (where (a,e) and (b,d) come together) is moved up to the binding energy of normal nuclear matter (E = -16). The k_f value of this point already corresponds to the density of normal nuclear matter due to the specific choice of the σ-model parameter. The details of including this vector meson in the calculation are exactly the same as in Ref. 4 and will not be reproduced here. One sees from Fig. 3 that even if a finite system were to exhibit a stable solution near conventional nuclear density (due to the collective phenomena associated with the finite system) the properties of such a solution would be very much unlike normal nuclei. For example,

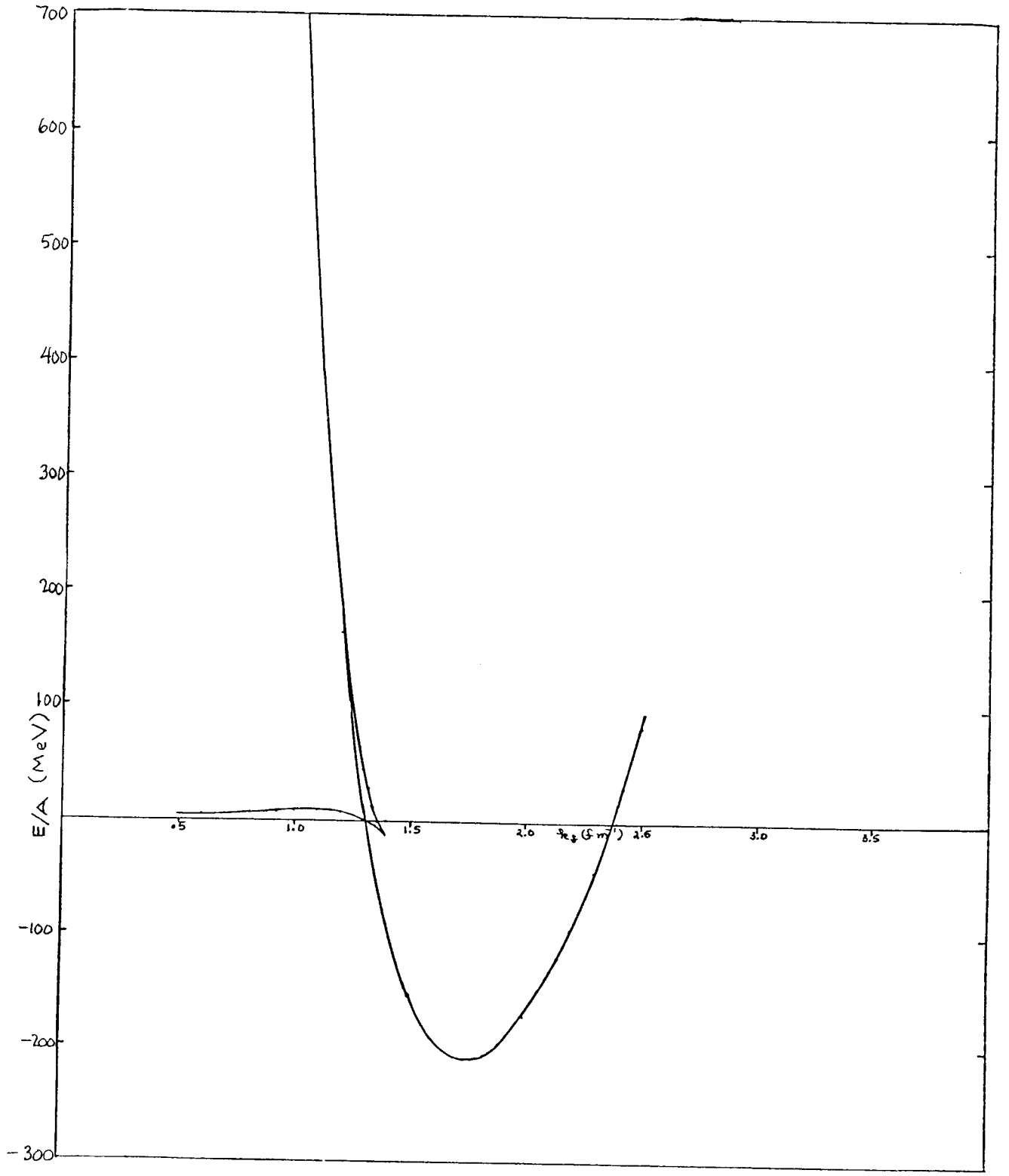

Fig. 3

any finite solution would have to have a very sharp nuclear surface or else the surface energy would cause the total binding energy to be much smaller than it is for conventional nuclei. This is due to the fact that the normal solution is unbound below $k_f = 1.3\ \mathrm{fm}^{-1}$ whereas conventional saturation curves show attraction in this region.

Another method of introducing repulsion into the nuclear model is through a hard core interaction. An exact treatment of a hard core would involve the Brueckner formalism which has not yet been developed for relativistic nuclear matter. However, an approximate phenomenological treatment of a hard core for the σ-model has been given by Lee and Wick.[6] Their method involves replacing the fermi momentum in the Fermion contribution to the binding energy per particle (first term of Eq. (IV-6) by an effective fermi momentum k_f' where,

$$k_f' = \frac{k_f}{1 - .525\, c\, k_f} \qquad \text{(IV-7)}$$

The parameter c is the radius of the hard core. By choosing a core radius of .56 fm, Lee and Wick obtain a minimum in the saturation curve at the parameters of normal nuclear matter. They then obtain a minimum in the abnormal saturation curve corresponding to a binding energy of 130 MeV per nucleon.

One does not obtain a minimum corresponding to normal nuclear matter with this core radius when the nonlinearities are included in the normal solution. One can however obtain a second minimum by increasing the core radius. The saturation curve which results

from a core radius of .677 fm is shown in Fig. 4. One notes that here a second minimum occurs which has the energy and density of normal nuclear matter. Note, however, that the core repulsion is so strong that the energy of the abnormal state is moved up to 28 MeV. Note also that the barrier separating the two minima is less than an MeV. An even stronger form of repulsion would be necessary to build up a significant barrier which would prevent copious decays of the normal state into the abnormal state; however, the core radius c = .677 fm is already unphysically large.

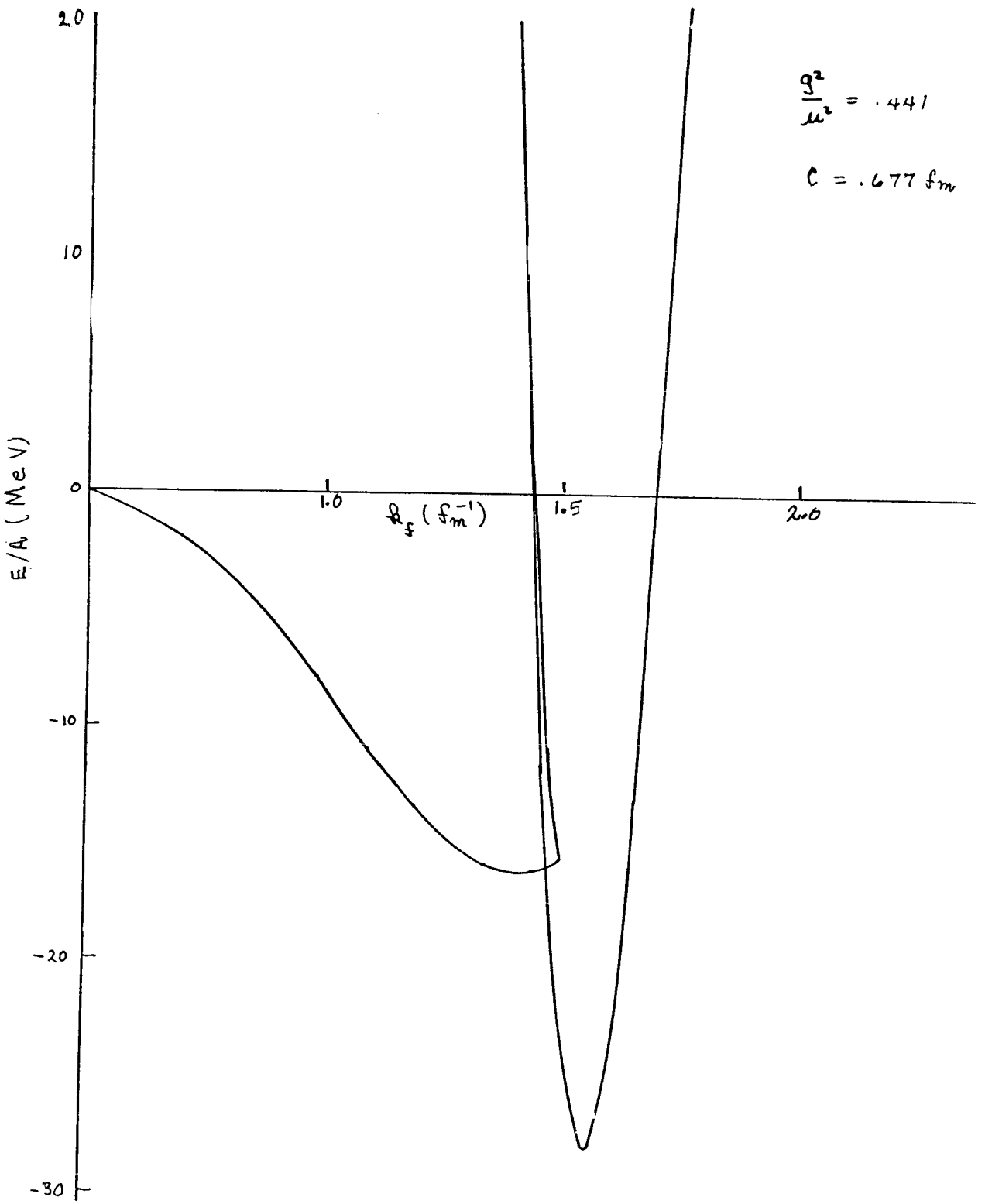

Fig. 4

V. FINITE NUCLEI

The scalar meson and nucleon equations of motion for a finite system (in Hartree approximation) are already given in Eqs. (III-5) and (III-6) respectively. The scalar potential ($V_s(r) = g\Phi(r)$) may be obtained from Eq. (III-5) by using the Green's function for the Klein-Gordon operator:

$$V_s(r) = -g^2 \int \frac{e^{-\mu_\sigma|\vec{r}-\vec{r}'|}}{|\vec{r}-\vec{r}'|} \left[\rho_s(r') + \frac{3}{2}\frac{\mu_\sigma^2}{g^2}\frac{V_s^2(r')}{4\pi m} + \frac{1}{2}\frac{\mu_\sigma^2}{g^2}\frac{V_s^3(r')}{4\pi m^2} \right] d^3r'. \qquad (V-1)$$

The derivative terms in the total binding energy equation (Eq. III-7) can be eliminated in analogy with conventional Hartree theory to obtain:

$$E = \sum_{n=1}^{A} E_n - \frac{1}{2}\sum_{n=1}^{A} \int \bar{\Psi}_n(\vec{r}) V_s(r) \Psi_n(\vec{r})\, d^3r - \frac{1}{4}\frac{\mu_\sigma^2}{g^2}\int \frac{V_s^3(r)}{4\pi m} d^3r - \frac{1}{8}\frac{\mu_\sigma^2}{g^2}\int \frac{V_s^4(r)}{4\pi m^2} d^3r . \qquad (V-2)$$

In Eq. (V-2) one recognizes the conventional Hartree expression for the total binding energy in the first two terms of the RHS while the last two terms represent the corrections due to the nonlinear nature of the field theory.

The computer program which was used to do the relativistic Hartree calculations in Ref. 5 has been modified to include the nonlinear corrections inherent in Eqs. (V-1) and (V-2). Since the solutions were already being obtained by iteration, the

fact that Eq. (V-1) is now a nonlinear integral equation does not force one to introduce a separate iteration procedure in order to solve it.

Several attempts have been made to calculate the properties of ^{40}Ca using the σ-model; however, all have met with instabilities which have prevented the program from obtaining self-consistent solutions. Nothing can be proved from such calculations; nevertheless, the instabilities have implications that can be used to make speculations about the nature of the true solutions.

First the results obtained with the pure σ-model ($g^2 = 15$, $\mu_\sigma = 1150$ MeV) are presented. Attempts to obtain stable nuclei with a central density corresponding to the minima of the normal curve (a,e) in Fig. 2 all lead to higher densities and large scalar potentials in successive Hartree iterations. It seems that if one is to prevent a finite nucleus calculation from seeking the more deeply bound abnormal state, one must introduce constraints into the Hartree iteration procedure which prevent the collapse. This is not at all surprising, when one considers the saturation curve in Fig. 2. What is somewhat surprising, however, is the fact that the Hartree calculation of ^{40}Ca does not exhibit a stable solution corresponding to the minima in the abnormal curve (c) of Fig. 2 either. For such a solution, one would expect the scalar potential to approximately cancel the nucleon mass in the interior

of the nucleus and go smoothly to zero at the surface. One would further expect the central nucleon density to correspond approximately to the k_f value at the minima of curve c in Fig. 2. When these conditions are introduced as the starting point of a Hartree iteration, however, the scalar potential becomes even larger in successive Hartree iterations. This surprising instability is related to the curious fact that Dirac particles tend to congregate on the surface of an attractive scalar well whenever the well depth exceeds the nucleon mass.[9]

The stability of the abnormal state ($\Phi = -\frac{m}{g}$) of infinite nuclear matter is due to the fact that $\rho_s(\Phi)$, the scalar density in Eq. (IV-2), goes from a positive to a negative value as Φ continues to decrease through the value $-m/g$ as shown in Fig. 1. In the absence of nuclear matter, the value $\Phi = -m/g$ is actually a maximum point in the meson field energy. This can be seen by setting ρ_s to zero in Eq. (IV-2) and noting that any perturbation of Φ about the point $-m/g$ will cause the resulting equation to collapse upon iteration to either the normal vacuum ($\Phi = 0$) or an abnormal vacuum excitation ($\Phi = -2\ m/g$) which is degenerate in energy with the normal vacuum.

For a finite system, the scalar density does not go through zero and become negative as one increases the depth of the scalar potential beyond the nucleon mass. Instead the nucleon

densities (both scalar and baryon) tend to collect on the surface of the well while the scalar density remains positive everywhere. This point is illustrated in Figs. 5 and 6 where the baryon and scalar nucleon densities respectively are shown for $1s\frac{1}{2}$ wave functions calculated in a scalar well of 1500 MeV (solid curves) and 1877 MeV (dashed curves) well depths. These wells are of Woods-Saxon form and both have radius and diffuseness parameters of 2.97 fm and .17 fm respectively. This latter parameter is the Compton wave length of the σ mass parameter. Note the strong surface peaking of the baryon density in Fig. 5 even though $s\frac{1}{2}$ densities are usually peaked at the center of the well. The surface peaking is even more pronounced when one goes to the higher well depth. Note in Fig. 6 that the scalar density (also surface peaked) is very small (about two orders of magnitude smaller than ρ_B), but that it refuses to become negative, even at potential values at which the scalar density of an infinite system would be highly negative. This behavior may or may not persist in the limit where the well radius gets very large and many single particle states are occupied.

If this curious "well climbing" behavior persists in large systems, one may speculate that the stable solutions of all finite systems calculated via the Hartree approximation to the σ-model will be hollow spherical shells. The interior of these shells will be devoid of nuclear matter, but will have

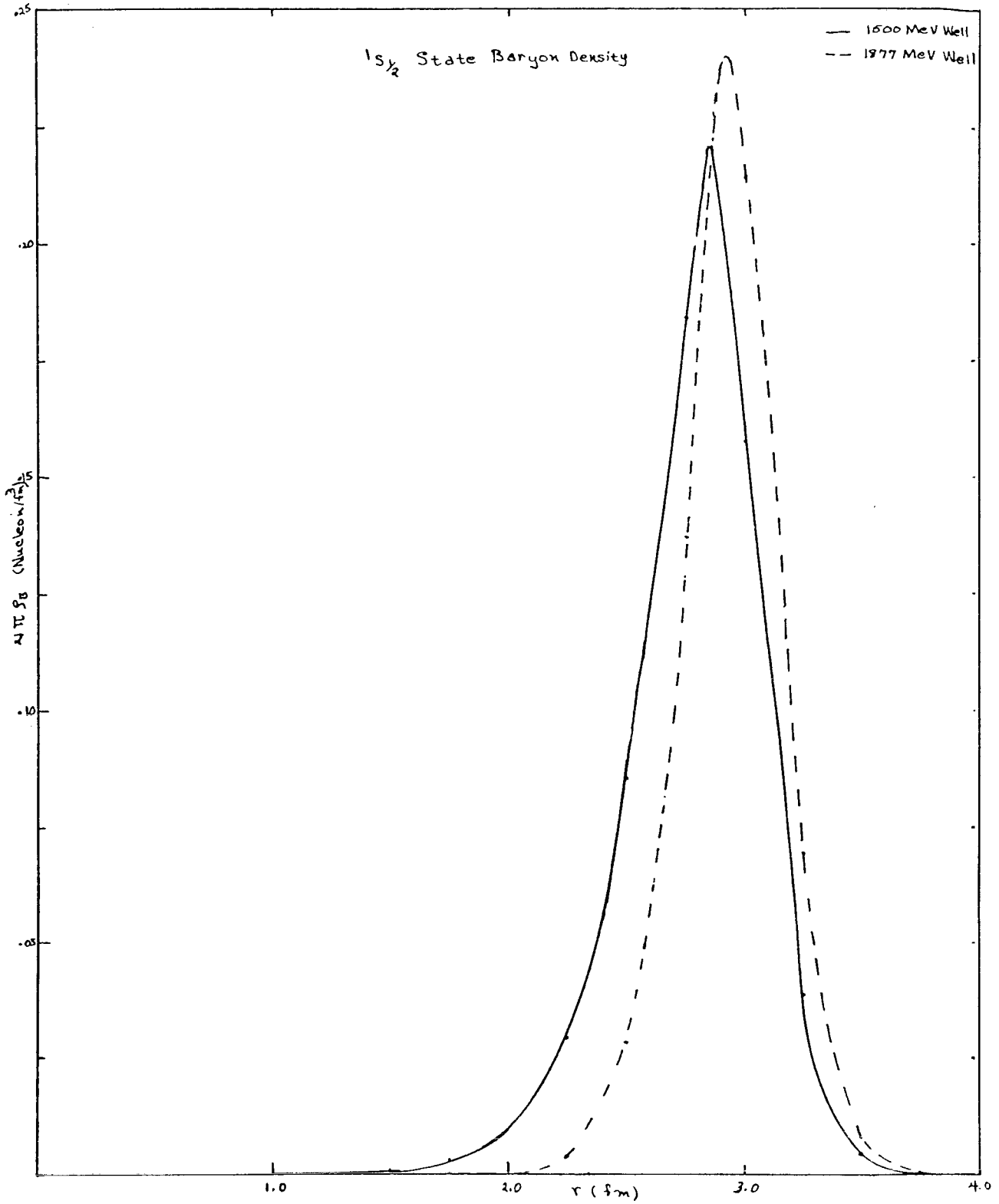
1500 MeV Well
1877 MeV Well
$1s_{1/2}$ State Baryon Density
.25
.20
.15
.10
.05
$4\pi\rho_B$ (Nucleon/fm^3)
1.0
2.0
3.0
4.0
r (fm)

Fig. 5

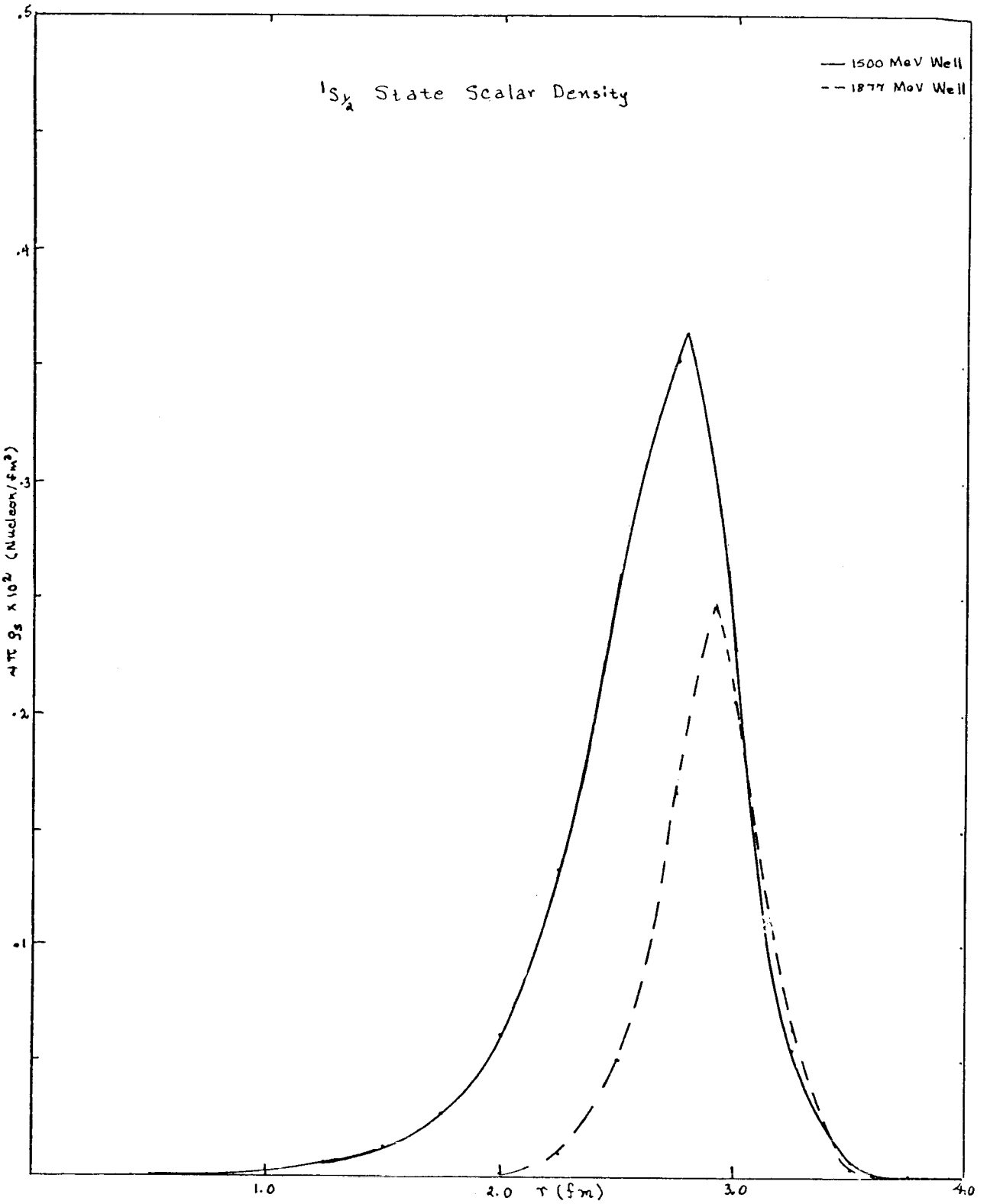
$^1S_{1/2}$ State Scalar Density
— 1500 MeV Well
-- 1877 MeV Well
$4\pi\, \rho_s \times 10^2$ (Nucleon/fm^3)
.5
.4
.3
.2
.1
1.0
2.0
r (fm)
3.0
4.0

Fig. 6

the abnormal meson field strength $\Phi = -2$ m/g. This is the abnormal vacuum excitation discussed by Lee and Wick.[6] The exterior will be the normal vacuum ($\Phi = 0$). The surface will contain the nuclear matter and the meson field strength will go smoothly from its interior value of -2 m/g to zero. While such a system will probably be stable, the numerical difficulties associated with such an unusual object are too great to permit self-consistent calculations with the existing computer program.

Calculations of ^{40}Ca were also attempted for the σ-model and vector meson combination used to generate the saturation curve in Fig. 3. The ω meson mass (782.8 MeV) was used and the coupling constant ($g_\omega^2 = 6.726$) was chosen so that the vector parameter used in the infinite calculation ($g_v^2/\mu_v^2 = .426$) is satisfied. The starting solution which corresponded to the normal density and surface thickness of ^{40}Ca became unbound on the first Hartree iteration. This adds to the suspicion already voiced in a previous section that any finite solutions which have densities corresponding to normal nuclei will have abnormally large surface energies because of the importance of the nonlinearities of the σ-model in this region.

The calculations of finite systems with the σ-model are still at a tentative stage and much work remains to be done before the speculations presented in this section can be confirmed or denied. Numerical calculations of nonlinear problems are always tricky and it would be naive to suppose that one could predict all the important and interesting aspects of the problem on the basis of these first crude attempts at calculations.

VI. CONCLUSIONS

On the basis of an exact treatment of the Hartree approximation to the σ-model for infinite nuclear matter, one may conclude that the nonlinearities have important consequences not only for nuclear densities in the abnormal region discussed by Lee and Wick, but also at nuclear densities corresponding to normal nuclei. This feature of the nonlinearities prevents the saturation curve from having a minimum at the density corresponding to normal nuclei unless one introduces an unphysical form of repulsion.

Tentative calculations for finite systems seem to support the conclusions drawn from the infinite case that the σ-model, even in combination with a repulsive interaction coming from vector meson exchange, is incapable of yielding stable Hartree solutions whose properties are similar to those of normal nuclei. Finite stable solutions corresponding to the abnormal nuclei predicted by Lee and Wick do not appear to be possible either, although this failure results from a curious property of Dirac single-particle wave functions in finite attractive scalar wells which could not have been predicted on the basis of calculations for an infinite system. Instead, the only stable finite system appears to consist of an abnormal vacuum excitation (predicted by Lee and Wick) which is separated from the normal vacuum by a spherical shell of nuclear matter. The baryon density in this shell will probably be comparable to the densities predicted by Lee and Wick for their abnormal

nuclei.

In conclusion, it appears that the σ-model is a poor candidate for predicting the behavior of nuclear matter at densities greater than those found in normal nuclei. This should not dissuade experimentalists from making searches for abnormal configurations of nucleons or density isomers as soon as reasonable extensions of present technologies permit them. Whether the σ-model is the appropriate vehicle for theoretical investigations or not, the nuclear force is certainly a highly nonlinear phenomenon. Otherwise the multipion resonances would not be so important in understanding it. The utility of theoretical studies of nonlinear field theory models like the σ-model is that they give one a feeling for the wide range of unusual objects which could exist. In view of our lack of knowledge about the nuclear force, this is not an inconsequential service.

We would like to acknowledge several conversations with T. D. Lee.

REFERENCES

1. H. Yukawa, Proc. Phys.-Math. Soc. Japan 3, 17,18 (1935).
2. A. Gersten, R. H. Thompson, and A. E. S. Green, Phys. Rev. D3, 2076 (1971); K. Holinde, K. Erkelenz, and R. Alzetta, Nucl. Phys. A194, 161 (1972); R. A. Bryan and A. Gersten, Phys. Rev. D6, 341 (1972).
3. M. H. Partovi and E. L. Lomon, Phys. Rev. D2, 1999 (1970); G. E. Brown and J. W. Durso, Phys. Lett. 35B, 120 (1971).
4. J. D. Walecka, Ann. of Phys. (N.Y.) 83, 491 (1974).
5. L. D. Miller and A. E. S. Green, Phys. Rev. C5, 241 (1972).
6. T. K. Lee and G. C. Wick, Phys. Rev. D9, 2291 (1974); and preprints.
7. B. W. Lee, Chiral Dynamics (Gordon & Breach, 1972).
8. A. K. Kerman and A. Klein, Phys. Rev. 132, 1326 (1963); A. Klein and A. K. Kerman, Phys. Rev. 138, B1323 (1965).
9. This feature of the Dirac equation has been used as a model for quark containment by hadrons; W. A. Bardeen, M. Chanowitz, S. D. Drell, M. Weinstein, and T. M. Yan, preprint.

The Charged Vacuum in Overcritical Fields and its Test in H.I. Collisions*

Bernd Müller, R.K. Smith

and

Walter Greiner**

Institut für Theoretische Physik

der Johann Wolfgang Goethe Universität

Frankfurt am Main, Germany

1. Introduction

The solutions of the Dirac equation are well known. We learned in school, that, if coupled to the electromagnetic four-potential $A_\mu = \{\vec{A}, A_o(r)\}$ it reads

$$(\gamma_\mu (p_\mu - \frac{e}{c} A_\mu) + mc^2)\psi = 0 \quad . \tag{1}$$

If $\vec{A}$ is neglected and the Coulomb potential is that of an external point charge, i.e. $A_o(r) = \frac{Ze^2}{r}$, the spectrum of (1) can be obtained analytically and is known as the Sommerfeld fine-structure formula

$$E = mc^2 \left[1 + \left(\frac{\alpha Z}{N + \sqrt{K^2 - \alpha^2 Z^2}} \right)^2 \right]^{-1/2} \tag{2}$$

$$K = \pm 1, \pm 2, \ldots \; ; \; N = 0, 1, 2 \ldots$$

It is schematically depicted in Fig.1 as a function of Z.

*This work was supported by the Deutsche Forschungsgemeinschaft, by the Bundesministerium für Forschung und Technologie and by the Gesellschaft für Schwerionenforschung (GSI).

**Invited speaker at the International Symposium on Physics with Relativistic Heavy Ions, LBL, Berkeley, July 1974.

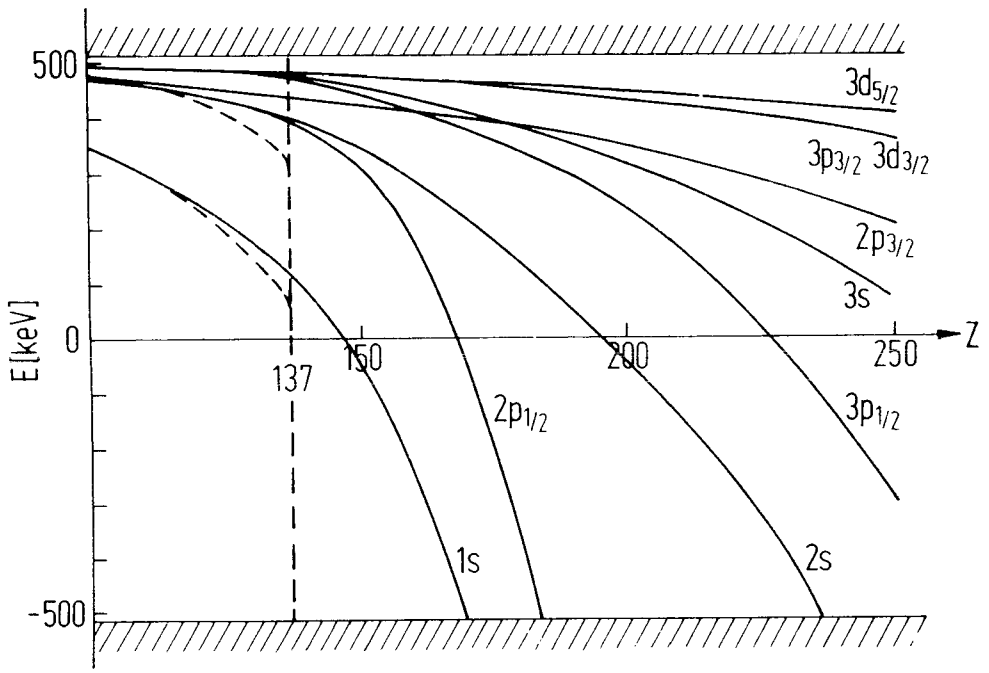

Fig.1: Schematic representation of the solutions (2) of the fine structure formula. At Z=137 the solutions with j=1/2 disappear. The dashed curve indicates the $s_{1/2}$-energy for modified Coulomb potentials belonging to extended nuclei[1]. The solutions for higher j are disappearing correspondingly at higher Z-values.

What happens to the j=1/2 solutions at this critical point? The answer is simple: Their radial wave functions $R_{j=1/2}(r) \sim r^{\sqrt{1-(\alpha Z)^2}}$ are, because of the imaginary square root, non-normalizable for $Z\alpha>1$. Since normalizability is an important quantization condition, the solutions disappear for $Z\alpha>1$. For modified Coulomb-potentials as they are necessary for extended nuclei (see Fig.2),

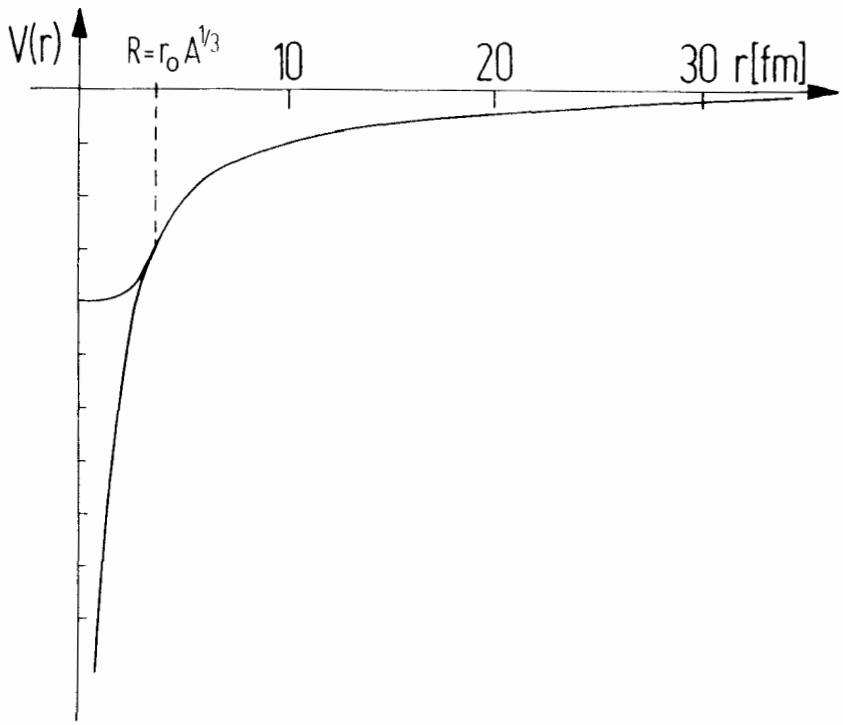

Fig.2: Coulomb and modified Coulomb potential.

this problem can be postponed up to a critical value of the charge $Z_{cr} \approx 170$. Indeed one obtains for such potentials bound state solutions up to Z_{cr}, where the bound state dives, i.e. disappears in the negative energy continuum (see Fig.1). It will be an important task for us to clarify the physics before and after this diving. As we will see, it has fundamental consequences for our understanding of quantum electrodynamics and the physics of the vacuum state.

2. The Autoionization of Positrons

We are facing here a problem similar to that of ordinary autoionization of nuclear and atomic physics, where one or several bound states are imbedded into one or several continua. The common autoionization process of nuclei is illustrated in Fig.3, which shows a bound 2p-2h-state degenerated with a 1p-1h continuum. Both configurations mix because of residual interactions, which leads to the decay of the bound state.

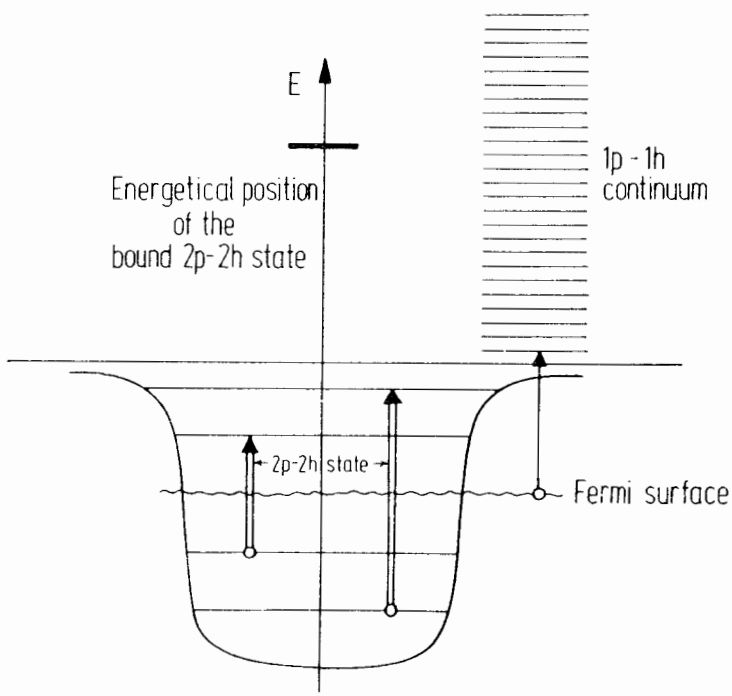

Fig.3: Illustration of the autoionization process in nuclear physics. The 2p-2h configuration (double arrows) is built of bound single particle states and imbedded into the 1p-1h continuum.

In our case the mechaninism of imbedding the bound state(s) into the negative energy continua is different from the ordinary autoionization, but the mathematical structure is the same; i.e. bound state(s) ($s_{1/2}, p_{1/2} \ldots$ etc.) are imbedded into continua ($s_{1/2}$, $p_{1/2}$, etc...). We will handle the problem therefore analogously to the former [1,2,5] by using Fano's formalism.[3] This will be useful for the physical understanding; an exact field theoretical treatment will be given later.

Let $D = i\gamma_\nu \frac{\partial}{\partial x_\nu} + m$ be the free electron Dirac operator. We then have to search for bound states of the Hamiltonian $\hat{H}=\hat{D}+V(r,Z)=\hat{H}(Z)$

$$\hat{H}(Z)|\phi_{nj}> = E_{nj}|\phi_{nj}> \tag{3}$$

where $V(r,Z) \equiv Z \times U(r,Z)$ is the "rounded off" Coulomb potential of the nucleus. $U(r,Z)$ is depending on Z only via the Z-N-dependent radius of the nuclear charge distribution. Within the range of atomic nuclei considered by us ($170 < Z < 200$) this dependence is very weak and may be omitted for convenience

$$V(r,Z) = Z \times U(r) \quad . \tag{4}$$

We now use the fact that we know the solution to our problem for $Z = Z_{cr} \approx 170$ and diagonalize $\hat{H}(Z=Z_{cr}+Z')$ in the basis of eigenstates given by $\hat{H}(Z_{cr})$. $|\phi>$ be the $\hat{1}s$ bound state eigenfunction for $Z = Z_{cr}$, i.e.

$$\hat{H}(Z_{cr})|\phi> = E_o|\phi> \approx -m_e c^2|\phi> \tag{5}$$

and $|\psi_E>$ may denote the S-continuum wave functions to the same

$$\hat{H}(Z_{cr})|\psi_E> = E|\psi_E> \ , |E|>m_e c^2 \ , <\psi_{E'},\psi_{E''}> = \delta(E'-E'') \ . \qquad (6)$$

$|\phi>$ and all $|\psi_E>$ serve as a basis for our diagonalization procedure. In doing this we neglect the small contribution from the higher bound ns states $(n > 1)$ (see ref.2a), which are separated by more then 500 keV from the 1s bound state. We need the matrix elements of $\hat{H}(Z_{cr}+Z')$ in our (restricted) basis

$$<\phi|\hat{H}(Z_{cr}+Z')|\phi> \equiv E_o + \Delta E_o \ , \qquad (7)$$

where

$$\Delta E_o = <\phi|Z'U(r)|\phi> = Z'<\phi|U(r)|\phi> \ . \qquad (8)$$

$$<\psi_{E'}|\hat{H}(Z_{cr}+Z')|\phi> = <\psi_{E'}|\hat{H}(Z_{cr})|\phi> + <\psi_{E'}|Z'U(r)|\phi> =$$

$$= Z'<\psi \quad |U(r)|\phi> \equiv V_{E'} \qquad (9)$$

and finally

$$<\psi_{E''}|\hat{H}(Z_{cr}+Z')|\psi_{E'}> =$$

$$= <\psi_{E''}|H(Z_{cr})|\psi_{E'}> + <\psi_{E''}|Z'U(r)|\psi_{E'}> \equiv$$

$$\equiv E'\delta(E''-E') + Z'U_{E''E'} \qquad (10)$$

The matrix elements $U_{E''E'}$ describe the rearrangement of the continuum states under the additional potential $U(r)$. For small Z' this, clearly, can be neglected since its influence upon the diving-in bound state is a second order effect. For large Z' the continuum states Ψ_E may be prediagonalized (continuum solutions for $Z > Z_{cr}$ are numerically available (see ref.2).

Now be $|\Psi_E\rangle$ a continuum solution to the Dirac equation for $Z > Z_{cr}$:

$$\hat{H}(Z_{cr} + Z')|\Psi_E\rangle = E|\Psi_E\rangle \quad . \tag{11}$$

We may expand $|\Psi_E\rangle$ within the approximations stated above into

$$|\Psi_E\rangle = a(E)|\phi\rangle + \int_{|E'|\geq m_e c^2} b_{E'}(E)\Psi_{E'}\rangle dE' \quad . \tag{12}$$

The coefficients $a(E)$ and $b_{E'}(E)$ are readily determined from the solution given by Fano. We are mainly interested in the effect from the bound state $|\phi\rangle$:

$$|a(E)|^2 = \frac{|V_{E'}|^2}{[E - (E_o+\Delta E) - F(E)]^2 + \pi^2|V_E|^4} \tag{13}$$

where $F(E)$ is the principal value integral

$$F(E) = P\int_{|E'|>m_e c^2} dE' \frac{|V_{E'}|^2}{E-E'} \tag{14}$$

The continuum functions $|\Psi_E\rangle$ are normalized in the usual way

$$\langle\Psi_{E'}|\Psi_E\rangle = \delta(E'-E) \quad ,$$

so $|a(E)|^2$ gives the probability that an electron bound in $|\phi\rangle$ is promoted to $|\Psi_E\rangle$ when an additional charge Z' is "switched on". It can be understood as well as the admixture of the bound state $|\phi\rangle$ to the new continuum state $|\Psi_E\rangle$. This admixture has an obvious resonance behaviour. If V_E does not depend too strongly on the energy E, we may neglect $F(E)$ with respect to ΔE_o and

set

$$\Gamma = 2\pi|V_E|^2 \quad .$$

Then the bound state amplitude obtains a Breit-Wigner shape

$$|a(E)|^2 \doteq \frac{1}{2\pi} \frac{\Gamma}{[E-(E_o+\Delta E_o)]^2+\Gamma^2/4} \quad , \tag{15}$$

with the resonance peaked around $E_o+\Delta E_o$.

Because we have chosen $E_o \approx -m_e c^2$,

$$\Delta E_o = Z'<\phi|U(r)|\phi> \equiv -Z'\delta \tag{16}$$

describes the energy shift of the bound 1s-state due to the additional charge Z'. The width Γ of the resonance is specified as

$$\Gamma = 2\pi|V_E|^2 = 2\pi|Z'<\psi_E|U(r)|\phi>|^2 \equiv Z'^2\gamma \quad . \tag{17}$$

Calculations show that

$$\delta \approx 30 \text{ keV} \quad , \quad \gamma \approx 0.05 \text{ keV} \quad . \tag{18}$$

Thus we may explicitly indicate the Z'-dependence of Eq.(15):

$$a(E)^2 = \frac{1}{2\pi} \frac{Z'^2\gamma}{[(E+m_e c^2)+Z'\delta]^2+1/4Z'^4\gamma^2} \tag{19}$$

Obviously, the bound state $|\phi>$ "dives" into the negative energy continuum for $Z>Z_{cr}$ proportional to $Z' = (Z-Z_{cr})$. At the same time it obtains a width Γ_E in energy distribution proportional to $Z'^2 = (Z-Z_{cr})^2$. This is illustrated in Fig.4.

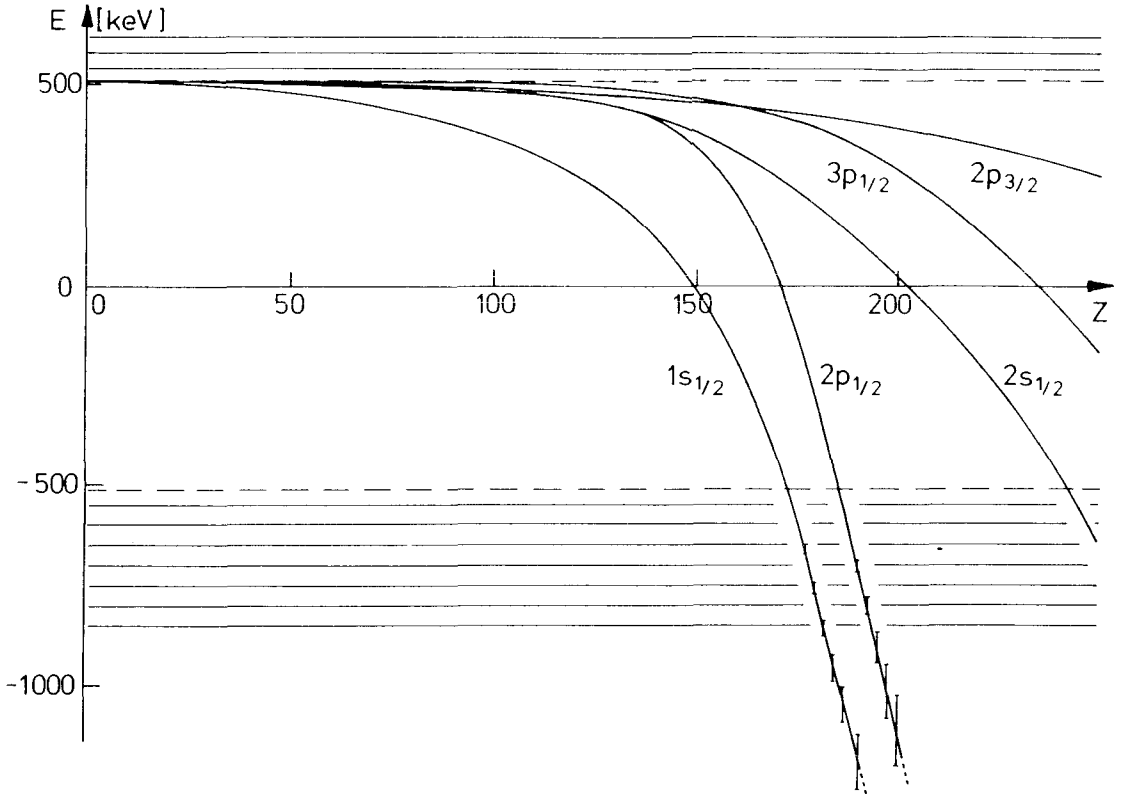

Fig. 4: Electronic binding energies for extended ($R=1.2\ fm \cdot A^{1/3}$) superheavy nuclei. Fermi charge distributions have been used. The diving points for the $1s_{1/2}$-, $2p_{1/2}$- and $2s_{1/2}$ levels are Z_{cr} = 170, 185 and 245 respectively. The influence of the other electrons are taken care of by a Thomas-Fermi distribution. The energy spreading of the states is shown by indicating the spreading width after the diving point (magnified by a factor 10). As shown in the text it is the same as the positron decay width of the bound state.

To these mathematical results we give the following physical interpretation:

If the proton number of a nucleus with $Z<Z_{cr}$ is steadily increased, the energy of K-shell electrons is decreased until at $Z=Z_{cr}$ it reaches $-m_e c^2$. During this process the spatial extension of the K-shell electron charge distribution is also decreasing, i.e. the bound state wave function becomes more and more localized. When Z grows beyond Z_{cr} the bound 1s-state ceases to exist. But that does not mean that the K-shell electron cloud becomes delocalized. Indeed, according to Eq.(12) the bound state ϕ is shared by the negative energy continuum states in a typical resonance type manner over a certain range of energy given by Eq.(13) and the negative energy continuum wave functions become - due to the bound state admixture - strongly distorted around the nucleus. This additional distortion of the negative energy continuum due to the bound state can be called <u>real charged vacuum polarization</u>, because it is caused by a real electron state which joined the "ordinary vacuum states", i.e. the negative energy continuum. The charge densities induced by all the continuum states superpose to form an electron cloud of K-shell shape. This electron cloud created by the collective behaviour of all continuum states contains the charge of two electrons, since the total probability for finding the 1s-electron state ϕ in any of the continuum states is ($\gamma \ll \delta$):

$$\int_{-\infty}^{-m_e c^2} |a(E)|^2 \, dE = 1 \quad . \tag{20}$$

Thus, the K-electron cloud remains localized in r-space. The surprising fact that it obtains an energy width Γ though it does not decay is resolved by the fact that it is composed of many stable states spread in energy, i.e. the bound state has obtained a spreading width in the negative energy continuum. This can be illustrated in the following way: Consider the gedanken-experiment of solving the Dirac equation with the cut-off Coulomb potential inside a finite sphere of radius a. Certain boundary conditions on the sphere have to be fulfilled. In this way the continuum is discretized (see Fig.5). Fig.5a shows the situation at $Z=Z_{cr}$, i.e. before diving. After diving (Fig.5b) the 1s-bound state has joined the lower continuum and is spread over it.

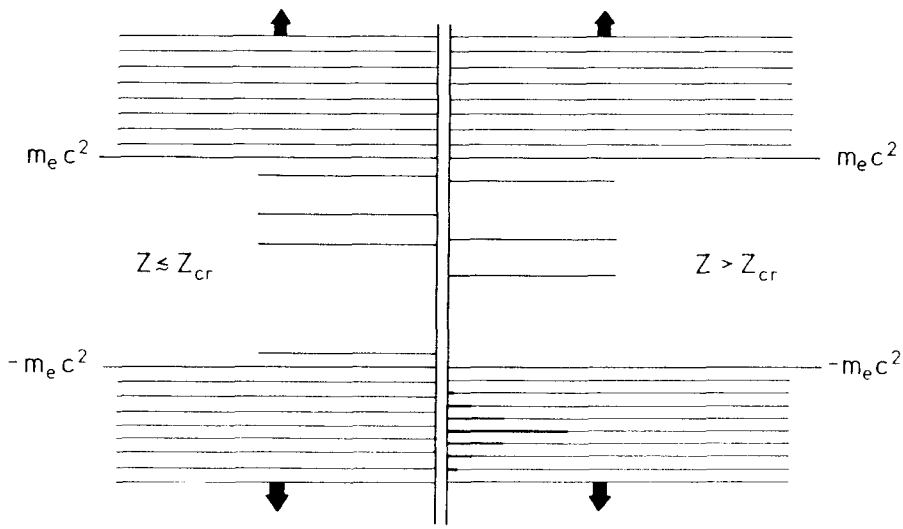

Fig. 5: Spreading of the bound state (solid line) over the negative energy continuum states (weak lines). After diving, i.e., $Z>Z_{cr}$, the negative energy continuum has obtained one more state; the 1s-bound state. It is now spread, however, over the negative energy continuum states. a) spectrum before and b) after diving.

If all levels are occupied (occupied K-shell), one sees that the K-shell still exists, but is spread out energetically. Therefore a γ-absorption line from a 1s-2p-transition would acquire an additional width, the spreading width. This is identical with the positron escape width. If one interprets this behaviour as a kind of strong vacuum polarization, it should be noticed that the vacuum thus defined is doubly charged. The formerly bound state K-electrons have now become a member of the vacuum. See in this connection also refs.[4,5].

The situation is changed if the bound state $|\phi\rangle$ is unoccupied during the process of "diving in". Then - on grounds of charge conservation - one of the resulting continuum states $|\psi_E\rangle$ has to be unoccupied, i.e. a positron escapes. The kinetic energy of the escaping positron is not sharp, but has a Breit-Wigner type spectrum given by Eq.(15). Of course, the positron-escape-process can be reversed. If positron scattering from nuclei with $Z > Z_{cr}$ is observed, the scattering cross-section has a resonance at $E = |\Delta E_o|$ with width Γ. The phase shift of the $s_{1/2}^-$ positron waves should go through $\pi/2$ at this energy. This can be used to independently determine the energy shift ΔE_o of the 1s-bound state according to the over-critical charge Z'. The probability per unit time for emission of positrons in the energy interval dE is given by Fermi's "Golden Rule"

$$P(E)\,dE = \frac{2\pi}{h}|\langle\phi|H_{int}|\psi_E\rangle|^2\rho(E)\,dE \qquad (21)$$

Thus, the K-electron cloud remains localized in r-space. The surprising fact that it obtains an energy width Γ though it does not decay is resolved by the fact that it is composed of many stable states spread in energy, i.e. the bound state has obtained a spreading width in the negative energy continuum. This can be illustrated in the following way: Consider the gedanken-experiment of solving the Dirac equation with the cut-off Coulomb potential inside a finite sphere of radius a. Certain boundary conditions on the sphere have to be fulfilled. In this way the continuum is discretized (see Fig.5). Fig.5a shows the situation at $Z=Z_{cr}$, i.e. before diving. After diving (Fig.5b) the 1s-bound state has joined the lower continuum and is spread over it.

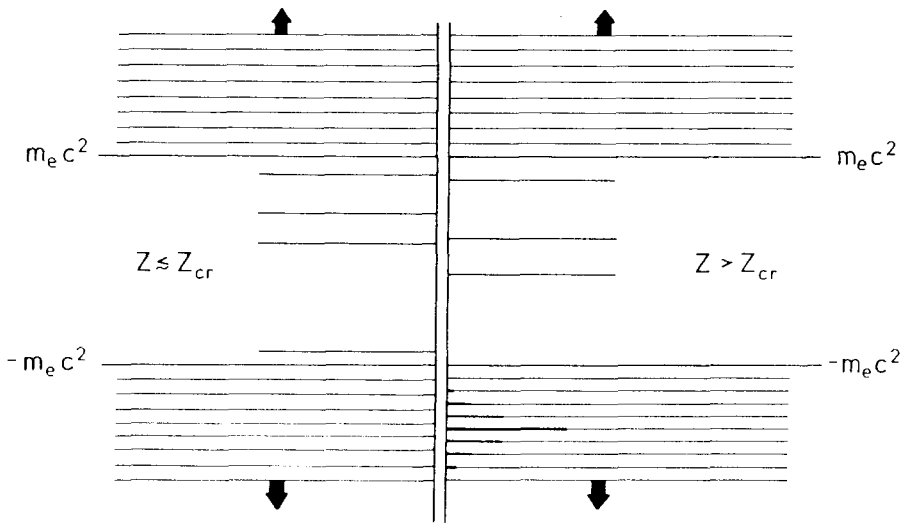

Fig. 5: Spreading of the bound state (solid line) over the negative energy continuum states (weak lines). After diving, i.e., $Z>Z_{cr}$, the negative energy continuum has obtained one more state; the 1s-bound state. It is now spread, however, over the negative energy continuum states. a) spectrum before and b) after diving.

If all levels are occupied (occupied K-shell), one sees that the K-shell still exists, but is spread out energetically. Therefore a γ-absorption line from a 1s-2p-transition would acquire an additional width, the spreading width. This is identical with the positron escape width. If one interprets this behaviour as a kind of strong vacuum polarization, it should be noticed that the vacuum thus defined is doubly charged. The formerly bound state K-electrons have now become a member of the vacuum. See in this connection also refs.[4,5].

The situation is changed if the bound state $|\phi\rangle$ is unoccupied during the process of "diving in". Then - on grounds of charge conservation - one of the resulting continuum states $|\psi_E\rangle$ has to be unoccupied, i.e. a positron escapes. The kinetic energy of the escaping positron is not sharp, but has a Breit-Wigner type spectrum given by Eq.(15). Of course, the positron-escape-process can be reversed. If positron scattering from nuclei with $Z > Z_{cr}$ is observed, the scattering cross-section has a resonance at $E = |\Delta E_o|$ with width Γ. The phase shift of the $s_{1/2}^-$ positron waves should go through $\pi/2$ at this energy. This can be used to independently determine the energy shift ΔE_o of the 1s-bound state according to the over-critical charge Z'. The probability per unit time for emission of positrons in the energy interval dE is given by Fermi's "Golden Rule"

$$P(E)\,dE = \frac{2\pi}{h}|\langle\phi|H_{int}|\psi_E\rangle|^2\rho(E)\,dE \qquad (21)$$

In our problem the ψ_E are normalized to δ-functions and the probability for finding the bound state ϕ at the energy E is according to (12) given by $\rho(E)dE = |a(E)|^2 dE$, and $H_{int} = Z'U(r)$. Hence the decay probability of the ionized K-shell, i.e. the autoionization rate per unit time, is, using Eq.(15)

$$p(E)dE = \cdot \frac{\frac{1}{2\pi}\,\Gamma_E dE}{[E-(E_o+\Delta E)]^2 + \Gamma_E{}^2/4} \cdot \frac{\Gamma_E}{h} \tag{22}$$

It can easily be generalized to several "diving states",[2] This decay must be interpreted as the decay of the normal, neutral vacuum into a charged vacuum (charge 2) in over-critical fields. Indeed, the Fermi surface has always to be at least at $E = -mc^2$; it cannot be at $E < -mc^2$, because otherwise we would immediately have strong contradictions to the experience. The vacuum state, which is to be identified with $E_F = -mc^2$ obviously is absolutely stable up to $Z=Z_{cr}$ and becomes instable (spontaneous decay) in over-critical fields. Only the charged vacuum (two positrons are emitted) is stable in over-critical fields. The vacuum proceeds to become higher charged as the over-critical fields (over-critical charge) are further increased.

3. The Change of the Vacuum in Overcritical Fields - Formal Aspects

Due to the excellent agreement between experiment and theory quantum electrodynamics (QED) is one of the most succesful parts of modern physics. This has been achieved by a power series expansion of all results in terms of the parameter α and $Z\alpha$. Unfortunately, little is known about the convergence of the expansion. In practice, this was no source of grief, since α and $Z\alpha$ are usually small parameters. In very heavy atoms, however, we have $Z\alpha = 0.7$ and in superheavy atoms we would be confronted with $Z\alpha \approx 1$ or even $Z\alpha > 1$.

Consequently, it seems to be worthwhile to extend atomic physics to the case where $Z\alpha > 1$. This means that we have to deal with the unpleasant situation of having neither weak ($g^2 << 1$) nor strong ($g^2 >> 1$) coupling, but working in the intermediate region. A first simplification is obtained by the remark that the finestructure constant $\alpha = 1/137$, which couples charged particles to the radiation field, remains small and these effects may be treated in perturbation theory. This suggests an expansion

$$B = \sum_{n=0}^{\infty} f_n(Z\alpha)\alpha^n \tag{23}$$

of observables with exact coefficients $f_n(Z\alpha)$. Conceptually, this corresponds to solving for the exact single particle solutions in the classical external field of the nucleus with charge Z and calculating all higher order effects in perturbation theory.

When dealing with the real electrons alone the most important higher order corrections are conveniently treated by the nonlinear Hartree-Fock equations. It is desirable to generalize these equations so that they include virtual effects as vacuum polarization and selfenergy. We start[4,5] from the operator equations for the coupled electron and photon fields

$$(\gamma\cdot p-m)\psi = \frac{e}{2}\{\gamma^{\mu}\psi, A_{\mu}\} \tag{24}$$

$$\Box A_{\mu} = e(j_{\mu}^{ex} + j_{\mu}) \tag{25}$$

where j_{μ}^{ex} takes into account the classical external field of the nucleus and

$$j = -\frac{1}{2}[\bar{\psi},\gamma^{\mu}\psi] \quad . \tag{26}$$

The second equation can be formally solved for A_{μ}:

$$A_{\mu}(x) = A_{\mu}^{ex}(x) + 2e\int_{-\infty}^{t_x} d^4y\, D_{\mu\nu}^{F}(x-y)\, j^{\nu}(y) + A_{\mu}^{rad}(x) \tag{27}$$

In the absence of photons $A_{\mu}^{rad} = 0$ and we may substitute (27) into (24). After some manipulations this leads us to the operator equation[6]

$$\begin{aligned}(\gamma\cdot p - e\gamma\cdot A^{ex} - m)\,\psi(x) &= e^2\int d^4y\, \gamma^{\mu}\langle j^{\nu}(\vec{y})\rangle D_{\mu\nu}^{F}(\vec{x}-\vec{y}; -t_y)\,\psi(x) \\ &- e^2\int d^4y\, \gamma^{\mu} S^{F}(\vec{x},\vec{y}; -t_y)\,\gamma^{\nu}\psi(\vec{y}, t_x + t_y) D_{\mu\nu}^{F}(\vec{x}-\vec{y}; -t_y) \ .\end{aligned} \tag{28}$$

In order to derive particle equations we have to take matrix elements between a complete set of particle states. First we have to specify which states we intend to regard as occupied, i.e. we have to define a fermi surface F (Fig.6).

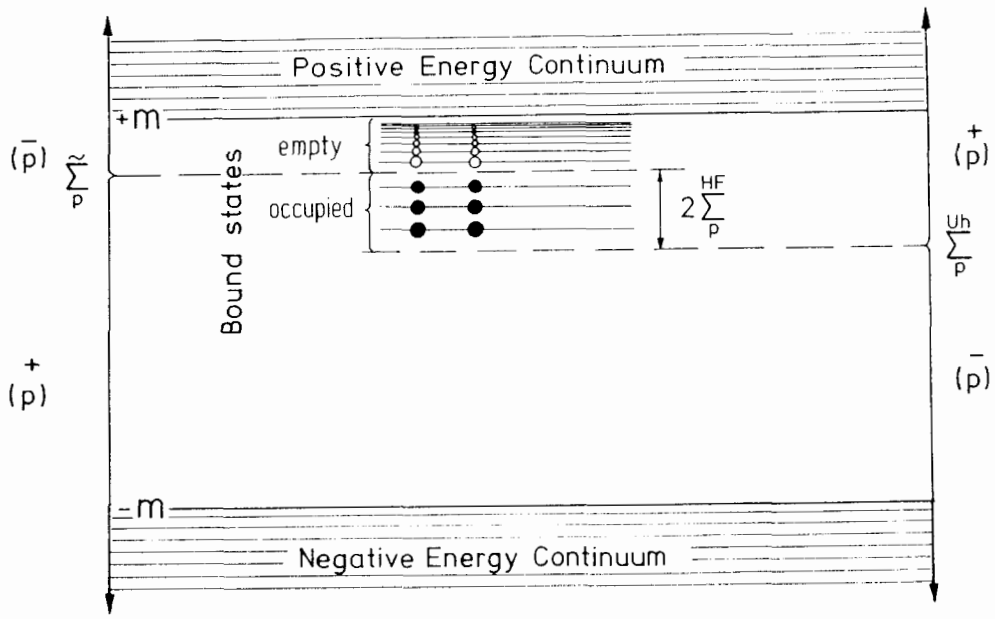

Fig. 6: The single particle spectrum and the Fermi surface; definition of the tilde ($\tilde{\Sigma}$) and the Uehling sum (Σ^{Uh})

The field operator is

$$\Psi(x) = \sum_{p>F} b_p \phi_p(\vec{x}) e^{-iE_p t_x} + \sum_{p<F} d_p^+ \phi_p(\vec{x}) e^{-iE_p t_x} \tag{29}$$

The Hartree-Fock approximation is introduced by restricting the basis to a single configuration, i.e. not allowing for any particle-hole excitations. Then the matrix elements are reduced to those between the vacuum and single particle states

$$\langle o| \ldots b_q^+ |o\rangle \quad \text{or} \quad \langle o| d_q \ldots |o\rangle \quad . \tag{30}$$

The resulting nonlinear equations are [4,5,6]

$$(\gamma_o E_q - \vec{\gamma}\cdot\vec{p} - e\gamma\cdot A^{ex} - m)\phi_q(\vec{x}) = \tag{31}$$

$$= \frac{e^2}{4\pi} \gamma_\mu \int d^3y \sum_p \bar{\phi}_p(\vec{y})\gamma^\mu \phi_p(y) |x-y|^{-1} \phi_q(\vec{x}) -$$

$$- \frac{e^2}{4\pi} \gamma^\mu \int d^3y \sum_p \bar{\phi}_p(\vec{y})\gamma^\mu \phi_q(\vec{y}) \frac{F_{pq}(|\vec{x}-\vec{y}|)}{|\vec{x}-\vec{y}|} \phi_p(\vec{x}) \quad .$$

We have now developed the general basis for atomic physics with $Z\alpha>1$. In Fig.4 the binding energies of the lowest lying atomic states are shown as a function of nuclear charge Z. At $Z_{cr} \approx 172$ the 1s-state is bound with the states of the negative energy continuum. It is obvious that a single-particle description will break down at this stage.[2,4,5]

For simplicity we assume all higher bound states as empty. We have two complete bases of single particle states to describe different situations. The states $|q, Z_{cr}+Z'\rangle$ of a

supercritical atom without a 1s-state and the just critical $|n,Z_{cr}>$ with a bound 1s-state. They are connected via a unitary transformation:

$$|q,Z_{cr}+Z'> = \sum_n <n,Z_{cr}|q,Z_{cr}+Z'>|n,Z_{cr}> \equiv \sum_n a(n,q)|n,Z_{cr}> \tag{32}$$

The critical 1s-state can be constructed from the supercritical continuum states

$$|1s,Z_{cr}> = \sum_q a^*(1s,q)|q,Z_{cr}+Z'> \quad . \tag{33}$$

The a(n,q) can be derived explicitly, if one neglects the interaction with higher bound states and among the continuum states. If Z'U(r) is the supercritical part of the Coulomb potential, we have

$$\left.\begin{aligned} <1s,Z_{cr}|Z'U(r)|1s,Z_{cr}> &= E_{1s} + mc^2 \\ <1s,Z_{cr}|Z'U(r)|E,Z_{cr}> &= V_E \\ <E,Z_{cr}|Z'U(r)|E',Z_{cr}> &= U_{EE'} \end{aligned}\right\} \tag{34}$$

with the solution

$$a(1s,E) \approx V_E^*[E - E_{1s} - F(E) + i\pi|V_E|^2]^{-1} \tag{35}$$

$$a(E,E') \approx U_{EE'}(E' - E)^{-1} + \delta(E - E') \tag{36}$$

where $F(E) = p\int|V_{E'}|^2 (E-E')^{-1} dE'$. This is analogous to our more "anschauliches" treatment in the foregoing section (Eqs.7 f.f.).

When two electrons occupy the 1s-states, the state vector ψ can be expanded in both the critical and the supercritical basis:

$$\psi = \sum_{E>F} \tilde{b}_E |E,Z_{cr}> + \sum_{\varepsilon} \tilde{d}^+_{1s,\varepsilon} |1s,\varepsilon,Z_{cr}> + \sum_{E<-m} \tilde{d}^+_E |E,Z_{cr}> =$$

$$= \sum_{E>-m} b_E |E,Z_{cr}+Z'> + \sum_{E<-m} d^+_E |E,Z_{cr}+Z'> \qquad (37)$$

where ε denotes the two spin orientations.
According to (33) the "critical" hole operator $\tilde{d}^+_{1s}$ is connected with the supercritical ones by[5]

$$\tilde{d}^+_{1s} = \int dE' \; d^+_E \; a(1s,E) \; . \qquad (38)$$

The familiar vacuum $|o>$ is defined by

$$|\tilde{o}> = \tilde{d}^+_{1s\uparrow} \tilde{d}^+_{1s\downarrow} |o> \qquad (39)$$

We shall show that $|\tilde{o}>$ is unstable for supercritical fields and decays into the twice charged supercritical vacuum defined by the state vector (37). Let us therefore prepare a K-hole in an atom with $Z = Z_{cr} + Z'$. The complete time-dependent state will be $(y(o)=1)$:

$$|\psi(t)> E \; y(t) \; \tilde{d}^+_{1s} \; |o> + \sum_{E<-m} W_E(t) d^+_E |o> \qquad (40)$$

Here d^+_{1s} is the "collective" 1s-state defined in (38) and d^+_E are the operators for a positron in supercritical fields. The time dependence of (40) is determed by the Hamiltonian

$$H = : \Psi^+ \; H_D(Z_{cr}+Z')\Psi \; : \qquad (41)$$

and the Schrödinger equation

$$H|\psi(t)> = i \frac{\partial}{\partial t} |\psi(t)> \quad . \tag{42}$$

Explicit solution yields[5]

$$y(t) = e^{i \tilde{E}_{1s} t} e^{-\frac{1}{2} \Gamma t} \tag{43}$$

with $\tilde{E}_{1s} = E_{1s} + F(\tilde{E}_{1s})$ and $\Gamma = 2\pi |V_{\tilde{E}_{1s}}|^2$,
and finally

$$|W_E(\infty)|^2 = |a(1s,E)|^2 \quad . \tag{44}$$

This result shows that the K-vacancy brought into the supercritical atom decays with the resonance width Γ from (33) as decay width. It produces positrons in the continuum states with an energy distribution equal to that of the spread out supercritical 1s-state. Fig.7 shows this spreading for an atom with Z = 184.

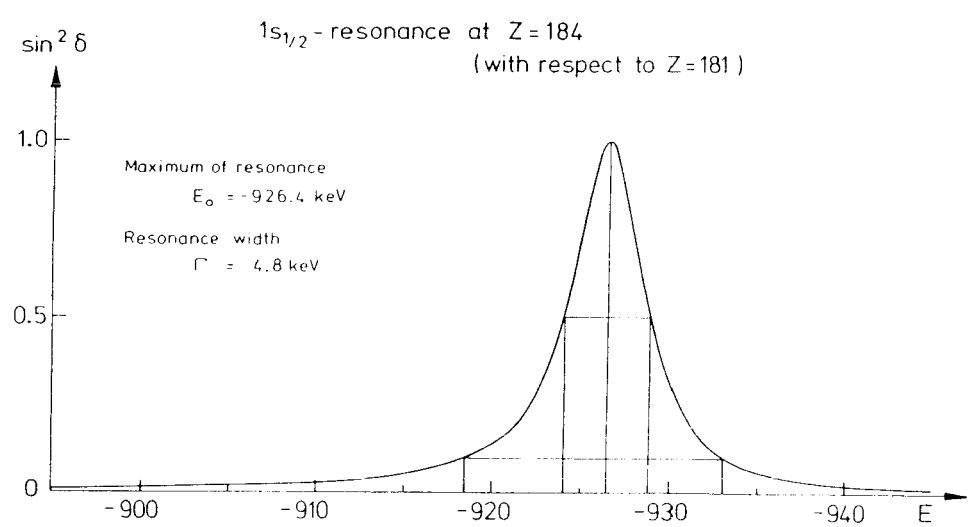

Fig. 7: Spreading of the "K-Shell" in the overcritical, charged vacuum of the element Z = 181.

Having shown the instability of the uncharged vacuum in supercritical fields, let us return to the charged vacuum. This does not contain a 1s-eigenstate, but a <u>collective 1s-state</u> can be extracted from the continuum. The total charge distribution of the charged vacuum is given by:[2,4,5]

$$\rho_{ind}(\vec{x}) = -\frac{1}{2}\int_m^\infty \{\varphi_E^+(x)\varphi_E(x) - \varphi_{-E}^+(x)\varphi_{-E}(x)\}dE - \frac{1}{2}\rho_{BS}(\vec{x}) \qquad (45)$$

where the φ are the continuum solutions to $Z_{cr}+Z'$ and ρ_{BS} is the charge distribution of the higher bound states. When the integral is restricted to the region of the resonance (33) we find the charge distribution of the old K-shell:

$$\tilde{\rho}_{1s}(x) = \int_{-\tilde{E}_{1s}-\Delta E}^{-\tilde{E}_{1s}+\Delta E} dE\ \{\varphi_E^+(x)\varphi_E(x) - \varphi_E^+(x)\varphi_{-E}(x)\}\ , \qquad (46)$$

and the remaining part of (45) yields (approximately) the standard vacuum polarization. Thus the K-shell has become part of the vacuum polarization,[2,5] so to say real part since $\int d^3x\ \tilde{\rho}_{1s}(x) = 2$. In contrast the familiar virtual part of vacuum polarization has a zero integral.

Fig.8 shows the charge distributions for several (collective) supercritical bound state resonances in comparison to the 1s-eigenstate at $Z_{cr} = 172$. Also for the higher bound states there exist critical nuclear charges, e.g. $Z_{cr}(2p_{1/2}) \approx 185$, $Z_{cr}(2s) \approx 245$. With the exception of the $2p_{1/2}$ - criticality, however, all higher critical points seem to be an academical problem, but can be treated in the very same way. Fig.9 demon-

strates the transitions between the vacua of different charge (isospin) at the critical points.

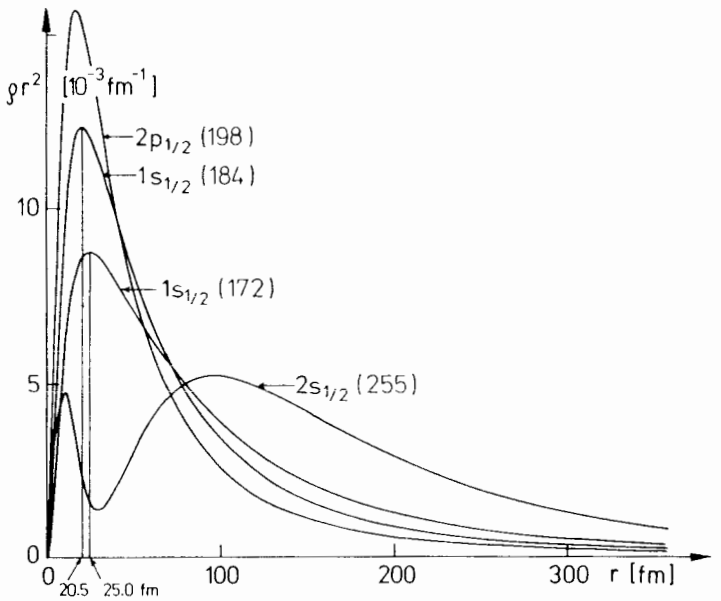

Fig. 8: Charge distribution of the vacuum in overcritical fields (Z=184,198,155) and of the K-shell in undercritical fields (Z=172).

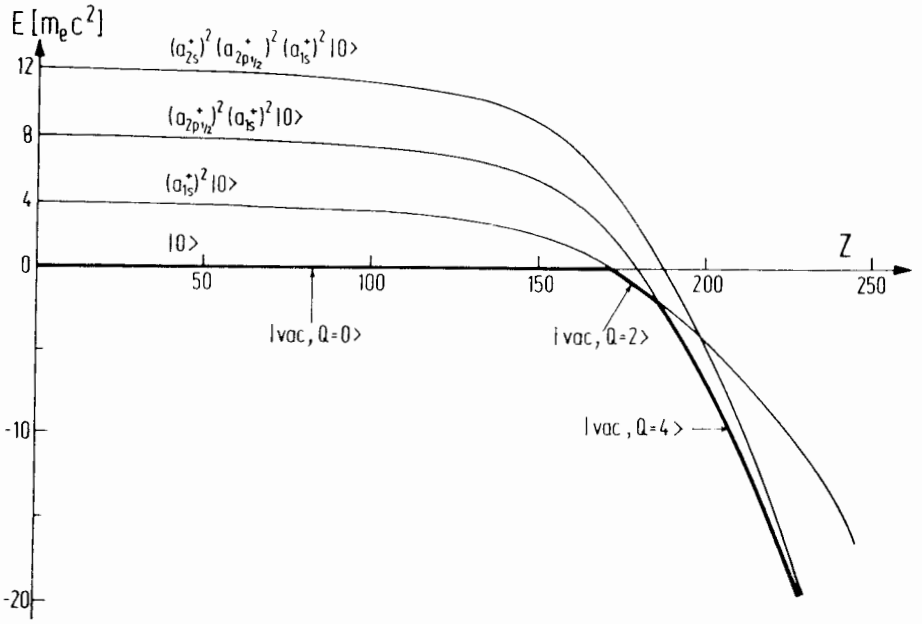

Fig. 9: The change of the vacuum to higher charge (isospin) as the overcritical field increases.

4. The Effects of Vacuum Polarization and Nonlinearities in the Electromagnetic and Spinor Fields

We are asking now for possible mechanisms which can prevent the diving of bound state levels into the negative energy continuum, i.e. which stabilize the neutral vacuum also in overcritical fields. The first such mechanism to think of is the field effects themselves; in particular the vacuum polarization, which is expected to be of greatest significance for high z atoms. For that it is necessary to investigate the vacuum polarization charge of Eq.(45) and to renormalize it. This is a quite mathematical game and has recently been carried out by M. Guylassi.[7] His results indicate, that the Uehling potential, which has already been calculated by Pieper et al.,[1] shifts the diving point by $\Delta Z \approx -1$ and the higher order vacuum polarizations by $\Delta Z \approx +1.5$, so that a net shift of $\Delta Z \approx 0.5$ results. His main result thus is, that vacuum polarization cannot prevent diving, and practically does not alter the critical charge Z_{cr}. This result has already been anticipated on quite physical grounds in refs.[2,8] by studying the effects of nonlinear electrodynamics. More precisely, consider a limiting field electrodynamics in the sense of Born and Infeld,[9] which is based on a Lagrangian of the type

$$\mathcal{L} = E_o^2 \left(\sqrt{1 - \frac{E^2 - B^2}{E_o^2}} - 1 \right) \tag{47}$$

which is constructed in analogy to the relativistic Lagrangian

$$\mathcal{L} = mc^2 \left(\sqrt{1 - \frac{v^2}{c^2}} - 1 \right) \tag{50}$$

which is a "limiting velocity Lagrangian". The Lagrangian (49) reduces for weak fields ($\frac{E^2-B^2}{E_o^2} << 1$) to the Maxwell Lagrangian for free fields, i.e. $L_{max} = \frac{1}{2}(E^2-B^2)$. Clearly, the analogy of (49) and (50) shows that E_o is a limiting field as c is the limiting velocity in special relativity. It is important to notice now, that a limiting field electrodynamics is a model electrodynamics for maximal vacuum polarization. If we plot, for example, the applied field E against the effective electric field E_{eff} (Fig.10), vacuum polarization can have at most the effect of saturating the applied field; i.e. leading to a limiting field E_o.

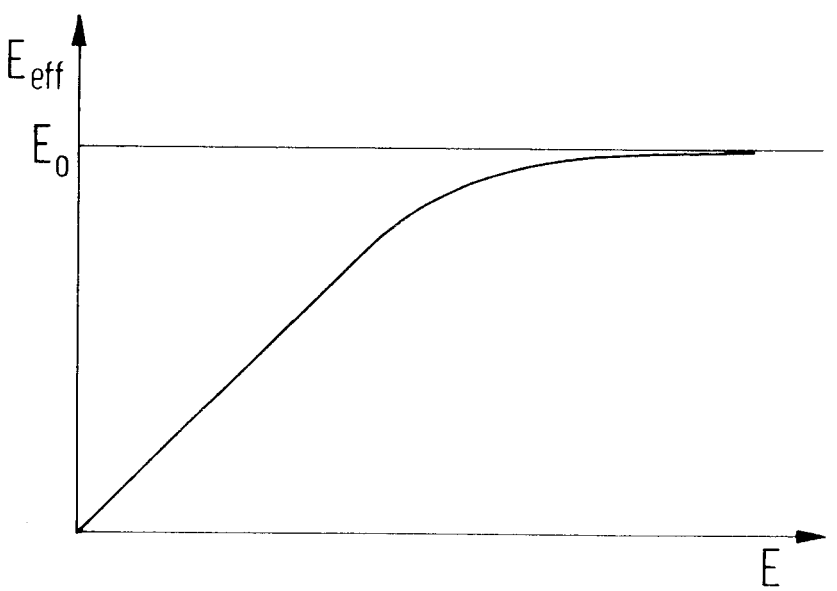

Fig. 10: The effective field E_{eff} as a function of the applied field E in a model of maximum vacuum polarization.

The Born-Infeld electrodynamics as a prototype of a limiting field electrodynamics have been investigated by Rafelski et al.[10]. In such limiting field electrodynamics the energy, i.e. the T_{44}-component of the energy momentum tensor is integrable. Born requested

$$\int_{\text{space}} T_{44} d^3x \stackrel{!}{=} m_o c^2 \tag{51}$$

where m_o is the electron mass. This leads to a limiting field $E_o \approx 10^{18}$V/cm. After recalculating with such a limiting field the modified electrostatic electron-nucleus interaction and coupling this into the Dirac-equation, one still obtains diving, but Z_{cr} is shifted up to $Z_{cr} \approx 250$ (see Fig.11)

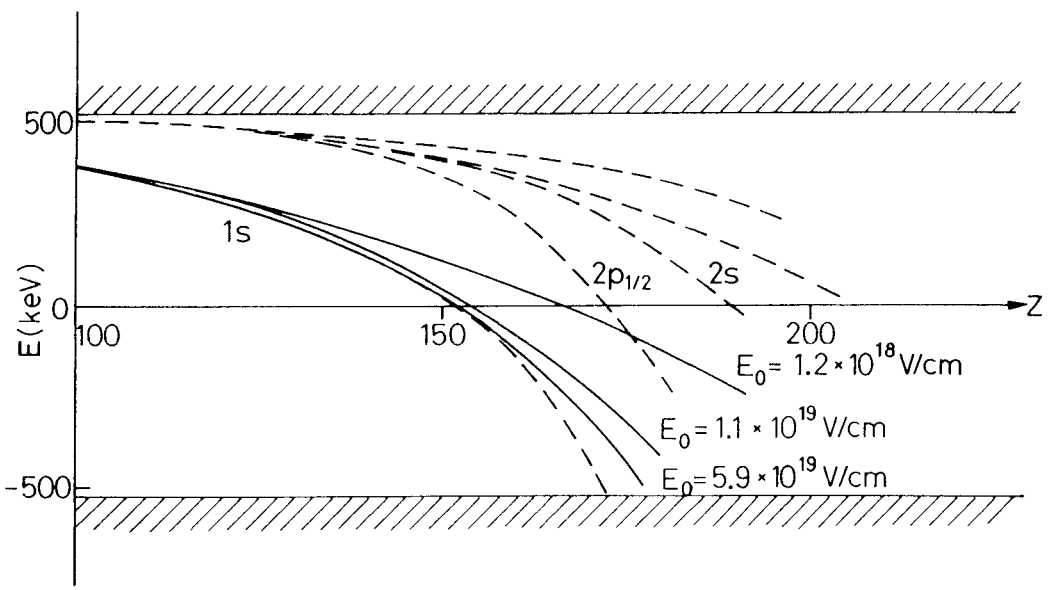

Fig. 11: The diving of the electronic K-shells in limiting field electrodynamics. The limiting field E_o is indicated. These theories serve as models for maximal vacuum polarization.

These relatively low limiting fields are, however, unrealistic, because such theories contradict high precision experiments. Soff et. al.[8] have investigated the Lambshift experiments, the precision measurements of the electronic K-binding energies in Fm and Pb,and the spectra of muonic atoms of heavy nuclei, and found that the limiting field E_o has to be at least $E_o \geq 10^{20}$V/cm in order to not disturb the obtained agreement between theory and experiments in these cases. With that value E_o the diving is practically occuring at the same critical charge as in the Maxwell theory, i.e. $\Delta Z_{cr} \approx 1$ (see Fig.11). Therefore we can conclude that 1) diving is not prevented by vacuum polarization, because it is even not prevented in the models of maximum vacuum polarization, i.e. limiting field electrodynamics and 2) that vacuum polarization can only shift the critical charge by not more than one charge unit.

Another mechanism to prevent diving (stabilize the vacuum) would occur if the Dirac field equations are changed by nonlinear term, e.g.

$$\gamma_\mu\left(\frac{\partial}{\partial x_\mu} - A_\mu\right) \psi + m\,\psi + \lambda_1(\bar{\psi}\psi)\psi + \lambda_2(\gamma_\mu\gamma_5\bar{\psi}\gamma_\mu\gamma_5\psi)\psi = 0 \qquad (52)$$

Such nonlinear terms can, if the coupling constants λ_1 or λ_2 are strong enough, indeed stabilize the vacuum. This is quite plausible. Let us take for example, the term $(\bar{\psi}\psi)\psi$. It acts like a repulsive potential when the electron densities $\bar{\psi}\psi$ becomes high. This "counter potential" can cancel or weaken Coulomb-potential so much that a further increase in Z does not lead to more binding. Waldeck[11] has shown, however, that such strong coupling constants λ_1 and λ_2 again would contradict the above

mentioned high precision experiments. In fact, one can determine upper limits for λ_1 and/or λ_2 from these experiments, and finds, that again diving is not prevented and occurs at practically the same critical charge as in the linear spinor theory. We can therefore conclude, that the electron positron vacuum cannot be stable in overcritical fields, and has to decay into a charged vacuum. We further comment, that we could exclude in this case of the electron-positron fields and its interaction with the electromagnetic fields violent nonlinear interactions, because high precision measurements were available. This is not the case for the strong interactions, i.e. the pionic field and its coupling to the nuclear field. Therefore, in this latter case, our knowledge is much more restricted, predictions for the overcritical strong field case much less reliable as in the present case. We will come back to these questions in our other talk on shock waves and pionization of matter.[12]

5. Experimental Possibilities

It is clear that superheavy elements around $Z = 170$ or 180 cannot be formed in the near future even though we predicted some years ago the existence of quasistable superheavy island around $Z=164$ (see ref.[13]). There is, however, a promising way out of this difficulty. Underlying all the various possible tests of QED of strong fields is the fact that in heavy ion collisions at energies around the Coulomb barrier the velocity of the ions, $v_{ion} \sim \frac{c}{20}$, is relatively slow compared with the highly relativistic electrons ($v_e \sim c$) bound with equal or more than twice their restmass. Therefore there exists a kind of adiabaticity

$$\frac{v_{ion}}{v_e} \sim \frac{1}{20} \tag{53}$$

which is not terribly good, but sufficient. In fact, we will see that the deviations from adiabaticity bring advantages for the possible experiments which are absolutely necessary. This adiabaticity led us[14] to the prediction of <u>intermediate superheavy molecules</u> in the heavy ion collision, which exist only during the time of collisions. The study of the intermediate molecules requires the solution of the Two-Center-Dirac-Equation, to which we will address ourselves now:

The motion of an electron under the influence of two charged nuclei is one of the fundamental problems in quantum mechanics theory of chemical binding.[15] Today the solutions of the one-electron spinless Schrödinger equation for two point charges are known analytically[15] and extensive numerical calculations

have been done to obtain binding energies in many-electron problems.[16,17] All these treatments, however, are non-relativistic, since the binding energies encountered in chemistry are of the order of some eV and relativistic effects are negligible. This comes from the fact that in diatomic molecules formed by heavy atoms, e.g. Ni-Ni, AuI, the internuclear distance is of the range of a few Å and only the outermost electronic orbitals overlap.

In heavy ion collisions with several MeV/nucleon scattering energy, the nuclei are for a short period of time so close that even the K-electrons feel the attraction of both centers. The typical collision time of heavy ions inside the K-shell is $T_c \sim 10^{-19}$sec whereas the "orbiting" time associated with a 1s-electron in very heavy atoms is $T_e \sim 10^{-20}$sec. The same holds true if the ratio of the correspondigly velocities is examined. Therefore the molecular electronic states have time to adjust to the varying distance $\vec{R}$ between the nuclei. This process can therefore be treated adiabatically in first approximation. The treatment, however, must be relativistic if the total nuclear charge involved, i.e. $Z=_1+Z_2$, is comparable to $\alpha^{-1} = 137$. Only one attempt has been made to account for relativistic corrections by Luke et al.[18] in ordinary molecular physics using first order perturbation theory in $Z\alpha$. This method, clearly, is inapplicable for systems with $Z > 90$.

The relativistic wave equation for an electron (with mass M) in the field of two electrical charges (located at $\underset{\sim}{R}$ and $-\underset{\sim}{R}$ resp.)

is given by[19]

$$[c\underset{\sim}{\alpha}\cdot\underset{\sim}{p}+\beta Mc^2 -E + V_1(\underset{\sim}{r}-\underset{\sim}{R}) + V_2(\underset{\sim}{r}+\underset{\sim}{R})]\Psi = 0 \ . \tag{54}$$

The two charges are considered as fixed in space. It is convenient to introduce prolate spheroidal coordinates ξ,η,φ by defining

$$\left.\begin{aligned} x &= R[(\xi^2-1)(1-\eta^2)]^{1/2}\cos\varphi \\ y &= R[(\xi^2-1)(1-\eta^2)]^{1/2}\sin\varphi \\ z &= R\xi\eta \end{aligned}\right\} \tag{55}$$

where the z-axis cuts through the two charges, which are foci of the ellipsoids ξ = const.. The φ-coordinate can be easily separated by setting ($m + \frac{1}{2}$ is the quantum number of angular momentum around the x-axis):

$$\Psi(r) = \begin{pmatrix} e^{im\varphi} & & & \\ & e^{i(m+1)\varphi} & & \\ & & ie^{im\varphi} & \\ & & & ie^{i(m+1)\varphi} \end{pmatrix} \Psi'(\xi,\eta) \tag{56}$$

and one is left with the equation

$$\frac{\hbar c}{R(\xi^2-\eta^2)}\begin{pmatrix} 0 & 0 & \pi_Z & \pi^- \\ 0 & 0 & \pi^+ & -\pi_Z \\ -\pi_Z & -\pi^- & 0 & 0 \\ -\pi^+ & \pi_Z & 0 & 0 \end{pmatrix} + \beta Mc^2 - E + V_1(\xi+\eta) + V_2(\xi-\eta) \quad \Psi'(\xi,\eta) = 0 \tag{57}$$

with the operators

$$\left.\begin{aligned}
\pi^+ &= W(\xi\frac{\partial}{\partial\xi} - y\,\frac{\partial}{\partial\eta}) - \frac{m}{W}\,(\xi^2-\eta^2)\\
\pi^- &= W(\xi\,\frac{\partial}{\partial\xi} - y\,\frac{\partial}{\partial\eta}) + \frac{m+1}{W}\,(\xi^2-\eta^2)\\
\pi_Z &= \eta(\xi^2-1)\,\frac{\partial}{\partial\xi} + \xi(1-\eta^2)\,\frac{\partial}{\partial\eta}
\end{aligned}\right\} \qquad (58)$$

This equation is known not to be separable in the ξ and η coordinates and has to be solved numerically. We have chosen a diagonalization procedure with an appropriate set of basis functions. In analogy to non-relativistic two-center functions we have used the set

$$\psi^m_{n\ell s}\,(\xi,\eta) =$$

$$= (\xi^2-1)^{\frac{m+\varepsilon_s}{2}}\; e^{-\frac{\xi-1}{2a}}\; L_n^{m+\varepsilon_s}(\frac{\xi-1}{a})\,P_e^{m+\varepsilon_s}(\eta)\,\chi_s \qquad (59)$$

where χ_s are the unit spin vectors, $\varepsilon_s = 0$ for s odd and $\varepsilon_s = 1$ for s even. L_i^α and P_i^α are the associated Laguerre and Legendre polynomials, respectively. a is a scaling factor to describe the asymptotic behaviour in the region $\xi\to\infty$. It is easy to see that Eq.(59) form a complete set of basis functions from the completeness of the L_i^α and P_i^α. Due to the common factor $(\xi^2-1)^{\frac{m+\varepsilon_s}{2}}$, which has been added to account for the structure of the differential equation (57) in the vicinity of the z-axis (ξ=1), and the volume element $R^3(\xi^2-\eta^2)d\xi d\eta$ in spheroidal coordinates, however, the $\psi^m_{n\ell s}$ are not orthogonal:

$$\langle\psi^m_{n'\ell's'}|\psi^m_{n\ell}\rangle = \delta_{ss'}\;B^m_s(n'\ell',n\ell) = \delta_{ss'}\,\delta_{nn'}\,\delta_{\ell\ell'}\;. \qquad (60)$$

Taking matrix elements of Eq.(57) we have

$$<\psi^m_{n'\ell's'}|\frac{\hbar c}{R(\xi^2-\eta^2)}\begin{pmatrix} 0 & \pi \\ -\pi & 0 \end{pmatrix}+\beta Mc^2+V_1(\xi+\eta)+V_2(\xi-\eta)|\psi^m_{n\ell s}> =$$

$$= A^m(n'\ell's',n\ell s) = E\ \delta_{ss'}\ B^m_s(n'\ell',n\ell) \tag{61}$$

as eigenvalue problem for E. It can be solved by standard procedures, i.e. first diagonalizing $B^m_s(n'\ell',n\ell)$, forming $[B^m]^{-1}\ A^m = C^m$ and subsequently diagonalizing C^m. This method circumvents Schmidt's orthogonalization of the basis functions $\psi^m_{n\ell s}$. The eigenvalues of C^m give the eigenenergies of our problem, depending on R and the explicit form of the potentials V_1 and V_2. For point charge

$$V_1^P(\xi+\eta) = \frac{Z_1e^2}{\xi+\eta} \qquad\qquad V_2^P(\xi-\eta) = \frac{Z_2e^2}{\xi-\eta} \tag{62}$$

all matrix elements in Eq.(61) can be evaluated analytically by use of recurrence formulae for the L_i^α and P_i^α (see ref.[19]). This convenience is due to the special choice of the basis functions Eq.(59) and is lost by even slight modifications, especially in the spin-orbit coupling terms. For $Z_1+Z_2>\alpha^{-1}$ and close distances R the extended structure of the charges becomes important and the additional matrix elements

$$<\psi^m_{n'\ell's}|V_i(\xi,\eta) - V_i^P(\xi,\eta)|\psi^m_{n\ell s}> \quad , \ i = 1,2$$

are computed by numerical integration over the nuclear volumes. We have chosen homogeneously charged spheres with a radius given by $r_N = 1.2\ (0.00733Z^2 + 1.3Z + 63.6)^{1/3}$fm (see ref.[13]).

For numerical calculations we have used a set of 100 basis functions (n=0,...,4) ; ℓ=m,...,m+4). The diagonalization then gives about 15 correct eigenstates and several states in the positive and negative energy continua. Figs.12-16 show the level schemes for the system $_{35}$Br -$_{35}$Br, examined by Meyerhof et.al., Ni-Ni investigated by Greenberg et.al.[21], $_{53}$I -$_{79}$Au and $_{92}$U -$_{92}$U investigated by Mokler et al.[22], Cl-Pb investigated by Burch et.al.[23].

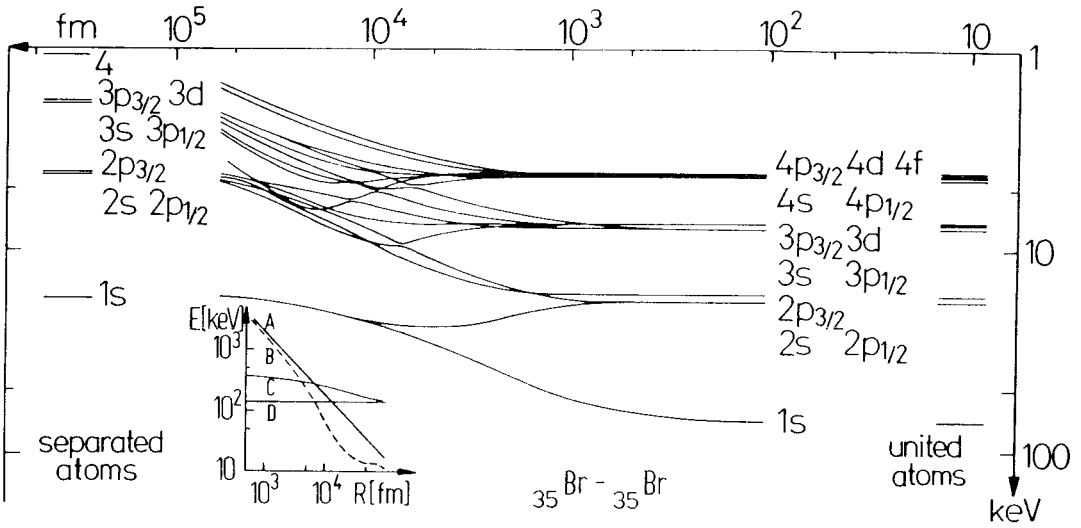

Fig. 12: The level scheme for the symmetrical system $_{35}$Br-$_{35}$Br. Since parity is a good quantum number, adiabatic states of opposite parity may cross. The small figure shows the molecular potential as function of the internuclear distance: A) the Coulomb repulsion between the nuclei; D) the electronic binding energy in separate atoms; C) electronic energy in the separate atoms; C) electronic energy in the molecule; B) the total molecular potential.

The Br-Br-system has been investigated by Meyerhof et.al.[20].

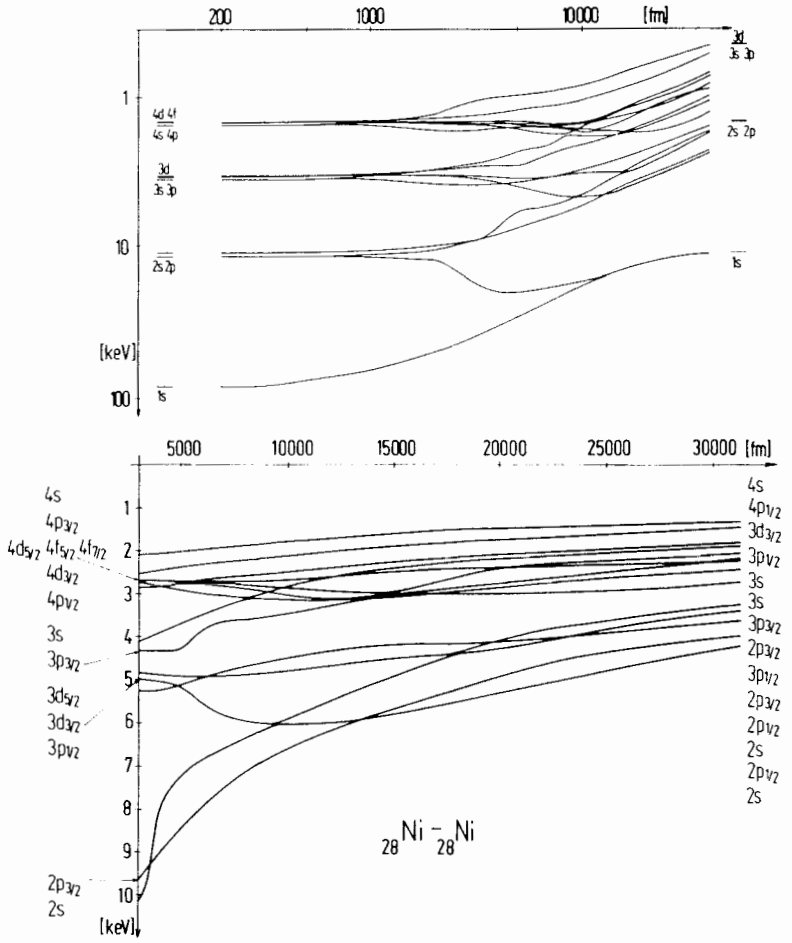

Fig. 13: The level scheme for the symmetrical Ni-Ni-system,[38] which has been investigated by Greenberg et.al.[21].

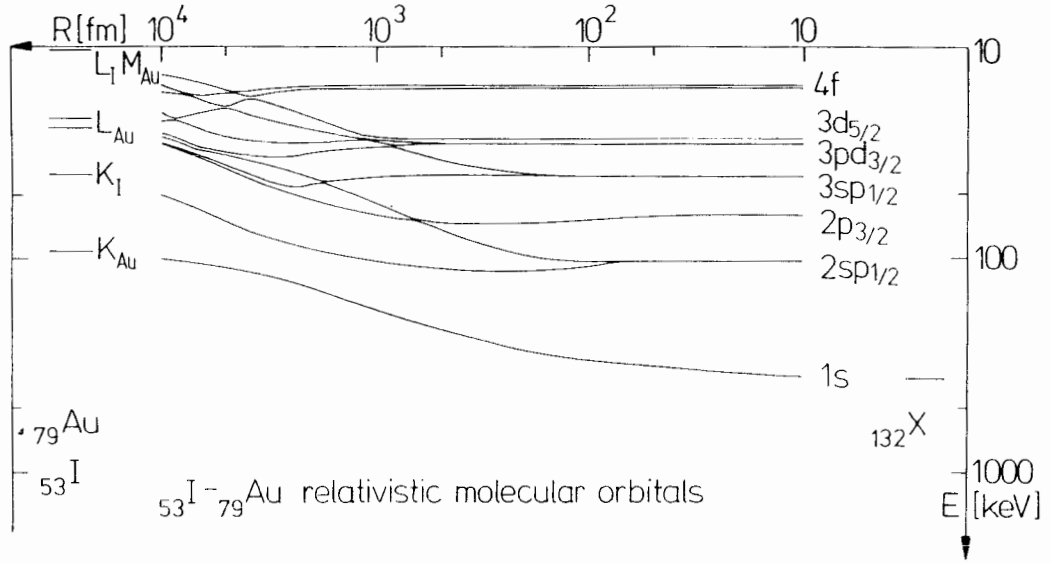

Fig. 14: The level scheme for the asymmetrical system $_{53}$I-$_{79}$Au.[38] Parity is not a good quantum number. This system has been investigated by P. Mokler et.al.[22] and more recently by H. Gove et.al.[45].

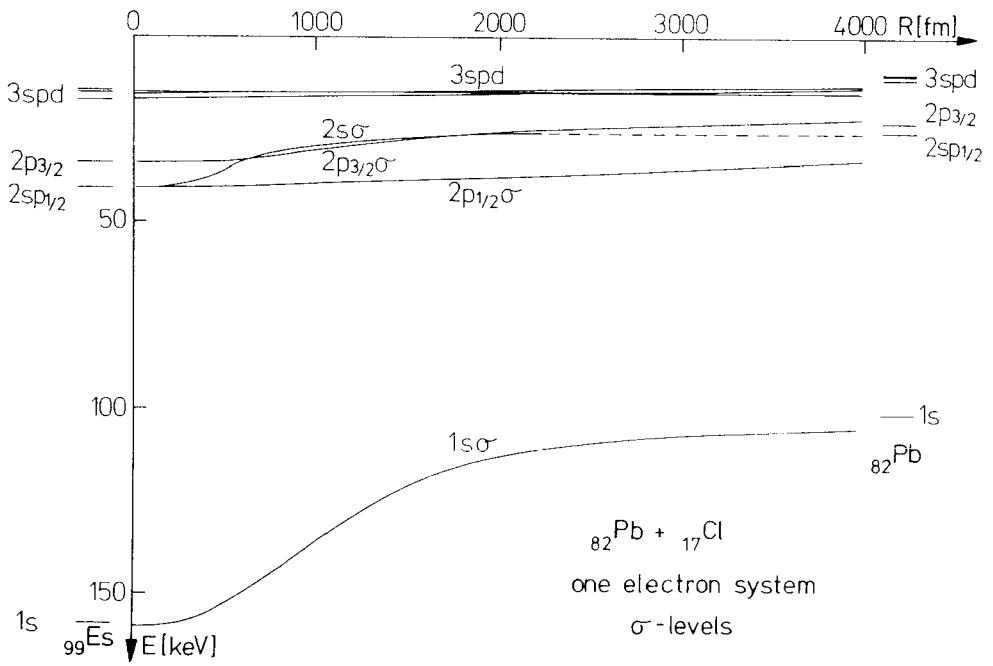

Fig. 15: The level scheme for the very asymmetrical Cl-Pb-system, which has been calculated by D. Burch et.al.[23].

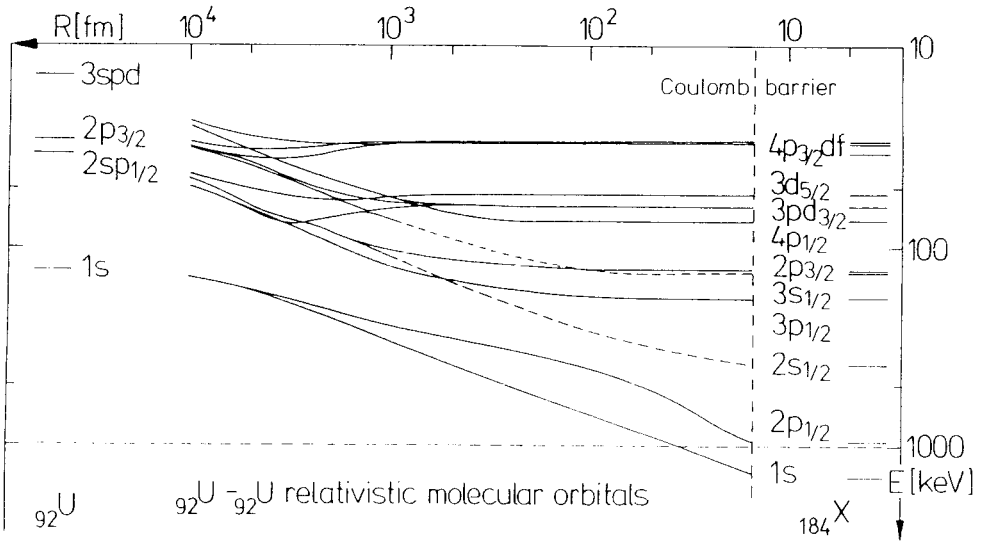

Fig. 16: The $_{92}U$-$_{92}U$ system with extended nuclei. The lowest molecular state reaches the negative energy continuum at $R_{cr} \approx 34$ fm. It can be traced even further down due to the discretization of the continuum states by the mathematical method of diagonalization.

The I-Au and Cl-Pb systems are interesting because the electronic states have no good parity and no level crossings are allowed. In the U-U system the nuclear charge distribution plays an important role for $R < 60$ fm. The critical distances R_{cr}, i.e. the internuclear separation where the deepest bound state acquires $2Mc^2$ binding energy and joins the negative energy continuum - is shifted from 36 fm for point-like to 34 fm for extended nuclei.

The comparison of these results shows that for the lighter molecular systems like Br-Br the asymptotic spectrum is already reached at distances of the order 10^3 - 10^4 fm, while for heavy systems like U-U the asymptotic spectrum is only reached when $R \approx 0$. Thus, considering the dynamics, there exists a kind of a "<u>run way</u>" for the final molecular spectra in light systems with a distance of the order 10^3 fm along which the <u>same</u> K_α, K_β etc. lines can be emitted, independent of R. This is probably the reason for observing enhanced molecular X-rays, while the great tail of molecular X-rays stems from the transition region between 10^5 and 5×10^3 fm. The level schemes thus obtained are exact for one electron in the electric field of two motionless nuclei. In heavy ion scattering, one will be confronted with many-electron problems in the field of two (rapidly) moving nuclei. Then several corrections will arise:

1. Screening of outer electrons by inner ones (Thomas-Fermi or Hartree-Fock methods). It can be estimated from calculations in superheavy atoms[24] to decrease the binding energy of

1sσ electron at R_{cr} by 50 - 100 keV for the U-U molecular system.

2. Corrections due to non-adiabacity, i.e. transitions between different molecular levels that lead to ionization and unsharpening of the level energy. These effects are treated by time-dependent perturbation theory on the adiabatic basis[25,26].

These new two center energy diagrams can be applied to the following problems: a) The exact shape of molecular X-ray spectra obtained in high energetic collisions of heavy ions[20,23,27,28]; b) the shape of positron autoionization spectra in the collisions of overcritical systems of heavy ions ($Z_1+Z_2>172$) (see ref.[26]); c) the ionization cross sections for inner molecular shells due to Coulomb excitation[26], which is of emminent importance for the positron autoionization experiments; d) deviations from the Rutherford scattering cross section (especially angular distribution) due to effects of electronic molecular binding[30].

The latter effect is shown in Fig.12b for the Br-Br case and shows that indeed strong deviations from the $\frac{Z^2\alpha}{R}$ potential occur.

5.2 X-rays from Intermediate Molecules

It is quite clear from our discussion so far that the intermediate molecules must be observable through the emission of their X-rays. Indeed, the first MO-X-rays (L-shell-X-rays) have been observed by F. Saris and his coworkers[27]. The first MO-X-rays for the M-shell, but for the superheavy I-Au-system (see Fig.14) have been observed by Mokler, Stein and Armbruster[22]. The MO-K-X-rays have been pionered by W. Meyerhof and his coworkers[20]. In these cases one observed spectra as shown in Fig.17 for the monoatomic Ni-Ni-system which has been investigated by J. Greenberg et.al. from the Yale-University[21]. The long tail of spectrum above the atomic K_α-,K_β-lines is interpreted as being due to molecular X-rays. Clearly, as Greenberg has shown, their exists no "united atom limit" for these X-rays, if the background is suppressed sufficiently. This is particularly so, since in this monoatomic system the dipole-bremsstrahlung-background (nucleus-nucleus bremsstrahlung) vanishes. These and many other arguments made it necessary to look for a unique signature for the identification of molecular X-rays. This has recently been achieved by recognizing that their exist induced transitions in the intermediate molecules.[30 - 33] The experimentum crucis has been performed by Greenberg and collaborators[33] at Yale. We will describe this theoretical and experimental work here shortly.

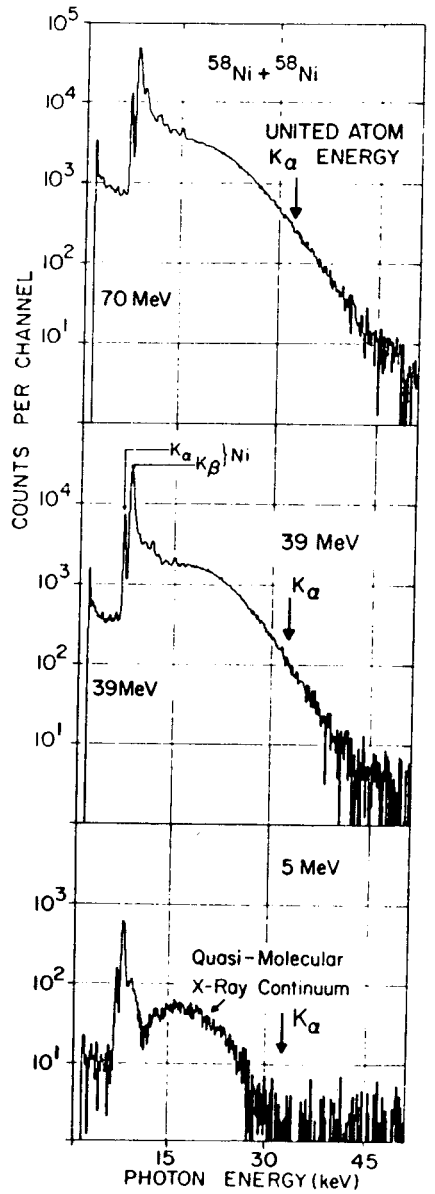

Fig. 17: MO-K-X-ray spectrum observed for various ion energies (70 MeV, 39 MeV, and 5 MeV) by J. Greenberg et.al. at Yale[33]. The united atom K_α-energy is indicated by an arrow. Clearly, the MO-X-rays are observed far beyond this limit. This is an effect of the collision broadening[32]. At 5 MeV ion energy the MO-X-rays join the background below the K_α-united atom limit; as it must be, because of the Two-Center-Level-Diagram and the small collision broadening.

Reports on the detection of molecular X-rays have been given by various experimental groups[20-23;27,28]. However, as mentioned above, ground effects such as electronic and nuclear bremsstrahlung occur as competing effects in these measurements. Only recently Greenberg and Davis[21] have carried out experiments with monoisotopic Ni beam and target where nuclear dipole bremsstrahlung is forbidden.

The unique signature of molecular X-rays comes from the fact, that - contrary to atomic X-rays - in addition to the spontaneous X-rays also induced radiative transitions occur, which can be recognized by their asymmetric angular distribution relative to the beam axis. It is the purpose of this note to discuss the X-ray spectrum due to both spontaneous and induced transitions including the most important dynamical effects.

The adiabatic molecular states have been given by the Two-Center-Dirac-Equation discussed in the foregoing paragraph. Non-adiabatic effects and radiative coupling can be described by writing the generally covariant form of the Dirac equation[31,34] in a rotating, instantaneous coordinate system whose z-axis is along the line connecting the two scattering nuclei[19b]

$$\gamma^k \left(\frac{\partial}{\partial x^k} - \frac{ie}{hc} A_k + \Gamma_k \right) \psi + \frac{m_e c}{h} \psi = 0 \qquad (63)$$

The $\Gamma_k = \frac{1}{4} \gamma^i (\gamma_{i/k} - \{ {}^{\ell}_{ik} \} \gamma_\ell) - \frac{1}{32}$ trace $(\gamma\gamma^i\gamma_{i/k})\gamma$ are the generalized connections for spinor differentation and the Dirac-matrices γ^k are determined via the metric g^{ik} of the coordinates in the rotating frame[31,19b]. Explicit evaluation for a

system rotating with angular velocity $\vec{\omega}_{rot}(t)$ gives

$$i\hbar \frac{\partial\psi}{\partial t} = [c\vec{\alpha}\cdot(\vec{p}-\frac{e}{c}\vec{A})+V+\beta m_e c^2]\ \psi - \vec{\omega}_{rot}\cdot[\vec{r}\times(\vec{p}-\frac{e}{c}\vec{A}+\frac{\hbar}{2}\sigma]\psi - \frac{i\hbar}{4c}(\vec{\omega}_{rot}\times\vec{r})\cdot\vec{\alpha}\ \psi \tag{64}$$

Two mechanisms for photon emission, a spontaneous one via the operator $H_{rad\ spon} = -c\vec{\alpha}\cdot\vec{A} = -i\frac{e}{\hbar}[H,\vec{r}]\cdot\vec{A}$ and an induced emission caused by $H_{rad\ ind} = \frac{e}{c}\vec{\omega}_{rot}\times(\vec{r}\cdot\vec{A})$, where the former current is imaginary while the latter is real. Therefore no interference occurs and the cross section for the two processes is given in the approximation of Fermi's Golden Rule by[25,31,32]

$$\frac{d\sigma}{d\omega\ d\Omega_k\ d\Omega_{ion}} = \frac{\omega^3}{2\pi\hbar c^3}|d_{fi}|^2\ \sin^2\Theta_{kd}\left(\frac{d\sigma}{d\Omega_{ion}}\right)_{Ruth},\ \frac{d\sigma_{ind}}{d\omega\ d\Omega_k d\Omega_{ion}} =$$

$$= \frac{\omega\ \omega^2_{rot}}{2\pi\hbar c^3}\left|\frac{\vec{I}}{|I|}\times\vec{d}_{fi}\right|^2 \sin^2\Theta\left(\frac{d\sigma}{d\Omega_{ion}}\right)_{Ruth} \tag{65}$$

Averaging over all possible orientations of the molecular dipole $\vec{d}_{fi}$ (closed shells!) gives an uniform distribution for the spontaneous radiation and for the induced radiation a distribution $\frac{d\sigma_{ind}}{d\omega d\Omega_k d\Omega_{ion}} \propto 1 - \frac{1}{2}\sin^2\Theta_{KI}$ where Θ_{KI} is the angle between the photon and the rotation axis $\frac{\vec{I}}{I}$ or if we integrate also over the azimuthal ion scattering angle

$$\frac{d\sigma_{ind}}{d\omega d\Omega_k \sin\Theta_{ion}\ d\Theta_{ion}} \propto \frac{1}{2} + \frac{1}{4}\sin^2\Theta_k$$

where Θ_k is the angle between photon and beam axis. Only the $2p_{3/2}\sigma$ and π and $2p_{1/2}\sigma$ to $1s_{1/2}\sigma$ transitions are included in

our calculations. They are so far assumed to be equally occupied with electrons. Uneqal population (alignment) of the $2p_{3/2}\pi$, $2p_{3/2}\sigma$ and $2p_{1/2}\sigma$ MO's with probabilities A^2, B^2 and C^2 respectively, leads to the following asymmetry as a function of photon energy $h\omega$, photon sacttering angle Θ_K and ion energy E

$$y(\omega,\Theta_k,E)=\frac{d\sigma(\Theta_k)}{d\omega d\,\Theta_k}\left(\frac{d\sigma(\Theta_k=0)}{d\omega d\,\Theta_k}\right)^{-1}-1=\frac{3}{2}\sin^2\Theta_k\frac{(A^2-B^2)-(\gamma A^2-7/3\ B^2-C^2)\,\alpha_3^2}{3A^2+5\ B^2+6\beta C^2\ +(3A^2+B^2+3\gamma C^2)\,\alpha_3^2} \tag{66}$$

where $\beta = \frac{D_1^2}{D_3^2}$ is the ratio of the squared reduced dipole matrix elements of the $p_{1/2}\sigma$ and $2p_{3/2}\pi,\sigma$ to the $1s_{1/2}\sigma$states,

$$= \frac{D_1^2}{D_2^2}\,\frac{\alpha_1^2}{\alpha_2^2} \quad \text{and} \quad \alpha_\nu = \frac{v}{R_\nu(\omega)\,\omega} = \frac{\sqrt{2ME}}{R_\nu(\omega)\,\omega}\ . \quad R(\omega) = R_o\cdot\frac{\sqrt{\omega_s\omega_s}}{\omega-\omega_s}$$

is the (approximate) two center distance as a function of the photon energy. For the $2p_{1/2}$ MO one has $\hbar\omega_s=0$, $\hbar\omega_c=31.8$ keV and for the $2p_{3/2}$ MO, $\hbar\omega_s=7.5$ keV and $\hbar\omega_c=32.2$ k3V. $R_o=2100$ fm. Obviously η is largest perpendicular to the beam axis ($\Theta_K=90^o$). The comparison of (66) with experiments[33] can serve as a determination of the alignments A^2/B^2, A^2/C^2.

Due to the non-adiabatic effects the molecular states obtain a width $\Gamma(t)$ which is composed of three different parts[25]

$$\Gamma_{\text{rad spon}} = \sum_{nk\varepsilon} \left| e \sqrt{\frac{2\pi}{\hbar\omega}} \int_0^t dt' \; e^{i \int_0^{t'} d\tau' \, \omega_{mn}(\tau) + i\omega t'} \; \omega_{mn} \langle n(R) | \vec{r}\cdot\vec{A} | m(R) \rangle \right|^2$$

$$\Gamma_{\text{rad ind}} = \sum_{nk\varepsilon} \left| e \sqrt{\frac{2\pi}{\hbar\omega}} \int_0^t dt' \; e^{i \int_0^{t'} d\tau' \, \omega_{mn}(\tau) + i\omega t'} \; \vec{\omega}_{rot} \times \langle n(R) | \vec{r}\cdot\vec{A} \; m(R) \rangle \right|^2$$

$$\Gamma_{\text{non rad}} = \sum_{n=m} \left| \int_0^t dt' \, e^{i \int_0^{t'} d\tau \, \omega_{mn}(\tau)} \langle n(R) | \dot{R} \frac{\partial}{\partial R} + \frac{\vec{\omega}_{rot}\cdot\vec{j}}{h} | m(R) \rangle \right|^2$$

(67)

In our present calculations an effective parameter Γ has been chosen for the sum of these widths[25], which has been varied between 1 and 5 keV to establish the dependence of the spectra on the width which is a function of scattering energy ($\Gamma \sim \sqrt{E}$). It leads to a smooth transition from the molecular X-ray spectrum into the quadrupole bremsstrahlung background,[35] which can serve for its determination (see Fig. 18b). Moreover, we have negelcted interference effects of the radiation for high energetic X-ray radiation.[36] The cross sections are calculated here by integrating (65) along the trajectory and, for the single spectrum, by further integrating over all ion scattering angles. The transition energies and dipole matrix elements are taken from the exact relativistic one-electron states for the Ni-Ni system shown in Fig. 13. For the symmetric Ni-Ni collision, the symmetrized Rutherford cross section is used. The results for a coincidence experiment (equal population assumed) at various scattering angles and energies are shown in Fig.18a. The spectra at moderate forward angles exhibit a

pronounced peak at the high energy end which is essentially due to the additional induced radiation that is strongly peaked at high photon energies. The induced radiation also grows with increasing scattering energy, whereas the spontaneous yield per K-vacancy drops. Of course, the K-vacancy production will increase with rising energy. For low scattering energy (e.g. 5 MeV) the molecule no longer reaches the asymptotic "runway" region and no peak structure occurs. For very forward or more backward angles ($\Theta<10^{o}, \Theta>45^{o}$) the contribution from induced radiation decreased with respect to the spontaneous X-ray yield. Especially for very forward angles ($\Theta<3^{o}$) the runway region is forbidden and the peak vanishes altogether (Fig.18a). The width of the peak at the end of the spectra at forward angles is almost completely determined by the collision broadening $\Gamma(t)$ and not so much by the shape of the level diagram. For the singles experiment the spectra shapes look essentially exponential (Fig. 18b). The calculation assumes that a K-vacancy is brought into the collision (two-step process). For a one-step process (ionization and X-ray in the same collision) the impact paramameter dependence of K-vacancy production has to be folded into the integration over Rutherford cross-section. The end point of the spectrum is a function of scattering energy, because Γ itself increases with scattering energies, e.g. 5 MeV in Fig.18b. The experimental endpoint of the spectrum may even lie before the united atom limit as the asymptotic region of the level diagram (Fig. 13) is not reached in the collision. For comparing theory with experiment we note that the background of the tales of the atomic $K_{\alpha,\beta}$-lines, the

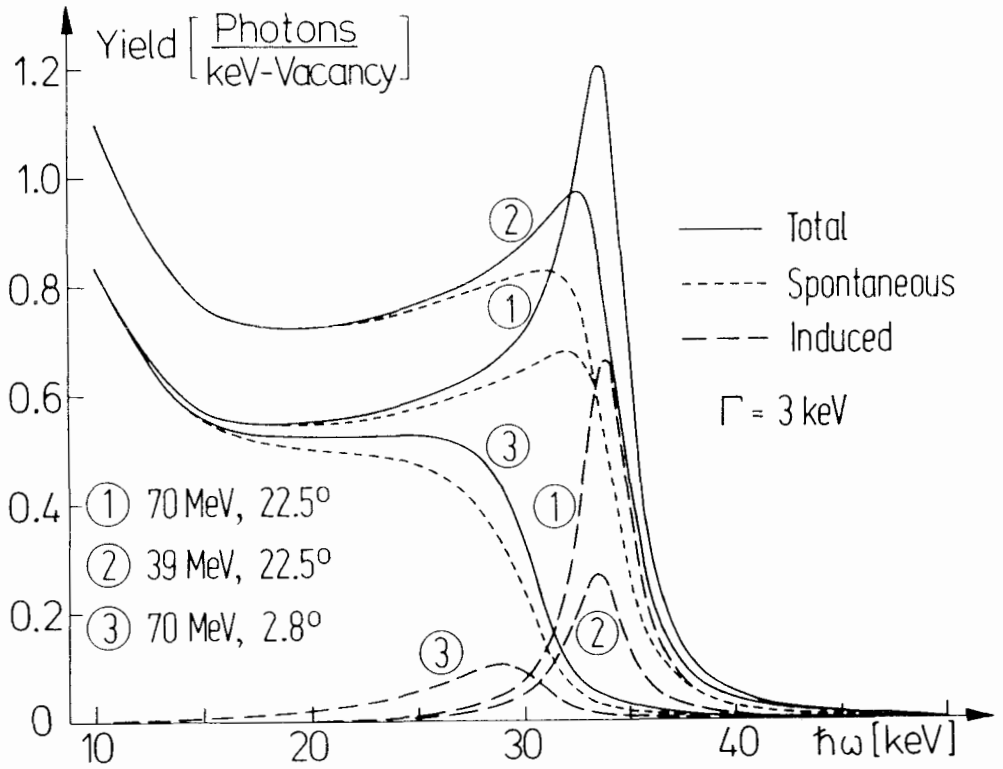

Fig.18: a) The MO-X-ray yield for coincidence experiments with 70 MeV Ni-Ni at (1) 11.2° and (3) 1.4° scattering angle, and (2) 39 MeV Ni-Ni at 11.2° scattering angle (all quantities in the Lab system). The solid lines show the total yield; the dotted and dashed lines the spontaneous and induced contributions, respectively. Observe that the peaks are strongly enhanced by the induced emission mechanism.

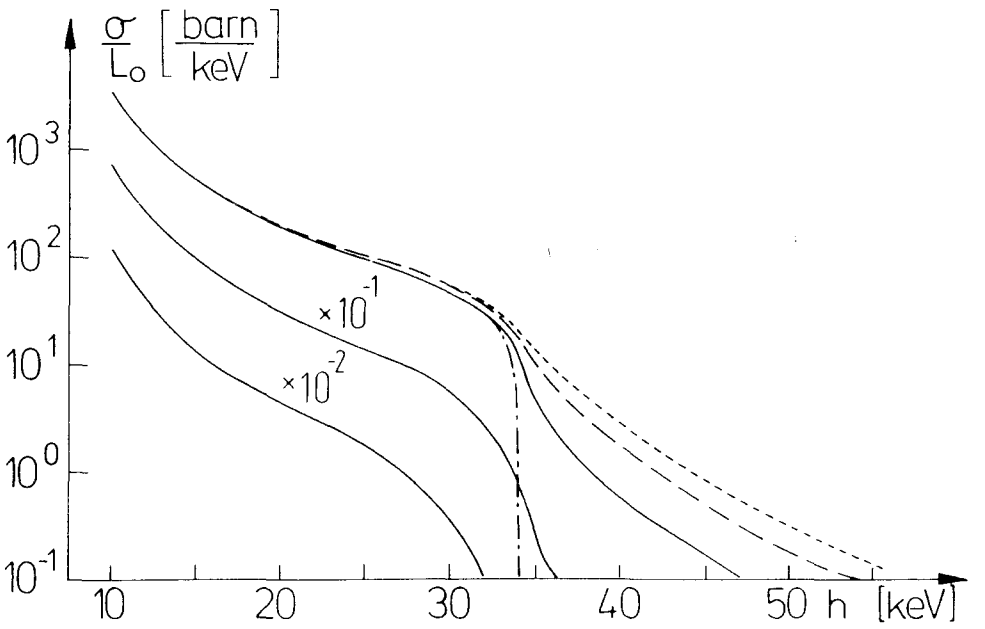

Fig. 18: b) MO-X-ray cross sections for the singles experiment Ni-Ni. (1) yield for 70 MeV collision. The solid line corresponds to Γ=1 keV, the dashed and dotted lines to 3 and 5 keV, respectively. The dashed-dotted lines give the spectrum without collision broadening which sharply cuts off at the limiting atom K_α-energy. (2) spectrum for 19 MeV collision, (3) for 5 MeV, both with Γ=1 keV. All quantities in the Lab system.

electron bremsstrahlung, transitions from higher MO's, interference effects between atomic and MO-X-rays,[37] and also the contribution of the slower recoil ions to the MO-X-ray production[33] are expected to contribute mostly in the low energy part of the X-ray continuum. This leads to a greater "filling up" of the spectrum shown in Fig. 18b at lower energies. It will be discussed in a forthcoming paper. The asymmetries (66) are shown in Fig. 19 for various alignments.

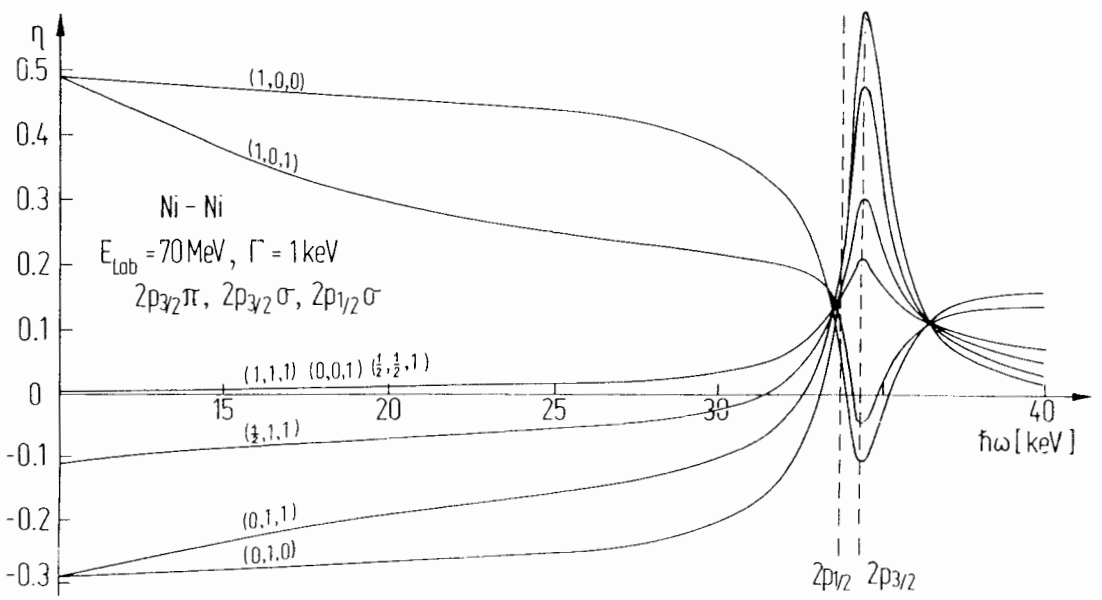

Fig. 19: The asymmetry as a function of photon energy for 70 MeV Ni-Ni collisions. The alignemnt (A^2,B^2,C^2) is indicated.

For not too small scattering energies they show a practically linear dependence on energy, which is to a large extent compensated by the inverse energy dependence of the width Γ. They exhibit a strong dependence on photon energy $\hbar\omega$, which is entirely due to the induced transitions. The observation of this effect by J.S. Greenberg and C.K. Davis[32,33] uniquely proves the existence of molecular X-rays and of induced transitions at the same time. We mention that recently P. Mokler and his collaborators[41] have also observed the asymmetry for the molecular m X-rays. The most important $\hbar\omega$-dependence of this asymmetry has also been established; which independently supports the observations of Greenberg et.al. and indicates further the Coriolis-induced radiations. Also Groeneveld et.al. find indications for the asymmetry in Ne-Si collisions, as does Meyerhof et.al.[43] for the Kr-Zr-system at high energies. These latter observations are less conclusive, however, because of the thick targets used in these experiments and the thus resulting mixture of asymmetries of two different molecular systems and the unknown Doppler- and recoil-effects in the secondary and multiple collisions.

The shape (peaking) of the coincidence spectra gives great hope for future spectroscopy of two center orbitals: Shifting of the peak with heavy ion energy, which in turn is related to the internuclear distance. In Ni-Ni collisions, e.g. it should ultimately be possible to determine the center of the peak to within a few hundred eV. This general feature should also hold for much heavier systems because the induced radiation always

comes from the "compound atom"-region of the two center level diagram. Experimentally this opens up the completely new field of X-ray spectroscopy of superheavy molecules which is of fundamental interest for quantum electrodynamics of strong fields. For example, in a system with $Z_1+Z_2 \sim 150$ the contribution of vacuum polarization from the Uehling potential is expected to be of the order of 5 keV for the $2p_{3/2}$-$1s_{1/2}$ transition and exceeds the selfenergy contribution. Thus it would be for the first time possible to measure vacuum polarization as the dominant quantum electrodynamical effect.

5.3 Induced Decay of the Neutral Vacuum in Overcritical Fields

The intermediate superheavy molecules can also be used to test the predicted decay of the vacuum in overcritical fields. The idea is pictorially shown in Fig.20.

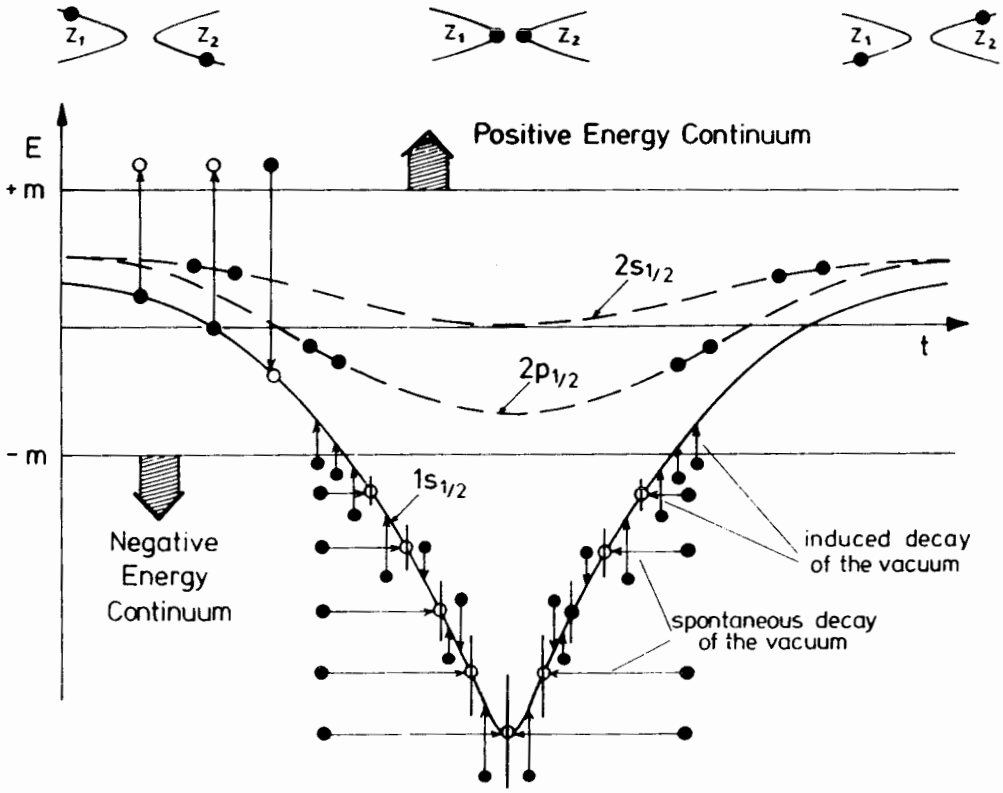

Fig. 20: The dynamical process occuring in connection with the decay of the vacuum in overcritical fields.

At large distances of the approaching nuclei the Fourier-frequencies descended from the changing Coulomb field should give rise to ionization of the K-shells. Such K-vacancies can also be produced by the Fano-Lichten[39] double collision process. At present it is unclear theoretically and experimentally which of the two processes is contributing dominantly and how much. We assume here, because we do not know better at this time, that 1 K-hole will be created in hundred collisions. After the field has become overcritical at distances $R < 36$ fm in e.g. an U-U-collision, it will be populated by e^+e-creations. The escaping positrons can then be observed experimentally as the indication for the decay of the vacuum. We shall study this process now more quantitatively.

Up to now calculations were done for the spontaneous positron creation (see sections 2 and 3). The cross sections will be increased, however, by two effects due to the nonadiabacity of the heavy ion collision: First, during the "diving"-process e^+e^--pairs are created in addition to the spontaneous ones by induced autoionization. Second, before and after the diving a large number of positrons will be created by induced transitions from the negative energy continuum to the $1s_{1/2}$-level. The latter transitions will occur even if there is no level-diving during the collision.

To calculate the total transition amplitude, all the transitions may be, approximately grouped into, first, pre- and after-diving amplitudes, $C_{PA,E}$ and, secondly, the during-

diving amplitudes, C_D. Then we have

$$C_{PA,E} = \int_{-\infty}^{-t_{CR}} dt' \exp \frac{i}{\hbar} \int_{-\infty}^{t'} dt''(E-E_{1s_{1/2}}(t'')) - \frac{1}{2\hbar} \int_{-\infty}^{t'} \Gamma(t'')dt'' \, M_E(t')$$

$$+ \int_{t_{CR}}^{\infty} dt' \exp \frac{i}{\hbar} \int_{-\infty}^{t'} dt''(E-E_{1s_{1/2}}(t'')) - \frac{1}{2\hbar} \int_{-\infty}^{t'} \Gamma(t'')dt'' \, M_E(t') \tag{68}$$

with

$$M_E(t') = - \langle\psi_E(t')|\frac{\partial}{\partial t'}|\varphi(t')\rangle \tag{69}$$

and $\Gamma(t'')$ represents the decay of the $1s_{1/2}$-level due to the interaction with the continuum (to be determined later). $|\psi_E\rangle$ and $|\varphi\rangle$are the wave functions for positron (negative energy continuum) and the $1s_{1/2}$-vacancy respectively. The time integration can be replaced by an integration over dR/v_R along the ion hyperbola, where R is the distance of the two ions and v_R the radial velocity.

The matrix element $M_E(t')$, can be computed by expanding the bound state, $|\varphi\rangle(t') \rangle = |\varphi(R)\rangle$, and the continuum states, $|\psi_E(t') = |\psi_E(R)\rangle$, which are eigenstates of the Hamiltonian, $H(R)$, about the $1s_{1/2}$ diving radius, $H(R)_{CR})$, i.e.

$$\begin{aligned} |\varphi(R)\rangle &= f(R)\{|\varphi_{CR}\rangle + \int dE' g_{E'}(R)|\psi_{E',CR}\rangle\} \\ |\psi(R)\rangle &= a(E,R)\{|\varphi_{CR}\rangle + \int dE' b_{E'}(E,R)|\psi_{E',CR}\rangle\} \end{aligned} \tag{70}$$

with the following normalizations

$$\langle\varphi(R)|\varphi(R)\rangle = 1$$

$$\langle\psi_E(R)|\psi_{E'}(R)\rangle = \delta(E-E') \tag{71}$$

$$\langle\psi_E(R)|\varphi(R)\rangle = 0$$

In this expression (70), the higher bound states, i.e. $2p_{1/2}$, $2s_{1/2}$, etc., have been neglected. Such effects are expected to be most important at large ion separations where the matrix element, $M_E(t)$, is small.

The matrix element (69) can now be written in terms of the expansion coefficients and reduces by use of Eq.(71) to

$$M = [a^*(E,R)f(R) \quad dE' b_E^*(E,R) \; [\frac{\partial}{\partial R} g_{E'}(R)]]v_R \tag{72}$$

To solve for the expansion coefficients, the following matrix elements are needed

$$\varepsilon(R) = \langle\varphi_{CR}|V(R)|\varphi_{CR}\rangle$$

$$V_E(R) = \langle\psi_{E,CR}|V(R)|\varphi_{CR}\rangle \quad (\gamma(E)/_{2\pi})^{1/2} \; \varepsilon(R) \tag{73}$$

$$V_{EE'}(R) = \langle\psi_{E,CR}|V(R)|\psi_{E',CR}\rangle$$

where $V(R) \equiv H(R) - H(R_{CR})$.

When the small contribution from the continuum-continuum matrix elements, $V_{EE'}(R)$, are neglected, the set of coupled channel equations may be easily solved[25,26] for the expansion coefficients. Upon substituting these coefficients into Eq.(72), the matrix element $M_E(t)$ may be readily computed. Once this matrix element is specified, the contribution from induced

transitions to the total transition probability may be approximated by (Eq.68))

$$W_{PA}\ (E_p, E_I, \theta) = |C_{PA}|^2 dE_p \tag{74}$$

where E_p is the positron energy. The dependence of this probability on the ion energy E_I, and the scattering angle θ enters through the time integrations over the Rutherford trajectory.

The during diving amplitude C_D is given by[25,26]

$$C_D = \frac{i}{h} \int_{-t_{CR}}^{t_{CR}} dt\ V_E(t) e^{\frac{i}{h} \int_{-\infty}^{t} dt'(E-E_{1s_{1/2}}(t')) - \frac{1}{2\hbar} \int_{-\infty}^{t} \Gamma(t')dt'} \tag{75}$$

with the corresponding diving probability

$$W_D(E_p, E_I, \theta) = |C_D|^2 dE_p \tag{76}$$

The total probability for producing a positron with an energy between E_p and $E_p + dE_p$ is then

$$W_T(E_p, E_I, \theta) = |C_{PA} + C_D|^2\ dE_p \tag{77}$$

To compute these probabilities, the functions $\gamma(E)$ and $\varepsilon(R)$ must be specified. The $\gamma(E)$ dependence, was extracted from the resonance in the one center continuum wave functions. $2\pi|V_E(R)|^2$ depend on both the charge Z and the separation R, as seen in Fig.21, the ratio $\gamma(E) = M_e c^2 \Gamma_E(R)/\varepsilon^2(R)$ depends only on energy to a good approximation. We used the approxi-

mation $\gamma(E) = \gamma_o (E-E_o)^2 \, e^{-\alpha (E-E_o)}$ where γ_o, E_o and α are parameters in the present calculations. While this energy dependence is based on one center calculation, we assume $\gamma(E)$ does not change appreciable when two center wave functions are used. The large width of $\gamma(E)$ enables one to use $\Gamma(R) = \overline{\gamma}_o \varepsilon^2(R)$ in the calculation of the line broadening (Eq.68)). The remaining function to be determined, $\varepsilon(R)$, was extracted from the Two-Center-Dirac-Model eigenvalues.

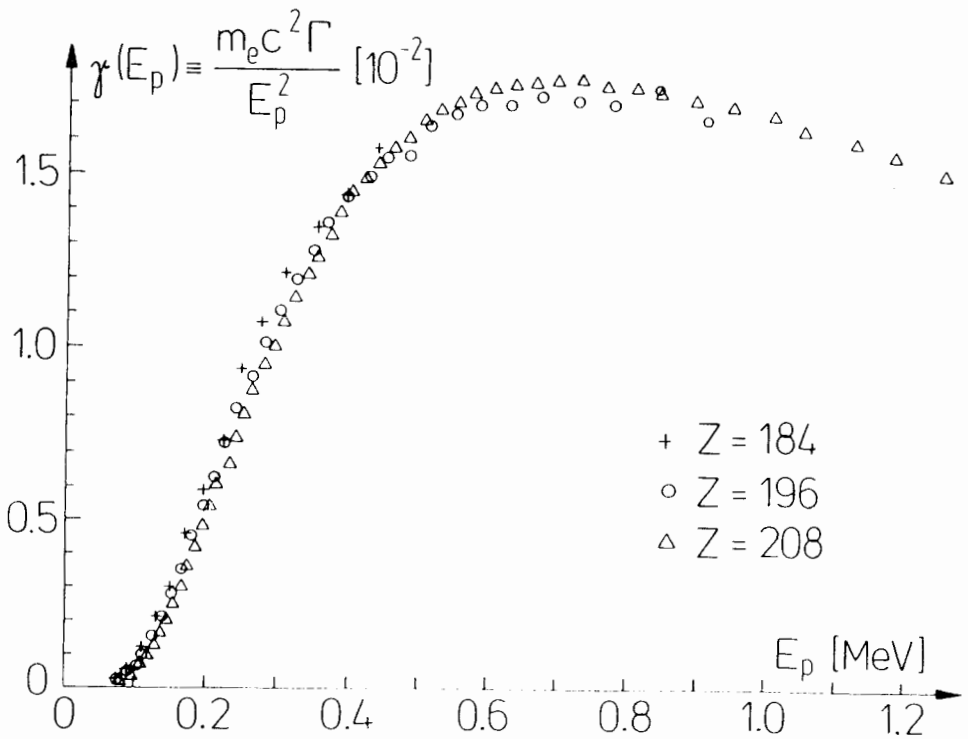

Fig. 21: The $\gamma(E_p)$-dependence plotted for $180 \leq Z \leq 210$, for distances greater than 15 fm (i.e. below the Coulomb-barrier). Obviously, $\gamma(E_p)$ does not depend on Z and R.

The quantities $W_{PA}(E_p,\Theta)$, $W_D(E_p,\Theta)$ are shown for the U-U-system in Fig. 22a). They are related to the cross section for positron production by $\frac{d\sigma}{dE_p d\Omega_{ion}} = \frac{d\sigma_R}{d\Omega_{ion}} L_o W(E_p,\Theta)$ where $d\sigma_R$ is the differential Rutherford cross section and L_o the initial K-hole probability, which has been taken in all our calculations to be $L_o = 10^{-2}$ (see Refs.[25,26]). This number has no justification. It is a simple guess. The present results of Meyerhof[43] contradict this guess; he estimates from his data $L_o \sim 10^{-5}$. This in turn is in contradiction to results of Burch, Vandenbosch et.al.,[44] who estimate from their findings in Cl-U-U-collisions $L_o \sim \frac{1}{2}$. Thus the situation is at present not quite clear, but encouraging and exciting.

Fig. 22b) shows the total ionization probability $W_T(E_p,\Theta)$. The full curves demonstrate that with decreasing ion energy E_I, the energies $\bar{E}_p$ for the maximal positron cross sections are shifted to smaller values. This possibly allows to some extent a spectroscopy of the diving mechanism. For fixed ion energy and varying scattering angle Θ, the energy maximum is only slightly shifted, as can be seen from the dashed curves.

The positron production cross section in the energy interval between E_p and $E_p + dE_p$ is given by integration of (30) over the angles

$$\frac{d\sigma}{dE_p} = L_o \int_o^{\pi} W_T(E_p,\Theta)\, d\sigma_R(\Theta) \quad . \tag{78}$$

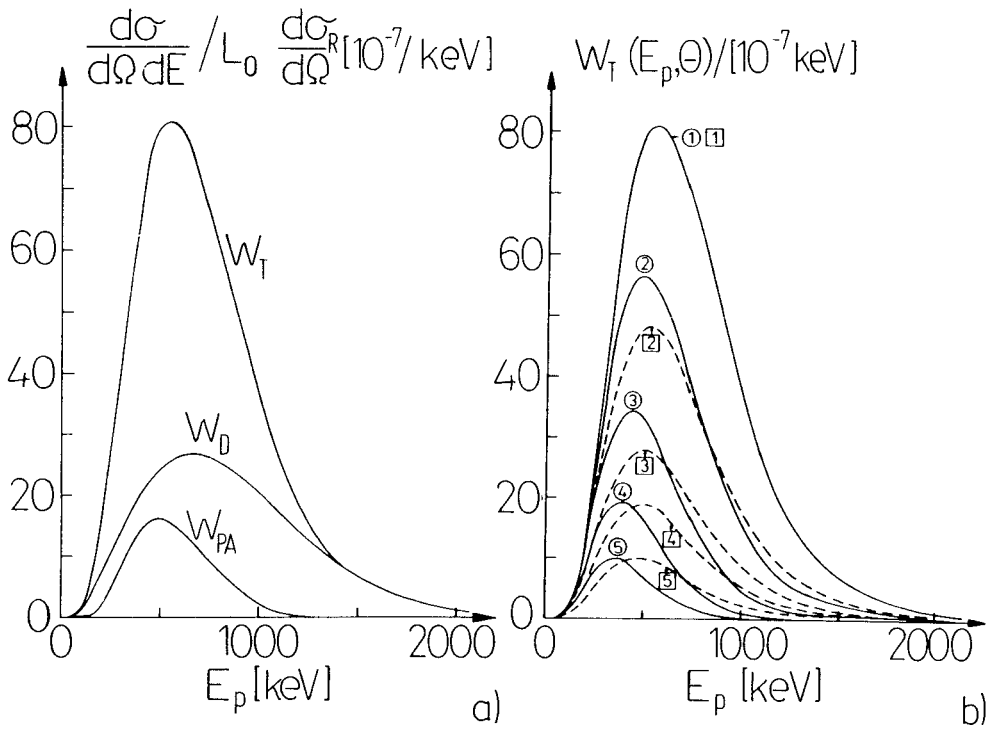

Fig. 22: a) The probabilities $W_{PA}(E_p,\Theta)$, $W_D(E_p,\Theta)$ and $W_T(E_p,\Theta)$ for the system $U \rightarrow U$ in the case of central collision with E_I = 812.5 MeV.

b) The full lines show $W_T(E_p,\Theta)$ at $\Theta = 180^o$ for the system $U \rightarrow U$ and its dependence on R_{Min} (distance of closest approach in fm), which corresponds to different ion energies (denoted in the brackets, units are MeV). (1) 15(815.5) (2) 20(609.4) (3) 25(478.5) (4) 30(406.3) (5) 35(348.2). In the last case $W_T(E_p,\Theta)\Theta = W_{PA}(E_p,\Theta)$ (no diving). The dashed curves show for fixed ion energy E_I=815.5 MeV the Θ-dependence (1) $\Theta=180^o$ (2) $\Theta=75^o$ (3) $\Theta=50^o$ (4) $\Theta=50^o$ (5) $\Theta=30^o$.

For different ion energies, $d\sigma/dE_p$ is shown for $U \rightarrow U$ in Fig.23 a). Compared with the purely spontaneous positron autoionization,[40] the dynamical, nonadiabatic effects lead to a "smearing out" of the sharply peaked excitation functions and to a considerable increase of the cross section by nearly two orders of magnitude.

To get the total positron cross section σ one has to integrate (78) over the positron energy E_p. As a function of the ion energy E_I, σ is shown in Fig.23 b).*

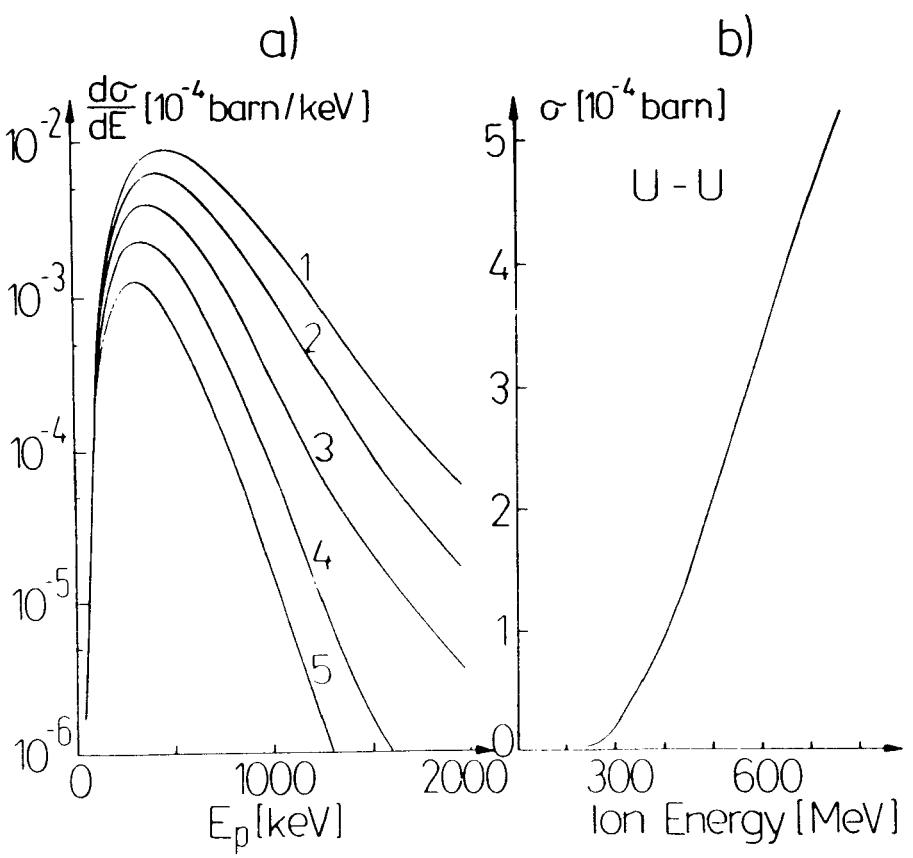

Fig. 23: a) The positron production cross section $d\sigma/dE_p$ for the system $U \rightarrow U$ for various ion energies. The energies are the same as in Fig.22 b)*.

b) The total positron cross section in dependence of the ion energy.*

It is considerably larger than the corresponding one for purely spontaneous positron autoionization.[40] This is due to the induced transitions (nonadiabatic effects). The vacuum thus decays - due to the nonadiabaticity introduced by the dynamics - as well spontaneously as by induction. In systems with higher total charge Z_1+Z_2, the transitions to higher levels ($2p_{1/2}$, $2s_{1/2}$) which come close to diving or are just diving ($2p_{1/2}$) must be taken into account and will further increase the cross sections. A spectroscopy of the diving orbitals, i.e. of the structure of the charged vacuum, should be possible by either studying the positron spectra in their dependence on heavy ion energy and their change with the total charge Z_1+Z_2 in the superheavy system. This, if done for lighter systems in a systematic fashion, should also yield information on the background effects. The vacuum structure can also be observed perhaps even more accurately, by spectroscopy of the molecular X-rays of the superheavy, overcritical system.

---

*The abscissa of the analogous figure in our original publication[26] was erroneous by a factor 10^{-4}. We thank Walter E. Meyerhof for drawing our attention to this scale error.

6. Broken Symmetry and Summary

Let us come back now to the question we started with in the introduction, which is the break down of the Sommerfeld-finestructure formula for $\frac{Ze^2}{r}$ -potentials at $Z \sim 137$. We can understand the physics at this "catastrophy" now as follows: In the finite radius of our supercritical systems ($Z > 137$) is made smaller and smaller, i.e. if the finite nuclei are made more and more point-like (highly compressed), the critical charge Z_{cr} (ocurrence of diving) will shift towards smaller values and approach Z=137 in the limit $R \to 0$. All $s_{1/2}$- and $p_{1/2}$-configurations dive in the limit at $Z = \frac{1}{\alpha} = 137$ perpendicular, i.e. the normal vacuum becomes tremendously unstable and decays into an infinitely charged vacuum.*

The change of the vacuum in overcritical fields is a most fundamental effect. It is a zero'th order effect unknown to the "waek-field-QED" commonly investigated. Its observation may shed now light to our understanding of field theories, and, in fact, may open a new and exciting field for experimental investigation. The concept of overcritical fields and the change of the vacuum state is not restricted to the electron-positron fields and electromagnetic interactions. It may also occur for other spinor fields (nucleons, quarks) and be caused by strong interactions. Indeed, J. Wolf,[46] has constructed along these ideas a quark-model of elementary particles, where nucleons, pions etc. are considered as <u>charged quark vacua</u>. The overcritical phenomena happen, of course, also for boson fields.

---

* The positron production due to the decay of the vacuum in highly relativistic heavy ion collisions should, because of the point-like structure of the intermediate system due to shock waves[48], tremendously increase.

Rafelski and Klein[47,48] have investigated and summarized various attempts for the understanding of overcritical pion fields. What is still lacking, and, in fact, quite unknown is the question to what extend such bosons are real bosons. If a pion is, for example, built out of the quark-antiquark Fermi-particles and if - as it seems - the pionic orbitals near the overcritical phenomena are rather small ($r_{pion} \sim$ 2-3 fm) it could very well happen that the complex structure of the bosons plays an important role. This has to be seen in analogy with the α-particles, which are the best massive bosons we know (superfluidity of Helium etc.) and still are no bosons if put together in e.g. an O^{16}-nucleus. In other words, their should occur again a stabilization of the overcritical vacuum for complex boson because of the Pauli-principle to which the constituent particles are subject to.

The study of overcritical systems in superdense nuclear matter occuring in shock-waves[48] of relativistic heavy ion collisions should thus shed light on very fundamental questions.

We finally remark that we are dealing here with a master example of a <u>broken symmetry</u>, which were invented mathematically by Goldstone[49], investigated and understood further by Higgs[50] and recently speculated about by Weinberg[51] in connection with a unification of the theory of weak and electromagnetic interactions. To understand this comment, let us make plausible the concept of broken symmetries with the following remarks:
The theory of electromagnetism and the electron-positron fields is generally gauge invariant. As a consequence of that we are

let to the continuity equation for the electric current, which in turn leads to charge conservation. Similarly both the electromagnetic theory and its coupling with the electron-positron field are generally invariant under charge conjugation, which leads directly to the symmetry between particles and antiparticles. Consider now our atoms built solely out of either protons (positive Z) with surrounding electrons and antiprotons (negative Z) with surrounding positrons. Then, for a given undercritical charge Z, we obtain the energy of the total system as a function of charge as shown in Fig.24 a). The groundstate of the total electron-positron field is obviously belonging to charge O; i.e. the vacuum has zero charge. This state has still the charge conjugation symmetry, as has the total system. The latter manifests itself in the left-right symmetry of Fig. 24a), while the former is indicated by the left-right symmetry of the minimum at Q=O. The local minima at higher energy correspond to stable charged atoms. Because the charge is quantized, they are separated along the abszissa in integers of e. These higher local minima as a function of e do no more show charge conjugation symmetry - though the overall world, i.e. the total Fig. 24a) shows it. We say, in these stable states the C-symmetry is spontaneously broken. In overcritical fields now we have a situation as shown in Fig.24 b). The groundstate has now become charged, i.e. the vacuum is charged and does no more show C-symmetry even though it exists globally. A tiny phsicist in an overcritical atom would perhaps not even notice that overall C-symmetry exists, because his vacuum (groundstate) does not show it. This situation is analogous to

the magnetization of a ferromagnet at temperature T (under-critical case) and near zero temperature (overcritical case).

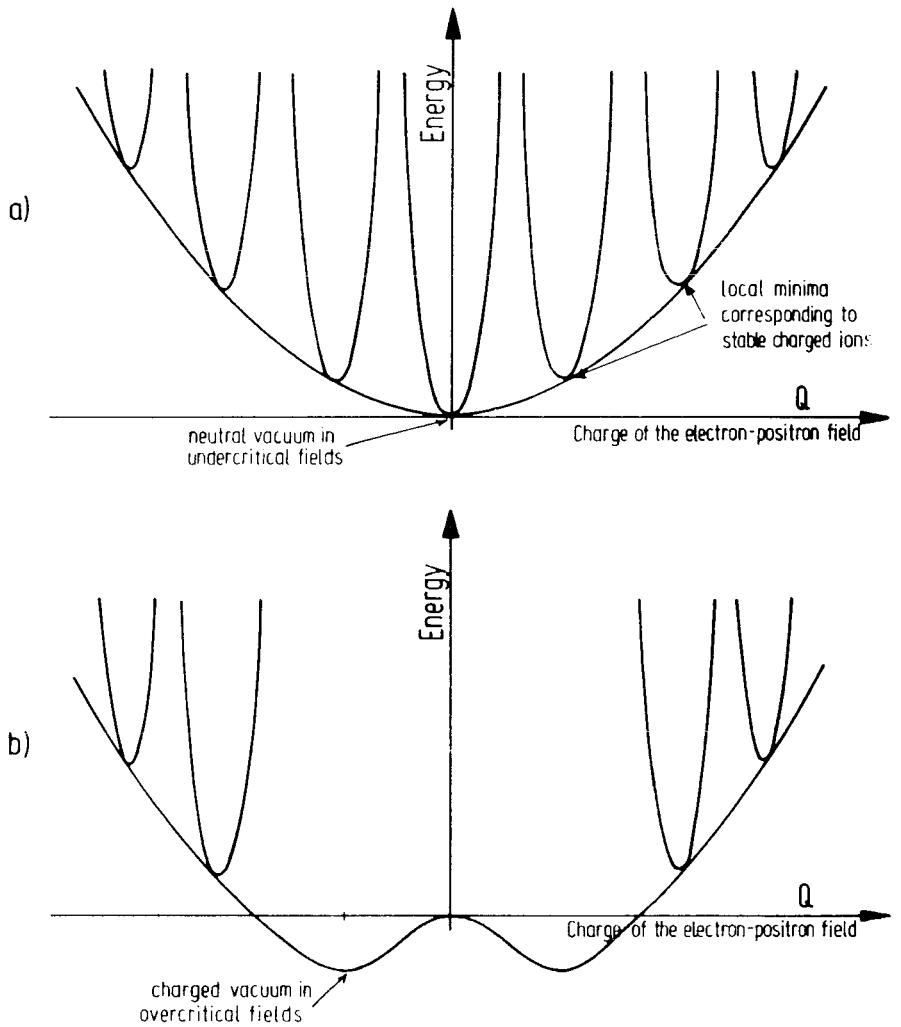

Fig. 24: Schematic drawing of the energy of the system against charge, which is thought to be continous. The quantization of charge at integer values can be imagined to occur because of stabilization potentials. In case a) the vacuum (groundstate) is symmetric under charge conjugation. This symmetry is broken in overcritical fields (case b)) where the vacuum is charged.

References

[1] W. Pieper and W. Greiner, Z. Physik 218 (1969) 327

[2] B. Müller, J. Rafelski, and W. Greiner, Z. Physik 257 (1972) 82 and 163

[3] U. Fano, Phys. Rev. 124 (1961) 1866

[4] P.G. Reinhard, W. Greiner, and H. Arenhövel, Nucl. Phys. A166 (1971) 173

[5] J. Rafelski, B. Müller, and W. Greiner, Nucl. Phys. B68 (1974) 585

[6] B. Müller and J. Rafelski, On the Hartree-Fock Appeoximation in Quantum Electrodynamics, to be published.

[7] M. Guylassi, thesis, University of California at Berkeley and Lawrence Berkeley Laboratory, 1974

[8] G. Soff, J. Rafelski, and W. Greiner, Phys. Rev. A7 (1973) 903

[9] M. Born, Am. Inst. Henri Poincaré 7 (1937) 155;
L. Infeld and B. Hofmann, Phys. Rev. 51 (1937) 765

[10] J. Rafelski, B. Fulcher, and W. Greiner, Il Nuovo Cimento, Vol. 13B (1973) 135

[11] J. Waldeck, diploma thesis, Institut für Theoretische Physik der Universität Frankfurt/Main, 1973

[12] W. Scheid, J. Hofmann, and W. Greiner, Nuclear Shock Waves and Pionization of Matter, Berkeley Symposium on Physics with Relativistic Ions, July 1974

[13] U. Mosel and W. Greiner, Z. Physik 217 (1968) 256;
J. Grumann, U. Mosel, B. Fink, and W. Greiner, Z. Physik 228 (1969) 371;
J. Grumann, T. Morović and W. Greiner, Z. Naturforsch. 26a (1971) 643;
A. Sobitcevsky, Proceedings of the Ronneby Conf., June 1974, see also contribution to the Intern. Conf. on Nucl. Physics, Munich (1973)

[14] The prediction of intermediate superheavy molecules in heavy ion collisions was made by the authors during the GSI-seminars 1969-1971 and first published in the article J. Rafelski, L. Fulcher, and W. Greiner, Phys. Rev. Lett. 27 (1971) 958

[15] W. Heitler, F. London, Z. Physik 44 (1927) 455;
E. Hylleraas, Z. Physik 71 (1931) 739;
E. Teller, Z. Physik 61 (1930) 458

[16] K. Helfrich and H. Hartmann, Theoret. Chim. Acta 3 (1965) 21

[17] see e.g. F.T. Smith, Phys. Rev. 179 (1969) 111

[18] S.K. Luke et.al., J. Chem. Phys. 50 (1969) 1644

[19] a) B. Müller, J. Rafelski, and W. Greiner, Phys. Lett. 47B, No 1 (1973) 5;
b) B. Müller and W. Greiner, The Two Center Dirac Equation, preprint, Institut für Theoretische Physik der Universität Frankfurt/Main, to be published

[20] W.E. Meyerhof, F.K. Saylor, S.M. Lazarus, W.A. Little, and B.B. Triplett, Phys. Rev. Lett. 30 (1973) 1279; Phys. Rev. Lett. 32 (1974) 502

[21] J.S. Greenberg, C.K. Davis and P. Vincent, Phys. Rev. Lett. 32 (1974) 1215

[22] P. Mokler, H.K. Stein, and P. Armbruster, Phys. Rev. Lett. 29 (1972) 827

[23] D. Burch, W.B. Ingalls, H. Wieman, R. Vandenbosch, preprints, University of Washington, Seattle (1973/74)

[24] B. Fricke, W. Greiner, and J.T. Waber, Theor. Chimica Acta 21 (1971) 235;
G. Soff and B. Fricke, GSI-report T 1-74 (1974)

[25] K. Smith, B. Müller, and W. Greiner, J. Phys.B, in print

[26] K. Smith, H. Peitz, B. Müller, and W. Greiner, Phys. Rev. Lett. 32 (1974) 554

[27] F.W. Saris, W.F. van der Weg, H. Tawara, and W.A. Laubert, Phys. Rev. Lett. 28 (1972) 717

[28] G. Presser, K.O. Groeneveld, and B. Knaf, Contribut. to the 4th Int. Conf. Atomic Physics, Heidelberg, July 1974

[29] J. Rafelski, B. Müller, and W. Greiner, Lett. il Nuovo Cim. 11 (1972) 469

[30] B. Müller, K. Smith, and W. Greiner, Phys. Lett. 49B (1974) 219

[31] B. Müller and W. Greiner, Phys. Rev. Lett. 33 (1974) 469

[32] J. Greenberg, C.K. Davis, and P. Vincent, Phys. Rev. Lett. 33 (1974) 473

[33] J. Greenberg, C.K. Davis, B. Müller, and W. Greiner, Proc. of the International Conference on Interactions between Nuclei, Nashville, Tenn., June 1974

[34] H. Tetrode, Ann. Physik 50 (1928) 336

[35] J. Reinhardt et.al., Multipole bremsstrahlung in heavy ion collisions, Inst. für Theoretische Physik der Universität Frankfurt/Main, March 1974

[36] Note that the expressions for the time dependent width and similar ones for the cross sections show rainbow-effects due to the time dependence of the matrix elements, of $\omega_{mn}(t)$ and $\Gamma(t)$ itself. Since these interference effects show up where the phase difference between contributions from approaching and separating ions along the scattering path are largest, they should occur most pronounced for low energetic transitions.

[37] K. Smith, B. Müller, and W. Greiner, Coherent effects in X-rays from intermediate molecular, preprint, Inst. für Theoret. Physik der Universität Frankfurt/Main, July 1974

[38] We aknowledge the help of W. Betz in the calculation of the level diagrams.

[39] U. Fano and W. Lichten, Phys. Rev. Lett. 14 (1965) 627

[40] H. Peitz, B. Müller, J. Rafelski, and W. Greiner, Lett. Nuovo Cim. 8 (1973) 37

[41] P. Mokler et.al., Invited paper at the 4th Int. Conf on Atomic Physics, Heidelberg, July 1974, and Phys. Rev. Lett. 33 (1974) 476

[42] K.O. Groeneveld and B. Knaf, Inst. für Kernphysik der Johann Wolfgang Goethe Universität Frankfurt/Main, private communication

[43] W.F. Meyerhof et.al., Contribution to the 4th Intern. Atomic Physics Conf., Heidelberg, July 1974

[44] D. Burch, V. Vandenbosch et.al., preprint from the University of Washington, Seattle (1974)

[45] H.E. Gove, F.C. Jundt, and H. Kubo, preprint University Rochester, Spring 1974

[46] J. Wolf, diploma thesis, Inst. für Theoretische Physik der Universität Frankfurt/Main, June 1974

[47] J. Rafelski and A. Klein, Instabilities of Matter in Strong External Fields and at High Density, Center for Theoretical Studies, Miami, Fla., January 1974

[48] See also W. Scheid, J. Hofmann, and W. Greiner, Nuclear Shock Waves and Pionization of Matter, Symposium on Physics with Relativistic Heavy Ions, Berkeley, July 1974

[49] J. Goldstone, Nuovo Cimento 19 (1961) 154

[50] P.W. Higgs, Phys. Rev. 145 (1966) 2156

[51] S. Weinberg, Phys. Rev. Lett. 29 (1972) 388; Phys. Rev. D8 (1973) 4482

Some Aspects of Nuclear Ion-Ion Potentials

Talk Given at Summer Study Group on Heavy Ions

Lawrence Berkeley Laboratory

July 1974

S.A. Moszkowski

University of California, Los Angeles

1. High Energy vs. Low Energy

a. Coulomb vs. Nuclear Interactions

I would like to discuss the nuclear aspects of ion-ion interactions at both low and high energies. At low energies, Coulomb effects are very important, Indeed, nuclear effects are significant only for small impact parameters, i.e., for large angle scattering. We can roughly say that for $\theta < \theta_{crit}$ Coulomb effects dominate, while for $\theta > \theta_{crit}$ nuclear interactions dominate, where θ_{crit} denotes a critical angle. According to a semi-classical description, the transition occurs when

$$V_{Coul}(R) = \text{Kinetic Energy}$$

where R denotes the distance between the ion centers when they are in contact, the sum of the ion radii. This implies that (if relativity is not taken into account):

$$\tan\left(\frac{\theta_{crit}}{2}\right) = \frac{Z_1 Z_2 \; e^2}{R\mu v^2} = \frac{V_{Coul}}{2 \times KE}$$

where

μ = reduced mass

v = relative velocity

As example, for two ions, each with $Z = 80$ and $A = 200$, we have

$R = 2 \times 6$ fm $= 12$ fm

$V_{Coul} \approx 1$ GeV

If $KE \approx 200$ GeV $\gg V_{Coul}$

$\theta_{crit} \sim 1^{o}$

Brink and Rowley[1] use the following criterion for the empirical determination of θ_{crit}, namely that at this scattering angle, the scattering cross-section is 1/4 of the Rutherford scattering cross-section (See Ref. 2).

b. Adiabatic vs. Sudden

In an adiabatic collision, the ions adjust to the different potential U when they get close. Thus, if and when the ions overlap, their density distributions spread out so that the total nucleon density is approximately the density of nuclear matter ρ_{NM}. On the other hand, if the collision happens suddenly, the nuclei do not have time to adjust their distributions. Thus in the region of overlap we have $\rho \sim 2\ \rho_{NM}$. (As we have heard from Greiner, we can get shock waves and even larger total densities in the region of overlap[3].)

A rough criterion for determining which of the two regimes is applicable is that for adiabatic (sudden) collision the kinetic energy per nucleon in the projectile is smaller (larger) than the average kinetic energy per nucleon in the target (i.e., about 30 MeV). An equivalent criterion is that the collision time is larger (smaller) than the time for a nucleon to cross the nucleus.

2. Zero Range Limit

A very simplified model of ion-ion interactions, but one that gives some useful insight, is the zero range model, i.e., that the nucleon-nucleon interaction is

$$V_{nn}(\vec{r}) = V_0 \delta(\vec{r})$$

We denote nucleons by n and nuclei by N. Then the nucleon-nucleus interaction is

$$U_{nN}(\vec{r}) = V_0 \rho(\vec{r})$$

(We neglect exchange terms throughout this talk.)

The nucleus-nucleus interaction is then given by

$$V_{NN} = V_0 \int \rho_A(\vec{r}) \rho_B(\vec{R} - \vec{r}) d^3r$$

where $\vec{r}$ (and $\vec{R} - \vec{r}$) are the positions relative to the centers of the nuclei A and B, and R is the distance between their centers, as sketched in Figure 1. The nuclear interaction occurs only when the two nuclei overlap, at least partially. This was studied by Vary and Dover[4]. Instead of using V_0 they determined V_{NN} directly from the nucleon-nucleon forward scattering amplitudes deduced using realistic nucleon-nucleon interactions

$$V_0 \rightarrow \frac{-2\pi\hbar^2}{m} f(0)$$

This will be discussed further by Vary later on.

3. Energy Dependence

a. At Low Energies

At low energies the nucleon-nucleus optical potential U_{nN} is strongly energy

dependent. On the other hand, V is proportionally less so. As a simple and very crude example, for A = 100 and E = 1 GeV, each nucleon has an average energy of 10 MeV. Now if U is written as

$$U_{nN} \sim U_0 \ (1 - \alpha E)$$

then

$$V_{NN} \sim AU_0 \ (1 - \alpha \frac{E}{A})$$

A more detailed derivation of the energy dependence of V_{NN} was given by Jackson and Johnson[5].

b. At High Energies

In the high energy region, say 1 Gev per nucleon, the use of a potential is questionnable. However, we can express the V_{NN} in terms of nucleon-nucleon scattering amplitudes, as was done by Vary and Dover[4] at lower energies.

The real part of V_{NN} is proportional to the real part of the forward scattering amplitude f(0) and is only weakly energy dependent. However, the imaginary part of f(0) must increase with energy, i.e., the scattering becomes absorptive and much larger than Re f(0). This can be seen directly from application of the optical theorem.

$$\text{Im } f(0) = \frac{p\sigma_T}{4\pi}$$

Here p is the momentum in units of $\hbar$. At high energy the total nucleon-nucleon cross-section σ_T is approximately constant. Thus Im F(0) for ion-ion scattering increases with energy. However, the nucleus-nucleus cross-sections approach constants

namely the geometrical values of $2\pi R^2$.

4. Finite Range Effects

a. Potential at Large Distances

The zero range approximation predicts no nuclear interaction unless the nuclei overlap. This is unrealistic since the nucleon-nucleon interaction has finite range. In fact, precision measurements of ion-ion cross-sections can give information regarding deviations from pure Coulomb interactions. This problem was studied by Brink and Rowley[1]. They considered the interaction between ^{84}Kr and ^{232}Th. They assumed a Woods-Saxon density distribution and assumed that the ρ and U_{nN} have the same surface thickness, but U extends out beyond ρ. This is sketched in Fig. 2. They fit the data,in particular θ_{crit}, quite well with $R \sim 1.04\ A^{1/3}$fm, slightly too small radii. Outside the surface, the density falls off exponentially

$$\rho \sim e^{-r/a}$$

and thus at large ion-ion distance the interaction is roughly given by

$$U \sim \rho^2 \sim e^{-2R/a}$$

When the nuclei just touch, their centers are apart by about 12 Fermis, and the nuclear interaction is calculated to be 50 MeV. When $R \sim 15$ fm, the ion-ion potential is still 4 MeV. This is a slight perturbation on the Coulomb energy of about 300 MeV. At low energies, the elastic ion-ion cross-sections depend mainly on the nuclear potentials at large R, as the Coulomb repulsion keeps the ions from approaching closely. Thus at low energy the finite range of the nucleon-nucleon potential is important. On the other

hand, at higher energies, the cross-sections depend more on V_{NN} at smaller distances.

b. Short Range Expansion

This is an improvement over the zero range approximation, and it may not be too bad. We consider a finite range nucleon-nucleon interaction $V_{nn}(r)$. Then $f(0)$ is proportional to $\int V(r)\, d^3r$ in the Born approximation (we ignore exchange terms). For a singular interaction (e.g., one containing a hard core), we use an effective interaction g which can be deduced from many body theory. Then,

$$f(0) \sim \int g(r)\, d^3r$$

The elastic nucleon nucleon cross-section is proportional to the square of the scattering amplitude $f(q)$

$$f(q) = \int g\, e^{i\vec{q}.\vec{r}}\, d^3r \simeq \int g\, d^3r - \frac{1}{6} q^2 \int g\, r^2 d^3r \;\; . \; . \; . \; .$$

where q is the momentum transfer.

The second term on the r.h.s represents the finite range effect. The ion-ion interaction is a series, of which the first two terms are written above. The first term

$$\int g\, d^3r \int \rho_A\, (\vec{r})\, \rho_B\, (\vec{R} - \vec{r})\, d^3r$$

is the same as for zero range, but the second:

$$\int g\, r^2 d^3r \int \vec{\nabla}\, \rho_A\, (\vec{r}) . \vec{\nabla}\, \rho_B\, (\vec{R} - \vec{r})\, d^3r$$

the finite range term, depends on the gradient of the density distributions at overlapping points. Thus even in this finite range approximation, there

has to be some overlap to get a finite V_{NN}.

c. Energy Density Formalism

This method can gives a somewhat more realistic formulation of V_{NN}. From nuclear many-body theory, the energy density e of nuclear matter is calculated[6] where

$$\int e\ [\rho(\vec{r})]\ d^3r = E$$

E = total energy of nucleus. However, the energy density of nuclear matter at very high density (say at twice or more of the normal nuclear density) is not well known. In any case, the nuclear ion-ion interaction is, according to the energy density formalism, given by the following expression[7].

$$V_{NN}(R) \equiv \int e\ [\rho_A(\vec{r}) + \rho_B\ (\vec{R} - \vec{r})]\ d^3r - (E_1 + E_2)$$

where E_1 and E_2 denote the energies of the separate nuclei.

d. Use of Density-Dependent Nucleon-Nucleon Interaction

This may be the best approach. It was recently used by Sinha.[8] He expressed the nucleon-nucleon interaction as the sum of a finite ranged interaction and a density dependent term to get saturation. Saturation means that the V_{NN} varies less strongly than linearly with ρ at high ρ. Such saturation, which is closely related to the saturation of nuclear matter, is an important result of the energy density formalism.[6] The simplest way to get a density dependence leading to saturation is to include zero range nucleon-nucleon repulsion with strength proportional to the density, i.e.,

$$V_{nn} \simeq \rho\delta\ (\vec{r})$$

The contribution of this interaction to V_{NN} is of the form

$$V_{NN} \sim \rho^3$$

for perfect overlap. The nuclear ion-ion potentials due to the total finite ranged plus density dependent delta interactions are calculated by Sinha[8] and are shown in Fig. 3. Sinha also includes terms involving gradients of the overlapping densities, such as of the kind mentioned in Section 4b.

5. Glauber Theory for High Energy Ion-Ion Scattering.

a. Basic Equations

The Glauber theory (known also as Eikonal approximation) has been used for many analyses of high energy nucleon scattering by nuclei[9], and recently also for heavy ion scattering. The first application of theory for high energy ion-ion scattering was given by Czyz and Maximon.[10] They assumed

(i) Small scattering angle elastic scattering, and

(ii) Colliding particles have a composite structure.

The elastic scattering amplitude is given by

$$F(q) = \frac{ip}{2\pi} \int d^2b \; e^{i\vec{q}.\vec{b}} \; (A\ B|\Gamma(\vec{b})|A\ B)$$

where b denotes impact parameter, A B is the wave function of the ion A-ion B system, and Γ is related to the absorption probability. The Γ can be expressed as a series:

$$\Gamma\ (b,s^A,s^B) = \sum_j^A \sum_k^B \Gamma_{jk}\ (\vec{b} - \vec{s}_j^{\,A} + \vec{s}_k^{\,B}) - \sum\sum\sum\sum \Gamma\ \Gamma + \ldots$$

The significance of s^A and s^B is illustrated in Fig. 4. The first sum represents the various possible single scatterings, the next term the double scatterings, etc. The bracket $\langle AB||AB\rangle$ can be replaced by an integral of the matter densities ρ_A, ρ_B

$$\langle A\ B|\Gamma(b)|A\ B\rangle = \iint \Gamma_{jk}(\vec{b} - \vec{s}_j^{\,A} + \vec{s}_k^{\,B})\ \rho_A\ (\vec{s}_j^{\,A})\ \rho_B(\vec{s}_k^{\,B})\ d^2s_j^{\,A}\ d^2s_k^{\,B}$$

for the single scattering jk term. Here $\rho_A(s) = \int \rho(\sqrt{s^2 + z^2})\ dz$, i.e., the integral of the density over the path $\vec{r} = \vec{s} + z\,\vec{k}$ $z = -\infty$ to ∞. Each Γ_{jk} is related to the nucleon-nucleon scattering amplitude by:

$$\Gamma_{jk}\ (b') = \frac{1}{2\pi ip} \int e^{-i\vec{q}'.\vec{b}'} f(\vec{q}')\ d^2q'$$

where the integration goes over momentum transfers $\vec{q}'$ perpendicular to the incident momentum.

At high energy, a good approximation of $f(q)$

$$f(q) = ip\ \frac{(1 - i\alpha)}{4\pi}\ \sigma_T\ e^{-\frac{1}{2}\beta^2\ q^2}$$

Note that the optical theorem is satisfied:

$$\mathrm{Im}\ f(0) = \frac{p}{4\pi}\ \sigma_T$$

The total cross-sections σ_T represent an average of np and pp cross-sections.

$$\sigma_T = (N\sigma_{pn} + Z\sigma_{pp})/A$$

For 1 GeV protons scattered by a nucleon at rest, an analysis of the empirical scattering crosssections yields:

$$\alpha = \frac{\mathrm{Ref}(0)}{\mathrm{Imf}(0)} = -0.27$$

and

$$\beta^2 = 4.7\ (\mathrm{Gev/c})^2$$

If (i) A and B $\to \infty$ (very heavy ions) and (ii) All pairs contribute equally to the scattering amplitude and (iii) Γ is strongly peaked compared to the matter distribution (short range interaction), then application of the Glauber theory gives:

$$F(\vec{q}) = \theta_{CM} \frac{ip}{2\pi} \int d^2b\ e^{i\vec{q}\cdot\vec{b}}\ (1-S)$$

$$S = e^{i\kappa}\int d^2s\ \ \rho_A(\vec{s})\ \rho_B(\vec{b}-\vec{s})$$

where θ_{CM} denotes a correction for center of mass motion, and S is the S-matrix at impact parameter b.

$$\kappa = \frac{1}{2} \; i \; (1 - i\alpha) \; A \; B\sigma_T$$

This expression represents the optical limit of the Glauber theory, i.e., the nucleus-nucleus interaction can be described by a potential V_{NN}, which is proportional to the exponent in S. In fact, V_{NN} turns out to be exactly the potential derived in the zero-range approximation by Vary and Dover.[4] At very high energy, $\alpha << 1$, κ is pure imaginary (since f is) and the above equation defines κ uniquely in terms of the nucleon-nucleon cross-sections.

b. Droplet Model

Recently, Wang and Lipes[11] have given a slightly different formulation of the Glauber theory for very high energy ion-ion scattering (2 GeV per nucleon). They assume that the ions can be regarded as droplets without substructure. They assume further, that the absorption is proportional, for any value of b, to the total amount of interpenetrating nuclear matter.

Thus, they get the same equations for f(q) and S as above, but now κ is taken to be simply a proportionality constant. This can also be done in the angular momentum representation and one obtains

$$F(q) = \frac{i}{2p} \cdot \sum_{\ell} \; (2\ell + 1) \; \left\{1 - e^{i\kappa B_\ell(p)}\right\} P_\ell \; (\cos\theta)$$

and $b_\ell(p)$ is essentially the partial wave amplitude associated with the form factor of the target. The total σ_T can then be obtained using the optical theorem.

$$\sigma_T(p) = \frac{2\pi}{p^2} \sum_{\ell} (2\ell + 1)\,(1 - e^{-x_0 B_\ell(p)})\,\mathrm{Cos}\,(\alpha\, x_0\, B_\ell)$$

where $x_0 \doteq \kappa/(i + \alpha)$ = real. Their calculations show that the value of α affects the σ only near the diffraction minima, and does not change the pattern much even for α as large as 0.5. It is interesting to compare the diffraction patterns with that for n-n scattering to compare the amount of transparency in N-N scattering compared to n-n.

c. Black Sphere Model (Ref. 11)

This is a limiting case of the droplet model We assume

$$S(b) = 0 \qquad b < R_1 + R_2 = R$$

$$= 1 \qquad > R_1 + R_2 = R$$

Then one finds the well known results.

$$\frac{\sigma(q)}{\sigma(0)} = \left(\frac{2\, J_1(q\, R)}{qR}\right)^2$$

This Fraunhofer diffraction pattern is well approximated, especially if the nuclei have sharp surfaces. For forward scattering the black sphere model gives:

$$F(0) = \frac{ip}{4\pi}\,\sigma_T = \frac{ip}{2}\,(R_A + R_B)^2$$

and thus

$$\sigma(0) = |F(0)|^2 = \frac{p^2}{4}(R_A + R_B)^4$$

Comparing different ion-ion scatterings with center of mass momenta p and p' respectively, we find

$$\frac{\sigma_{AB}(0)}{\sigma_{A'B'}(0)} = \frac{p^2}{p'^2} \quad \frac{(R_A+R_B)^4}{(R_{A'}+R_{B'})^4}$$

This provides a good first order estimate of any heavy ion elastic scattering at high energy.

d. Results of Calculations

The droplet model was applied by Wang and Lipes[11] to the calculation of σ_{NN} at very high energies (2 GeV per nucleon).Fig. 5 shows the calculated differential cross-sections vs. t, the negative square of the momentum transfer, for ^{4}He and ^{12}C ions. The ratio $\sigma(q)/\sigma(0)$ vs. αR for several pairs of ions is plotted in Fig. 6. This shows the approach to the black sphere case. The positions of the maxima and minima are the same for all cases, but the $\sigma(q)$ depend on the diffuseness, especially at large angles. The black sphere limit gives too much backscattering. Note that at these high energies, the total and forward elastic cross-sections are directly related via the absorption parameter κ , since Re f(0) << Im f(0). It

will be interesting to compare for example, high energy He and ^{16}O scattering to study the effect of the diffuseness in the two cases.

6. Short Concluding Remarks

High energy heavy ion-ion scattering experiments may shed light on the behavior of high density nuclear matter and possibly also on high energy behavior of effective nucleon-nucleon interactions, and of nuclear transparencies.

References

1. D.M. Brink and N. Rowley, Nucl. Phys. A 219, 79, 1974
2. W.E. Frahn, Ann. of Phys. 72, 524, 1972
3. W. Scheid, H. Müller and W. Greiner, Phys. Rev. Lett. 32, 741, 1974
4. J.P. Vary and C. B. Dover, Phys. Rev. Lett. 31, 1510, 1973
5. D.F. Jackson and R.C. Johnson, Phys. Lett. 49B, 249, 1974
6. K.A. Brueckner, J.R. Buchler, R.C. Clark, G. Jorna and R.J. Lombard, Phys. Rev. 171, 1188, 1968; Phys. Rev. 181, 1543, 1969
7. J. Galin, D. Guerran, M. Lefort and X. Tarrago, Phys. Rev. C9, 1018, 1974
8. B. Sinha, Phys. Rev. Lett. 33, 600, 1974
9. See, for example, R.J. Glauber and G. Matthiae, Nucl. Phys. B21, 135, 1970, and J.P. Auger and R.J. Lombard, Phys. Lett. 45B, 115, 1973
10. W. Czyz and L.C. Maximon, Ann. of Phys. 52, 59, 1969
11. W.L. Wang and R.G. Lipes, Phys. Rev. C9, 814, 1974

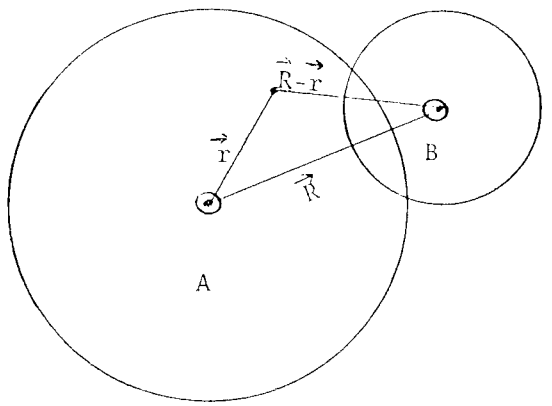

Figure 1. Geometry of ion-ion collision

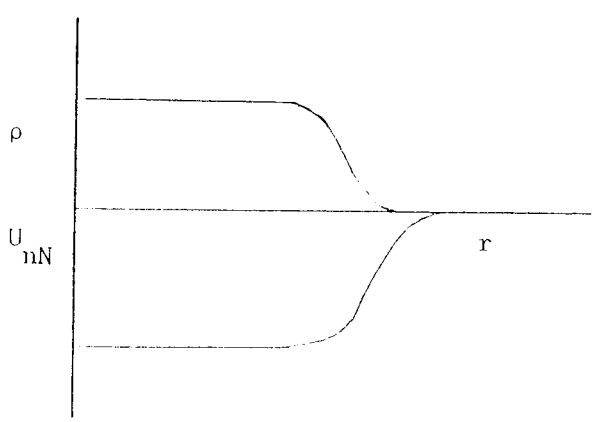

Figure 2. Illustrating the relation between nucleon density and nucleon-nucleus potential

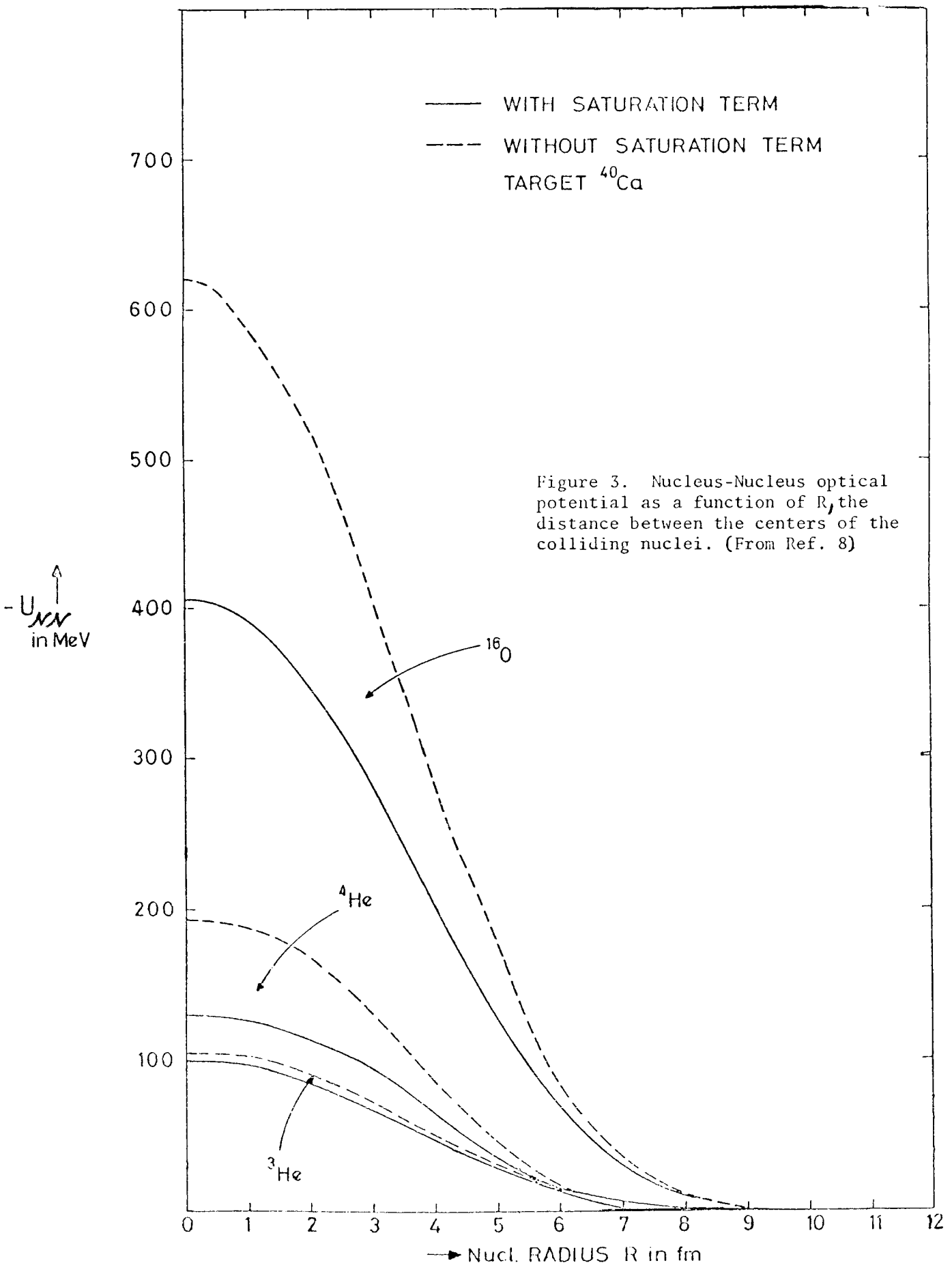

Figure 3. Nucleus-Nucleus optical potential as a function of R, the distance between the centers of the colliding nuclei. (From Ref. 8)

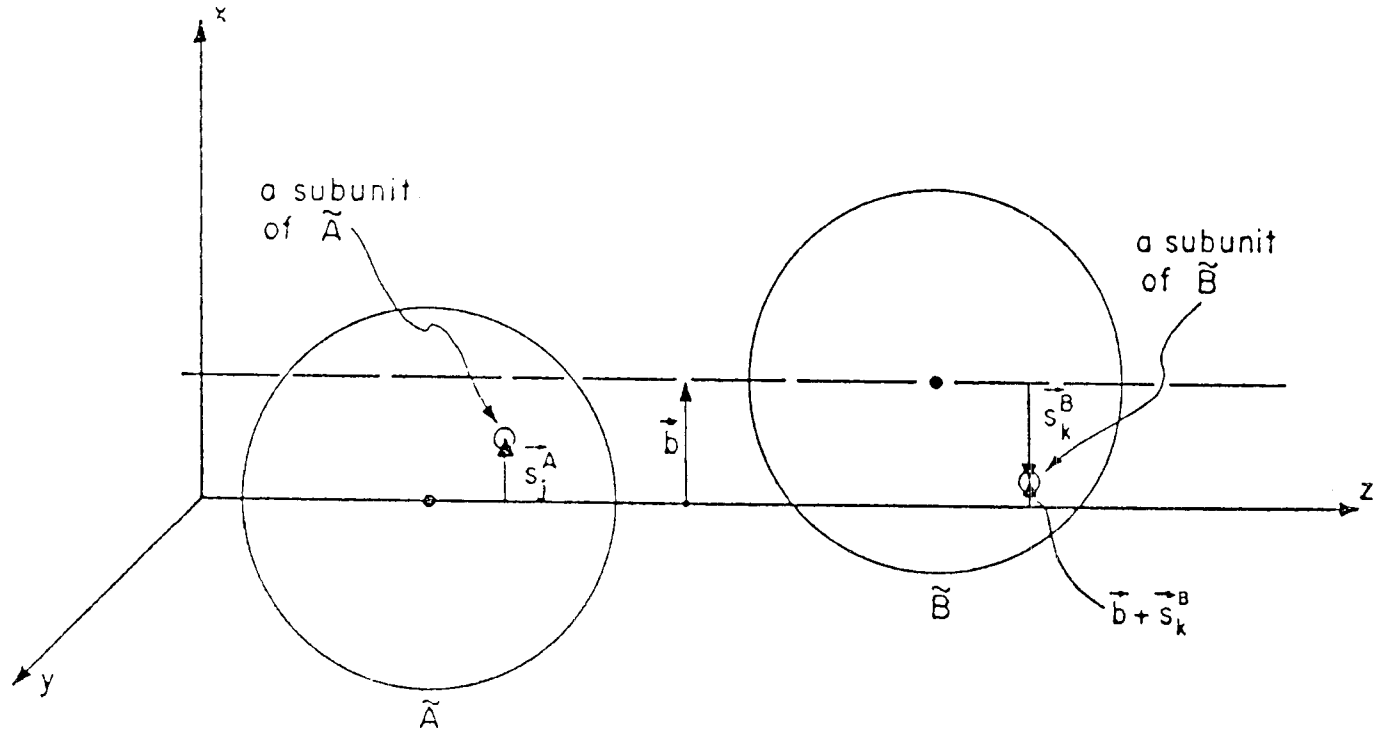

Figure 4. Definitions of the coordinates used in the formulae for the amplitudes of two composite objects colliding elastically. If we call Γ_{jk} the profile function of the collision of the subunits j and k, from the geometry depicted above we see that the argument of Γ_{jk} is $\Gamma_{jk}(\mathbf{b} - \mathbf{s}_j^A + \mathbf{s}_k^B)$.

(From Ref. 10)

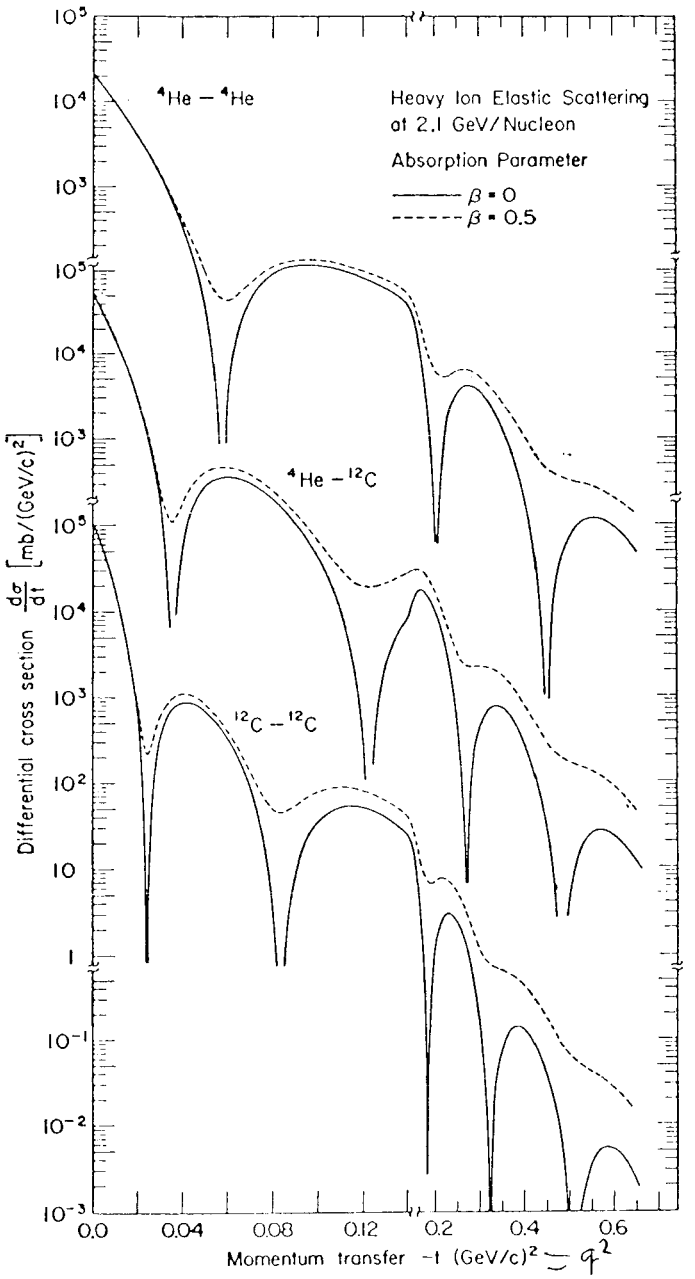

Figure 5. Differential cross sections for ^{4}He-^{4}He, ^{4}He-^{12}C, and ^{12}C-^{12}C elastic scattering. The solid line is obtained using a purely imaginary x, i.e., $x = ix_o$; the dashed line corresponds to $x = (\beta + i)x_o$, with a large real part $\beta = 0.5$. The real part does not affect the diffraction pattern very much, except at the minima or large momentum transfer. The diffraction patterns shown here are independent of the incident energy.

(From Ref. 11)

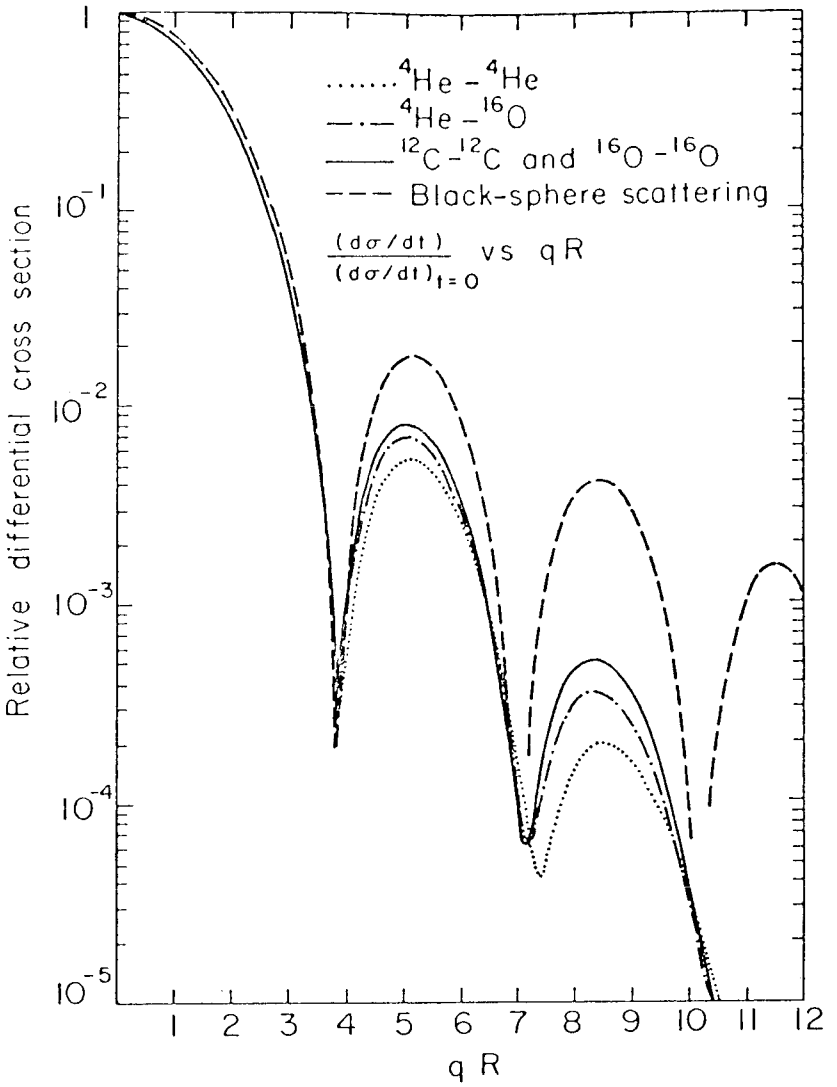

Figure 6. Differential cross sections in "scaling coordinates." We plot the relative cross section $(d\sigma/dt)$ to the forward cross section $(d\sigma/dt)_{t=0}$, versus qR, where q is the momentum transfer and R is the effective radius $R = R_1 + R_2$. The differential cross sections seem to scale. The ^{12}C-^{12}C, ^{12}C-^{16}O, and ^{16}O-^{16}O are essentially indistinguishable on this plot. The ^{4}He scattering deviates from asymptotic form, probably due to its diffused surface. The long dashed line is the prediction of a sharp cutoff model (black-sphere scattering).

(From Ref. 11)

Microscopic Models for Heavy Ion Scattering at Low, Intermediate and High Energies*†

J. P. Vary and C. B. Dover

Brookhaven National Laboratory, Upton, New York 11973

ABSTRACT and SUMMARY

We trace the evolution with energy of a lowest-order microscopic model for nucleus-nucleus interactions from 10 MeV/nucleon to 1 TeV/nucleon incident energies. There are three essential questions investigated; first, what is the interaction and how carefully must we obtain its ingredients; second, what is the appropriate dynamical framework in which to employ this interaction; and third, for what processes do we expect this lowest order model to be valid. To answer the first question, we present a development of an optical potential model obtained by folding the densities of the interacting nuclei with a suitably renormalized nucleon-nucleon force. At low energies (< 50 MeV/nucleon) there is sufficient data to demonstrate marked sensitivity to the choices of density and range of the elementary force. When the densities are taken with correct asymptotic properties and the interaction has a

---

* Work performed under the auspices of the U.S. Atomic Energy Commission.

† Invited paper for the Second High Energy Heavy Ion Summer Study, Lawrence Berkeley Laboratory (July 15-26, 1974), presented by J. P. Vary.

one-pion exchange range good agreement with the available α particle data is obtained in the diffractive region of elastic scattering. Comparison with the data in this lower energy region also demonstrates that all the parameters appear to be calculable. Predictive power is thus obtained. The energy dependence of the important density overlap region is then studied. In the elastic channel the density overlap is shown to increase with energy so that the surface and interior region of the nucleus-nucleus interaction becomes more important at higher energies. For the dynamical framework, in answer to the second question, we employ the Schrödinger equation at low energy and examine how the results may be approximated by an eikonal treatment at intermediate (40-70 MeV/nucleon) energies. The differences between an eikonal approximation and the optical limit of the Glauber approximation are seen to be very important in this region. Here, the Glauber approximation with, possibly, a Pauli correction can do better than the simple eikonal. This is possible since there are up to 40% differences in the interaction strengths required to fit the 40 MeV/nucleon data in the Schrödinger and Glauber frameworks. To answer the third question we show how the lowest order optical potential is useful for peripheral processes at low to moderate energies in the Schrödinger framework. However, with increasing energy, as the impulse approximation becomes more valid, the model may be extended for use with other processes as well. Results have been obtained by Barshay, Dover and Vary with a Glauber approach at Bevalac energies (0.1-4.0 GeV/nucleon) to examine the question of whether the nucleus-nucleus total, reaction, and elastic cross-sections factorize. We find that factorization holds to 20% if the radii of the projectile and target nuclei do not differ by more than 50%. This fact and the gross violation of factorization when the nuclei are very different in size

are interpreted in the context of a simple geometric model. Within this same microscopic framework we discuss mean multiplicites of particles produced in nucleus-nucleus collisions at high energies. We perform this calculation by an extension of the methods proposed by Dar and Vary to obtain multiplicities in nucleon-nucleus collisions. It is concluded that moderate to heavy target multiplicities and their energy dependence in nucleus-nucleus collisions will help distinguish between the various types of proposed production mechanisms. If, as is suspected based on present nucleon-nucleus results, a two step mechanism is involved, then nucleus-nucleus collisions are found to offer a unique opportunity to study the interactions of the intermediate particles (clusters, fireballs, or whatever). Production of a super fireball is contemplated and some consequences are delineated.

I. INTRODUCTION AND MOTIVATION

With the advent of heavy ions at high energies a very broad research field has opened up. It potentially bridges the gap between conventional nuclear physics, high energy physics and nuclear chemistry. Researchers from these fields have been drawn together by the exciting possibilities envisaged with beams of high energy heavy-ions.

It is our belief that the methods of microscopic nuclear theory will play an important role in many high energy heavy-ion studies. The simple approach we propose should provide a backdrop of results which forms a basis for analyses of experiments and comparison with other models. Two applications we discuss here in the microscopic framework are the questions of factorization and mean multiplicites in multiparticle production. These exemplify our viewpoint in two ways. First, as in the case of factorization, it provides

a set of predictions which could serve as a guide in mapping out experimental programs that concentrate on regions of behavior where the conventional microscopic approach disagrees with other hypotheses. Second, as in the case of multiplicities, this model can be coupled with a selection of particle-physics models (for the multiparticle production mechanisms) to exploit the many nucleon media and determine which of the particle-physics models are tenable and which are not.

II. MODEL FOR THE POTENTIAL VIA ANALOGY

For pedantic purposes it is convenient to first sketch the main results by means of analogy with the static Coulomb potential between two distributed charges such as displayed in Fig. 1. If $\vec{r}$ is the radius vector separating the two centers of charge defined in analogy with the center of mass then the classical static potential is just

$$U_{coul}(\vec{r}) = \int d^3r_1 \; \rho_1(\vec{r}_1) \int d^3r_2 \; \rho_2(\vec{r}_2) \; \frac{e^2}{|\vec{r} + \vec{r}_1 - \vec{r}_2|} \tag{1}$$

where $\vec{r}_1$ and $\vec{r}_2$ are internal radial vectors locating points of charge within their respective distributions ρ_1 and ρ_2. In order to pass to the strong interaction situation we replace the Coulomb force, e^2/r, by an appropriate short ranged nucleon-nucleon interaction, $v(\vec{r})$

$$V(\vec{r}) = \int d^3r_1 \; \rho_1(\vec{r}_1) \int d^3r_2 \; \rho_2(\vec{r}_2) \; v(\vec{r} + \vec{r}_1 - \vec{r}_2) \tag{2}$$

If we, in addition, make the assumption of a zero ranged nucleon-nucleon interaction

$$v(\vec{r} + \vec{r}_1 - \vec{r}_2) \sim \gamma\delta^3(\vec{r} + \vec{r}_1 - \vec{r}_2) \tag{3}$$

we obtain

$$V(\vec{r}) \sim \gamma \int d^3 r_2 \; \rho_1(\vec{r}_2 - \vec{r}) \; \rho_2(\vec{r}_2) \tag{4}$$

It can be shown that the appropriate constant in the limit of high energy nucleus-nucleus scattering is

$$\gamma = -\frac{2\pi\hbar^2}{M} \; f(0) \tag{5}$$

where M is the nucleon mass and f(0) is the complex forward nucleon-nucleon scattering amplitude evaluated at the incident lab energy per nucleon. This then yields our first and simplest approximation to the lowest order optical potential for ion-ion interactions

$$V_{opt}(\vec{r}) = -\frac{2\pi\hbar^2}{M} \; f(0) \int d^3 r' \; \rho_1(\vec{r}' - \vec{r}) \; \rho_2(\vec{r}') \tag{6a}$$

It is already clear that this form of the model ignores the spin and isospin degrees of freedom of the nucleons though the above treatment is easily generalized to this level. Nowhere did the spin statistics enter so the Pauli principle has been ignored except to the extent it participates in the one body density distributions. Dispersive effects due to, among other things, the polarizability of the two distributions have not entered. Indeed, the analogy with Coulomb potentials clearly neglects <u>all</u> rearrangement processes. The internal Fermi motion of the constitutents and binding effects (off-shell effects) also remain to be included. Theoretical adjustments to f(0) that approximately correct for some of these inadequacies will be introduced and studied.

We explain in more detail below an extension to include finite

range which results in an improved form of V_{opt}, namely

$$V_{opt}(r) = -\frac{2\pi\hbar^2}{M}\frac{\bar{f}(0)}{(\pi\bar{\gamma}^2)^{3/2}}\int d^3r_1\rho_1(\vec{r}_1)\int d^3r_2\rho_2(\vec{r}_2)e^{-|\vec{r}+\vec{r}_1-\vec{r}_2|^2/\bar{\gamma}^2} \tag{6b}$$

where $\bar{\gamma}$ is a range parameter and $\bar{f}(0)$ includes certain many-body effects. This additional complexity is shown to be essential in achieving a high quality description of the low-energy data.

At this point all ingredients are, in principle, calculable or obtainable by independent measurements. Is this adequate to explain the ion-ion data at low energies? As a consequence of the many approximations one may suspect it is not. Therefore we assume that some of the remaining important corrections can be simulated by adjusting $\bar{f}$. This is the degree to which we are willing to confess our ignorance at low energies. A two-pronged effort is thus necessary to test a model whose geometry is fixed by our knowledge of nuclear densities and the range of the nucleon-nucleon force. We both calculate $\bar{f}(0)$ theoretically and fit the experimental data to obtain the "best fit" $\bar{f}(0)$. Comparing the thoeretical and best fit results for $\bar{f}(0)$ and the quality of the angular distributions instructs us on the validity and shortcomings of the model. This distinguishes the present effort from those of other investigators[1-11] of various semi-microscopic models.

The effort as outlined above was initially conducted[12] with densities taken from fits to electron scattering data. This approximation as well as a zero-ranged force with a phenomenological strength were found useful for some peripheral ion-ion processes. However, a desire to understand the strength constant on a theoretical basis has led to a set of improvements.

In this talk we outline the improved low energy results (10-40

MeV/nucleon) obtained with a more careful treatment of the densities coupled with a finite range nucleon-nucleon force. Only after carefully treating densities and range effects can one extract an understanding of the role of many-body effects exhibited in the ion-ion interaction data. Specifically, we concern ourselves with how these many body effects evolve with energy. It will also be argued why this complexity is considerably less important as one goes to higher energies and heavier projectiles.

III. DYNAMICAL FRAMEWORK

There is, of course, a vast body of literature dealing with theoretical approaches to the nucleon-nucleus potential and its appropriate dynamical framework. There is much overlap of ideas but also many subtle differences in these approaches. It is beyond the scope of this talk to attempt to summarize, categorize or even refer to these efforts. The model we deal with here may easily be obtained from some of the above mentioned efforts by straightforward extension.

In a forthcoming work[13] we present an approach which maintains close contact with standard non-relativistic many-body theory. Here we only summarize the assumptions and the conclusions of such a model.

In the center of mass of two interacting nuclei, 1 and 2, we describe the system by the total Hamiltonian

$$H = T_{12} + V_{12} + H_1 + H_2 \tag{7}$$

where H_1 and H_2 represent the internal Hamiltonians for the two nuclei which consist of A_1 and A_2 nucleons respectively, T_{12} represents the kinetic energy operator of relative motion and V_{12} is the interaction potential between them. We assume only two-body forces, v_{ij}, for the nucleus-nucleus interaction

$$V_{12} = \sum_{i=1}^{A_1} \sum_{j=1}^{A_2} v_{ij} \tag{8}$$

We assume a complete set of internal solutions are obtainable

$$\begin{aligned} H_1\Phi_1^n &= \epsilon_1^n\Phi_1^n \\ H_2\Phi_2^n &= \epsilon_2^n\Phi_2^n \end{aligned} \tag{9}$$

where n indexes solutions sequentially (n=0 being the ground state) and passes to a continuous variable for scattering solutions. The proper solutions are internally antisymmetric and functions of $3A_1$-3 and $3A_2$-3 variables respectively.

The problem to solve is

$$H\psi = E\psi \tag{10}$$

Let us restrict ourselves first to elastic scattering (throughout this talk "elastic" refers to the case where the projectile and target are in their ground states intially and finally while inelastic includes all other scattering states) for which a convenient expansion of the total wavefunction is just

$$\psi = \mathcal{a} \sum_{m,n} \varphi_{mn}\, \Phi_1^m\, \Phi_2^n \tag{11}$$

where $\mathcal{a}$ represents the operator that antisymmeterizes the nucleons of 1 with those of 2 and φ_{mn} is the ion-ion relative motion wave function.

If we denote by α_1 and α_2 the $3A_1$-3 and $3A_2$-3 internal coordinates and form the following inner product

$$\int (\Phi_1^0\, \Phi_2^0)^* \,(H-E)\, \psi\, d\alpha_1 d\alpha_2 = 0 \tag{12}$$

one may obtain an infinite set of coupled integro-differential equations[13]

$$(T_{12} + V - E)\varphi_{00} = \text{everything else} \tag{13}$$

where V is given by Eq. (2) when the nucleon-nucleon force is assumed local, and spin and isospin independent. Thus we have formally obtained the appropriate dynamical framework in which to employ the simple potential given by Eq. (2). All the exchange processes between the two ions, the coupling to breakup and other inelastic channels, etc., has been shifted to the right hand side of Eq. (13).

The formal solution to the model at this stage is not attainable for two reasons. First, the nucleon-nucleon potential may possess a hard core which would cause the nucleus-nucleus potential, V, to diverge. Second, the couplings to an infinite number of channels on the RHS of (13) are not numerically tractable.

In order to proceed we need to employ some multiple scattering summation. If we were to follow Kerman, McManus and Thaler[14] we would invoke the Watson, on-shell, multiple scattering formalism and expect the model only to be useful at very high energies since it neglects many body effects. Instead we wish to obtain results for lower energy regions where the comparison with data is feasible in order to test the model. Thus we follow the spirit of Hüfner and Mahaux[15] and invoke a Brueckner multiple scattering summation defined by

$$\mathcal{g}(E) = v + v \frac{Q}{E-H_0+i\epsilon} \mathcal{g}(E) \tag{14}$$

where H_0 is some appropriate two-center single particle Hamiltonian and Q is the Pauli operator that forbids intermediate two particle states

which are normally occupied. We interpret $\mathcal{G}(E)$ as the full two particle scattering operator in the two-ion medium. It represents a sum of an infinite series of v interactions where one nucleon in the projectile scatters with one in the target through all available one-particle one-hole excitations of the projectile and target.

In the limit of two heavy ions uniform over all space the $\mathrm{Im}\,\mathcal{G}(E,\theta=0)$ is proportional via the optical theorem to the probability that the final two-particle state is not the initial two-particle state. In this limit we establish a connection with the conventional interpretation of the ion-ion optical potential. That is, to some approximation, our substitution of v with a complex $\mathcal{G}$ operator yields a reduction in the number of coupled channels we have to consider explicitly in (13). All the 1p-1h excitations of the projectile and target have been taken out of the dynamical framework and lumped into an effective potential. Furthermore we do not wish to consider any of the remaining coupled channels initially so we merely neglect the remaining terms on the right hand side of Eq. (13).

This then yields our starting position for the potential model and the practical dynamical framework in which it can be employed. We must now assess the validity of this approach. After demonstrating its validity by comparing with low energy data we are encouraged to proceed to higher energies where our approximations should have greater validity.

IV. INGREDIENTS OF THE ION-ION POTENTIAL AND VALIDITY TESTS FOR THE MODEL

A. Densities - electron scattering versus shell model

In an initial effort[12] only electron scattering densities were employed and certain irregularities were observed in analyses of ^{16}O and

^{18}O data. An analysis of semiclassical paths followed by the heavy-ions indicated strong sensitivity to the densities in the asymptotic or "far tail" region. This region of the density is not well determined by electron scattering studies and, in fact, the 3-parameter charge distributions proposed as fits to that data often have physically undesirable properties in the far tail region. This indicated that if one ever wished a meaningful comparison between theoretical and best fit values of $f(0)$ and the consequent emergence of true predictive power one would have to exercise great care in obtaining mass densities for nuclei valid all the way into the far tail region. Later on in the talk we show why less care is required at higher energies. For shell model mass densities of light nuclei ($A < 66$) we have taken average single particle well parameters from the extensive study of Millener and Hodgson,[16] computed all the single particle wave functions and summed their absolute squares with appropriate occupation weights. For ^{208}Pb we have obtained the density dependent Hartree-Fock results of J. Negele.[17] All these densities should yield high quality agreement with electron scattering data and thus satisfy that constraint as well as proper behavior in the asymptotic density region.

Figure 2 displays the ^{40}Ca and α densities obtained in different ways where their centers have been separated by the "strong absorption radius" at 10 MeV/nucleon. This radius is defined, a posteriori, as the distance of closest approach of that semiclassical trajectory where the probability of inelastic processes reaches 1/2. One merely interpolates an "$\ell_{1/2}$" value from a standard calculation of the transmission coefficients, $(1 - |e^{2i\delta_\ell}|^2)$, such that the transmission coefficient would be 0.5, and converts $\ell_{1/2}$ to a radius using the Coulomb shifted semiclassical distance of closest approach:

$$kR_{SA}(kR_{SA}-2\eta) = \ell_{1/2}(\ell_{1/2}+1) \qquad (15)$$

where η is the Sommerfeld parameter $\frac{Z_1 Z_2 e^2}{\hbar v}$ and k is the ion-ion relative wave number. It is a fairly model independent quantity always being well determined by the data. The figure demonstrates that the densities contributing to V_{opt} are those in the far tails at 10 MeV/nucleon. Besides indicating the necessity for care in the selection of densities at low energies this substantiates the claim that a low-density expansion for the ion-ion potential should be quite valid for applications at low energy. This contrasts with the corresponding nucleon-nucleus potential at low energies since, there, more penetration occurs and interior dynamics are considerably more important. The more highly absorbing ion-ion situation enhances the validity of a lowest order theoretical model especially for peripheral processes. As energy increases more significant matter overlap can be expected for the elastic channel trajectories but this will be shown not to occur until quite high energies where the impulse approximation becomes valid. Thus a switch in dynamical framework to Glauber theory at high energies will preserve the usefulness of the lowest order microscopic interactions.

B. Nucleon-nucleon interaction

The basic ansatz for the renormalized nucleon-nucleon force is

$$\mathcal{g}(E) = -\frac{2\pi\hbar^2\bar{f}(0)}{M} N_\gamma e^{-r^2/\gamma^2} \qquad (16)$$

where N_γ is chosen to yield a normalization to unity of the Gaussian interaction. This simple ansatz satisfies the constraint discussed by Moszkowski in a previous talk[18] that the volume integral of $\mathcal{g}$ yields the above constant times the forward scattering amplitude. The ansatz also permits separation of

geometric range effects on the optical potential from the many body effects on the strength. With this simple isolation of many-body effects we shall easily see that the simple physical intuition goes a long way to understanding these effects. Before attempting to calculate $\bar{f}(0)$ (which contains all the energy dependence) let us examine whether the low energy data demand the finite range contribution to the geometry of V_{opt}. Figure 3 displays the χ^2/pt resulting from a fit of $\bar{f}(0)$ to the 140 MeV University of Maryland α data[19] as a function of the range parameter, γ. For all three targets there is sharp sensitivity to the choice of range with the best fit being in the vicinity of $\gamma = 1.25$fm. When corrected for finite proton size left in the α density this yields a nucleon-nucleon force of range $\sim 1.40 \pm 0.25$fm as determined by the data. We take this as an acceptable range consistent with current thinking on ranges of effective nucleon-nucleon forces. As one moves to heavier projectiles one may expect less sensitivity to this range parameter.

The next question is the effect on the best fit $\bar{f}(0)$ results due to different ranges. This is shown in Fig. 4. A simple, nearly linear, behavior with range is obtained for both the real and the imaginary parts and this can be easily understood. The finite range introduces a smearing function into V_{opt}, increasing the geometrical strength of its long range component smoothly with increasing γ. A reduction in strength of $\bar{f}(0)$ results to keep the strength of V_{opt} at the strong absorption radius approximately fixed. Clearly then, finite range effects on geometry must be included for meaningful comparison between theoretical and best fit values of $\bar{f}(0)$.

We calculate $\bar{f}(0)$ in the following way in order to elucidate the many-body effects as much as possible. First we start with the on-shell

phase shifts as obtained in fits to the two body scattering data by MacGregor, Arndt and Wright[20], and obtain f(0) by summing the s, p and d partial waves. Then, since we desire an average interaction corrected for many-body effects we perform two averages and two corrections sequentially in a Fermi gas approach as follows:

i) Average over spin and isospin statistics. We define the fraction of non-identical particle collisions

$$\zeta = \frac{N_1 Z_2 + Z_1 N_2}{A_1 A_2} \tag{17}$$

where N and Z represent neutron number and proton number, respectively of the interacting ions 1 and 2. Then we evaluate the average amplitude

$$f(0) = \zeta f_{np}(0) + (1-\zeta) f_{pp}(0) \tag{18}$$

For an N=Z projectile on an arbitrary target ζ=1/2 and the results of this procedure are demonstrated at the top of Figs. 5a and 5b for the real and imaginary components respectively of f(0). All quantities are plotted on a scale of incident lab kinetic energy from 0 to 70 MeV. At the highest energy depicted we expect about a 2-3% error in f_{np} and f_{pp} due to neglect of the higher partial waves.

ii) Average over the Fermi motion. This we do because we want to eliminate the complexity of the full momentum dependence of the nucleon-nucleon interaction. The nucleons colliding in the two-ion medium sample a wide range of momentum components of the interaction due to their Fermi motion. If both nuclei are represented by Fermi gases, the average amplitude is

$$\hat{f}(0) = \frac{\int_0^{K_F} d^3k_1 \int_0^{K_{F_2}} d^3k_2 \; f_{\vec{k}_1 + \vec{k}_D - \vec{k}_2}}{\int_0^{K_{F_1}} d^3k_1 \int_0^{K_{F_2}} d^3k_2} \tag{19}$$

where K_{F_1} and K_{F_2} are the appropriate Fermi momenta, and $\vec{k}_D$ is the incident lab momentum per nucleon (the drift momentum). We take K_F to be the same for projectile and target and speculate, based on the density overlap shown in Fig. 2, that the appropriate value of K_F (in the spirit of the local density approximation[17]) is somewhere in the broad range of $0.45 \lesssim K_F \lesssim 0.90$ (fm^{-1}). This corresponds to a local density in which the two nucleons collide in the range of 4% to 33% of nuclear saturation density. We confess a certain ignorance of how to choose this parameter accurately and therefore carry an upper and lower estimate throughout the remaining calculations leading up to $\bar{f}(0)$. The results for Fermi motion averaging are displayed in the bottom half of Figs. 5a and 5b for the real and imaginary amplitudes, respectively. Since the only variable is the drift momentum we choose to represent all results on a universal scale of incident lab energy per nucleon. For simplicity we continue to treat an N=Z projectile and we feel that the broad range of K_F results presented should cover most ion-ion collision possibilities in this energy region.

The Fermi motion averaging has an effect easily anticipated. It damps the energy dependence in proportion to the amount of internal motion.

iii) <u>Off-shell correction</u>. In some fashion we must take account of the fact that the nucleons in the media do not collide on the energy shell. They are bound in the nucleus and experience some average

attractive potential. A proper $\mathcal{g}$ matrix will account for this by employing off-shell propagators for the nucleons. It has been well established that the $\mathcal{g}$ matrix resulting from realistic nucleon-nucleon potentials is smoothly dependent on off-shell energy. Thus one may reliably estimate[13]

$$\tilde{f}_E(0) = \hat{f}_E(0) - (\langle U_1 \rangle + \langle U_2 \rangle) \frac{\partial}{\partial\omega} \hat{f}_\omega(0)\Big|_E \tag{20}$$

where $\langle U_1 \rangle$ and $\langle U_2 \rangle$ are average potential energies experienced by particles 1 and 2, respectively and E denotes the lab kinetic energy per particle. We take $\langle U \rangle$ to be -15 MeV for surface nucleons. Actually the correction is not very large but does go in the same direction as the Fermi motion average. It tends to completely eliminate energy dependence of both components of the amplitude as demonstrated at the top of Figs. 6a and 6b.

iv) <u>Pauli correction</u>. Until this point we have dealt with a matrix which would conventionally be called the reference $\mathcal{g}$ matrix. It has all the many-body effects except a correction for the Pauli principle. If we had an exact reference $\mathcal{g}$, denoted by $\mathcal{g}_R$, we could obtain the exact $\mathcal{g}$ via an operator identity

$$\mathcal{g}(\omega) = \mathcal{g}_R(\omega) + \mathcal{g}_R(\omega) \left[\frac{Q}{e} - \frac{1}{e}\right] \mathcal{g}(\omega) \tag{21}$$

We have evaluated[13] the second term in (21) in a Fermi gas model by employing approximations consistent with our above discussions. The analytic structure[13] of the answer is

$$\bar{f}(0) = \tilde{f}(0) + \left(\tilde{f}(0)\right)^2 F(k_D, K_F) + \left(\tilde{f}(0)\right)^3 F^2(k_D, K_F) + \ldots \tag{22}$$

$$= \tilde{f}(0) \left[1 + \sum_{n=1}^{\infty} \left[\tilde{f}(0) F(k_D, K_F)\right]^n\right] \tag{23}$$

where F is a complex function involving many algebraic terms not conveniently presentable here. The effect of the Pauli corrections is large and again cooperative with the direction of the previous corrections. A marked sensitivity to the selection of K_F emerges as displayed at the bottom of Figs. 6a and 6b. The physical meaning of the Pauli correction is intuitively obvious.[13] Without keeping the audience in suspense any longer, let us leap immediately to compare this crude approximation of the lowest order theory with fits to the available data to determine the "best" $\bar{f}(0)$. The best fit values are also displayed in Figs. 6a and 6b. The great consolation at the low energy region to be derived from this is the fact that the total target dependence seems to be well accounted for by this crude version of the model. The additional fact that almost no energy dependence is required by the data is also consistent with the $K_F = 0.45\ fm^{-1}$ results. Around 40 MeV/n one may conjecture that even the crude model with $K_F = 0.45$ is beginning to yield true predictive power to about a 20% accuracy in the strength parameters.

To recap the progress of these corrections we see that at the low energy of about 10 MeV/n the many-body effects can account for about a factor of 4 in the strength constant and that factor reduces the imaginary strength and increases the real strength from their respective statistics averaged on-shell values. What started out on-shell as strong energy dependence due primarily to the $^1S_0$ "resonance" and the $^3S_1$-$^3D_1$ deuteron pole has largely been eliminated or even reversed in trend by the many-body effects. Within the uncertainty in choice of K_F the theoretical $\bar{f}(0)$ seems consistent with the values required to give best fits to the data.

It should be pointed out that the lowest order model presented above should only be expected to work in the diffractive region. Thus, all least squares fits are restricted to that region. We relegate to a later work those improvements to the model that could handle the non-diffractive large-angle scattering phenomena.

Fig. 7 displays the fit for $\alpha + {}^{208}Pb$ at 139 MeV along with the Maryland[19] experimental data. A high quality description is obtained through the first 3 orders of magnitude in $d\sigma/d\sigma_R$. This is obtained only when the complexity of proper finite range and proper density tails are included in the geometry of V_{opt}.

We are confident that we have now fulfilled a fairly stringent set of criteria for the lowest order potential at low energies.

V. EVOLUTION FROM 40 MeV/n to 100 MeV/n

One is encouraged by the above results to extend the application of the model to this region to examine further the diminishing role of the many-body effects. One may hope that the model in its <u>present</u> crude form may have true predictive power here since most of the corrections should be smaller and more accurately handled by our methods. Furthermore, we will treat this region as the testing ground for alterations in the dynamical framework -- especially the question of the validity of the Glauber and eikonal approximations.

First, we define the eikonal approximation within the context of the present optical model and then proceed to examine some numerical results. We follow the discrete eikonal sum approach of Dar and Kirzon[21] in which the nucleus-nucleus elastic scattering amplitude is given by

$$F(\theta) = F_C(\theta) + \frac{1}{2ik}\sum_{\ell=o}^{\infty}(2\ell+1)\ \exp(2i\delta_\ell^C)\ \{\exp(2i\delta_\ell^N)-1\}\ P_\ell(\cos\theta) \qquad (24)$$

where $F_C(\theta)$ is the Coulomb scattering amplitude for point charge distributions (Rutherford scattering), δ_ℓ^C, δ_ℓ^N are the Coulomb and nuclear phase shifts, respectively, and k is the relative ion-ion wave number. Our approximate eikonal framework amounts to taking the nuclear phase shift for given ℓ to be that given by

$$\delta_\ell^N = \delta^N(b) = -\frac{1}{\hbar v}\int_{\infty}^{\infty} V_{opt}(b,z)dz \tag{25}$$

where v is the incident ion velocity, V_{opt} is given by Eq. (6b) and ℓ and b are related by the semiclassical expression, Eq. (15). The above result for the eikonal phase shift is easily obtained by an expansion of the complex WKB phase shift to first order in V/E and its expected region of validity should be thus limited to regions where WKB is valid and $V/E \ll 1$. In the ion-ion situation V, in the form of Eq. (6b), can be very deep. For α on ^{208}Pb it gets to be about 300 MeV deep in its real component. Thus one expects some trouble in employing the eikonal expansion at this low energy. On the other hand, the strong peripherality and localization of the ion-ion elastic scattering situation mitigates this tremendously and motivates one to consider only the constraint that the optical potential at the strong absorption radius obeys $V(R_{SA})/E \ll 1$. This should be acceptable since the smaller impact parameter portion of the incident wave is completely damped. For elastic scattering typical values of $V(R_{SA})$ range from 1 to 20 MeV with the larger values occurring with increasing lab energy. The correct criteria seems to lie somewhere in between the above two estimates as we now demonstrate by actual computation.

Fig. 8a displays the Orsay[3,22] elastic scattering data for α on ^{40}Ca at 166 MeV. The heavy solid curve depicts the results of a standard

Schrödinger calculation as described in the previous section while the dashed-dot curve represents our eikonal approximation results using the <u>same</u> V_{opt}. Through the first three diffractive oscillations about a 20% discrepancy emerges but the discrepancy is essentially constant after about 30°. Now, for forward angle scattering at this energy one may argue that the eikonal approximation is somewhat useful but one naturally wonders if one couldn't do better.

The other popular approximation to investigate is the Glauber approximation. The chief difference between eikonal and Glauber under our model setup is the fact that Glauber theory instructs us to use <u>on-shell</u> amplitudes with, possibly, a Pauli correction. This Pauli correction in the Fermi gas limit differs from the one previously described and has been worked out by Glauber[23] for particle-nucleus scattering. Otherwise, the analytic framework that results from eikonalizing our V_{opt} is formally the same as the extension of Glauber theory in the "optical limit" to the nucleus-nucleus situation.[21,24] We have not yet calculated the amplitudes, $\bar{f}(0)$, appropriate to a Glauber approximation but we can offer as an indication of its usefulness a fit of $\bar{f}(0)$ to the data in this approximation. This is in a spirit similar to fitting $\bar{f}(0)$ in the Schrödinger framework. The Glauber best fit curve is displayed in Fig. 8b and is remarkably close to the best fit curve in the Schrödinger framework. The difference in the best fit values in the two frameworks at this energy is a 40% increase in $\mathrm{Im}\bar{f}(0)$ obtained in the Glauber approximation. It remains to be seem whether this is consistent with the Glauber prescription for calculating $\bar{f}(0)$. As a side note, it should be indicated that we have kept the finite range nucleon-nucleon force in our calculation of (25).

Let us increase the energy of the α particle to 70 MeV/n and examine the same set of calculations again. Unfortunately, we do not have the guidance of experimental data here. We therefore take the Schrödinger results with theoretical $\bar{f}(0)$ values as "pseudo data." We display Schrödinger and eikonal results in Fig. 9a. Eikonal has improved dramatically as an approximation by this energy.

Taking the pseudo data as described and fitting to obtain the "Glauber" best fit value we find a 12% increase in the real strength and a 25% increase in the imaginary strength gives the curve depicted in Fig. 9b.

At the indicated rates of improvement one suspects that by 100 MeV/n the eikonal will be an excellent approximation to the results obtained in the Schrödinger framework. After 100 MeV/n Glauber, eikonal and Schrödinger should all be nearly the same since the many-body effects have died out substantially. In the region from 40 to 100 MeV/n the Glauber approximation should have some validity. However, at this stage of our results we can only say that the Glauber approximation is valid as long as $\bar{f}(0)$ is adjusted to fit the data. The actual calculation of $\bar{f}(0)$ for the Glauber approximation is very straightforward and we should have it shortly.

All the above has been preliminary to convince the audience that the microscopic approach can be useful to understand a vast body of ion-ion data without recourse to 4 or 6 free parameters as employed in conventional phenomenology. With the justification we have presented above we now wish to attempt to use the predictive power, such as it is, that a no free parameter model is supposed to yield.

As promised earlier we present here an argument why one can forego great care in density selection beyond 100 or 200 MeV/n. We do this by

examining the classical distance of closest approach in the elastic channel as a function of energy. This is the strong absorption radius described by Eq. (15). As a rather model independent quantity, it serves as a useful measure of the amount of matter penetration. In Fig. 10 we display the difference ΔR_{SA} between this strong absorption radius and the sum of the RMS radii of the colliding ions. As energy increases ΔR_{SA} shrinks yielding greater matter penetration. This implies less and less sensitivity of the elastic scattering to that part of the optical potential which depends most strongly on the tails of the matter distributions. Thus, for purposes of higher energy calculations (> 200 MeV/n) of elastic, total and reaction cross sections it should be a good first approximation to take all matter distributions from elastic electron scattering measurements of charge density. This we do for the results presented in the remainder of this talk.

VI. THE VALIDITY OF THE FACTORIZATION HYPOTHESIS AT INTERMEDIATE AND HIGH ENERGIES

We would like now to report on some recent results obtained in collaboration with Saul Barshay[25] from which the bulk of this section is extracted. This work was stimulated by the proposals[26] that nucleus-nucleus total cross sections should factorize because a simple exchange process should occur. These arguments have been briefly summarized by J. Jaros and M. Richardson in previous talks. We assume the validity of the Glauber multiple scattering framework to predict nucleus-nucleus and nucleon-nucleus total, reaction, and elastic cross sections at intermediate and high energies. Our results predict that factorization holds to 20% if the radii of the projectile and target nuclei do not differ by more than 50%. This fact and the gross violation of factorization can be explained in

the context of a simple geometric model. These results clearly indicate that if factorization is to be used to demonstrate the validity of the Chew[26] hypothesis it must be shown to hold for nuclei with vastly differing sizes. Let us introduce a geometric parameter which is a measure of the relative size of the colliding systems:

$$x = R_A/R_B \tag{26}$$

where A and B are the atomic numbers of the projectile and target, R_A and R_B are nuclear radii.

The factorization ratios defined by

$$r_{AB} = (\sigma_{AB})^2/\sigma_{AA}\sigma_{BB} \tag{27}$$

have also been of considerable recent interest.[25,29-31] We have numerically evaluated such ratios for a wide variety of nucleus-nucleus reactions, in order to see under what conditions the factorization hypothesis $r \approx 1$ is numerically valid. Order of magnitude deviations from $r \approx 1$ are observed in some cases, but are understandable in terms of a simple geometric limit

$$r^G = \frac{(1+x)^4}{16x^2} \tag{28}$$

Note that $r^G \gg 1$ for $x \ll 1$, i.e., when the target and projectile vary greatly in size. The fact that $r \approx 1$ to within 20% for many reactions does not necessarily imply that high energy concepts such as the Pomeron are required for the description of such reactions. If $x \approx 1$, values $r \approx 1$ are also produced by the simple geometrical model of Eq. (28). In order to substantiate a given high energy model, it seems likely that unless the total cross sections and factorization ratios deviate significantly from the dictates of geometry, one must look at more detailed properties of the nucleus-nucleus interaction. In all likelihood, these gross features will be explainable within the framework of conventional nuclear theory, at least in the domain of energy presently accessible.

For the purpose of these calculations we neglect the Coulomb potential and assume that $f_{np}(0) = f_{pp}(0) = f_{nn}(0)$. These should be satisfactory approximations for the energies we consider here. We also make the zero range approximation for the nucleon-nucleon interaction. The error thus introduced is partially cancelled by using densities obtained from electron scattering experiments without correcting for the finite size of the proton.

Using the relation $\sigma^T_{NN} = 4\pi \mathrm{Im} f_{NN}/k$ between the nucleon-nucleon total cross section σ^T_{NN} and the amplitude f_{NN} [k is the NN wave number], we can write Eq. (25) in the form

$$\delta^N(b) = \chi_{AB}(b) = \sigma^T_{NN}(i+\beta)T(b)/4$$
$$\beta \equiv \mathrm{Re} f(0)/\mathrm{Im} f(0) \tag{29}$$

where

$$T(b) = \int_{-\infty}^{+\infty} dx \int d\underset{\sim}{r}' \; \rho_A(\underset{\sim}{r}-\underset{\sim}{r}')\rho_B(\underset{\sim}{r}') \; . \tag{30}$$

Using the optical theorem, the total cross section σ_{AB}^{T} for reaction A+B is given by

$$\sigma_{AB}^{T} = 4\pi \int_0^\infty \{1-e^{-2\mathrm{Im}\chi_{AB}(b)} \cos(2\mathrm{Re}\chi_{AB}(b))\} b\,db \tag{31}$$

The total reaction cross section σ_{AB}^{R} and the total elastic cross section σ_{AB}^{E} are given by

$$\sigma_{AB}^{R} = 2\pi \int_0^\infty (1-e^{-4\mathrm{Im}\chi_{AB}(b)}) b\,db$$

$$\sigma_{AB}^{E} = \sigma_{AB}^{T} - \sigma_{AB}^{R} \tag{32}$$

Another quantity of interest is the slope b_{AB} of the elastic diffraction peak. This we obtain from the elastic scattering differential cross section $d\sigma/dt$ for small $t = -q^2$ via the equation

$$\frac{(d\sigma_{AB}^{E}/dt)}{(d\sigma_{AB}^{E}/dt)_{t=0}} = \left|\frac{F_{AB}(t)}{F_{AB}(0)}\right|^2 \underset{\approx}{t \to 0} e^{b_{AB}t} \tag{33}$$

By making a Taylor expansion of $F_{AB}(t)$ for small t, we obtain

$$b_{AB} = -\frac{k_{AB}}{2|F_{AB}(0)|^2} \{\mathrm{Im}F_{AB}(0)\mathrm{Re}G_{AB} - \mathrm{Re}F_{AB}(0)\mathrm{Im}G_{AB}\}$$

$$G_{AB} = \int_0^\infty \{e^{2i\chi_{AB}(b)} - 1\} b^3 db \tag{34}$$

The b^3 weighting in G_{AB} enhances the contribution of large impact parameters b and thus b_{AB} is more sensitive to the behavior of ρ_A and ρ_B in the surface and tail regions.

In addition to the cross sections, we are also interested in the <u>factorization ratios</u> r_{AB} defined by

$$r_{AB}^{T} = (\sigma_{ab}^{T})^2/\sigma_{AA}^{T}\,\sigma_{BB}^{T}$$

$$r_{AB}^{R} = (\sigma_{AB}^{R})^2/\sigma_{AA}^{R}\,\sigma_{BB}^{R}$$

$$r_{AB}^{E} = (\sigma_{AB}^{E})^2/\sigma_{AA}^{E}\,\sigma_{BB}^{E}$$

$$r_{AB}^{b} = (b_{AB})^2/b_{AA}\,b_{BB} \tag{35}$$

The factorization hypothesis, as usually formulated in high energy physics, refers to the ratio r_{AB}^{T} of <u>total</u> cross sections; <u>strict factorization</u> means $r_{AB}^{T} = 1$. One of the main purposes here is to investigate to what extent the factorization hypothesis applies to real nucleus-nucleus collisions. In the simple <u>geometrical</u> picture which we have outlined above, all of the quantities r_{AB} of Eq. (35) are on the same footing; there is nothing special about the ratio of total cross sections. Qualitatively, we find that the degree to which factorization is satisfied is much the same for each of the quantities $r_{AB}^{T,R,E,b}$; gross deviations from strict factorization are explainable in each case by a simple geometric formula (28).

The nucleon-nucleon cross sections σ_{NN}^{T} and the ratios β_{pp} of the real to imaginary parts of the amplitude which we used are shown in Table 1. The values for $0.52 \leq E_{LAB} \leq 7.0$ GeV are obtained from Ref. 33 and the values at 25 GeV from Ref. 34. In each of these cases, we assumed $\beta_{np} = \beta_{pp}$. At 0.1 GeV, the values of σ_{NN}^{T} and β were calculated directly from phase shifts.[20] In this case, $\beta_{np} = 1.18$. As

we see from Table 1, β varies from large positive values to sizable negative values as we pass from low to high energy, while the total cross section remains relatively constant. As we shall see explicitly below, these large variations in β produce only very minor variations in the nucleus-nucleus cross sections.

For a description of the nuclear densities ρ_A and ρ_B, we employ parametric representations obtained from analyses of electron scattering data,[35] and we refer to Ref. 25 for the details on this selection. Table 2 gives the rms radii of the nuclei discussed for rapid reference.

In Table 3, we show a selection of our numerical results for $\sigma_{AB}{}^{R}$, $\sigma_{AB}{}^{T}$ and b_{AB} at 1.05 GeV per particle. The reactions are ordered according to the parameter $x = \min\{R_A/R_B, R_B/R_A\}$, where R_A and R_B are the r.m.s. radii of the colliding nuclei, listed in Table 2.

Several points are to be noted about the results of Table 3, which are very similar to our results at other incident energies:

a) The reaction cross sections $\sigma_{AB}{}^{R}$ are generally quite close to a geometric limit $\pi(R_A{}^{EQ} + R_B{}^{EQ})^2$ where $R_A{}^{EQ} = (5/3)^{\frac{1}{2}} R_A$ is the equivalent spherical radius (i.e., the radius of a uniform distribution having the same r.m.s. radius). This corresponds to our most naive expectation on the basis of two colliding black spheres.

b) The ratio of total cross section to reaction cross section is generally of order 1.7-1.8, except for collisions between two relatively light nuclei. This is close to the geometric limit of 2.

c) The elastic slopes b_{AB} are close to the limit $b_{AB} \approx \frac{1}{4}(R_A^{EQ}+R_B^{EQ})^2$, which one would expect on the basis of the black sphere model, for which

$$\frac{d\sigma_{AB}^{E}/dt}{(d\sigma_{AB}^{E}/dt)_{t=0}} = 4\left|\frac{J_1(qR_{AB})}{qR_{AB}}\right|^2$$

$$R_{AB} = R_A^{EQ} + R_B^{EQ}$$

$$b_{AB} = \lim_{t \to 0} \frac{1}{t} \ln\left[4\left|\frac{J_1(qR_{AB})}{qR_{AB}}\right|^2\right]$$

$$= (R_A^{EQ} + R_B^{EQ})^2/4 \qquad (36)$$

If we assume that $R_A = \tilde{r}_0 A^{1/3}$, then in the geometrical limit we expect

$$\sigma_{AB}^{T} \cong 2\pi\, r_0^2 (A^{1/3} + B^{1/3})^2 \qquad (37)$$

with $r_0^2 = 5/3\, \tilde{r}_0^2$. In Fig. 11, we show the calculated total cross sections σ_{AB}^{T} at 2.1 GeV. The points correspond to the reactions listed in Table 3. The solid curve represents the geometrical approximation of Eq. (37), with r_0 adjusted to correctly reproduce the cross sections for the heaviest nuclei. Since $\tilde{r}_0$ is of the order of 1fm, we expect $r_0 \approx (\frac{5}{3})^{\frac{1}{2}} \approx 1.29$ fm, which is close to the value $r_0 = 1.27$fm used in Fig. 11.

We have also calculated proton-nucleus cross sections as a function of energy. Note that our proton-nucleus calculations can either be regarded as the folding of the extended proton density together with a zero range interaction or as the folding of a point proton together with a finite range Gaussian interaction. This latter interpretation is to be preferred, but the numerical calculations are identical. Some typical results are given in Table 4, for a proton energy of 800 MeV. This table may be of some qualitative interest to experimentalists engaged in intermediate energy proton-nucleus scattering at the Los Alamos Meson Physics Facility. We note that one only approaches the geometric limit $\sigma_{AB}^{T}/\sigma_{AB}^{R} = 2$ for heavy targets. Thus for light targets, we expect the proton to be sensitive to the whole nuclear volume, and hence $\sigma_{pB}^{T} \propto B$ for relatively small B. For heavier targets, the stronger absorption restricts the proton's interaction to the surface region, and hence $\sigma_{pB}^{T} \propto B^{2/3}$ for large B. These features are indicated in Fig. 12; one sees the change from a volume to a surface reaction as we increase B. Further results to substantiate this behavior is presented in a forthcoming work.[25]

The energy dependence of the cross sections in the region 0.1-25 GeV/particle is shown in Fig. 13 for three typical reactions. The nucleus-nucleus cross sections are seen to be essentially constant in this energy region, in spite of large variations in β, i.e., the real part of the NN amplitude. This is so because the nucleon-nucleon cross section σ_{NN}^{T} is sufficiently large so that we are near the

geometric limit at all the energies considered. Equivalently, if the optical potential is very absorptive (close to the black sphere limit), there is little sensitivity to the real part of the potential, within reasonable limits. It is worth noting that other aspects of ion-ion collisions need not be so energy independent and at Bevalac energies of 1-2 GeV/n it would be interesting to see the role played by β since it is almost exactly zero at 1.0 GeV but significantly large at 2.0 GeV/n.

As indicated, the total and reaction cross sections are close to the geometric limit, except for reactions where both projectile and target are very light nuclei. If we have $\sigma_{AB}{}^{T} \approx 2\pi(R_A{}^{EQ} + R_B{}^{EQ})^2$, $\sigma_{AB}{}^{R} \sim \sigma_{AB}{}^{E} \approx \pi(R_A{}^{EQ} + R_B{}^{EQ})^2$, $b_{AB} \approx (R_A{}^{EQ} + R_B{}^{EQ})^2/4$, then clearly <u>all</u> of the factorization ratios r^T, r^R, r^E, r^b will be close to the simple geometric limit

$$r^G = (1+x)^4/16x^2 \qquad (38)$$

where $x = \min\{R_A{}^{EQ}/R_B{}^{EQ},\ R_B{}^{EQ}/R_A{}^{EQ}\}$. In Fig. 14, we plot the calculated ratios as a function of x at 1.05 GeV. The geometric limit r^G of Eq. (38) is shown for comparison, and is seen to provide a semi-quantitative account of the calculated results. Note that for small x, the deviations from strict factorization are quite large. However, if $\frac{2}{3} \lesssim x \lesssim 1$ (i.e., the nuclei do not differ in radius by more than 50%), the deviations from strict factorization

are seen to be ≤ 20%. This is essentially the region of x considered by Fishbane and Trefil.[29]

In Table 5, we show the calculated factorization ratios for proton-nucleus interactions at 800 MeV. As x becomes smaller, order of magnitude deviations from strict factorization occur. As in the case of the nucleus-nucleus results in Fig. 14, the proton-nucleus factorization ratios of Table 5 exhibit two evident features:

a) the calculated ratios r (except for $p+\alpha$) <u>exceed</u> the geometric limit r^G.

b) the values of r are always greater than unity. Observation b) is a direct consequence of a), since the geometric limit r^G has the property

$$r^G(x) > 1 \text{ for } \underline{\text{all}}\ 0 < x < 1 \tag{39}$$

and $r^G = 1$ <u>only</u> for $x = 1$ (equal size nuclei). An experimental ratio $r < 1$ would then indicate the failure of the simple geometric picture.

Large deviations from strict factorization (r=1) are predicted if the colliding nuclei are of very different size. This result follows because the basic nucleon-nucleon interaction is of relatively short range and is strong, leading to a large absorptive part for the nucleus-nucleus potential. Because of the strong absorption, nucleus-nucleus elastic scattering is a peripheral process and for the actual observed value of the NN cross section, we are relatively close to the limit of black spheres. In view of this fact,

the gross features of nucleus-nucleus cross sections at high energies (1-25 GeV/particle) should be rather easy to interpret in terms of the geometrical model.

VII. MULTIPARTICLE PRODUCTION MULTIPLICITIES

It has been suggested[37,38] that particle-nucleus multiplicities at high energies would provide a sensitive test of the mechanism underlying multiparticle production. Most models of multiparticle production fall into two categories.[38] The first category includes those models which assume that the final multiparticle state is directly produced in a single step from the colliding particles. This includes the particle fragmentation model[39], the multiperipheral model[40] and its multi-Regge generalizations,[41] and the bremsstrahlung analogy.[42] The second category consists of those models which assume a two-step mechanism, where in the first step one or two compound systems are produced which subsequently decay into the final multiparticle states with lifetimes long compared to the collision time. Such model include the diffraction excitation model[43] and the one or two fireball thermodynamic models.[44]

It has been shown[37,38,45,46] that under apparently reasonable assumptions the one-step mechanisms, via a cascading phenomena, yield large increases with energy in the ratio ($\langle N(E)\rangle/\langle n(E)\rangle$) of nucleon-nucleus multiparticles $\langle N(E)\rangle$ to nucleon-nucleon multiplicities $\langle n(E)\rangle$ at the same energy. This result is illustrated by the results of Dar and Vary[38] in Fig. 15. Similar results were obtained

with similar assumptions by other authors. Due to the cascading phenomena, the heavier the target, the larger the number of average mean free paths per event and thus the larger the multiplicities as compared to the pp results.

The two step mechanism[38] yields a sharply different prediction illustrated by Fig. 16. Here there is no energy dependence to the ratio provided enough energy is available in the incident beam to supply all the collisions with essentially the initial energy. The calculated result shows an $A_t^{0.26}$ behavior which is interpretable as an average linear dimension of the nucleus. This average arises because this mechanism is sensitive only to an average over impact parameters of the depth of the nucleus as measured in numbers of mean free paths. It is indeed noteworthy that the Heckman Group[47] presented data that shows that the partial cross sections for a given beam fragment produced in heavy-ion collisions is proportional to $A_t^{0.26}$. It is conceivable that this same average depth of the target nucleus is again involved here.[48]

Recent data[49] supports an energy independent ratio and seems to exclude any possibilities of cascades.[50] Putting aside what consequences this implies to those at this conference that are proponents of π condensates and such, let us examine what we might like to learn from nucleus-nucleus multiplicities and its energy dependence up to 1 TeV beam energies. Let us propose via analogy with the particle-nucleus situation[38] a model for nucleus-nucleus multiplicities

involving an intranucleus formation and transport of resonances consistent with present leanings towards two-step mechanisms. Let us then examine the range of results possible depending on the subsequent hypotheses that must be proposed to make the model for nucleus-nucleus multiplicities complete. It is this range of possibilities that suggests nucleus-nucleus collisions can help unravel the as yet undertermined features of multiparticle production mechanisms.

Specifically, let us consider the diffractive excitation models.[43] According to these models, one or both of the colliding particles are first excited into resonant states which have the same internal quantum numbers, excepting spin and parity, and approximately the same momenta as the original particles. These resonances subsequently decay via cascading (mainly via pion emission) with small Q values (typically 300 MeV) into the final multiparticle states. Since the average multiplicity increases very slowly with energy (as the log of the energy, in fact), and since the average Q value for the cascading decay of the resonances is also small, the important resonances are therefore of low-mass excitation and one may expect them to have lifetimes of familiar low excitation states, say $< \Gamma > \sim 100$ MeV. Consequently, at high energy, a projectile particle which is diffractively excited behaves in the target nucleus like a stable particle due to time dilatation. On the other hand, resonances which are produced by diffractive excitation of target nucleons have only small momenta in the lab frame. Thus, in both the projectile and target nuclei, the resonances will start their

cascading decay sometime after the nuclei are outside their interaction region. However, due to the small Q values, the decay products will not have sufficient energy to multiply via secondary collisions while escaping out of their respective nuclei.

Due to the complexity of the nucleus-nucleus situation we have now to examine some new possibilities. For example, it is possible that one resonance can be produced in the projectile and collide with another resonance produced in the target by a previous collision. What shall we assume happens in such a situation? Let us summarize three global hypotheses that could be distinguished by actual nucleus-nucleus experiments.

A - The saturated resonance hypothesis

Let us represent an unexcited nucleon by p and an excited nucleon by F. Let F represent that excitation which yields the appropriate average number of decay products to reproduce the measured pp multiplicities. Then in a nucleus-nucleus collision we hypothesize that only the following processes occur:

1) $p+p \rightarrow p+F$ or $p+p \rightarrow F+F$

2) $p+F \rightarrow F+F$

3) $F+F \rightarrow F+F$

that is, in subsequent resonance-resonance collisions, no additional mass is created so the resonance stays at its initial excitation energy. Only Steps 1) and 2) were required to obtain predictions for particle-nucleus multiplicities at high energies in the two-step approach.[38]

B - Linear Bootstrap hypothesis - Stacking

Let us now introduce the notation that F^* represents an excitation of F with an energy addition ΔE, about the same as the difference in mass between p and F. Thus F^* will decay with twice the mean multiplicity as F. Similarly, F^{**} has an excitation energy about ΔE again above F^* and decays with a mean multiplicity three times that of F, etc. We now hypothesize that the following processes occur:

1) $p+p \rightarrow F+F$

2) $p+F \rightarrow F+F^*$

3) $F+F \rightarrow F^*+F^*$

4) $F+F^* \rightarrow F^*+F^{**}$

etc.,

but the cross sections for all processes will be assumed to be the <u>same</u>.

C - Statistical bootstrap hypothesis

It is conceivable that the increasing phase space for further excitations of resonances will yield an appropriately <u>rising</u> cross section for the processes described under hypothesis B. This hypothesis would yield the fastest rise in mean nucleus-nucleus multiplicities as a function of projectile and target mass.

where E is expressed in GeV.

Now, we are able to readily evaluate the nucleus-nucleus mean multiplicities under hypothesis B. Every elementary collision yields the measured pp mean multiplicity since it "stacks" this mass on top of the mass increases due to previous collisions. The total number of collisions, N, at impact parameter b is just

$$N(E,b) = \sigma T(b) \tag{43}$$

so that, in analogy with the general definition (40) we can define the mean multiplicity for particles (charged and uncharged) <u>produced</u> in nucleus-nucleus collisions at very high energies

$$< N(E) > = \frac{4\pi \int_0^\infty N(E,b) < n(E) > \sigma_{AB}{}^T(b)\ bdb}{\sigma_{AB}{}^T} \tag{44}$$

where $\sigma_{AB}{}^T$ is given by eqn. (31) and $\sigma_{AB}{}^T(b)$ is just integrand in eqn. (31) . Since $\sigma_{AB}{}^T(b) \sim 1$ in the interior region, we have the useful approximation from (44)

$$\frac{< N(E) >}{< n(E) >} \propto \frac{\int T(b)\ bdb}{\sigma_{AB}{}^T} \propto \frac{AB}{(A^{1/3} + B^{1/3})^2} \tag{45}$$

Fig. 17 displays calculated results for ^{14}N on various targets. The energy is assumed large enough so that nucleons in the projectile loose insignificant amounts of energy when resonances are produced. The elementary cross-sections for all processes is taken to be 38 mb.

Because of the mathematical simplicity that emerges we have chosen hypothesis B for actual numerical applications. It is clear that A would yield lower multiplicities and less dependence on the projectile and target masses. It is also clear that C yields the steepest dependence on masses and the largest multiplicities. Thus, hypothesis B also serves as a guide.

We recall that the standard definition for mean charged particle multiplicities in pp collisions is

$$< n'(E) > \; = \; \frac{\sum_{n'} n'\sigma_{n'}}{\sigma} \tag{40}$$

where n' is the number of charged particle tracks including the two protons, $\sigma_{n'}$ is the partial cross section for n' tracks and σ is the total nucleon-nucleon cross section at that energy. For our purposes, however, we want as an input to our results, the average number of particles <u>produced</u> per collision, which we take to be[38]

$$< n(E) > \; = \; \frac{3}{2} \; < n_c(E) > = \frac{3}{2} \{< n'(E) > - 2\} \tag{41}$$

where the $\frac{3}{2}$ is inserted to account for unobserved neutral particles produced and in recognition of the fact that most of the produced particles are π's. A satisfactory fit to the measured pp data is obtained with[51]

$$< n(E) > \; \cong \; 0.63 \; \ell n(E/1.71) \tag{42}$$

The approximation (45) is seen to be well satisfied and thus simple geometry dominates the picture under hypothesis B.

It is worthwhile remarking once again for the sake of emphasis that the two-step mechanism yields a prediction for $< N(E) >/< n(E) >$ which is energy independent. Hypothesis B has been employed for simplicity and the results that emerge have a simple dependence on projectile and target mass.

For lower energies, such as those attainable at the Berkeley Bevalac, the above treatment should be modified mainly to accommodate the energy loss since it is a significant fraction of the incident energy. The effect, at Bevalac energies, will be to shift the curve down somewhat and flatten it out especially for heavier targets where the large number of mean free paths cannot be used entirely.

SUMMARY

The reader is asked to read the Abstract again.

Table 1. Nucleon-nucleon Cross Sections and β Values as a Function of Energy.

LAB KINETIC ENERGY (GeV)	σ_{np}(mb)	σ_{pp}(mb)	β_{pp}
0.10	68.0	32.0	1.87
0.52	35.22	34.03	0.550
0.65	38.45	42.90	0.443
0.80	39.61	46.76	0.144
0.90	39.61	47.34	0.0017
1.05	40.39	47.50	-0.073
2.1	43.14	44.45	-0.292
4.2	42.06	41.17	-0.330
7.0	41.3	40.0	-0.320
25.0	38.9	38.90	-0.154

Table 2. Nuclear r.m.s. radii

Nucleus	$R_{r.m.s.}$(fm)
^{4}He	1.71
^{40}Ar	3.47
^{58}Ni	3.73
^{90}Zr	4.26
^{120}Sn	4.64
^{208}Pb	5.49

Table 3. Calculated Cross Sections and Elastic Slopes at 1.05 GeV/particle

Reaction A+B	x	σ_{AB}^{R}(barns)	$\sigma_{AB}^{T}/\sigma_{AB}^{R}$	b_{AB}(fm^2)
$\alpha + {}^{208}Pb$	0.312	2.58	1.78	19.24
$\alpha + {}^{90}Zr$	0.399	1.66	1.72	12.43
${}^{12}C + {}^{208}Pb$	0.450	3.39	1.82	25.37
${}^{14}N + {}^{208}Pb$	0.452	3.46	1.82	25.93
$\alpha + {}^{58}Ni$	0.458	1.28	1.70	9.57
${}^{16}O + {}^{208}Pb$	0.501	3.70	1.82	27.71
${}^{12}C + {}^{90}Zr$	0.576	2.32	1.77	17.31
${}^{14}N + {}^{90}Zr$	0.578	2.38	1.78	17.77
$\alpha + {}^{16}O$	0.622	0.68	1.58	5.31
${}^{40}Ar + {}^{208}Pb$	0.627	4.81	1.83	36.06
${}^{16}O + {}^{90}Zr$	0.641	2.58	1.78	19.20
${}^{12}C + {}^{58}Ni$	0.662	1.85	1.76	13.76
${}^{14}N + {}^{58}Ni$	0.665	1.90	1.77	14.14
$\alpha + {}^{12}C$	0.692	0.56	1.55	4.47
${}^{16}O + {}^{58}Ni$	0.737	2.07	1.77	15.44
${}^{90}Zr + {}^{208}Pb$	0.776	5.86	1.85	44.12
${}^{40}Ar + {}^{90}Zr$	0.802	3.49	1.79	26.06
${}^{120}Sn + {}^{208}Pb$	0.845	6.40	1.86	48.28
${}^{12}C + {}^{16}O$	0.898	1.10	1.67	8.27
${}^{14}N + {}^{16}O$	0.902	1.14	1.69	8.56
${}^{90}Zr + {}^{120}Sn$	0.918	4.86	1.84	36.51
${}^{40}Ar + {}^{58}Ni$	0.922	2.89	1.78	21.57
${}^{3}He + \alpha$	0.966	0.26	1.35	2.51
${}^{14}N + {}^{12}C$	0.996	0.98	1.67	7.38

Table 4. Proton-Nucleus Cross Sections and Elastic Slopes at 800 MeV

Reaction	σ_{AB}^{R}(barns)	$\sigma_{AB}^{T}/\sigma_{AB}^{R}$	b_{AB}(fm^2)
p + ^{3}He	0.093	1.18	1.38
p + α	0.108	1.24	1.37
p + ^{6}Li	0.174	1.20	2.38
p + ^{9}Be	0.223	1.28	2.50
p + ^{12}C	0.267	1.33	2.64
p + ^{14}N	0.280	1.38	2.71
p + ^{16}O	0.340	1.36	3.25
p + ^{18}O	0.361	1.38	3.33
p + ^{24}Mg	0.449	1.41	3.98
p + ^{28}Si	0.498	1.43	4.34
p + ^{32}S	0.554	1.44	4.86
p + ^{40}Ar	0.637	1.47	5.42
p + ^{48}Ti	0.715	1.51	5.83
p + ^{58}Ni	0.785	1.55	6.18
p + ^{68}Zn	0.943	1.54	7.565
p + ^{90}Zr	1.068	1.60	8.26
p + ^{120}Sn	1.285	1.63	9.83
p + ^{140}Ce	1.414	1.66	10.69
p + ^{197}Au	1.723	1.70	12.91
p + ^{208}Pb	1.815	1.70	13.62

Table 5. Proton-Nucleus Factorization Ratios at 800 MeV

Reaction	x	r^T	r^R	r^E	r^b	r^G
p + ^{3}He	0.452	1.14	1.24	0.80	1.67	1.36
p + α	0.468	1.24	1.34	1.05	1.55	1.33
p + ^{6}Li	0.332	1.42	1.67	0.88	2.36	1.78
p + ^{9}Be	0.331	1.82	2.08	1.55	2.18	1.79
p + ^{12}C	0.324	2.27	2.49	2.38	2.10	1.83
p + ^{14}N	0.323	2.55	2.70	3.02	2.06	1.84
p + ^{16}O	0.291	2.77	3.00	3.10	2.37	2.05
p + ^{18}O	0.289	3.03	3.20	3.70	2.36	2.06
p + ^{24}Mg	0.264	3.74	3.82	5.01	2.63	2.29
p + ^{28}Si	0.256	4.16	4.15	5.93	2.75	2.37
p + ^{32}S	0.256	4.46	4.42	6.46	2.96	2.37
p + ^{40}Ar	0.233	5.25	5.03	8.28	3.17	2.66
p + ^{48}Ti	0.222	6.28	5.78	10.90	3.35	2.83
p + ^{58}Ni	0.215	7.44	6.59	13.98	3.55	2.95
p + ^{68}Zn	0.196	8.17	7.33	15.00	4.09	3.33
p + ^{90}Zr	0.186	10.15	8.58	20.83	4.44	3.57
p + ^{120}Sn	0.172	12.48	10.23	27.10	5.15	3.99
p + ^{140}Ce	0.165	14.50	11.55	33.09	5.65	4.23
p + ^{197}Au	0.150	18.31	13.98	44.59	6.69	4.86
p + ^{208}Pb	0.146	19.14	14.56	46.88	6.98	5.06

REFERENCES

1. J.S. McIntosh, S.C. Park and G.H. Rawitscher, Phys. Rev. 134, B1010 (1964).
2. G.W. Greenlees, G.J. Pyle and Y.C. Tang, Phys. Rev. 171, 1115 (1968).
3. B. Tatischeff and I. Brissaud, Nucl. Phys. A155, 89 (1970).
4. A.M. Bernstein and W.A. Seidler, Phys. Letters 34B, 569 (1971).
5. B. Tatischeff, I. Brissaud and L. Bimbot, Phys. Rev. C 5, 234 (1972).
6. P. Mailandt, J.S. Lilley and G.W. Greenlees, Phys. Rev. Letters 28, 1075 (1972); Phys. Rev. C 8, 2189 (1973).
7. R.S. Mackintosh, Nucl. Phys. A210, 245 (1973).
8. A.M. Bernstein and W.A. Seidler, Phys. Letters 39B, 583 (1973).
9. D.R. Alexander and F.B. Malik, Phys. Letters 42B, 412 (1972); A. Budzanowski, A. Dudek, K. Grotowski, Z. Majka and A. Strzalkowski, Particles and Nuclei 6, 97 (1973).
10. A.R. Barnett and J.S. Lilley, Phys. Rev. C 9, 2010 (1974).
11. D.M. Brink and N. Rowley, Nucl. Phys. A219, 79 (1974).
12. J.P. Vary and C.B. Dover, Phys. Rev. Letters 31, 1510 (1973).
13. C.B. Dover and J.P. Vary (to be published).
14. A.K. Kerman, H. McManus and R.M. Thaler, Ann. Phys. (N.Y.) 8, 551 (1959).
15. J. Hüfner and C. Mahaux, Ann. Phys. (N.Y.) 73, 525 (1972).
16. D.J. Millener and P.E. Hodgson, Nucl. Phys. A209, 59 (1973).
17. J. Negele, Phys. Rev. C 1, 1260 (1970).
18. S.A. Moszkowski, "Some Aspects of Ion-Ion Potentials", presented at this conference.
19. D.A. Goldberg and S.M. Smith, Phys. Rev. Letters 29, 500 (1972); D.A. Goldberg, S.M. Smith, H.G. Pugh, P.G. Roos and N.S. Wall, Phys. Rev. C 7, 1938 (1973); D.A. Goldberg, S.M. Smith and G.F. Burdzik, Univ of Maryland Technical Report No. 74-107, June (1974) and private communication.
20. M.H. MacGregor, R.A. Arndt and R.M. Wright, Phys. Rev. 182, 1714 (1969), Table VI.

21 A. Dar and Z. Kirzon, Phys. Letters 37B, 166 (1971).

22. I. Brissaud, Y. Le Bornec, B. Tatischeff, L. Bimbot, M.K. Brussel and G. Duhamel, Nucl. Phys. A191, 145 (1972).

23. R.J. Glauber in High Energy Physics and Nuclear Structure, ed. G. Alexander (North-Holland Publishing Co., Amsterdam (1967)).

24. W. Czyz and L.C. Maximon, Ann. Phys. (N.Y.) 52, 59 (1969): G. Faldt, H. Pilkuhn and H.G. Schaile, Ann. Phys. (N.Y.) 82, 326 (1974); this latter article contains a number of references to earlier work on relativistic nucleus-nucleus collisions; see also A. Tekou, Nucl. Phys. B46, 141 (1972) and B46, 152 (1972); T.W. Donnelly, J. Dubach, and J.D. Walecka, Heavy Ion Scattering at Intermediate and High Energies Nucl. Phys. (to be published`

25. S. Barshay, C.B. Dover and J.P. Vary, Nucleus-Nucleus Cross Sections and the Validity of the Factorization Hypothesis at Intermediate and High Energies, May 1974, BNL preprint 18972 (to be published).

26. G.F. Chew, Comments on Nuclear and Particle Physics 2, 107 (1968), plus various internal Berkeley reports.

27. J. Jaros, "High Energy Heavy Ion Total Cross Sections", presented at this conference.

28. M. Richardson, "Diffraction Dissociation with Heavy Ions", presented at this conference.

29. P.M. Fishbane and J.S. Trefil, Phys. Rev. Letters 32, 396 (1974).

30. V. Franco, Phys. Rev. Letters 32, 911 (1974).

31. J. Pumplin and G.L. Kane, Phys. Rev. Letters 32, 963 (1974).

32. S. Barshay, C.B. Dover and J.P. Vary, Phys. Letters 51B, 5 (1974).

33. D.V. Bugg et al., Phys. Rev. 146, 980 (1966).

34. K.J. Foley et al., Phys. Rev. Letters 19, 857 (1967).

35. H.R. Collard, L.R.B. Elton and R. Hofstadter, in Landolt-Börnstein: Numerical Data and Functional Relationships in Science and Technology ed. K.H. Hellwege and H. Schopper (Springer, Berlin (1967)), Group I, Vol. 2, p. 21 and references therein. Further details are found in Ref. 25.

36. Very similar results at 2.1 GeV/particle are given in Ref. 32.

37. P.M. Fishbane and J.S. Trefil, Phys. Rev. D 3, 238 (1971).

38. A. Dar and J. Vary, Phys. Rev. D 6, 2412 (1972).

39 J. Benecke, T.T. Chou, C.N. Yang and E. Yen, Phys. Rev. 188, 2159 (1969); T.T. Chou and C.N. Yang, Phys. Rev. Letters 25, 1072 (1970).

40. D. Amati, A. Stanghellini and S. Fubini, Nuovo Cimento 26, 896 (1962).

41. F. Zachariasen and G. Zweig, Phys. Rev. 160, 1322 (1967); 160, 1326 (1967).

42. R.P. Feynman, Phys. Rev. Letters 23, 1415 (1969); in High Energy Collisions, ed. C.N. Yang et al., (Gordon and Breach, New York (1969)).

43. R.K. Adair, Phys. Rev. D 5, 1105 (1972); M. Jacob and R. Slansky, Phys. Letters 37B, 408 (1971).

44. R. Hagedorn, Suppl. Nuovo Cimento 3, 147 (1965); R. Hagedorn and J. Ranft, ibid. 6, 169 (1968).

45. I.Z. Artykov et al., Nucl. Phys. B6, 11 (1968) and references cited therein.

46. P.M. Fishbane et al., Phys. Rev. Letters 29, 685 (1972).

47. H.H. Heckman et al., Data presentation at this conference.

48. J.P. Vary, Summary talk presented at this meeting.

49. R. Holynski, S. Krzywdzinski and K. Zalewski, Krakow preprint No. 856/Ph.

50. K. Gottfried, CERN preprint TH 1735 (1973).

51. D.E. Lyon, Jr., C. Risk and D. Tow, Phys. Rev. D 3, 104 (1971) and G.R. Charlton and G.H. Thomas, Argonne National Laboratory Report No. ANL/HEP 7217 (unpublished).

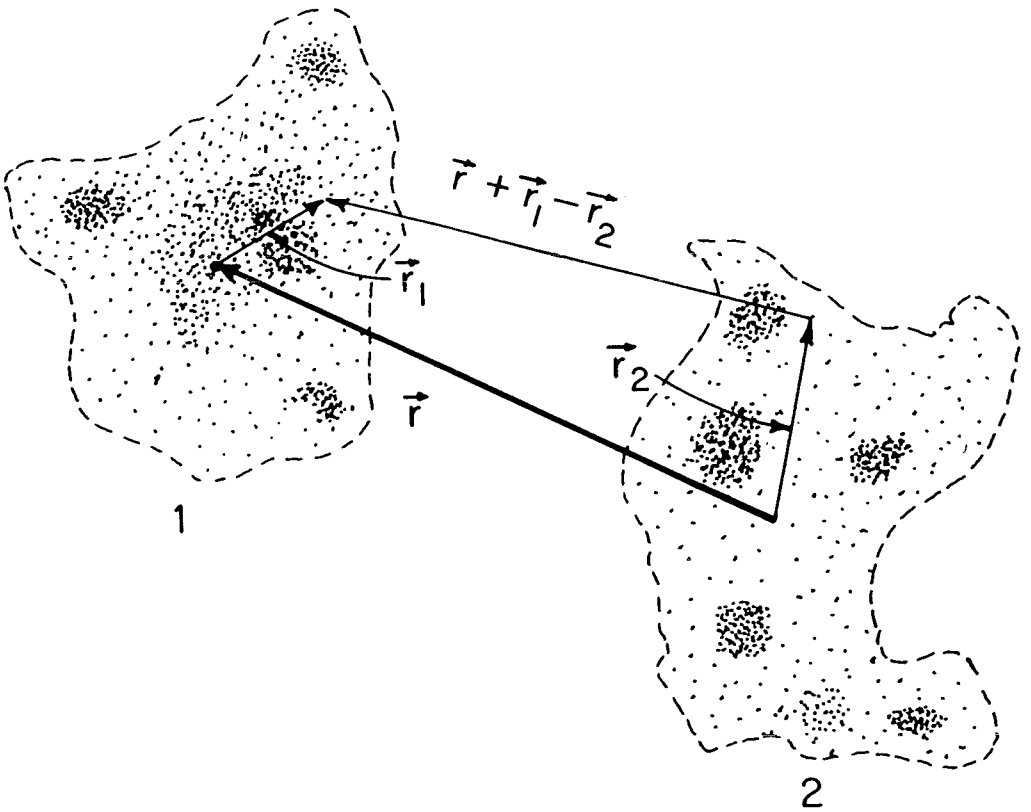

Fig. 1 Representation of two generalized distributions of interacting particles. $\vec{r}$ is the radius vector separating their centers of mass while $\vec{r}_1$ and $\vec{r}_2$ are internal vectors locating arbitrary particles. Then $\vec{r}+\vec{r}_1-\vec{r}_2$ is the vector argument of the particle-particle interaction.

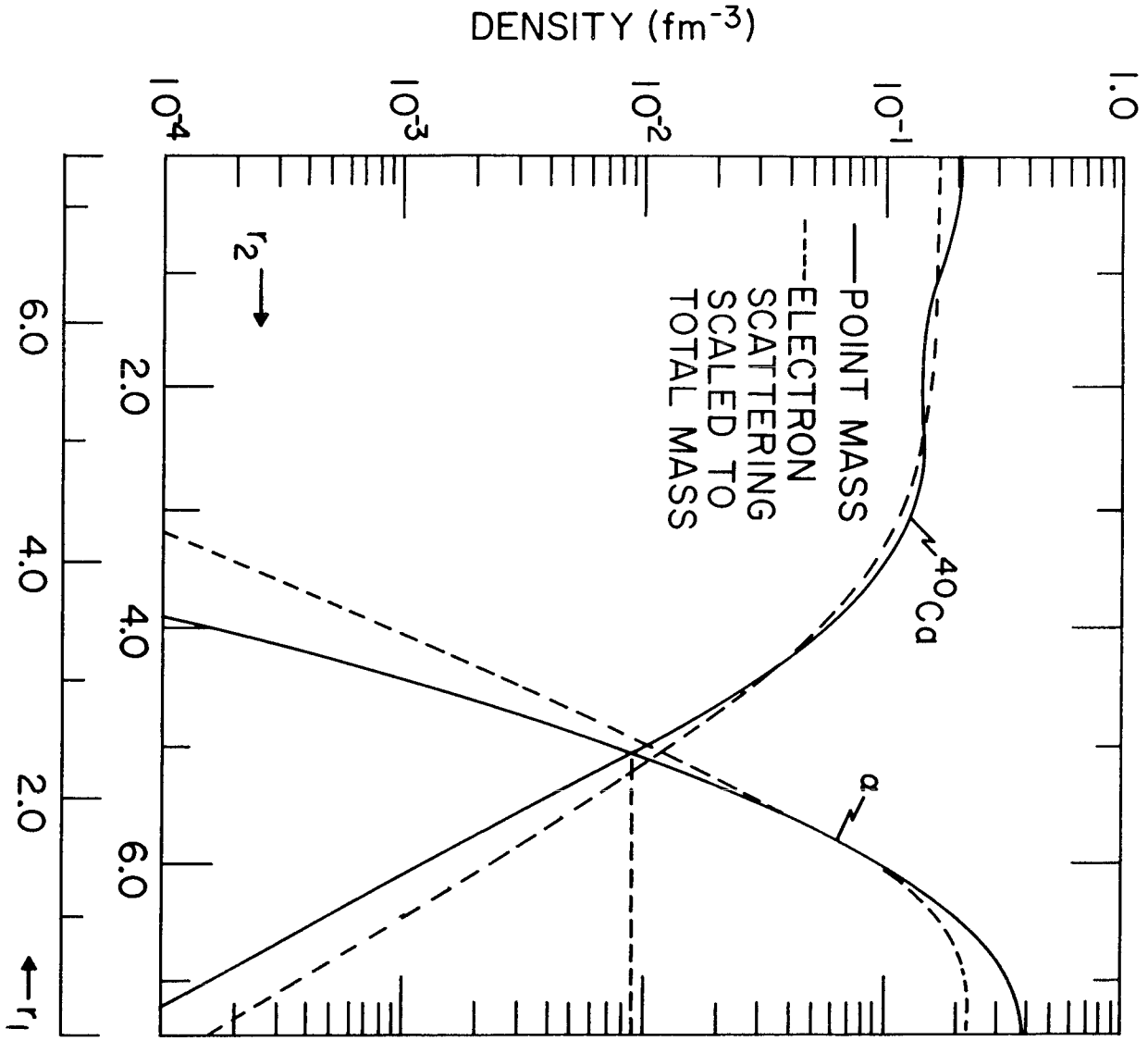

Fig. 2 Mass distributions for ^{40}Ca and α. The point mass distribution for ^{40}Ca is the result of shell model calculations based on potentials of Ref. 16 while the α point mass distribution is obtained by unfolding the finite proton size from the density determined by fits to electron scattering.

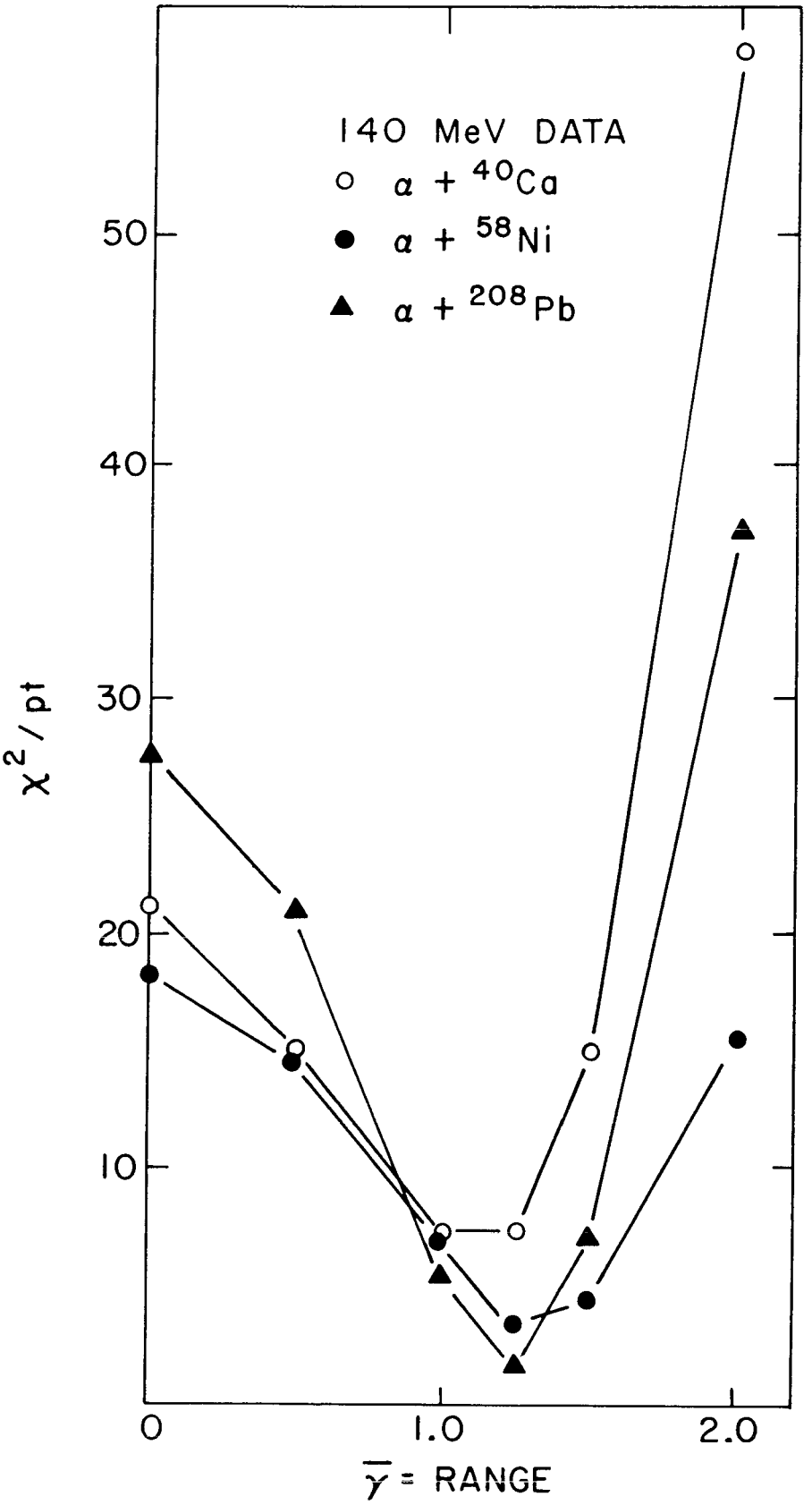

Fig. 3 Minimum square/pt. in fits to α data with the folding model versus the range in femtometers of the complex nucleon-nucleon $\mathcal{g}$ matrix. The actual range is $\gamma = (\gamma^{-2} + 0.64)^{1/2}$ to account for the use of the scaled electron scattering density for the α particle. No cneter of mass corrections were employed for the target densities.

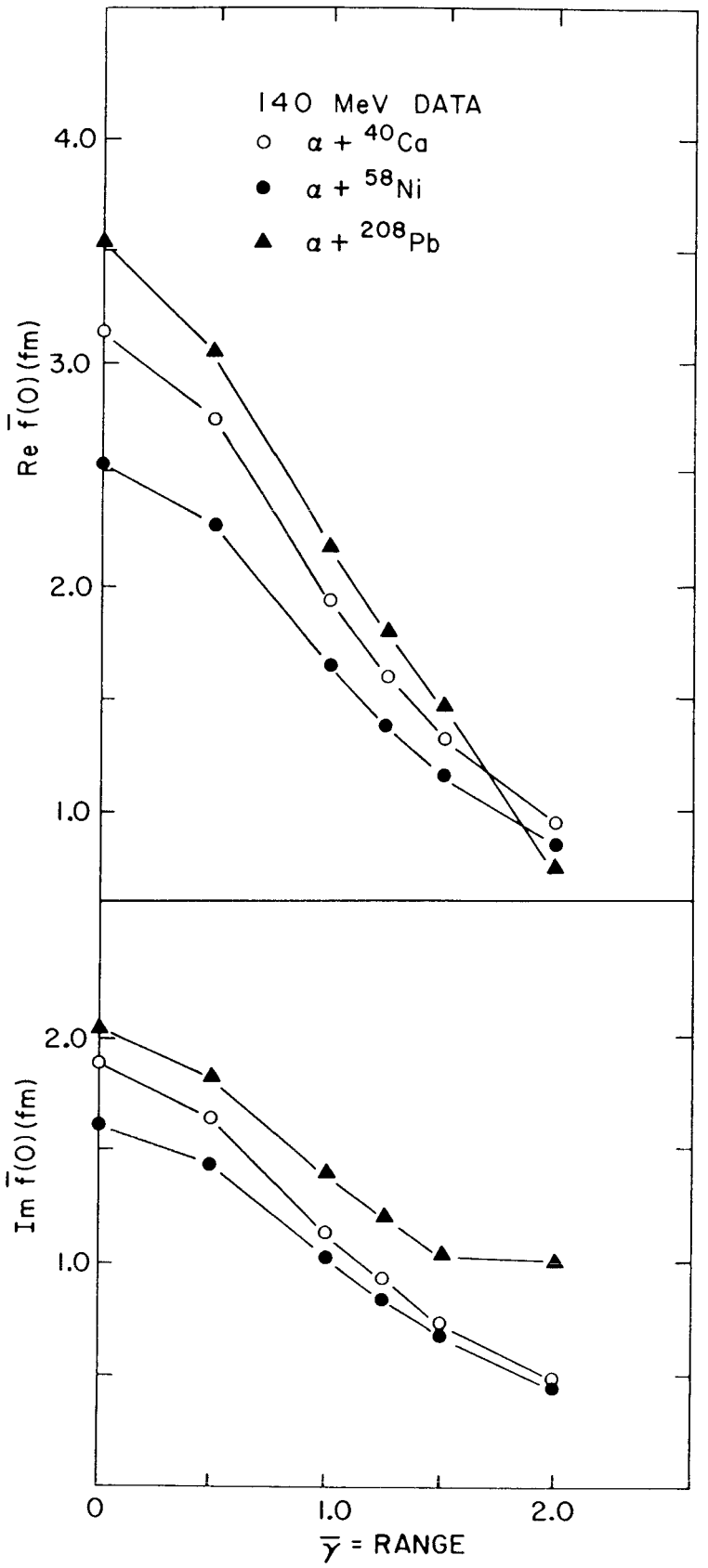

Fig. 4 Behavior of the best fit values of $\bar{f}(0)$ versus the range in femtometers of the complex nucleon-nucleon $\mathcal{g}$ matrix. See caption to Fig. 3.

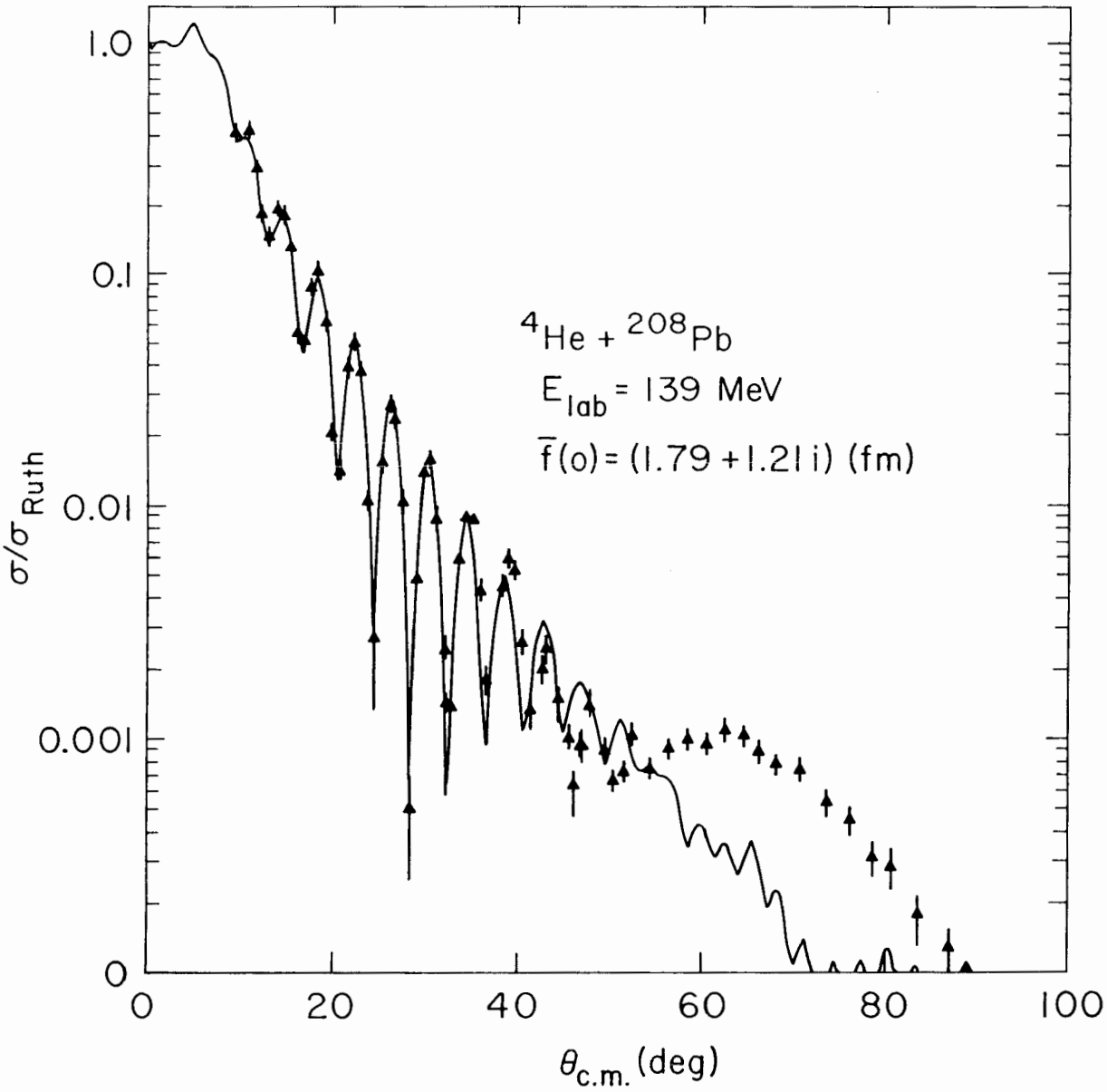

Fig. 5 The statistics average (top) and Fermi motion average (bottom) of the measured nucleon-nucleon forward scattering amplitude versus the incident nucleon's lab energy. K_F is the Fermi momentum in inverse femtometers employed in a Fermi gas average as described in the text. The solid curve represents the statistics average result and is labelled by $K_F = 0$ at the bottom to indicate it contains no many-body effects.

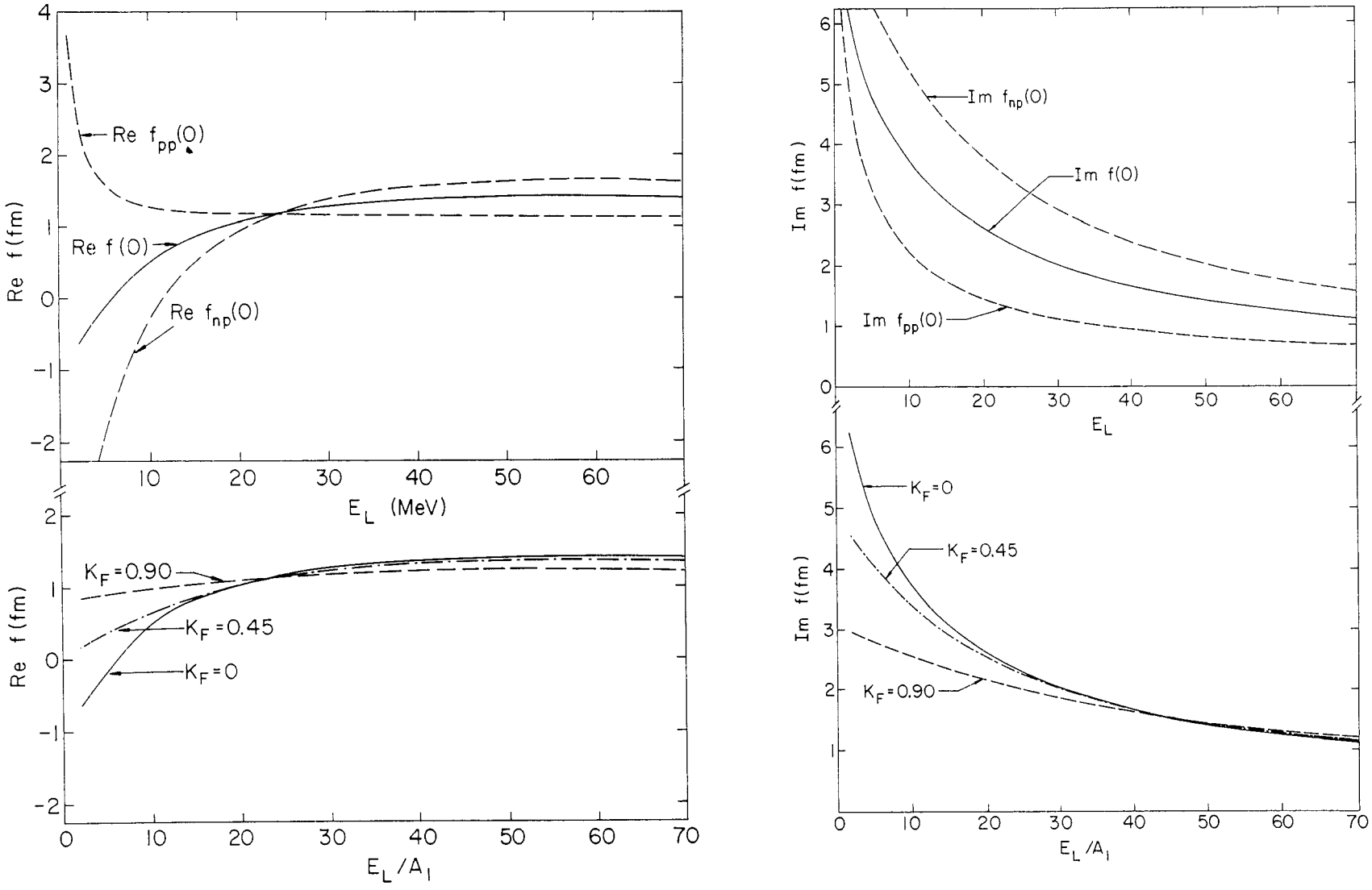

Fig. 6. The off-shell corrected (top) and Pauli corrected (bottom) forward scattering amplitude versus the incident nucleon's lab energy. The discrete points are the value of $\bar{f}(0)$ determined by least squares fits to available experimental data in the folded model with the range $\bar{\gamma}$ = 1.25fm. The remarkable degree of independence of $\bar{f}(0)$ and the near absence of energy dependence is noteworthy.

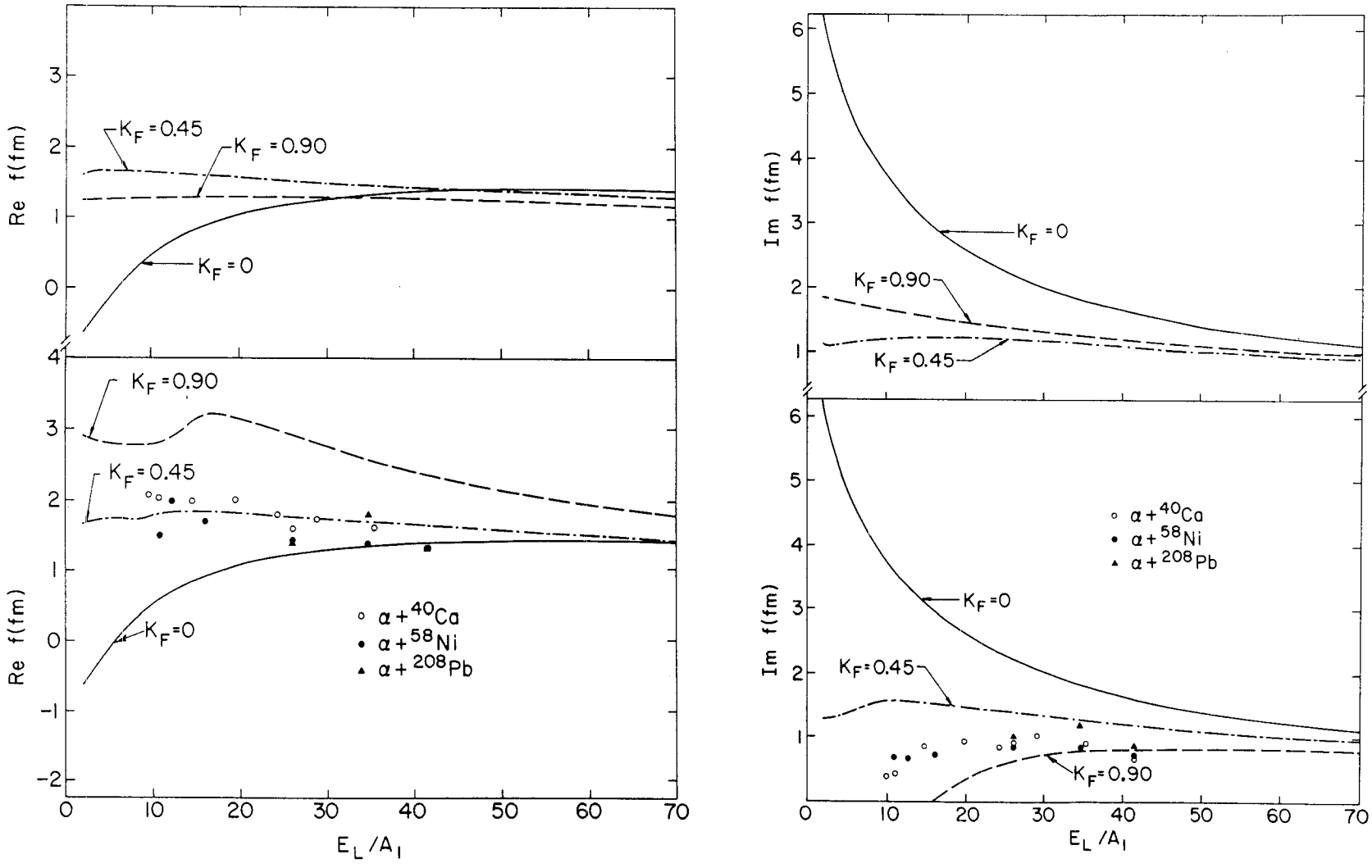

Fig. 7. Example of the results of a least squares fit within the folded model ($\bar{\gamma}$ = 1.25fm) to the measurements (Ref. 19) of cross section divided by the Rutherford cross section. No attempt is made to fit the data beyond center of mass scattering angle, θ_{cm}, of 40° since this lowest order model is not expected to be viable beyond the diffractive scattering region.

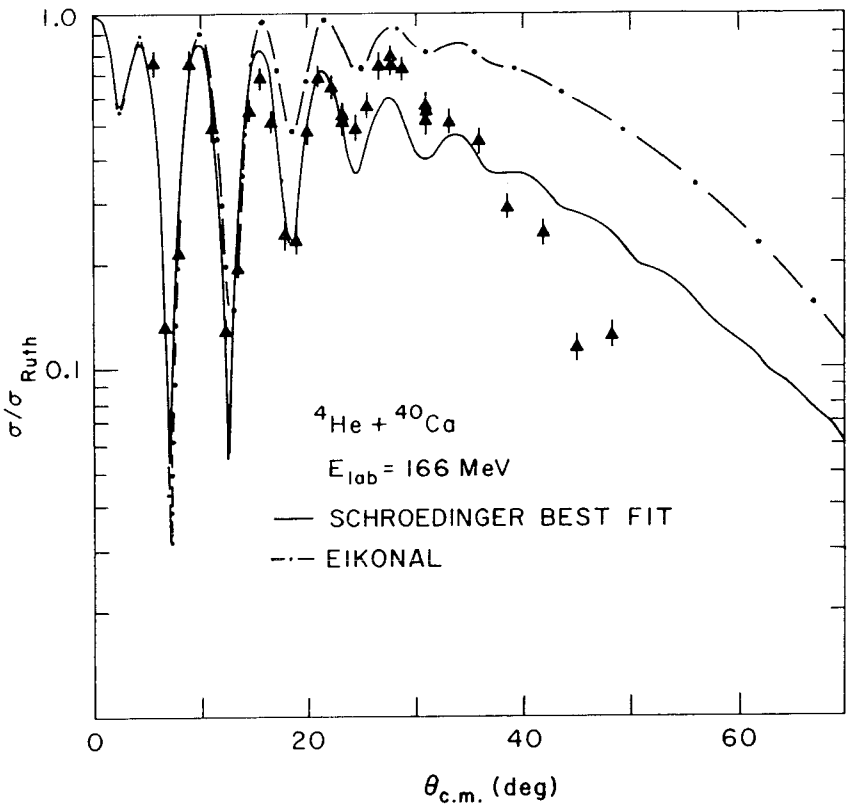

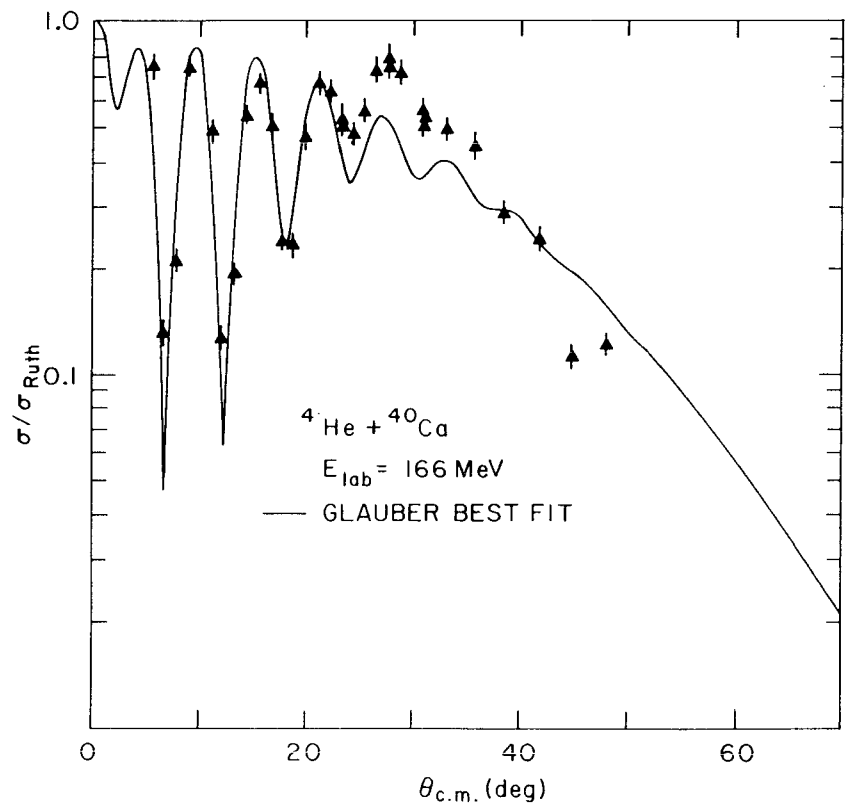

Fig. 8 Comparison of various dynamical frameworks for fixed (folded density) interaction with the experimental data for α + ^{40}Ca at 166 MeV. The eikonal and Glauber frameworks are functionally identical but eikonal employs the Schrödinger best fit value of $\bar{f}(0)$. For Glauber, $\bar{f}(0)$ is adjusted to give a least squares fit to the data.

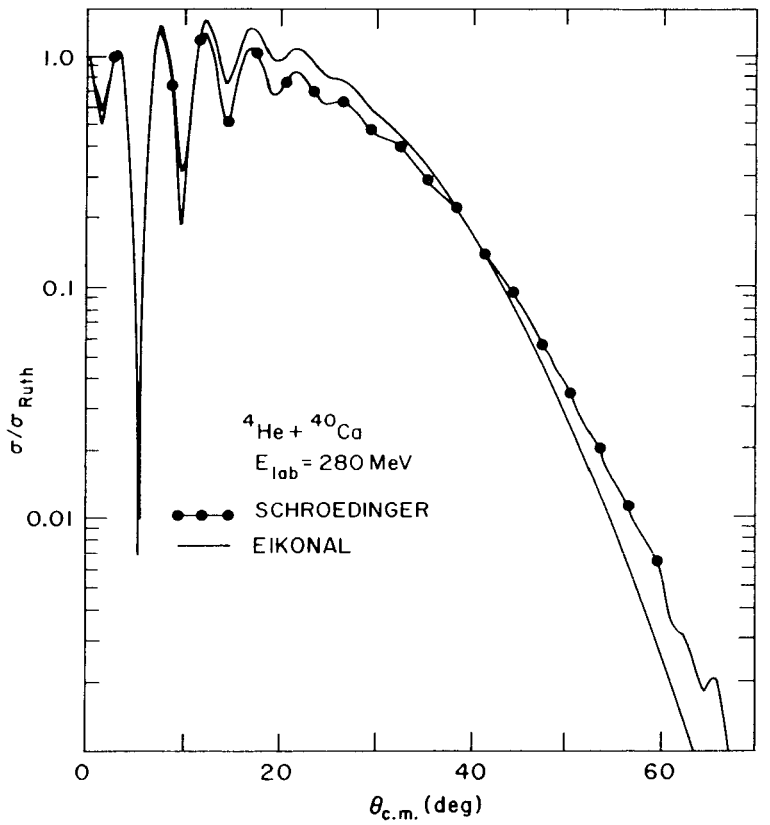

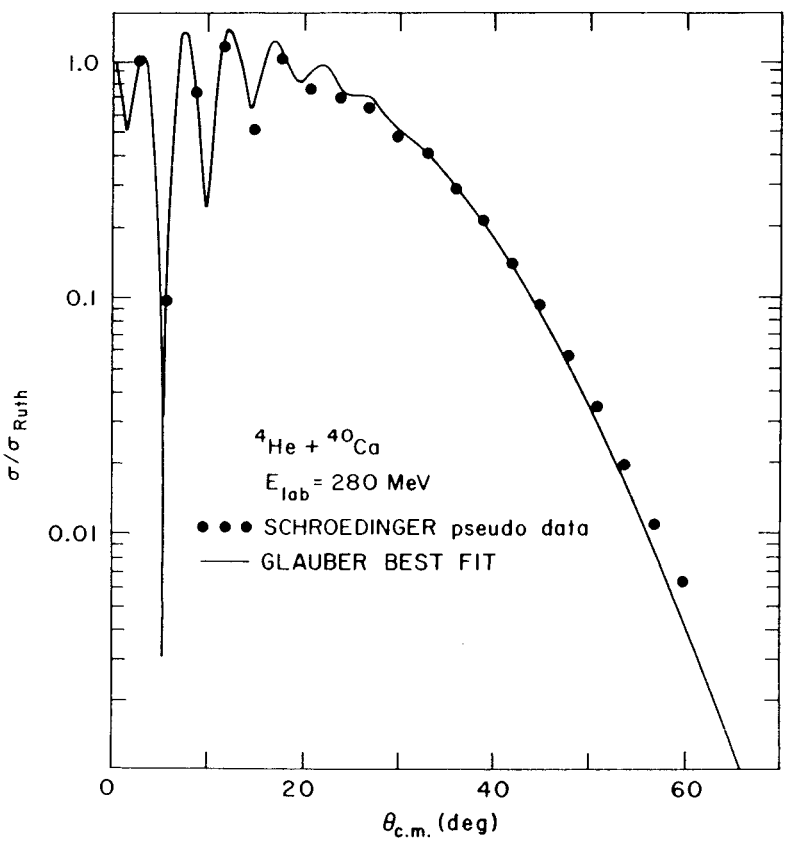

Fig 9 Comparison of various dynamical rrameworks for fixed (folded density) interaction with pseudo data for α + ^{40}Ca at 280 MeV. The pseudo data are the Schrödinger results at 5° intervals with the strength parameter taken from theory. A noticeable improvement in the eikonal approximation is observed when compared with the results in Fig. 8.

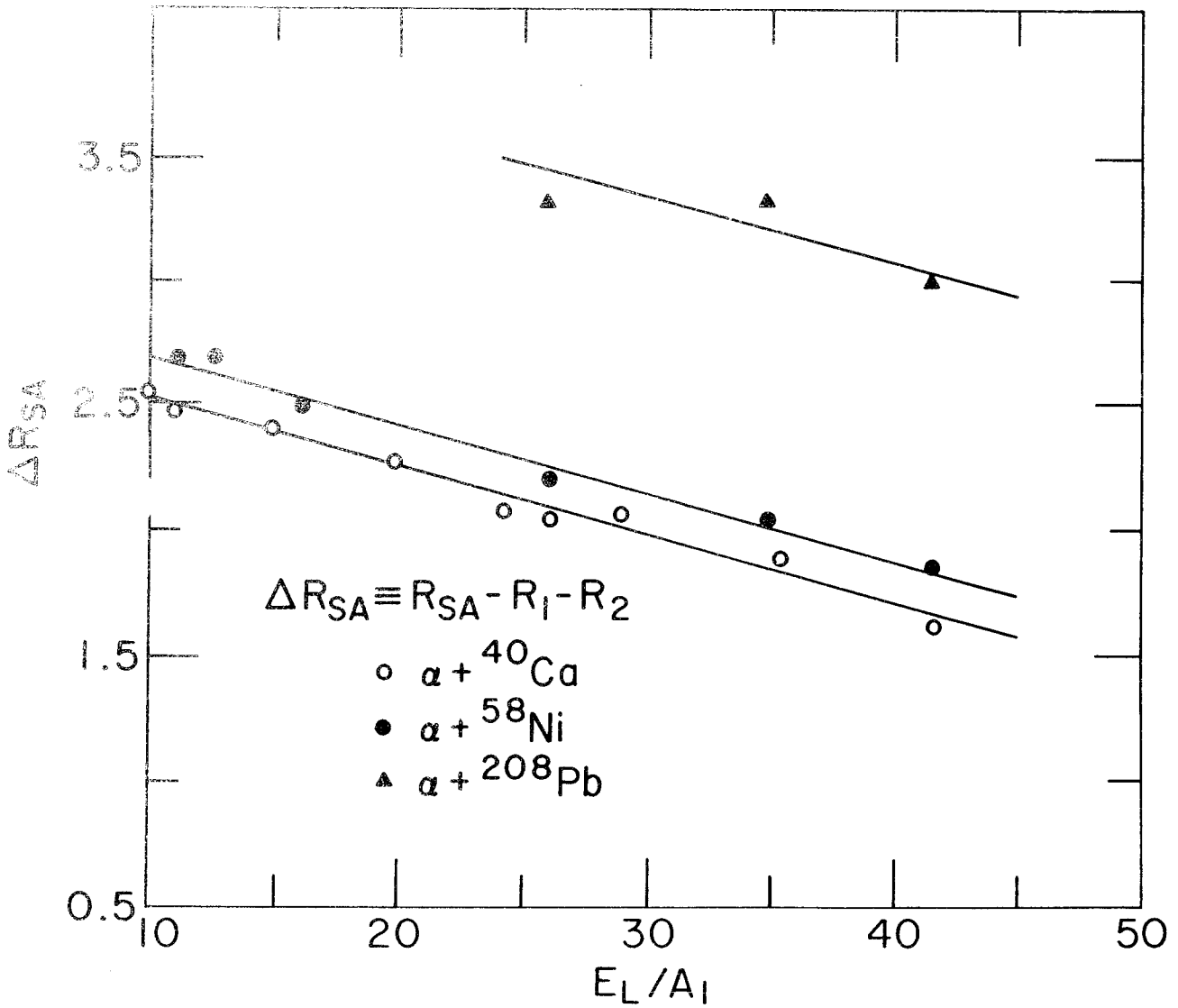

Fig. 10 Behavior of the strong absorption radius, R_{SA}, in fm with the energy per nucleon for α scattering on various targets. ΔR_{SA}, the difference in fm between the strong absorption radius and the sum of the r.m.s. radii of the colliding objects is actually plotted for convenience.

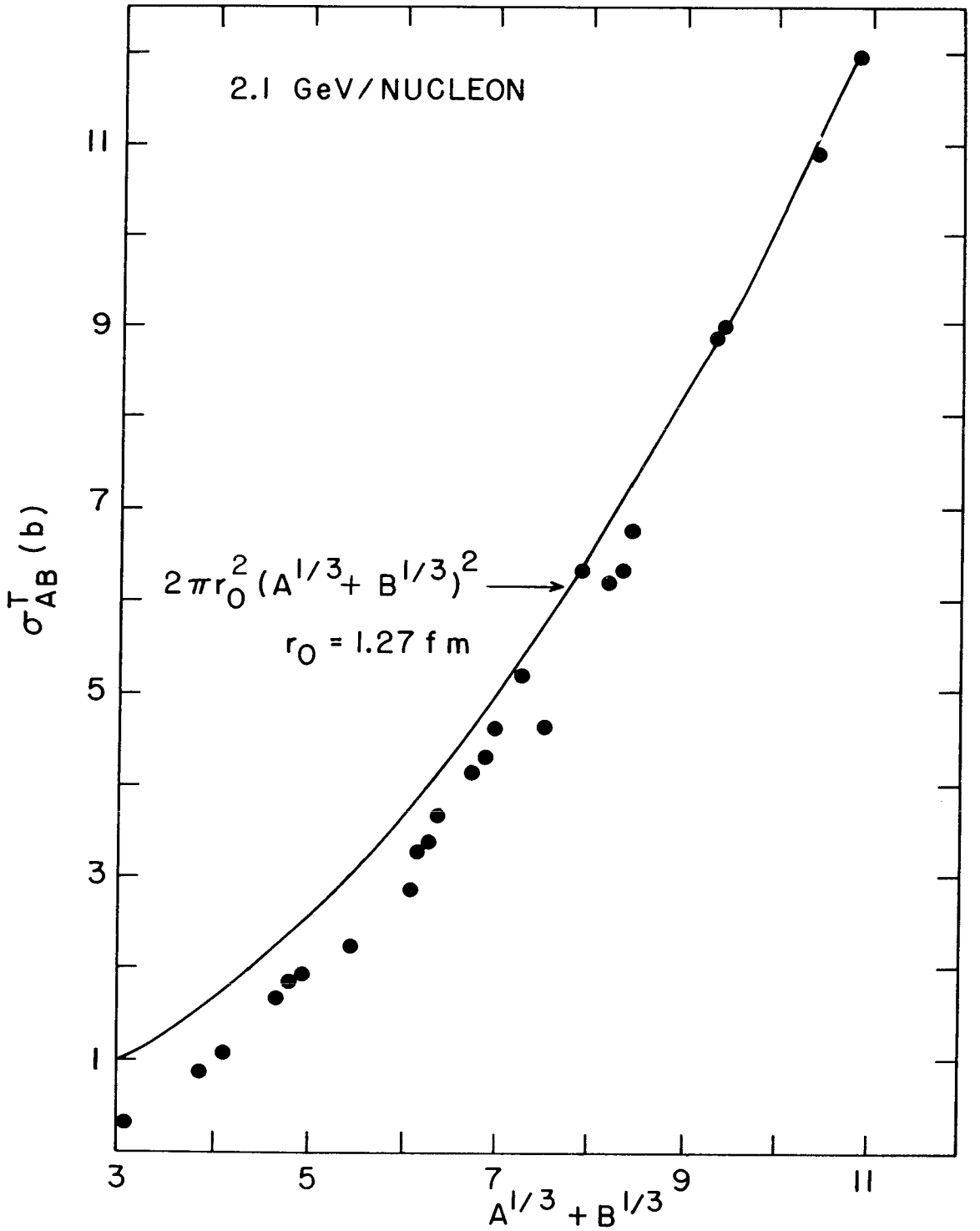

Fig. 11 Total nucleus-nucleus cross sections σ_{AB}^{T} at 2.1 GeV per particle, as a function of $A^{1/3} + B^{1/3}$. The points correspond to the reactions listed in Table 3. The solid curve represents the geometrical approximation.

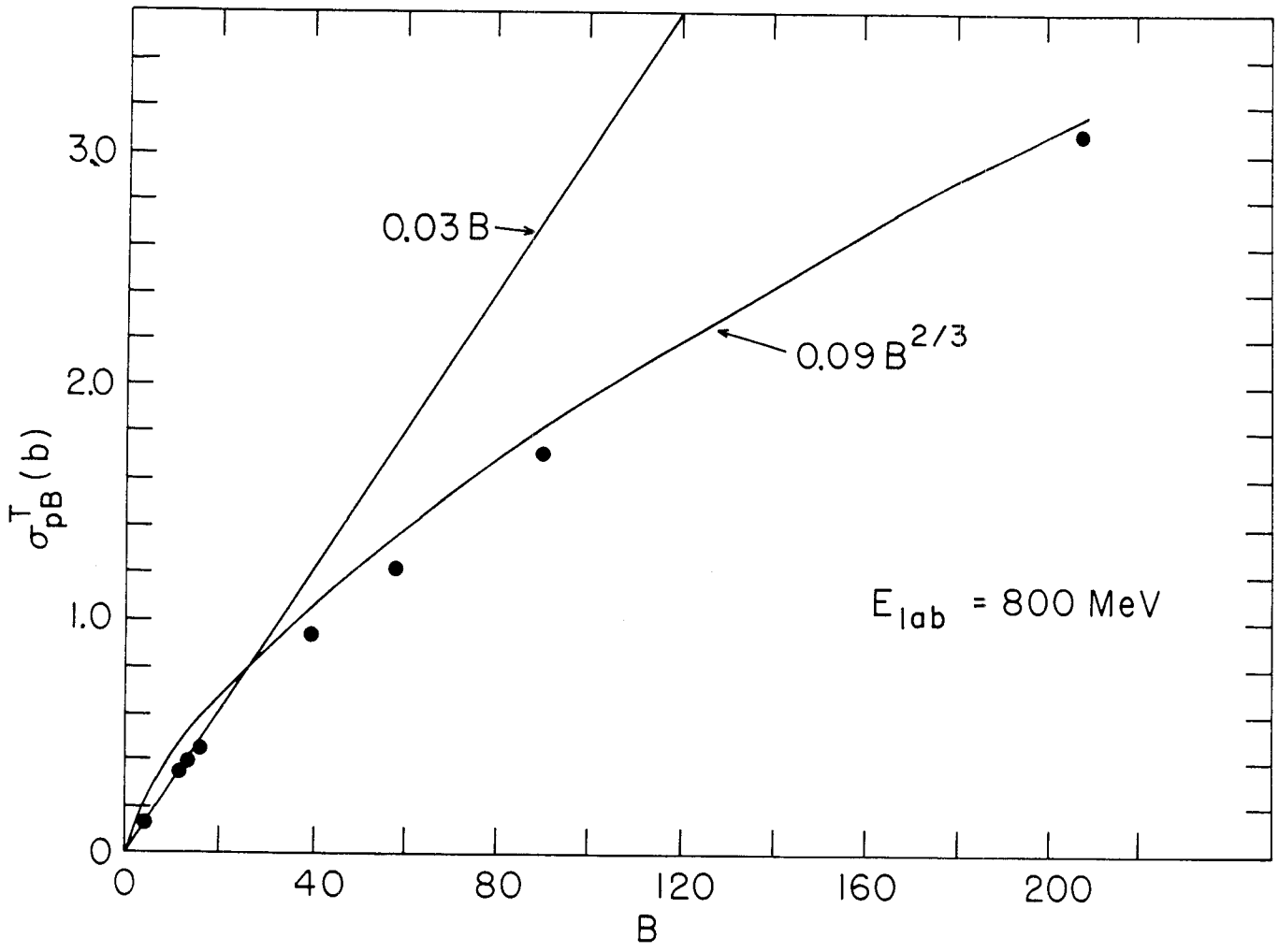

Fig. 12 Calculated proton-nucleus total cross sections σ_{pB}^{T} at 800 MeV lab energy. The points correspond to the reactions listed in Table 4. The two solid curves proportional to B and $B^{2/3}$ are obtained by approximately fitting the small B and large B behavior of σ_{pB}^{T}. See Ref. 25 for more complete results.

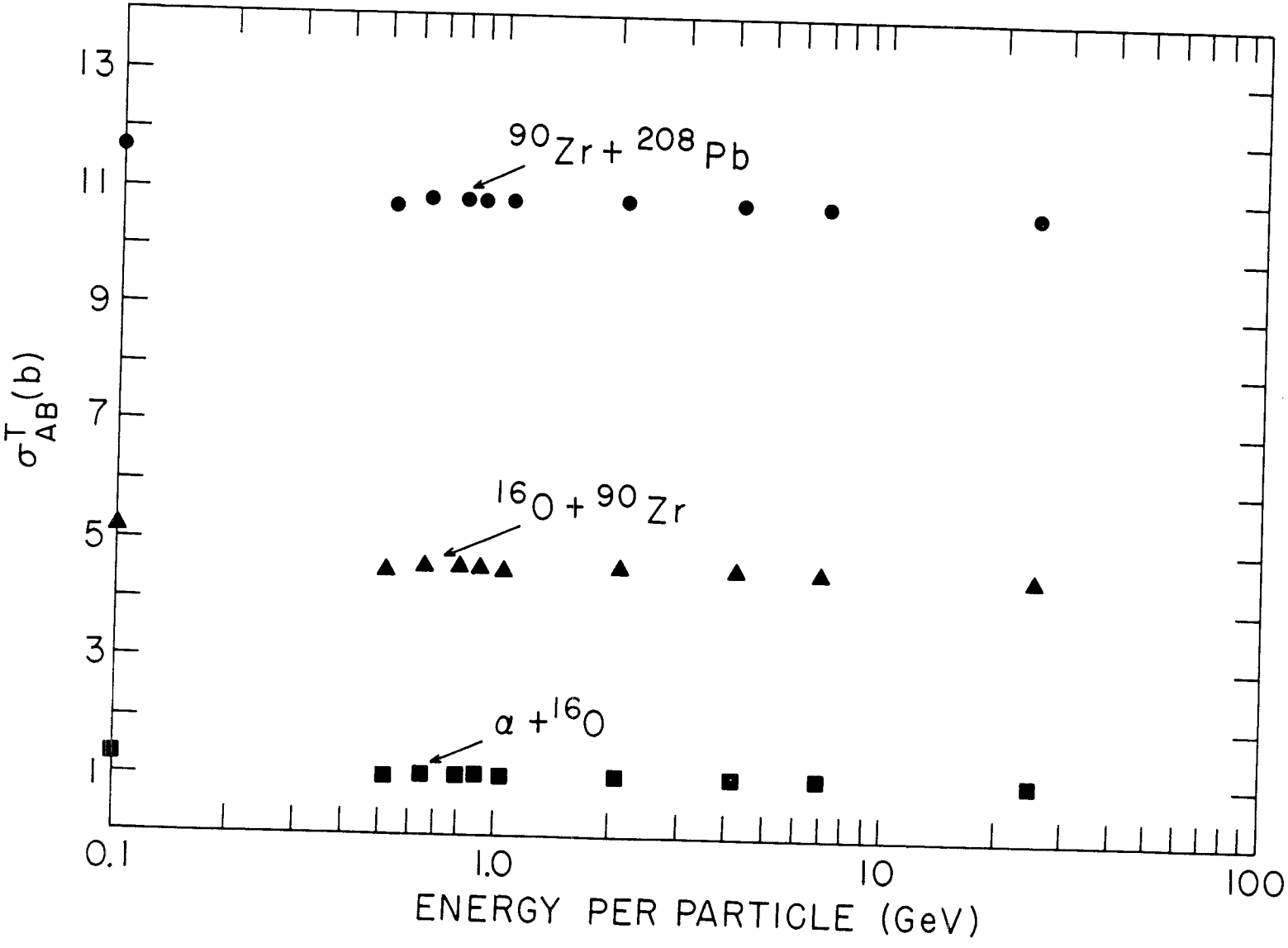

Fig. 13 Predicted energy dependence of nucleus-nucleus total cross sections in the energy range 0.1-25 GeV per particle. The points correspond to the energies and elementary cross sections listed in Table 1. Three typical reactions have been chosen from Table 3.

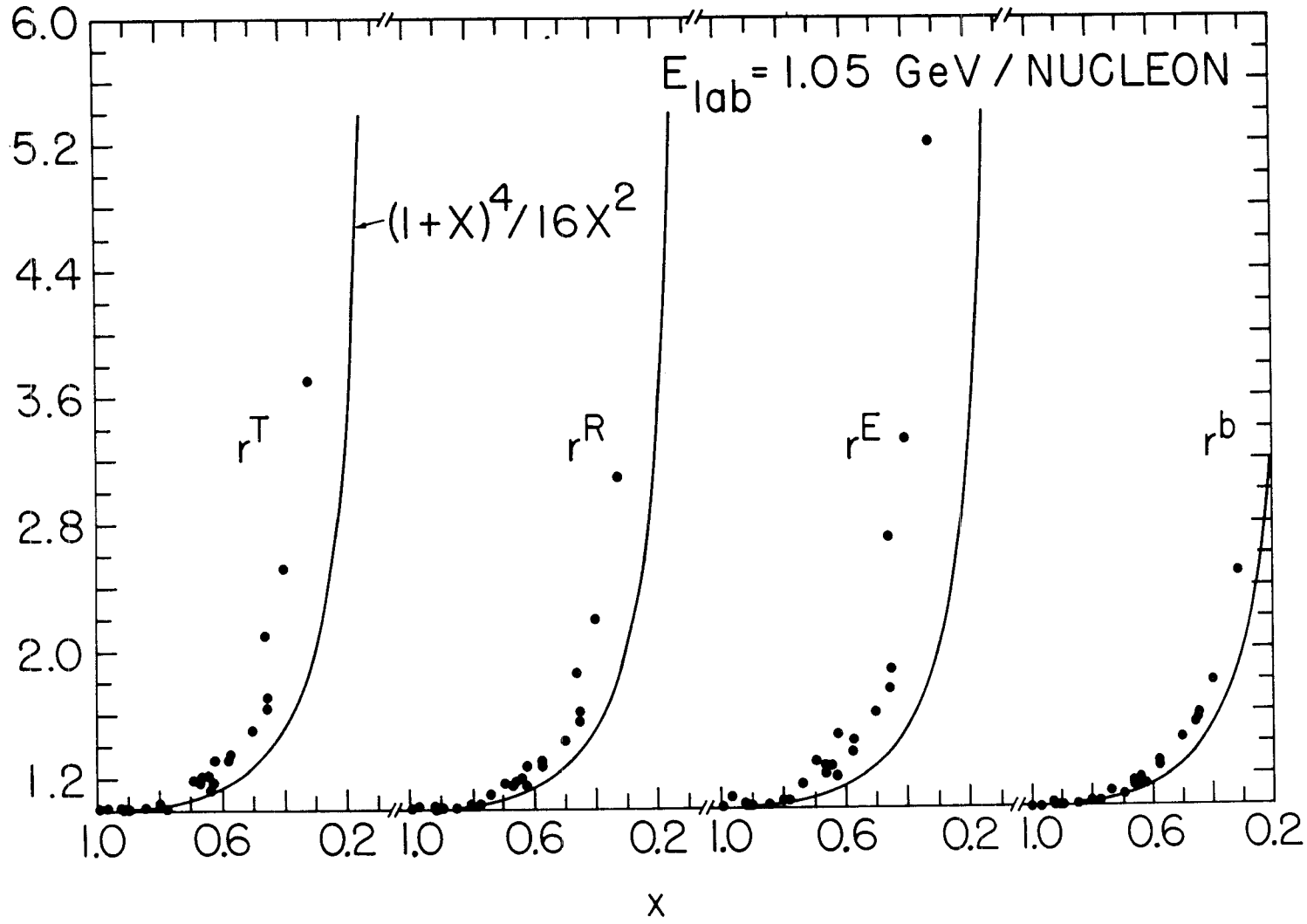

Fig. 14 Factorization ratios r^T, r^R, r^E and r^b of Eq. (35) at 1.05 GeV per particle as a function of the relative size parameter x. The points correspond to the reactions listed in Table 3. The solid curves represent the geometrical limit r^G of Eq. (38).

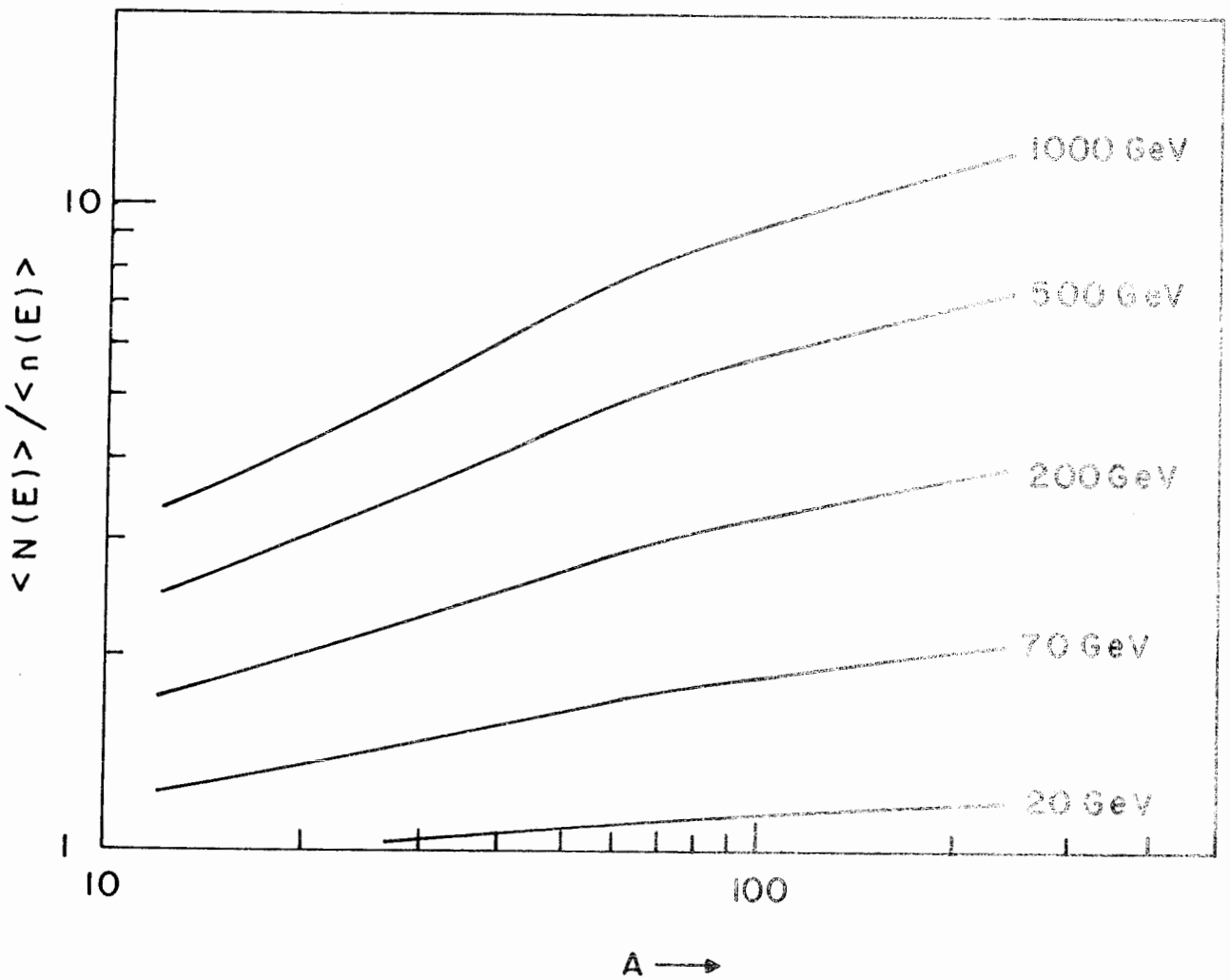

Fig. 15 Ratio of the average particle multiplicity in proton-nucleus collisions $< N(E) >$, based on an intranucleus cascading model described in Ref. 38, to the measured average multiplicity in pp collisions $< n(E) >$ as a function of incident energy and atomic number of the target nucleus. These results are extracted from Ref. 38 for pedantic purposes.

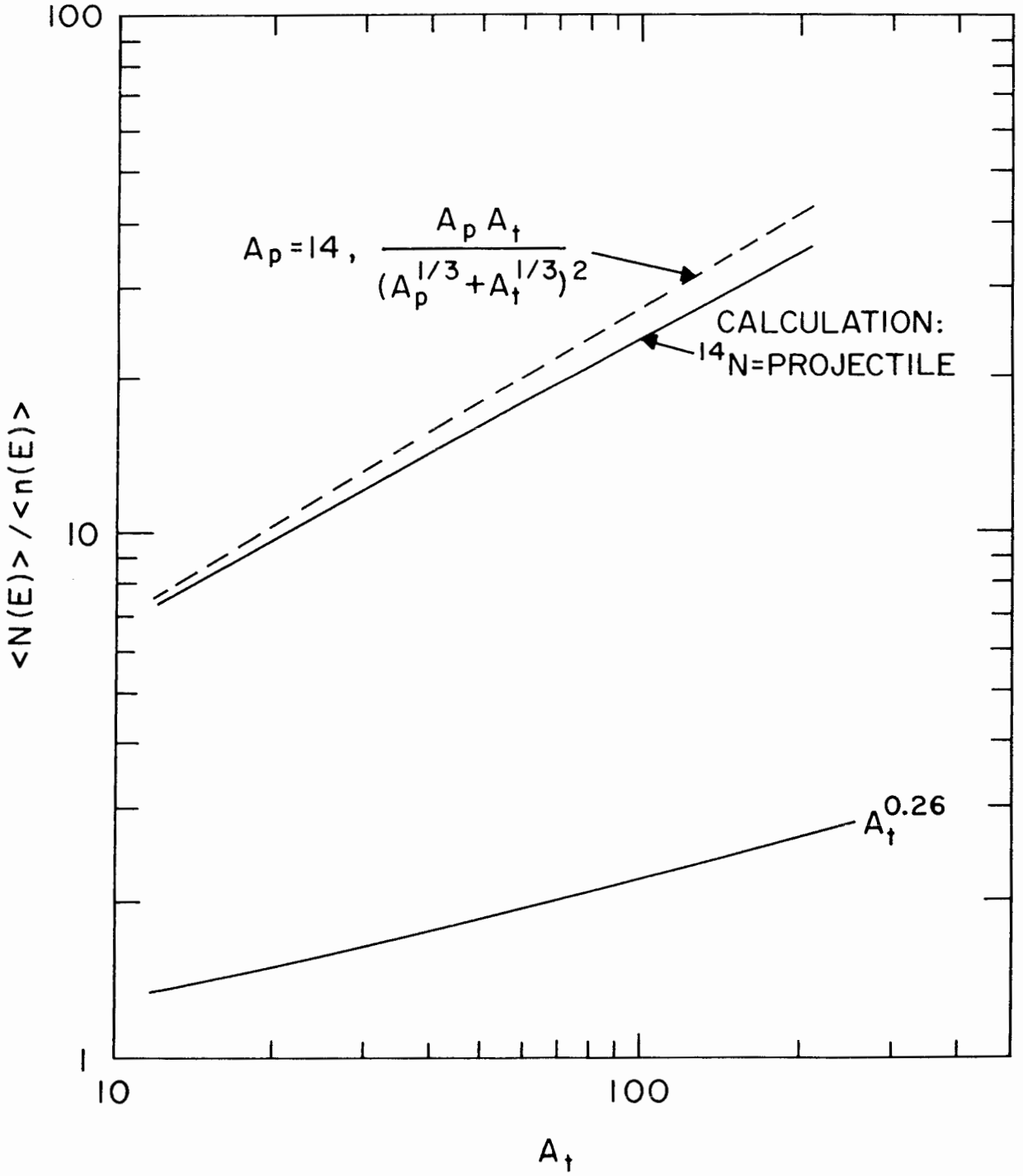

Fig. 17 Ratio of the average multiplicity in ^{14}N-nucleus collisions $< N(E) >$, based on a two-step mechanism with subsidiary assumptions as described in the text, to the measured average multiplicity in pp collisions $< n(E) >$ as a function of atomic number of the target nucleus. The dashed curve provides a comparison with the simple approximate analytic result of Eq. (45).

CAN ONE SEE N*'S IN NUCLEI ?+

by

R. SCHAEFFER

Service de Physique Théorique
Centre d'Etudes Nucléaires de Saclay
BP n° 2 - 91190 - Gif-sur-Yvette

FRANCE

I. INTRODUCTION.

With the availability of medium energy projectiles (say from a few 100 Mev to several Gev per particle), a new area is opened in Nuclear Physics. We shall comment here on a particular field which looks very promising : the physics of baryon resonances : N^* particles (with isospin I = 1/2) and Δ particles (I=3/2). More specifically, we shall ask ourselves the question whether there are such particles in a nucleus, and how they might manifest themselves. For this purpose, one might be guided by the experience with the backward proton-deuteron scattering, i.e. the d(p,d)p pick-up reaction. There it has been shown[1] that the meson degrees of freedom can be very important. Moreover, there are now some data[2] for the (p,d) pick-up on a nuclear target at energies up to 700 Mev and there is hope to have data at much higher energies. One might therefore hope this reaction partly proceeds by the pick-up of a baryon resonance in the target nucleus, instead of a neutron (fig. 1).

If such a process can be seen, it will be a direct measure of the wave function of an N^* in the nucleus.

II. THE BORN APPROXIMATION

Let us first, for simplicity, assume the proton and deuteron waves are not distorded by the presence of the target nucleus. The scattering amplitude is the sum of the usual neutron and of the N^* pick up amplitude (fig 1).

+ This talk is to a large extend based on a work currently done in collaboration with L.S. KISSLINGER and E. ROST

In addition, in this range, one has[1] $F_D \simeq F_D*$, so that :

$$T \sim F_N(Q) + F_N*(Q) \tag{4}$$

The values of Q for which F_N is large correspond of course to $Q \sim k_F$, the Fermi momentum ($k_F \sim 1.4\ m^{-1}$) . For $Q > k_F$, $F_N(Q)$ is a rapidly decreasing function of Q (roughly $F_N(Q) \sim F_N(0)\ e^{-\frac{3}{4}\left(\frac{Q}{k_F}\right)^2}$). On the other hand, one expects $F_N*(Q)$ not to decrease so rapidly, therefore it will eventually show up for large enough momentum transfer. As an example, some typical values of Q are given in table I for 700 Mev and 3 Gev protons

E	θ	Q fm^{-1}
700 Mev	0°	2.0
	30°	3.9
3 Gev	0°	3.4
	20°	6.2

Table I. Values of the momentum transfer Q at the nuclear vertex for the $^{12}C(p,d)^{11}C$ pick-up experiments as a function of the incident proton energy E and scattering angle θ.

Of course whether the N^* pick-up contribute co the (p,d) reaction will to a large extend depend on the distorsions of the proton and deuteron waves. This point will be investigated later.

III. THE NUCLEAR VERTEX $F_N*(Q)$.

The target wave function can be expanded as

$$|\psi_A\rangle = |\psi_A^{(0)}\rangle + \sum |\varphi_N* \psi_{A-1}^{(0)}\rangle \tag{5}$$

where $M_{N^*} - M_N$ is the N^* and N mass difference. A typical probability P_{N^*} for having in ^{12}C a given N^*, and the remaining nucleons in a given state of ^{11}C is of the order of 10^{-4} which is quite small. But the wave function φ_N of a nucleon is a rapidly decreasing function of the momentum transfer, whereas φ_{N^*} decreases slowly. For a high enough momentum, the probability of finding an N^* will eventually be larger than the probability of finding a nucleon. From (8) it is easy to see, from dimension arguments, that the probability P_{N^*} varies like $1/A^2$ where A is the mass of the considered nucleus. Since φ_{N^*} is built up with the product of three bound state function, its momentum distribution is roughly $e^{-\frac{Q^2}{2k_F^2}}$, that is

$$|\varphi_{N^*}(Q)|^2 \sim \frac{C}{A^2} e^{-\frac{Q^2}{2k_F^2}} \qquad \text{with } C \sim 10^{-2}$$

compared to the nucleon momentum distribution

$$|\varphi_N(Q)|^2 \sim e^{-\frac{3}{2}\frac{Q^2}{k_F^2}}$$

This means that at momenta larger than

$$Q \sim \eta k_F \qquad (\text{with } \eta^2 \simeq \log A^2/C)$$

the N^*'s will show up.

IV. THE (p,d) REACTION.

The transition amplitude for the A(p,d)A-1 reaction is written in the post representation as

$$T_{pd} = \langle \chi_d^{(-)} \psi_D \psi_{A-1} | v | \chi_p^{(+)} \psi_A \rangle \qquad (9)$$

where v is the interaction between two baryons in the deuteron. The mesonic degrees of freedom are assumed to be included in all the wave functions of (9). Seperating the N and N^* pick-up, the scattering amplitude reads :

The situation, for instance is much more favourable for 3 Gev incoming protons, where the baryon resonance contribution will show up in a much stronger way, and be comparable to the nucleon transfer contributions.

These calculations are still preliminary in the sense we have only roughly estimated the deuteron vertex for the various N^*'s, generalising the results of ref 1). A more careful calculation is currently being done.

V. HEAVY-ION REACTIONS.

It is tempting to use the additional freedom for the quantum numbers of the interacting fragments to get transfers which favour N^*'s compared to nucleons (for instance isospin 3/2 transfer). Moreover, the high selectivity of the heavy ion transfer reactions in terms of energy-momentum matching conditions can be used to search for N^* transfers reactions. Favoured regions are often called windows and have been explained using semi-classical arguments[4,5]. Let us consider the pick-up reaction $a + A \rightarrow b + B$ where a is the projectile which may be comparable in mass with the target A. The factorisation assumption leads to a scattering amplitude of the form :

$$T \sim F_{ab}(\underset{\sim}{\Delta})\ F_{AB}(\underset{\sim}{Q})$$

$$\underset{\sim}{Q} = k_f - \frac{M_B}{M_A} k_i \qquad (12)$$

$$\underset{\sim}{\Delta} = \frac{M_a}{M_b} k_f - k_i$$

The strong absorption will cause both functions F_{ab} and F_{AB} to be sharply peaked about the values

$$\Delta_{max} \sim \lambda_a/R_a$$

$$Q_{max} \sim \lambda_B/R_B \qquad (13)$$

It can be seen that the N^* window is at appreciably higher energy than the N window, especially for light projectile on light targets. In addition, the window for N^*'s is broader, due to the high momentum components of their wave functions in a nucleus. One might therefore expect N^* transfer to occur up to very high energies (say 500 Mev per nucleon, or even more), in a region where the nucleon transfer is already prohibited.

One should therefore look for transfer reactions as a function of energy from 50 to 500 Mev per nucleon. The nucleon transfer will be smoothly decreasing, and baryon resonance transfer should show up.

VI. OTHER REACTIONS.

There are of course many other ways to search for baryon resonance in nuclei. The (π,p) or (γ,p) reactions will certainly cast some light on this subject. I just learned about a very exciting feature, namely the data presented by Heckman et al which observe the $(^{16}O, ^{15}C)$ reaction at an energy of about 3 Gev per nucleon. The ^{15}C nucleus has two protons less and one neutron more than ^{16}O. Whereas at the lower energies (say 50 Mev per nucleon) this could still be due to multiple transfer, at the energies considered, this is practically impossible, as just discussed previously. But there is a non negligible probability (say 10^{-3} - 10^{-4} if one sums over the relevant excited states in ^{15}C) that ^{16}O is built up with a Δ^{++} orbiting around ^{15}C. By projectile fragmentation, the Δ can be separated from the core, hence leading to the observed ^{15}C particles without any need for multi-step processes. If this mechanism is the relevant one, there should be a shift δE compared to the expected energy of ^{15}C ($E_{^{15}C} \sim \frac{15}{16} E_{^{16}O}$), where δE is the mass-difference of a Δ and a nucleon :

$$\delta E \sim 300 \text{ Mev}$$

Of course this shift will be broadened by the momentum distribution of the Δ (i.e. by the kinetic energy this particle takes away, which is related to its momentum distribution in ^{16}O).

There is a competing process, which is proton emission by ^{16}O preceded or followed by charge exchange, (exchange of a virtual pion between projectile and target). This can be estimated from the known rate of ^{16}N particles

REFERENCES

[1] - A.K. KERMAN and L.S. KISSLINGER - Phys. Rev. 180 (1969) 1483.

[2] - S.D. BAKER et al - Phys. Lett. 52B (1974) 57.

[3] - J.B. CUMMINO - Ann Rev. Nucl. Sci. (E. SEGRE, Ed.) 13 (1963) 261 ;
S. JENA and L.S. KISSLINGER - Ann. Phys. 85 (1974) 251.

[4] - D. BRINK Phys. Lett. 40B (1972) 37.

[5]- F. POUGHEON and P. ROUSSEL Phys. Rev. Lett. 30 (1973) 1223.

[6] - J. KNOLL and R. SCHAEFFER to be published.

[7] - J.M. LAGET to be published in Phys. Lett.

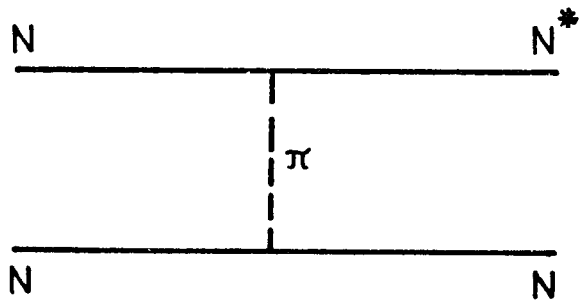

Figure 2. Elementary vertex for the creation of an N^*N pair by the one pion exchange process.

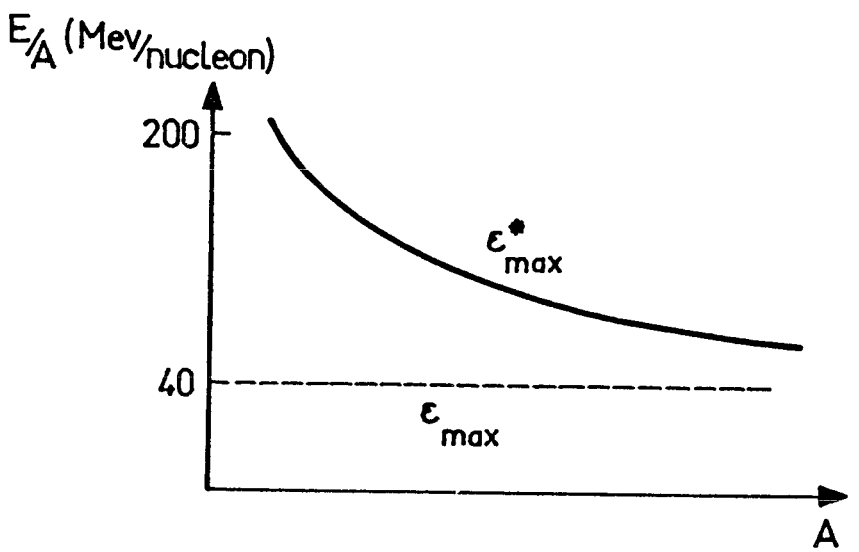

Figure 3. Comparison of nucleon transfer and N^* transfer cross-section for the $^{12}C_{G.S.}(p,d)\,^{11}C_{G.S.}$ reaction at $E_p = 700$ Mev.

STATISTICAL MODELS OF FRAGMENTATION PROCESSES

Alfred S. Goldhaber*

Institute for Theoretical Physics
Stony Brook, Long Island
New York 11794

July 15, 1974

Over a year ago, Heckman et al.[1] reported early results of experiments in which relativistic heavy ions (^{12}C, ^{16}O) impinged on various nuclear targets, and fragments of the projectile nucleus were observed. In the rest frame of the projectile, the fragments were found to have a momentum distribution $\exp(-p^2/2\,\sigma^2)$, with $\sigma \approx m_\pi c$, regardless of the mass of the fragment. Feshbach and Huang[2] attempted to understand this result in a model which described the projectile disintegration as a fast process governed by the distribution of nucleon momenta in the projectile before collision. Since then, more refined data[3] have shown that the quantity σ^2 does vary with fragment mass number K, in a manner well fit by the expression

$$\sigma^2 = \sigma_0^{\,2}\, K(A - K)/(A - 1) \qquad (1)$$

with $\sigma_0 \approx 90$ MeV/c.

We wish to show here that

(1) Equation (1) is an immediate consequence of the FH statistical hypothesis. Even the constant σ_0 is determined, and is only 10% higher than given by experiment.

* Supported by NSF GP-32998X.

This gives immediately

$$\langle \underset{\sim}{p}_K^{\,2} \rangle = \left\langle \left(\sum_{i=1}^{K} \underset{\sim}{p}_i \right)^2 \right\rangle = K(A - K) \langle \underset{\sim}{p}^2 \rangle / (A - 1). \tag{4}$$

Since the σ in Eq. (1) corresponds to a single Cartesian component of the three momentum $\underset{\sim}{p}_K$, we get

$$\sigma_0^{\,2} = \langle \underset{\sim}{p}^2 \rangle / 3 \quad . \tag{5}$$

FH quote, as a reasonable first approximation,

$$\langle \underset{\sim}{p}^2 \rangle = 3\, p_F^{\,2}/5 \tag{6}$$

where the Fermi momentum is taken as $p_F \approx 230$ MeV/c for ^{16}O.[2] This yields $\sigma_0 \approx 100$ MeV/c, 10% above the experimental value. There are qualitative arguments to suggest that the theoretical σ_0 could have a lower value because, on the one hand, the very light or very heavy fragments should exhibit the lower p_F of the nuclear surface, and, on the other hand, medium mass fragments are likely to have larger-than-average negative values of $\langle \underset{\sim}{p}_i \cdot \underset{\sim}{p}_j \rangle$ for their constituent nucleons. However, such claims require the existence of a far more complete theory for their evaluation.

2. Feshbach and Huang,[2] using a formalism developed earlier by Huang,[4] solved (in the large A limit) the following problem: Given that A nucleons are distributed among n fragments, each fragment labeled only by its three-momentum, what is the momentum distribution of any fragment? From the nature of their formulation,

of momentum of a given fragment K can be associated with a single degree of freedom, except that the center of mass motion of the remainder of the nucleus is perfectly correlated, since $\underset{\sim}{p}_A$ is zero. Therefore, we have

$$kT/2 = \langle p_{K\alpha}{}^2 \rangle / 2m_N K + \langle p_{K\alpha}{}^2 \rangle / 2m_N (A - K) \qquad (8)$$

or

$$\sigma^2 = m_N kTK(A - K)/A \qquad (9)$$

where k is Boltzmann's constant and m_N is the nucleon mass (we neglect binding corrections to fragment masses). This would correspond to an excitation temperature of about 9 MeV/k, remarkably close to the mean nucleon binding energy.

4. If the projectile nucleus received a mean squared momentum transfer $p_x{}^2$ in some direction, σ^2 in that direction would be changed to

$$\sigma'^2 = \sigma^2 + p_x{}^2 (K/A)^2 \quad . \qquad (10)$$

This means that the momentum distribution of the heaviest fragments is most sensitive to collisional momentum transfer.

We conclude that the momentum distribution of projectile fragments is not sensitive to the speed of the fragmentation process. Whether fragmentation occurred almost immediately after collision, with insignificant final state fragment-fragment interaction (sudden hypothesis), or whether it occurred only after a rough equilibrium

REFERENCES

1. H. H. Heckman et al., Proceedings 5th International Conference on High Energy Physics and Nuclear Structure (G. Tibell, ed.), Almqvist and Wiksell, Uppsala, 1974.

2. H. Feshbach and K. Huang, Phys. Letters 47B, 300 (1973), referred to as FH below. They compute a mean value of the number of ^{16}O fragments $\langle n \rangle \approx 7$. There are some misprints in their paper, but the result quoted here in eq. (7) is correct.

3. F. Bieser, B. Cork, D. Greiner, H. Heckman, and P. Lindstrom, report to Second Summer Study of Relativistic Heavy Ions, Lawrence Berkeley Laboratory, Berkeley, California, July 15-26, 1974. Experiment gives $\langle n \rangle \approx 7$, in agreement with the FH theory. The parabolic form, eq. (1), was suggested a year ago by W. A. Wenzel, using reasoning very similar to that given in the present paper (Section 1, below), but he was discouraged from pursuing the matter by the apparent disagreement with experiment. The same form was adopted by the experimenters in plotting their data. following work by J. V. Lepore and R. J. Riddell, who found the parabola in a simple model satisfying the assumptions of the present Section 1.

4. K. Huang, Phys. Rev. 146, 1075 (1966); Phys. Rev. 156, 1555 (1967).

5. Related to this, H. Feshbach (private communication), following remarks by T. E. O. Ericson, has shown that kinetic energies derived from Coulomb repulsion of initially tangent spherical fragment nuclei are comparable with the observed kinetic energies, when only two fragments are produced. However, for the more

FRAGMENTATION OF HEAVY NUCLEI AT HIGH ENERGY*

Joseph V. Lepore and Robert J. Riddell, Jr.

Lawrence Berkeley Laboratory
University of California
Berkeley, California 94720

July 17, 1974

ABSTRACT

Fragmentation of high-energy nuclei is treated using the quantum mechanical sudden approximation. Nuclear wave functions necessary for the method are constructed using the shell model. Momentum distributions for ^{4}He particles from ^{16}O and ^{12}C and for protons coming from ^{12}C are determined. They are dominated by a Gaussian factor whose standard deviation is simply related to the shell model parameters of projectile and fragment.

In a series of remarkable experiments carried out over the past two years Beiser, Cork, Greiner, Heckman and Lindstrom[1] have observed the fragmentation of heavy nuclei on various targets at energies of 1.05 and 2.1 GeV per nucleon. They find that when a nuclear projectile ruptures on collision it gives rise to nuclei with velocities narrowly distributed about that of the projectile. All possible "long-lived" ($> 10^{-9}$ sec) fragments (compatible with the quantum numbers involved) are observed; the spread in velocity (rapidity) is of the order of the "Fermi momentum" for the projectile. They further find that the ratios of the cross sections for various fragments is

$$A_{PT}^{NX} = \int \Psi_N^*(\xi_1, \cdots \xi_N)\, \Psi_X^*(\xi_{N+1}, \cdots \xi_{P+T}) \Psi_P(\xi_1, \cdots \xi_P) \Psi_T(\xi_{P+1}, \cdots \xi_{P+T}) d\tau, \tag{2}$$

where $d\tau$ represents the integration element over all variables. Our wave functions are not symmetrized between P and T or N and X, but a consideration of effects resulting therefrom, show these to be unimportant since there is essentially no overlap between such wave functions because there is a negligible component of 1-2 GeV particles in a nuclear state. The variables ξ_i represent an appropriate collection for description of the system: we find it convenient to use magnitude of momentum, angular momentum, and spin variables for these.

The fragmentation experiments are carried out in the manner of an "inclusive" measurement, in the language of high energy particle physics. Thus if we ask for the probability, W_{PT}^{N}, of finding a nuclear fragment N we have

$$W_{PT}^{N} = \sum_X \int \Psi_N^*(\xi_1, \cdots \xi_N) \Psi_X^*(\xi_{N+1}, \cdots \xi_{P+T}) \Psi_P(\xi_1, \cdots \xi_P)$$

$$\times \Psi_T(\xi_{P+1}, \cdots \xi_{P+T}) \Psi_N(\xi_1', \cdots \xi_N') \Psi_X(\xi_{N+1}', \cdots \xi_{P+T}') \Psi_P^*(\xi_1', \cdots \xi_P')$$

$$\times \Psi_T^*(\xi_{P+1}', \cdots \xi_{P+T}') d\tau \ .$$

Using the closure relation

$$\sum_X \Psi_X^*(\xi_{N+1}, \cdots \xi_{P+T}) \Psi_X(\xi_{N+1}', \cdots \xi_{P+T}') = \delta(\xi_{N+1} - \xi_{N+1}') \cdots \delta(\xi_{P+T} - \xi_{P+T}')$$

In this equation $\vec{Q}_N$ is the momentum of the nucleus "N". This type of wave function, when appropriately modified to take into account spin and the Pauli exclusion principle, has been used for the evaluation of the transition probability. A Slater determinant embodying these features is easily constructed.

Before giving the results of elaborate calculations involving such wave functions, we give a basic result which is independent of such complication. Note first that regardless of the state of a particle, each harmonic oscillator wave function contains a Gaussian factor. (To exhibit the aforementioned result we could assume that each particle is in an S state and that spin may be neglected.) All calculations are imagined to be done in the projectile rest frame. Upon inserting wave functions of the form of Eq. (5) into Eq. (3) we have

$$W_{PT}^{NX} = N_P^2 N_N^2 \int f(\vec{p}_1, \cdots) \prod_{i=1}^{N} \exp\left\{-\alpha_N\left[(\vec{p}_i - \vec{Q}_N/N)^2 + (\vec{p}_i' - \vec{Q}_N/N)^2\right] - \alpha_P(p_i^2 + p_i'^2)\right\}$$
$$\times \prod_{i=N+1}^{P} \exp\left\{-2\alpha_P p_i^2\right\} \delta\left(\sum_{i=1}^{N} \vec{p}_i - \vec{Q}_N\right) \delta\left(\sum_{i=1}^{N} \vec{p}_i' - \vec{Q}_N\right)$$
$$\times \delta\left(\sum_{i=1}^{P} \vec{p}_i\right) \delta\left(\sum_{i=1}^{N} \vec{p}_i' + \sum_{i=N+1}^{P} \vec{p}_i\right) d\tau ,$$

where N_P and N_N are normalization constants, and $f(\vec{p}_1, \cdots)$ is a polynomial in the momenta of the various particles which results from

calculation of relative probabilities. The dependence of W_{PT}^{N} on the fragment's momentum is now easily found to be

$$W_{PT}^{N} = C \exp\left[-Q_N^2/2\sigma^2\right] . \tag{5}$$

In this expression the standard deviation is

$$\sigma = \left[N(P - N)/4\alpha_P^{P}\right]^{1/2} \tag{6}$$

These simple formulas give a good account of the experimental data. The Gaussian formula fits individual results and the observed standard deviation for production of N from P is in good accord with Eq. (6) as shown in Fig. 1.[3] It is to be noted that the only parameter is α_P, which is related to the harmonic oscillator force constant. In the figure, the basic harmonic oscillator level spacing has been chosen as[4]

$$\hbar\omega_0 = 45\ A^{-1/3} - 25\ A^{-2/3} . \tag{7}$$

Figure 1 is plotted using a value of α_P which may be deduced from Eq. (7).

We now turn to the question of the evaluation of W_{PT}^{N} using shell model wave functions which correctly take into account orbital and spin angular momentum and the Pauli exclusion principle. This is not an easy task because one encounters large numbers of terms in any calculation. Simplification of integrals because of rotational invariance is spoiled because of the need for dealing correctly with total momentum as in Eq. (5). One feature which remains in any

FOOTNOTES AND REFERENCES

* This work was supported by the U. S. Atomic Energy Commission.

1. Beiser, et al., Bull. Am. Phys. Soc. 19, 518 (1974).

2. Compare L. I. Schiff, Quantum Mechanics, McGraw-Hill Book Co., New York, N. Y. (1949), p. 211.

3. Preliminary data presented by Beiser et al. at the High Energy Heavy Ion Summer Study, Lawrence Berkeley Laboratory, July 15-26, 1974.

4. G. F. Bertsch, The Practioner's Shell Model, American Elsevier Publishing Co., New York, N. Y. (1972), p. 33.

PHENOMENOLOGICAL APPROACH TO NUCLEAR FRAGMENTATION*

Fumiyo Uchiyama

Lawrence Berkeley Laboratory and
Space Sciences Laboratory
University of California
Berkeley, California 94720

ABSTRACT

The nova model of hadron-hadron scattering is extended to treat the fragmentation of heavy nuclei, and the results are in agreement with recent experiments.

To motivate the choice of the nova production spectrum ρ_{AB}, we recall the multi-Regge expression for double diffractive dissociation,[5] corresponding to Fig. 1b:

$$\frac{d^3\sigma}{dt\,dm_1\,dm_2} = \frac{1}{s^2}\ \beta_{AAR}(0)\ \beta_{BBR}(0)\ g^2_{PPR}(t) \left(\frac{s}{m_1^2 m_2^2}\right)^{2\alpha_P(t)}$$

$$\times\ (m_1^2)^{\alpha_R(0)+\frac{1}{2}}\ (m_2^2)^{\alpha_R(0)+\frac{1}{2}} \tag{3}$$

Here, $\beta_{AAR}(0)$ is the forward coupling of some Reggeon R to nucleus A; similarly, for $\beta_{BBR}(0)$, α_R and α_P are the trajectories of the Reggeon R and the Pomeron, and $g_{PPR}(t)$ is a triple-Regge coupling. Since the energies involved in the experiments of interest are not very high (2.1 GeV/c of beam momentum per nucleon), triple-Pomeron terms are unlikely to contribute appreciably and we assume R is the highest-intercept secondary Reggeon of appropriate quantum numbers, the f, with $\alpha_f(0) = \frac{1}{2}$. Using a linear trajectory $\alpha_P(t) = \alpha_P(0) + \alpha' t$ and exponential triple coupling $g_{PPf}(t) = g_{PPf}(0)\, e^{\gamma t}$ we can integrate over t to obtain a prototype missing mass distribution

$$\frac{\rho_{AB}(m_1, m_2)}{dm_1\ dm_2} = \beta_{AAf}(0)\ \beta_{BBf}(0)\ s^{2\alpha_P(0)-2} \left(\frac{1}{m_1^2 m_2^2}\right)^{2\alpha_P(0)-\alpha_f(0)-\frac{1}{2}}$$

$$\times \left[2\alpha' \log \frac{s}{m_1^2 m_2^2} + 2\gamma\right]^{-1} \exp\left[\left(2\alpha' \log \frac{s}{m_1^2 m_2^2} + 2\gamma\right) t_{min}\right] , \tag{4}$$

where the minimum momentum transfer t_{min} is a known complicated function of s, m_A, m_B, m_1, and m_2 (Ref. 6) and its appearance will

behavior has been found consistent in an analysis of $K_L - K_S$ regeneration by charge-exchange degeneracy on nuclear targets.[8]

In Fig. 3 we compare the experimental inelastic cross section with the results of a calculation using Eq. (2, 5, 6) normalized at lead and the agreement is satisfactory.

It is interesting to notice here that there are two pieces of preliminary experimental results on target dependence to be investigated further: The target dependence of total inelastic cross section, σ^{AB}_{incl}, is $A^{0.42}$ (Fig. 3) while that of partial cross section $\frac{d\sigma^C_{AB}}{d^3q}$ is $A^{0.256}$ which was observed for γ_A assuming factorizability of target and beam

$$\frac{d\sigma^C_{AB}}{d^3q}(\theta^C_L < 12mv) \equiv \gamma^C_B \, \gamma_A$$

These two information on target dependence implies that the average multiplicity should decrease as target mass increases as

$$n_C \equiv \frac{1}{\sigma^{AB}_{incl}} \int \frac{d\sigma^C_{AB}}{d^3q} \, d^3q \propto A^{-0.16}$$

if we assume that the target dependence is factorizable and has the same dependence at all angles.

The decay distribution of a nova is conventionally[2] considered to be a Gaussian in the nova rest frame

$$D^C_B(m_2, \vec{k}) = N_C(m_2) \exp\left\{-\frac{(k_L^2 + k_T^2)}{[K_C(m_2)]^2}\right\} , \qquad (7)$$

where we have resolved k into longitudinal (k_L) and transverse (k_T)

the rest frame of the nova (of mass m_2), then conservation of energy implies

$$m_2 = \sqrt{m_C^2 + P^2} + \sqrt{m_D^2 + P^2} .$$

In the case of interest, $P \ll m_C, m_D$ so we can rewrite the last equation as

$$P^2 = 2 m_C m_D [(m_2 - m_B + \delta)/m_B] .$$

Averaging over nova mass, we obtain

$$K_C^2 \equiv P_C^2 = 2 \frac{m_C m_D}{m_B^2} \int m_B (m_2 - m_B + \delta)\, \rho(m_1, m_2) dm_1 dm_2 / N$$

$$\equiv 2 \left(\frac{m_C}{m_B}\right) \left(\frac{m_B - m_C}{m_B}\right) \bar{Q}^2, \qquad (8)$$

where N is normalization and

$$N = \int \rho(m_1, m_2)\, dm_1\, dm_2,$$

where the constant Q^2 is independent of C. Thus K_c^2 is a parabola as a function of m_C, with a maximum at $m_C = m_B/2$. This formula is compared to experiment in Fig. 4, for an ^{16}O nova, and the agreement of the shape is quite good for its simplicity. The parabolic shape of the target dependence is also predicted from the quantum mechanical sudden approximation[12] and the statistical model.[13]

At the peaks of the nova mass spectrums, $m_{1,2} = m_{A,B} + \beta/2n_{A,B}$, the momentum P of the fragment C at mass number 8 for ^{16}O nova, and the target recoil momenta are calculated as a function of β and shown in Table I. The best result is obtained at $\beta = 0.5 \pm 0.1$. The fragment momentum is rather sensitive on δ at small β and could have

Footnote and References

*Work done under the auspices of the U. S. Atomic Energy Commission and NASA Grant NGR-05-003-513.

1. H. H. Heckman, D. E. Greiner, P. J. Lindstrom and F. S. Bieser, Phys. Rev. Lett. 28, 926 (1972) and private communication. See also H. Steiner, LBL-2144 (1973), for a review of research with high-energy heavy ions.

2. M. Jocob and R. Slansky, Phys. Rev. D 5 1847 (1972).

3. R. C. Hwa, Phys. Rev. D 1, 1790 (1970).

4. The experimental evidence for the double nova dominance is observed in the interaction of 2.1-GeV/c ^{16}O beam in emulsion. (D. E. Greiner, private communication.)

5. H. D. I. Abarbanel, G. F. Chew, M. L. Goldberger, and L. M. Saunders, Phys. Rev. Lett. 26, 937 (1971); G. F. Chew, Large and Small Baryon Numbers in High Energy Collision Theory, unpublished LBL Report (1973). The author would like to thank J. Koplik for discussions on this point.

6. H. Pilkuhn, The Interactions of Hadrons (Wiley, New York, 1967).

7. D. P. Ray and R. G. Roberts, Rutherford Laboratory Report RL-74-022-T79 (1974); R. D. Field and G. C. Fox, Cal Tech Report CALT-68-434 (1974).

8. F. Uchiyama, Phys. Rev. D 9, 673 (1973) and its addendum.

9. J. Harte, J. Rawls, and H. C. Yen, unpublished Yale report (1972).

10. Preliminary data presented by D. E. Greiner at the High-Energy Heavy-Ion Summer Study, Lawrence Berkeley Laboratory, July 15-26, 1974.

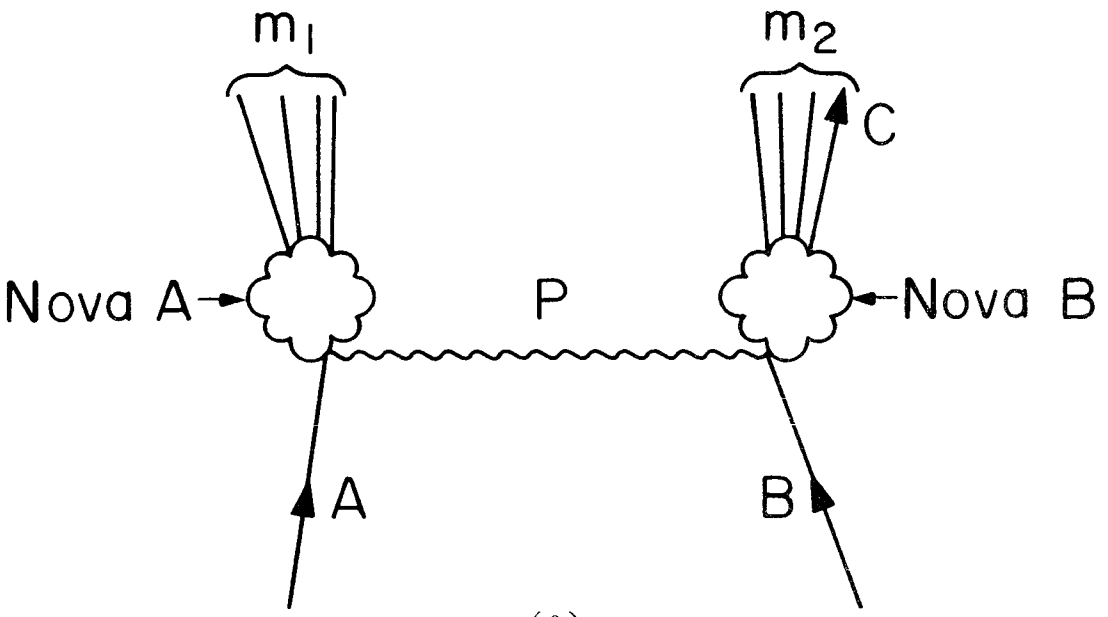

(a)

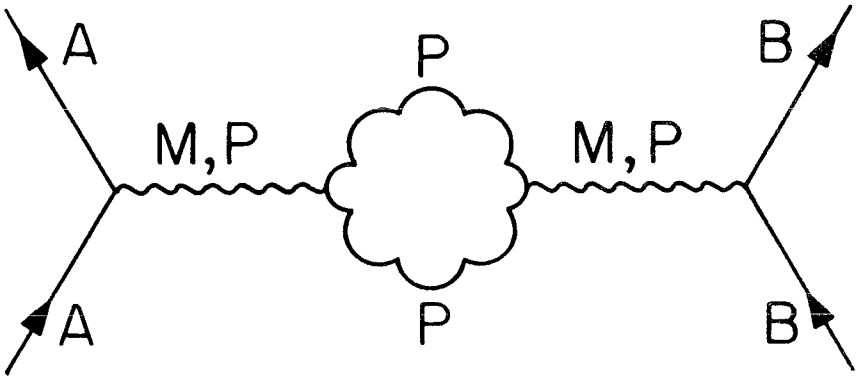

(b)

XBL 749-4145

FIG. 1a. Diffractive double-nova production and subsequent decay into fragments.

1b. Multi-Regge approximation to double-diffractive nova production.

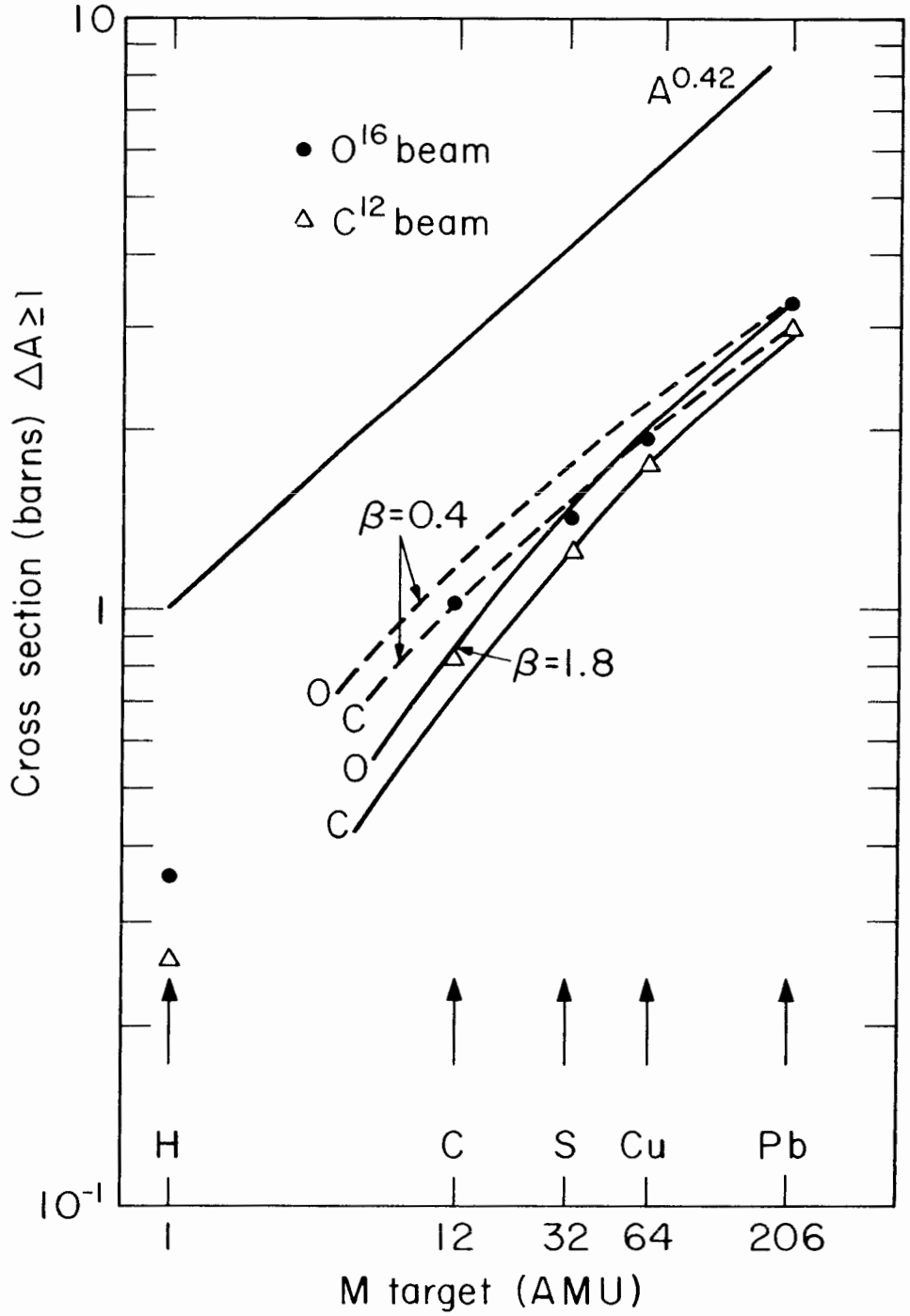

XBL 749-4147

FIG. 3. Target dependence of the total inelastic cross section. The data points are from Ref. 11. • = ^{16}O beam, △ = ^{12}C beam at 2.1 GeV/nucleon. The continuous curves are the results from calculation which is normalized at Pb for ^{16}O beam.

HIGH ENERGY REACTIONS IN NUCLEOSYNTHESIS

James W. Truran

Department of Astronomy, University of Illinois

Urbana, Illinois

High energy reaction mechanisms are directly responsible for the formation of a number of lighter nuclei in astrophysical environments. They are very likely responsible as well for the anomalous abundance features observed in the spectra of "peculiar" stars and for the synthesis of some heavy nuclei in supernova shock waves. Their most important contribution to nucleosynthesis may ultimately prove to be an indirect one - that of allowing the disintangling of the cosmic ray abundances to provide detailed information concerning the nature of cosmic ray sources. A brief review of these various problems is presented.

Introduction. Current theories of nucleosynthesis relegate to high energy reaction mechanisms a secondary role. Supporting arguments for this view are straightforward. Nucleosynthesis, as we understand it today, involves the synthesis of heavy nuclei in stars and supernovae as a consequence of fusion reactions starting with hydrogen and helium - the primordial galactic constituents, nuclear remnants of the cosmological fireball. Higher energy reactions (above $\sim$ 10 MeV/nucleon) are characteristically destructive by nature and are not suitable for this task. Rather, thermonuclear reaction mechanisms involving relatively low energy particles play the dominant role. Note further that for typical conditions in stars and supernovae, equilibrium exists between matter and radiation; high temperatures $T \gtrsim 10^{10}$ ^{o}K thus imply photonuclear breakdown of heavier species - but the kT energy equivalent at 10^{10} ^{o}K is only 1 MeV.

Elaborating upon this picture, extensive numerical investigations carried out over the past several years have established the likely roles played by various astrophysical sites in the synthesis of the elements. Hydrogen and ^{4}He represent the major products of the cosmological "big-bang" for a rather broad range of conditions. For more restrictive choices of boundary conditions, significant concentrations of ^{2}D, ^{3}He and ^{7}Li can also be formed, but universal synthesis of the heavy elements by this mechanism is not possible (Peebles 1966; Wagoner 1973).

The role of nuclear transformations in supernova shock precursors provides a new and active area for research. Substantial nuclear data concerning proton and alpha-particle reactions at energies $\sim$ 10-100 MeV/nucleon may be required to allow reliable predictions of relative nuclear abundances. The answers to date are surely not definitive - too many parameters are simply too poorly defined. Recent work by Weaver and Chapline (1974), for example, has posed serious fundamental questions concerning many details of this picture. They argue that radiation diffusion, not ion viscosity, represents the dominant dissipative mechanism for shock energies up to 30 MeV/nucleon - hence that a high ion-temperature shock precursor can only exist at higher energies. If this view is correct, deuterium production would certainly not be possible.

Nucleosynthesis and Cosmic Ray Sources. Supernovae and their remnants are generally considered to be the most likely source of cosmic rays in our galaxy. The energy requirements for filling the galaxy with cosmic rays are easily met and the relative heavy element enrichment of cosmic rays (see for example Shapiro and Silberberg 1970) suggests their origin is at a site of nucleosynthesis.

If this view is correct, it necessarily follows that cosmic rays represent both a potentially powerful probe of supernova environments and a test of nucleosynthesis theories. In order to utilize this probe, however, one must first correct the distribution of cosmic rays arriving at the top of the earth's atmosphere for the effects of propagation from the sources through the interstellar medium. An enormous research effort has been addressed to this problem over the past ten years (Shapiro and Silberberg 1974). These studies have been successful in providing measures of the mean path length traversed by the cosmic rays ($\sim$ 6 gm/cm^2) and of the cosmic ray dwell time in the galaxy ($<10^7$ years). Spallation reactions occurring as a result of cosmic ray traversal of 6 gm/cm^2 can give rise to enormous enhancements particularly of less abundant nuclear species (witness: lithium, beryllium and boron). The process of sorting out the secondary nuclei produced en route demands realistic estimates of fragmentation yields at high energies, as elaborated by Dr. Raisbeck in these proceedings. Source compositions of heavy cosmic ray nuclei have been obtained in this manner.

There are two major groups of heavy nuclei whose origin in supernova events we believe to be firmly established. The first of these groups, involving elements from neon to nickel, can be formed in solar system proportions in the explosive thermonuclear burning of matter composed initially of ^{12}C and ^{16}O at temperatures ranging $T \sim 2\text{-}7 \times 10^9$ ^oK. This can presumably occur in a single event - the explosion of a massive star. If the cosmic ray abundances of these nuclei have their origin in the same events, then their relative concentrations should be consistent with solar system matter. Within the uncertainties in both experiment and theory, the two distributions are consistent.

While this agreement is suggestive, it does not conclusively demonstrate that these cosmic rays are accelerated in the immediate vicinity of a supernova event. One could argue that a solar system mix of hydrogen, helium and these heavy nuclei has been subjected to a mechanism which preferentially accelerates the heavier component. Mogro-Campero and Simpson (1972) have in fact discovered an enrichment of heavy elements in solar cosmic rays indicating the operation of such a preferential acceleration mechanism. It is the second group of heavy nuclei formed in supernovae - the "r-process" heavy nuclei - which may ultimately provide a definitive test.

The solar system abundances of nuclei in the mass range $A > 60$ are largely attributable to two neutron-capture mechanisms, distinguished by the typical time between successive neutron captures. The "s-process", characterized by low neutron fluxes and time scales for successive captures at least of the order of years, is believed to occur during the red giant phase of a star's evolution. The "r-process" demands high neutron fluxes with neutron captures proceeding on a time scale short compared to beta decay lifetimes in the vicinity of the valley of beta stability. The operation of this mechanism on a hydrodynamic time scale in supernova environments has been demonstrated (Cameron, Delano and Truran 1970; Schramm 1973). Both mechanisms provide distinct signatures, evident in the abundance distribution of heavy nuclei in solar system matter. In both instances, these signatures reflect the increased stability of nuclei with "magic numbers" of neutrons. The s-process, constrained to the vicinity of the valley of beta stability, shows abundance peaks at masses $A \sim 88$, 138 and 208 corresponding to the closed neutron shells at $N = 50$, 82 and 126. In contrast, r-process neutron captures proceed into the neutron rich region off the valley of beta stability where the neutron closed shells are encountered at lower values of Z; the observed abundance peaks at $A \sim 130$ and $A \sim 195$ are believed to have been formed in this manner.

The potential for probing the nature of cosmic ray sources is evident from this discussion. Certainly no pure preferential acceleration mechanism operating on a solar system abundance mix could selectively emphasize the r-process nuclei. Accumulating data suggests, however, that the heavy nuclei in the cosmic radiation shows a distinctly r-process signature (Price et al 1971). Should this be confirmed by further investigations, the origin of cosmic ray heavy nuclei at a side of nucleosynthesis would be demanded. Furthermore, Osborne et al (1973) have found the energy spectrum of heavy cosmic rays ($Z \gtrsim 60$) to be much steeper than measured spectra of the less massive components, suggesting that perhaps a second source (another type of supernova event?) is responsible for the formation and acceleration of cosmic rays in this heavy region. (We should note that conflicting evidence does exist (Fowler 1973) indicating an energy spectrum in this region consistent with that of the iron group.)

Further studies of cosmic ray abundances are required to clarify many aspects of this picture. One exciting area involves the determination of isotopic ratios for nuclei of $Z \geq 6$. Nucleosynthesis studies make very definite predictions of these ratios (Truran 1973b,c; Arnett 1973) which should provide more critical tests of the nature of cosmic rays sources. For these more sensitive tests, experimental determinations of the fragmentation yields for spallation reactions at energies up to ~ 1 GeV/nucleon involving nuclei in the mass range $12 \lesssim A \lesssim 24$ are essential.

This research was supported in part by the National Science Foundation under Grant GP-40696.

REFERENCES

Arnett, W. D. and Truran, J. W. 1970, Ap. J., 160, 959.

Arnett, W. D., Truran, J. W. and Woosley, S. E. 1971, Ap. J., 165, 87.

Arnett, W. D. 1973, Ann. Rev. Astro. Astrophys., 13, 73.

Audouze, J., Lequeux, J. and Reeves, H. 1973, Astron. Astrophys., 28, 86.

Bernas, R., Gradsztjan, E., Reeves, H. and Schatzman, E. 1967, Ann. Phys., 44, 426.

Brancazio, P. J. and Cameron, A. G. W. 1967, Can. J. Phys., 45, 3297.

Burbidge, E. M., Burbidge, G. R., Fowler, W. A. and Hoyle, F. 1957, Revs. Mod. Phys., 29, 547.

Cameron, A. G. W. 1957, Chalk River Rep., CRL-41.

Cameron, A. G. W., Colgate, S. A. and Grossman, L. 1973, Nature, 243, 204.

Cameron, A. G. W., Delano, M. D. and Truran, J. W. 1970, in Proceedings of the International Conference on the Properties of Nuclei far from the Valley of Beta Stability, Vol. 2, CERN.

Colgate, S. A. 1973, Ap. J. (Letters), 181, L53.

Colgate, S. A. 1974, Ap. J., 187, 321.

Epstein, R. I., Arnett, W. D. and Schramm, D. N. 1974, Ap. J. (Letters), 190, L13.

Fowler, P. H. 1973, in Proceedings 13th International Cosmic Ray Conference, Denver, Colorado.

Fowler, W. A., Burbidge, G. R. and Burbidge, E. M. 1955, Ap. J. Suppl., 2, 167.

Hoyle. F. and Fowler, W. A. 1973, Nature, 241, 384.

Meneguzzi, M., Audouze, J., and Reeves, H. 1971, Astron. Astrophys., 15, 337.

Michaud, G. 1970, Ap. J., 160, 641.

Mitler, H. E. 1972, Astrophys. Sp. Sci., 17, 186.

Mogro-Campero, A. and Simpson, J. A. 1972, Ap. J. (Letters), 171, L5.

Osborne, W. Z., Pinsky, L. S., Shirk, E. K., Price, P. B., Kobetich, E J. and Eandi, R. D. 1973, Phys. Rev. Letters, 31, 127.

Peebles, P. J. E. 1966, Ap. J., 146, 542.

Price, P. B., Fowler, P. H., Kidd, J. M., Kobetich, E. J., Fleischer, R. L. and Nichols, G. E. 1971, Phys. Rev. D, 3, 815.

Reeves, H. and Audouze, J. 1968, Astrophys. Letters, 1, 197.

Reeves, H., Fowler, W. A. and Hoyle, F. 1970, Nature, 226, 727.

Rogerson, J. B., Jr. and York, D. G. 1973, Ap. J. (Letters), 186, L95.

Ryter, C., Reeves, H., Gradsztjan, E. and Audouze, J. 1970, Astron. Astrophys., 8, 389.

Schramm, D. N. 1973, Ap. J., 185, 293.

Shapiro, M. M. and Silberberg, R. 1970, Ann. Rev. Nucl. Sci., 20, 323.

Shapiro, M. M. and Silberberg, R. 1974, Proc. Roy. Soc., in press.

Truran, J. W. and Cameron, A. G. W. 1971, Astrophys. Sp. Sci., 14, 179.

Truran, J. W. and Cameron, A. G. W. 1972, Ap. J., 171, 89.

Truran, J. W. 1973a, in Explosive Nucleosynthesis, ed. D. N. Schramm and W. D. Arnett (Austin: University of Texas Press).

Truran, J. W. 1973b, Sp. Sci. Revs., 15, 23.

Truran, J. W. 1973c, in Proceedings 13th International Cosmic Ray Conference, Denver, Colorado.

Wagoner, R. V. 1973, Ap. J., 179, 343.

Weaver, T. A. and Chapline, G. F. 1974, Ap. J. (Letters), 192, L57.

NUCLEAR SPALLATION OF COSMIC RAY NUCLEI IN THE INTERSTELLAR MEDIUM

Grant RAISBECK

Laboratoire René Bernas
Centre de Spectrométrie Nucléaire et de Spectrométrie de Masse
91406 ORSAY France.

INTRODUCTION

My understanding of the purpose of this meeting is an attempt to broaden the awareness amongst members of diverse scientific disciplines as to the relevance of high energy heavy ions in these various domaines. Therefore, before beginning to discuss the specific topic indicated in the title of this talk, I would like to take this opportunity of making a few general comments on the importance of high energy heavy ion accelerators to cosmic ray studies.

As we have seen already at this meeting, arguements can be made as to the potentialities of high energy heavy ions in a number of areas of physics. Some of these ideas are quite specific - many others of a highly speculative nature. The eventual impact in these areas is thus still uncertain, although I personally am persuaded that they will be very significant in the long run. In the case of cosmic ray physics, however, I believe a much firmer statement can be made. The reason is straightforward - a small (but, as we shall see, very important) fraction of cosmic ray particles are themselves high energy heavy ions. When one uses high energy heavy ions in other branches of physics, one is studying matter in an " abnormal " state in an attempt to better understand its normal state. In the field of cosmic ray research,

however, these high energy heavy ions effectively simulate the objects under study in their normal state. Therefore, it is clear that any investigations on the interaction of such cosmic ray particles with matter, whether it be in the domaine of particle physics, nuclear physics, atomic physics, solid state physics or biophysics, will benefit enormously by having available a known and controlable accelerator source of such projectiles. This is true whether one is considering a " basic " research problem of the type I will discuss today, a more indirect application to a basic problem, such as the calibration of a cosmic ray detector, or whether it is a very practical application such as designing cosmic ray shielding for manned space studies. It is also an arguement which is far reaching in time, since it will apply equally to aspects of such research in the future which we may not even be aware of today. I think I can speak for all members of the cosmic ray community, therefore, in expressing our pleasure at the importance the high energy heavy ion program is being given here at Berkeley, and in lending our wholehearted support to its continued development.

I now turn to the more specific topic which we are to consider today, namely nuclear spallation of cosmic rays during propagation. I would like to treat the subject in four sections ; (a) an overall view of the problem ; (b) what type of information we can learn from such studies ; (c) which nuclear reactions are important and (d) what is the present status of knowledge of these cross sections. Hopefully the above will provide the basis for a better appreciation of the aspect of greatest interest to this group - i. e. , how can the Bevalac, or other high energy heavy ion accelerators, contribute to progress in this field. For the reasons metioned above I will try to direct this discussion to the non-specialists in the field. I apologize in advance to those in the audience who are already familiar with this problem, and may find the treatment at a somewhat basic level.

THE PROBLEM

It may be useful to first make a schematic representation of the problem we are considering :

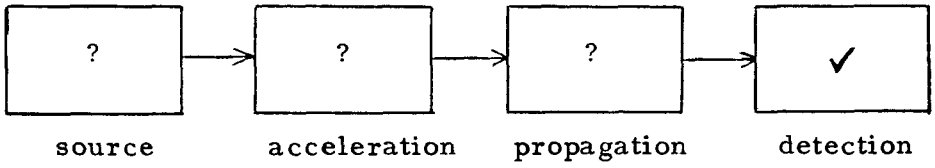

At the left we have a box which represents cosmic ray sources. The question mark indicates that we don't really know what these sources are. Next, is a box representing acceleration of cosmic ray particles. Again the question mark shows that we don't know the nature of this acceleration mechanism. In fact, we don't know whether boxes 1 and 2 should be separate or not. That is, is the event in which cosmic rays are born also responsible for their acceleration, or does that happen later ? And if so, when, where, and how ? In the third box we represent propagation. By this we mean everything that occurs to cosmic rays between their acceleration and their arrival here in the solar system. Again a question mark indicating we don't really know how, or even where, this propagation takes place. Finally we have a box representing detection of cosmic rays. Actually this box could be subdivided into several others, since, depending on the energy, altitude, and latitude of detection of the cosmic ray, it may be necessary to correct for other effects such as solar modulation, geomagnetic cutoff, reactions in the atmosphere etc... However, in principle at least, all of these factors can be accounted for. If we put a check in this box it is not because we know everything about the arriving cosmic rays, but because it is the area in which we know most, and in which further progress can be counted on.

In its simplest form, therefore, cosmic ray physics can be considered a study of this last box, with a view to having some understanding of the other three. We see immediately that interest in the propagation problem has two aspects. First, it represents one of those question marks. Secondly, it is a vital link between our detection box and those representing source and acceleration. In order to relate what we detect to any of the earlier phases, it is clear that we must understand what happens during the propagation phase.

In particular, if we consider the cosmic ray composition, then we must take account of nuclear reactions of the type :

$$A + H\,(He) \longrightarrow B + \ldots\ldots \qquad (1)$$

where A represents an initial cosmic ray nucleus , H (He) represents an interstellar atom of hydrogen (helium), and B represents a secondary nuclear reaction product. Now, although the large majority of cosmic ray particles are protons ($\sim$ 90 %) and alphas ($\sim$ 10 %), we shall see that the $\sim$ 1 % of heavier nuclei are very rich in the type of information they can provide.

MOTIVATION

The type of information we can learn from studying the nuclear reactions indicated above can be considered under the following three headings : (1) quantity and distribution of matter traversed ; (2) time and place of propagation ; (3) source composition.

Quantity and distribution of matter traversed

One of the earliest conclusions arrived at regarding cosmic ray propagation was that the primary cosmic rays (i. e. those emitted by the source) traversed a significant amount of matter between their

acceleration and their arrival in the solar system. This conclusion was based on the ratio Li Be B/C N O, which is believed to be very small universally ($\sim 10^{-6}$) but which is $\sim$ 0.23 in cosmic rays. Assuming a universal ratio at the source, and a knowledge of the relevant cross sections, one can calculate that the primary C N O nuclei must interact with the equivalent of a $\sim$ 4 gm/cm^2 slab of hydrogen in order to produce the observed cosmic ray Li Be B. Somewhat later a similar analysis of the spallation products near Fe led several workers to argue that this same " slab " of matter would lead to more of these heavier secondary products than were actually observed *. This has led to the idea of an exponential distribution of potential pathlengths, a concept which is also more satisfying from some other physical points of view. An improvement in both cosmic ray abundance determinations, and in cross section measurements, should eventually permit one to conclude whether a single distribution of matter can quantitatively account for all the observed secondary species. Such information is very important to the question of whether all cosmic ray nuclei originate in the same sources or whether, for example, Fe nuclei may be from different sources than C N O.

---

* It should be noted that this analysis is based to a very large extent on predicted cross sections for Fe spallation. However, since many reactions are involved, and because there are more radioactive products in this region on which to base cross section predictions, it was felt unlikely that systematic uncertainties in these estimates could be sufficient to invalidate the above conclusions. Recent measurements in our laboratory (1) tend to support this point of view.

Another question that has been brought to interest recently is whether cosmic ray primaries of different energies encounter the same amount of matter. While this was believed true for many years, recent cosmic ray composition measurements at high ($\geqslant$ 10 GeV) energies suggest the opposite. These observations show that the ratio of secondaries/primaries decreases with increasing energy. This phenomena has widely been attributed to the fact that the higher energy nuclei traverse a smaller quantity of matter. Such an interpretation has very important consequences for cosmic ray studies. It is clear that any quantitative evaluation of this effect must correctly account for variations due simply to changes in the relevant nuclear cross sections.

Time and place of propagation

Two of the basic unknowns regarding cosmic ray propagation are where and for what period of time it takes place. This problem has traditionally been considered from the point of view of cosmic ray " clocks " - i. e. spallation produced radioactive isotopes having lifetimes of the order of the expected propagation time. The most important of these species is ^{10}Be, with a rest half-life of 1.5×10^6 years. Other possible candidates are ^{26}Al (7.3×10^5 years) and ^{36}Cl (3.0×10^5 years). A measure of what fraction of these radioactive species survives can give us the time between their formation and detection.

It has often been stated that this temporal information, together with knowledge of the total amount of matter traversed, can, by means of the implied density of the propagation medium, tell us where propagation takes place. This is true if, (and <u>only</u> if,) production and propagation are contiguous. However, it is not impossible to imagine a situation in which spallation takes place in a relatively dense medium, followed by propagation in a very tenuous one. The density inferred from a radioactive " clock " in this case would be an " average " one, which would not be representative of either the spallation or the propagation environment.

A method of approaching this difficulty has been suggested by our group recently (2). It consists of using pure electron capture isotopes, and will be discussed in more detail in my other talk at this meeting.

It will also be important to eventually compare the " propagation age " determined by these techniques with the " genetic age " of cosmic rays (as determined, for example, by radioactive primary nuclei) in order to see whether birth and acceleration occur in the same event.

Primary composition

Information on the primary composition of cosmic rays can give us valuable clues as to the potential astrophysical sites for their formation and subsequent acceleration. For example, early observations that cosmic rays were enriched in heavier (Fe region) nuclei compared to " universal " abundances led to speculation that they came from highly evolved stars. This, together with a favourable energetic situation, suggested identification of such sources with supernova. More recently it has become apparent that a very significant fraction of all heavier element synthesis may occur in explosive events (3). If this is true, then cosmic rays may represent one of our most direct samplings of the results of explosive nucleosynthesis. Since different models of such events give different final compositions, it is important that we know as accurately as possible the composition of these " primary " cosmic rays. As we have seen earlier, the quantity of matter traversed during propagation is not negligible, and nuclear reactions give rise to a significant modification in the observed composition. In order to unfold these effects correctly we obviously need to know a large number of the relevant nuclear cross sections.

Another aspect of this problem involves the possibility of " selection " effects during acceleration. One extreme point of view for example, is to argue that the cosmic ray source composition is the same as universal composition, and that all the differences we observe are due to these selection effects. A method of testing such ideas is to compare the " enrichment " of two elements differing strongly in the physical property believed to be causing selection. If one wants to test the importance of ionization potential, for example, one might choose to compare Na and Ne. Again it is the abundances before propagation that we are interested in, and in some cases (Na in the present example) the spallation corrections are very significant.

WHICH CROSS SECTIONS ?

We should first note that, because of the astrophysical time scale involved, the reactions we are interested in are those leading to stable or very long lived products (including, of course, contributions of radioactive precursors which decay to these products). One often sees the statement that analysis of the cosmic ray propagation problem requires a knowledge of cross sections for all these interactions. While technically correct, such a position is somewhat misleading in that it fails to emphasize the variable importance of different cross sections. In reality significant information can be obtained from an accurate knowledge of a relatively modest number of carefully chosen cross sections.

This is indeed fortunate since if one examines the situation quantitatively, one begins to appreciate the magnitude of the complete problem. For example, restricting ourself only to the region of $Z \leqslant 26$ for the moment (and thus ignoring a group of rare but very interesting

heavier nuclei) we find about 70 stable or long lived isotopes. This means that about 70 x 70/2 $\simeq$ 2500 projectile-product combinations are involved in the complete transport equations. If we assume, as a very modest criterion , that we need results at 4 energies for a rough excitation function, this implies the necessity for $\sim$ 10,000 cross section measurements. And, of course, since the interstellar medium is $\sim$ 10 % by atom He, we should for completeness have an equal number of alpha induced cross sections. One sees that this is certainly a major undertaking - even by Bevalac techniques ! One is therefore relieved to realize that they are not all of equal importance.

The decision as to what cross sections are critical is naturally dependent on which of the previously discussed areas one is interested in : For example, if one is trying to evaluate the quantity of matter traversed then one looks for a product nuclide which is expected to have very low abundance at the source (eg. Li Be B, F, Sc). If one is looking at the question of cosmic ray " age " then one focuses on the favourable radioactive " clocks " (^{10}Be, ^{26}Al, ^{36}Cl). For the question of source composition one can summarize the important reactions as follows - those having parent nuclei that are abundant, and product nuclei that are scarce (i. e. those interactions which will significantly contribute to the observed abundances).

The above comments may appear trivial, and yet they often seem to be ignored in discussions of the subject. Application of the above criteria still leaves a long, but perhaps feasible list of cross sections that should be measured. Use of rough estimates for many others that are less critical will have relatively little effect on the final analysis.

PRESENT STATUS

Alongside the statement that a complete matrix of cross sections is needed, one often reads that almost none of these are yet measured. This is also a little misleading, although perhaps less so than the former. In fact, during the past ten years, due largely to efforts of the Orsay group, under the late René Bernas, several of the most important reactions have been studied using mass spectrometric techniques *. For example, the production of Li Be B from their most important progenitors ^{12}C and ^{16}O have been quite extensively examined (4 - 7). Many additional cross sections leading to the important nuclide ^{10}Be have also been reported (8 - 11). Some attempts have been made to investigate the importance of the helium interactions (6 , 12). More recently our efforts have been directed to measurements in Fe targets, and initial results will soon be available (1).

Because of the reasons alluded to earlier, even these rather limited data have permitted important conclusions to be reached regarding the amount and distribution of matter traversed, and the expected secondary product distributions. A more extensive cross section dampling is, nevertheless, still very much needed. Also, as in any experimental field, it is desirable that the existing measurements be checked by alternate techniques.

---

* In this type of measurement the cosmic ray " projectile " ion is simulated by a stationary " target " nucleous in the laboratory system, and an energetic proton (alpha) represents the interstellar H (He). At the same relative velocity (energy/nucleon) the nuclear cross sections are, of course, identical.

POSSIBILITIES WITH BEVALAC

The potential of high energy heavy ion accelerators for measuring nuclear cross sections applicable to the cosmic ray problem has been recognized for some time. The reason is implicit in an assumption that workers in the field have made for many years - i. e. that the spallation fragments from high energy heavy ion interactions will have essentially the same velocity (energy/nucleon) as the original projectile. The degree to which this expectation holds true appears, to date, quite impressive. Experimentally this means that virtually all the projectile fragments escape the target, and can be identified with counter techniques. This is in contrast to the situation in which the " projectile " nuclei is at rest in the laboratory system, and where the low laboratory energy of the fragments makes 100 % detection by counters very difficult. This latter limitation is the reason a mass spectrometric technique has been adopted at Orsay.

The overwhelming advantage of counter techniques, compared to mass spectrometry is their generality. Not only are the mass spectrometric methods used in our laboratory very painstaking (requiring the extraction and measurement of 10^{-9} - 10^{-12} gm of the product under consideration), they also require virtually a new technique for each target-product combination, and developments are therefore quite slow. For the Bevalac type experiment, on the other hand, essentially the same setup will serve for any desired measurement (providing, of course, the necessary beams are available). While no one would wish to minimize the effort necessary for constructing and setting up the original system, I think it is this generality which has given rise to such optimism over future possibilites of the Bevalac in this field.

There are other advantages of the Bevalac type measurements which are relevant to the propagation question. For example, they will permit the study of spallation of rare isotopes or even, through the use of secondary beams, radioactive nuclides. The latter may be quite important in the case of long lived or pure electron capture isotopes in cosmic rays. Energetic heavy ions also permit the simulation of cosmic ray breakup in the atmosphere or in detector materials. Corrections for such interactions are still a major source of uncertainty for all balloon observations of cosmic ray abundances.

Finally, are there any drawbacks or limitations to measuring cross sections in this way ? In reflecting on this question I have been able to think of only two*, and they are more present machine limitations rather than disadvantages in principle. The first involves the fact that, as we have been told, even with the new Hilac injector, the present Bevatron vacuum limitations will prevent acceleration of ions heavier than $\sim$ Kr. Thus we would have to forsake making measurements relevant to the very heaviest cosmic ray nuclei, a region, incidentally, where spallation effects are even more important because of larger

---

* I do not include here the purely technical problem associated with providing a suitable H target. One may use either a solid hydrocarbon, or liquid hydrogen. The first requires very accurate measurements in order to reliably subtract the carbon contributions, while a liquid hydrogen target presents certain experimental inconveniences. However, both methods are feasible and are being currently pursued by the Heckman group.

total interactions cross sections. Fortunately this situation can be overcome with a new vacuum system, and I am confident that it will be eventually done.

Perhaps more fundamental is the present energy limit imposed by the Bevatron. As we noted earlier, the cosmic ray problem has need of cross sections over a wide span of energies, and particularly up to the nuclear cross section asymptotic limit. While our own work has shown that 2.5 GeV/nucleon is probably well into this limit for light targets (projectiles) such as ^{12}C and ^{16}O, it is doubtful whether the same is true for a projectile as heavy as Fe. Therefore, while we are all still anxiously awaiting the first results from this wonderful new facility, perhaps we should be trying to convince those responsible for some of our even higher energy accelerators of the future importance of relativistic heavy ions.

REFERENCES

1 - C. Perron, Thesis (in preparation).

2 - G. Raisbeck, C. Perron, J. Toussaint and F. Yiou. 13th International Cosmic Ray Conference, Denver, Colorado (1973), paper 252.

3 - " Explosive Nucleosynthesis ", ed. D. N. Schramm and W. D. Arnett, University of Texas Press (1973).

4 - F. Yiou, Ann. Phys. (Paris), 3, 169 (1968).

5 - P. Fontes, C. Perron, J. Lestringuez, F. Yiou and R. Bernas, Nucl. Phys., A 165, 405 (1971).

6 - G. M. Raisbeck, J. Lestringuez and F. Yiou, Phys. Rev., C 6, 685 (1972).

7 - F. Yiou, P. Fontes, C. Perron and G. M. Raisbeck, 13th International Cosmic Ray Conference, Denver, Colorado (1973), paper 251.

8 - G. M. Raisbeck and F. Yiou, Phys. Rev. Lett., 27, 875 (1971).

9 - F. Yiou and G. M. Raisbeck, Phys. Rev. Lett., 29, 372 (1972).

10 - G. M. Raisbeck, J. Lestringuez and F. Yiou, Nat. Phys. Sc., 244, 28 (1973).

11 - G. M. Raisbeck and F. Yiou, Phys. Rev., C 9, 1385 (1974).

12 - J. Lestringuez, G. M. Raisbeck, F. Yiou and R. Bernas, Phys. Lett., 36 B, 331 (1971).

ATOMIC CAPTURE AND LOSS CROSS SECTIONS OF RELATIVISTIC HEAVY IONS AND THEIR ROLE IN COSMIC RAY PHYSICS

by G. M. RAISBECK

Laboratoire René Bernas
Centre de Spectrométrie Nucléaire et de Spectrométrie de Masse
91406 ORSAY - France.

INTRODUCTION

The subject I would like to discuss today, atomic charge exchange, may seem like a curious one to consider at a meeting on high energy heavy ions. Such projectiles, however, provide the possibility of carrying out studies which can help elucidate the fundamental atomic mechanisms involved, as well as having important implications for the field of cosmic ray physics. It is these latter implications which originally interested us at Orsay in this subject. I can thus in no way pretend to be an expert in the theoretical aspects of the field, and my description here will be based essentially on what I have been able to pick up while looking into this largely unexplored domaine.

I will first give a brief résumé of the relevance of this subject to the cosmic ray question. I will then discuss some theoretical aspects of the atomic charge exchange process at very high energies, and the present status of experimental verification (or lack thereof) for these theories. Finally I will return in somewhat more detail to the astrophysical potentialities that exist by combining an understanding of the charge exchange process together with certain cosmic ray measurements.

RELEVANCE TO COSMIC RAY STUDIES

Table I gives a list of nuclei which have two things in common : (a) they are all believed to be formed from nuclear spallation reactions of primary cosmic ray nuclei (most notably Fe) ; (b) they all decay by pure electron capture (in the nuclear sense) . In the absence of orbital electrons, these species will thus be stable. At the high energies characteristic of cosmic rays, one normally thinks of nuclei as being fully stripped of orbital electrons. However, because of the time scales involved, even a very small probability of picking up an electron may result in eventualy decay of these species. The problem therefore consists in trying to estimate or better yet, measure this probability.

HIGH ENERGY CHARGE EXCHANGE

Loss cross sections

There are two processes relevant to the present question, electron pickup and electron stripping. I will talk very little about the latter. Partly this is because this process appears to be fairly well understood theoretically, and partly because its parameter dependence is such that it is expected to have a relatively minor effect on the cosmic ray question. It can be noted the electron stripping is very closely related to the ionization process. Its cross section, in a light media, has been given for example by Bohr (1) as :

$$\sigma_1 = 4 \pi a_o^2 Z_p^{-2} (Z_t^2 + Z_t) \left(\frac{v_o}{v}\right)^2 \qquad (1)$$

where a_o = 2.8×10^{-17} cm^2

v_o = K electron velocity of hydrogen (2.2×10^8 cm/sec)

v = projectile velocity

Z_p, Z_t = projectile and target nuclear charges, respectively

This formula appears to be approximately valid at least for light projectiles at the highest energies so far explored (2).

Capture Cross Sections

The electron capture process can be divided into two distinct processes depending on whether bound or free electrons are involved.

(a) - Non-radiative capture

The mechanism normally considered for the pickup of an electron from the encounter of a fast ion with a neutral atom is non-radiative capture. The mechanism has been considered by Bohr (1), and phenomenologically can be considered to occur whenever the projectile ion imparts to the electron a velocity comparable to its own. Such a process is evidently enhanced when the original orbital electron velocity and the ion velocity are similar. At higher projectile energies, this probability falls off quickly, and the ion is considered " fully stripped " Quantitatively , the quantum mechanical solution to this problem was first worked out by Oppenheimer (3) and Brinkman and Kramers (4). The result quoted in the literature as the OBK solution, is :

$$\sigma_c\,(\mathrm{OBK}) = \pi\, a_o^{\,2} \left(\frac{2^{18}}{5}\right) Z_p^{\,5}\, Z_t^{\,5}\, S^8 \left[S^2 + (Z_p + Z_t)^2\right]^{-5} \times \left[S^2 + (Z_p - Z_t)^2\right]^{-5} \qquad (2)$$

where $S = v/v_o$ and other quantities are as defined in (1)

In the high energy (non-relativistic) limit this cross section is proportional to $(Z_p)^5$, $(Z_t)^5$ and E^{-6}. The applicability of this treatment has been discussed at length elsewhere (5), and we do not have time here to go into details. We note, however, that there seems to be general agreement that this analysis is not theoretically valid (it consists essentially of a first Born approximation which apparently does not converge). There is not as general consensus as to what is a correct treatment. However, it is noted that many other analysis give results which are similar (or proportional) to the OBK result in the high energy limit. Moreover, these other treatments are much more difficult and have to date only been applied to relatively simple systems. The OBK approach appears to offer the only reasonably simple prediction for the heavy ions we are interested in here.

There is a much more serious limitation to the OBK result, however, and that is that it is a non-relativistic treatment. For ions in the energy range of hundreds or thousands of MeV/nucleon, this is obviously a serious omission (especially when one consider that the non-relativistic solution involves a factor of v^{12} !). The only work we are aware of in which relativistic effects have been considered is a brief note by Mittleman (6), which suggest that the energy dependence of non-radiative capture will eventually be E^{-1}.

(b) - Radiative capture

The capture of free electrons by ions can occur by radiative capture. Since this is just the inverse of the photo electric effect, a completely relativistic, and presumably reliable theoretical treatment does exist and is given by (7)

$$\sigma_c\,(\text{rad}) = 3/2\,\frac{Z_p^{\,5}}{(137)^4}\,\phi_o\,\frac{k^2}{(k+m_o)^2 - m_o^{\,2}}\left(\frac{m_o}{k}\right)^5 (\gamma^2-1)^{3/2}$$

$$\times\left[\frac{4}{3} + \frac{\gamma(\gamma-2)}{\gamma+1}\left(1 - \frac{1}{2\gamma(\gamma^2-1)}\ \ln\frac{\gamma+(\gamma^2+1)}{\gamma-(\gamma^2-1)}\right)\right] \qquad (3)$$

where $\phi_o = 6.65 \times 10^{-25}\ \text{cm}^2$

m_o = electron rest mass

k = electron kinetic energy in projectile reference frame

$\gamma = \dfrac{k+m_o}{m_o}$

In the high energy limit the above result gives the radiative capture as proportional to $(Z_p)^5$ and E^{-1}. In cases where the projectile ion has a velocity much larger than the (electron) orbital velocities of a target atom, it should be possible to apply the free electron result to atomic electrons and therefore σ_c will depend directly on the number of electrons in the target, i.e. Z_t. By comparing equations (2) and (3), one can note immediately two things. First, because of the very different energy dependences, radiative capture should be expected to dominate at high enough energies. Second, because of the Z_t dependencies, the energy region of this domination will depend on the target medium.

Is there any experimental evidence for these effects ? Several years ago my colleague Françoise Yiou and I set out to examine this question. Not having relativistic heavy ions available to us at that time, we settled for protons, deuterons and alpha particles. Figs 1 and 2 show some interesting results of those experiments (7). Although the data have rather large uncertainties, the above effects do, in fact, appear to occur. One sees that the capture cross section in the mylar target material, (essentially carbon and oxygen) does take a sharp break at

high energies, which can be rather nicely accounted for by the onset of radiative capture. A smaller break is observed for Al, while no increase at all is seen for Ni and Ta, in accordance with the theoretical expectations. We also have similar indication for gas targets of He, N_2 and Ar. Unfortunately, because of uncertainties due to relativistic effects in the OBK type capture, such an interpretation of the data is not unique. In addition, these experiments were not able to test the very strong (Z_p^5) dependence which is expected from both radiative and non-radiative capture.

APPLICATION TO THE COSMIC RAY PROBLEM

On the basis of the above considerations (and especially recognizing their limitations) one can apply the above formulae to the cosmic ray problem. In figs 3 and 4 we show examples of effective capture cross sections calculated for high energy Be and V nuclei in a medium of interstellar composition (assumed " universal " abundances of Cameron (8)). One sees that the dependences noted above are also reflected in these curves. In both cases radiative capture dominates at sufficiently high energies. However for Be the magnitude of the capture cross sections are much smaller, and the " cross over " point at which the two processes are equal occurs at a higher energy. The result is that in the region where it becomes important ($\gtrsim 10^{-24}$ cm^2) the effective cross section for ^{7}Be is dominated by non-radiative capture, and is falling much more steeply than for ^{49}V, which is dominated by radiative capture. Finally, we show in Figs 5 and 6 the result of applying these type of cross sections to the decay of these species in the interstellar medium. The results are shown as " survival " curves i. e. the fraction of species formed by spallation which is expected to survive (compared to that which would survive in the absence of any decay) as a function of

its detection energy. Since the electron pickup cross sections increase with decreasing energy, this fraction becomes smaller at lower energies. The effect of the difference in the magnitude of the cross sections and steepness of their energy dependence can be seen more clearly in Fig. 7, where the two curves are plotted on the same scale. The lighter ^{7}Be survives to a much lower energy, and then decreases very abruptly, while the ^{49}V decreases gradually over a much wider energy range.

An electron which is captured can either lead to nuclear decay, or be stripped off again. It is clear therefore, that the above survival curves must be dependent on the density of the medium in which they are propagating. The calculations in Figs 5 and 6 were done for typical interstellar densities of $\sim$ 1 atom/cm^{2}. In Fig. 8 we show some recent calculations we have made where we have allowed this density to vary. One sees that at densities of $\gtrsim 10^{4}$ atom/cm^{3} restripping effectively inhibits decay even at low energies.

It should now be clear what the implication of these effects will be for the cosmic ray propagation question. In effect, these isotopes can act as probes (or " hydrometers ") of the medium in which they were formed. As such, they act in a complementary fashion to the radioactive " clocks " which we discussed elsewhere at this Conference. Those clocks give the " average " density of the medium between birth and detection, whereas the electron capture isotopes can give information on the instantaneous density at the time of their formation. A very interesting question, for example, is whether a significant portion of the material traversed by the cosmic rays could be in or around the sources. If so, the density should be high enough that a large fraction of the electron capture isotopes produced in that region will survive.

To be complete I should add that Cassé has suggested that a similar reasoning might be used to probe the time between the birth of the primary cosmic rays, and their acceleration (10). He notes, for example, that many explosive nucleosynthesis models suggest that ^{56}Fe is originally formed as ^{56}Ni. If this latter is accelerated immediately, he then argues that it might survive as ^{56}Ni. Actually, the fact that one observes ^{56}Fe and not ^{56}Ni in the cosmic rays would seem to be a strong arguement against this interpretation.

Finally I would like to return to one point which I have rather glossed over in the above treatment, that is, what happens if the spallation products are originally formed with an electron ? In a dense medium, of course, they will be immediately stripped off, and will not change the behaviour described above. In a density of 1 atom/cm^3 however, decay would occur before stripping. Although it has usually been assumed that nuclear spallation products will be formed " naked " of electrons, this is an area for some very fascinating experimental work. We at Orsay have already made some preliminary experiments in this direction at low energies, and along with the charge exchange measurements hope to continue such studies at the Bevalac.

IMPLICATIONS FOR HIGH ENERGY HEAVY ION ACCELERATORS

Many of the above ideas are fascinating, but it is clear that there is a woeful lack of experimental information. The Bevalac facility will provide a unique opportunity to carry out a comprehensive and systematic study of the charge exchange process in an energy domaine barely touched by earlier work. Such measurements will be important both for analyzing the basic mechanism involved at relativistic energies, and in providing necessary data for the cosmic ray problem.

REFERENCES

1 - N. Bohr, Kgl. Danske Videnskab. Selskab, Mat.-Fys. Medd, 18, 8 (1948).

2 - R. Smyth and J. W. Toevs, Phys. Rev., 139, A 15 (1965) : K. H. Berkner, S. N. Kaplan and R. V. Pyle, Phys. Rev., 134, A 1461 (1964).

3 - J. R. Oppenheimer, Phys. Rev., 31, 349 (1928).

4 - M. C. Brinkman and H. A. Kramers, Proc. Acad. Sci. Amsterdam, 33, 973 (1930).

5 - See for example, B. H. Bransden, Rep. Prog. Phys., 35, 949 (1972).

6 - M. H. Mittleman, Proc. Phys. Soc. (London), 84, 425 (1964).

7 - G. Raisbeck and F. Yiou, Phys. Rev., A 4, 1858 (1971).

8 - A. G. W. Cameron, Space Science Rev., 15, 121 (1973).

9 - G. M. Raisbeck, G. Comstock, C. Perron and F. Yiou (to be published).

10 - M. Cassé, 13th International Cosmic Ray Conf., Denver, Colo. (1973) Vol. 1, p. 546.

11 - F. Yiou and G. M. Raisbeck, Astrophys. Lett., 7, 129 (1970).

12 - G. Raisbeck, C. Perron, J. Toussaint and F. Yiou, 13th International Cosmic Ray Conference, Denver, Colo. (1973), Vol. 1, p. 534

TABLE I

Pure electron capture isotopes lighter than Fe

Nuclide	" Normal " half-life
^{7}Be	53.2 d.
^{37}Ar	36 d.
^{41}Ca	8×10^{4} yr.
^{44}Ti	48 yr.
^{49}V	330 d.
^{51}Cr	27.8 d.
^{53}Mn	3.7×10^{6} yr.
^{55}Fe	2.6 yr.
(^{54}Mn	303 d.) *

* The case of ^{54}Mn is special. While both β^- and β^+ decay are energetically possible these must procede through highly forbidden transitions, and thus are expected to have very long partial half lives.

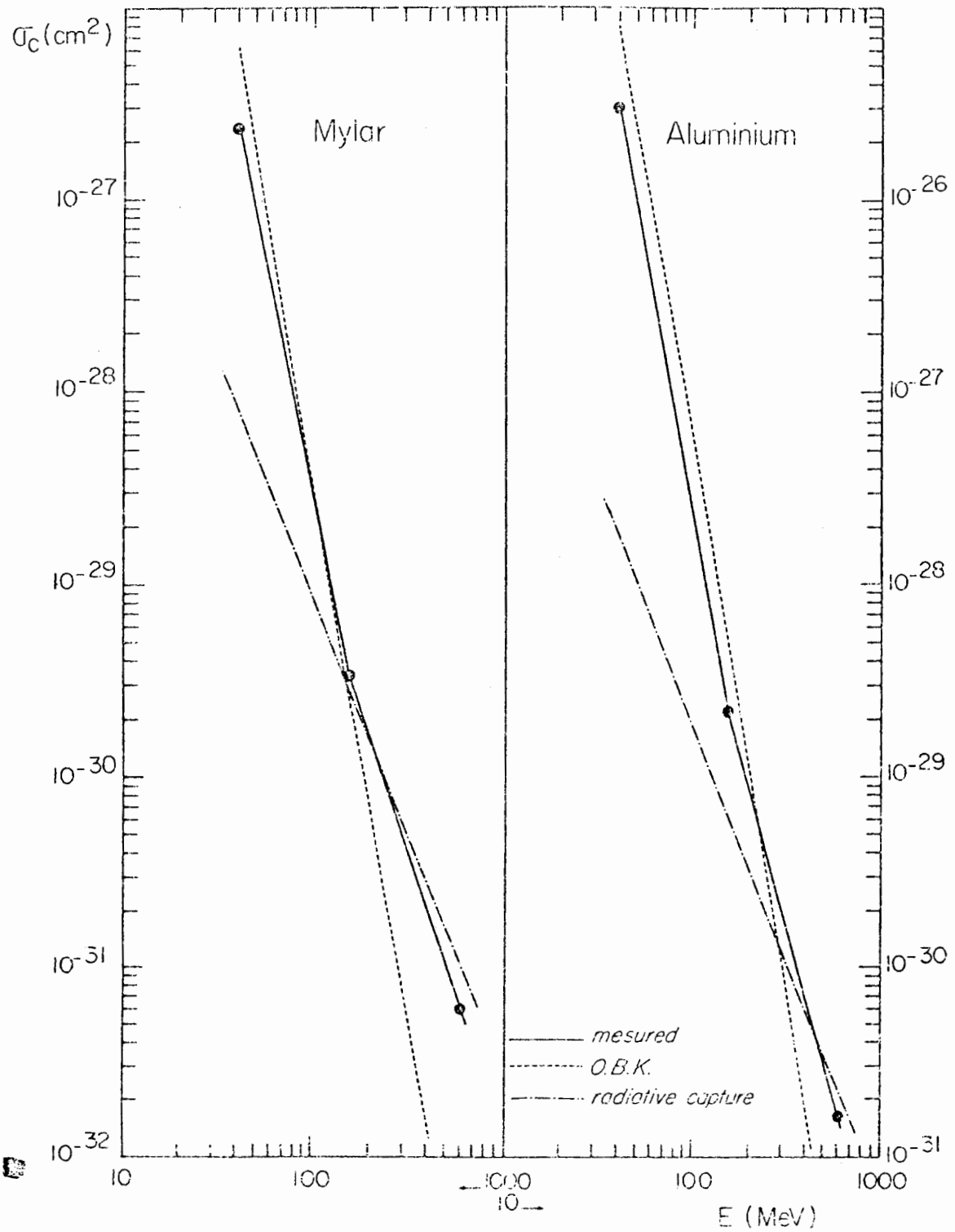

Fig. 1 Theoretical and experimental electron capture cross sections for high energy protons in mylar and aluminum (From ref. 7).

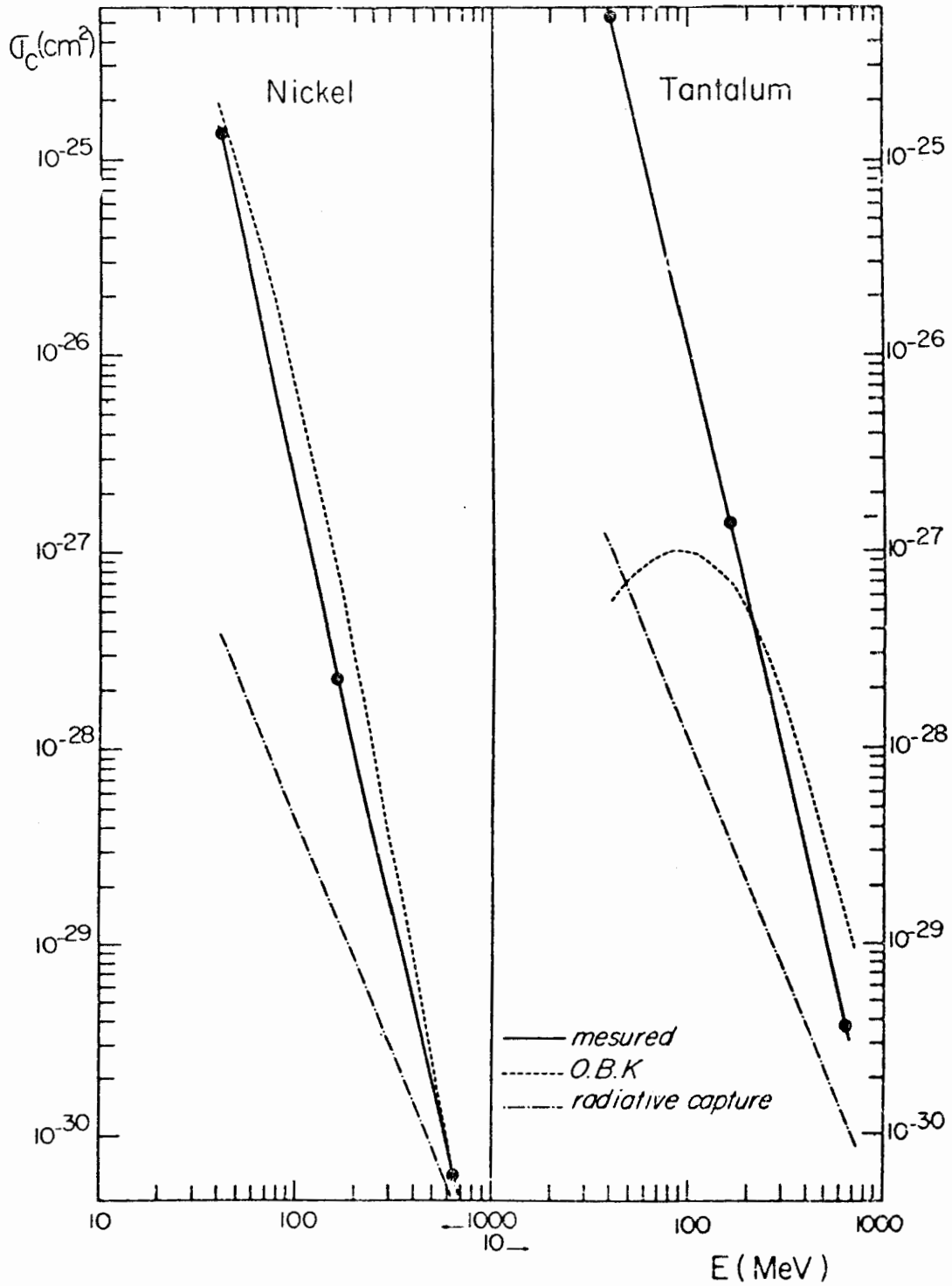

Fig. 2 Same as Fig. 1 in nickel and tantalum (From ref. 7).

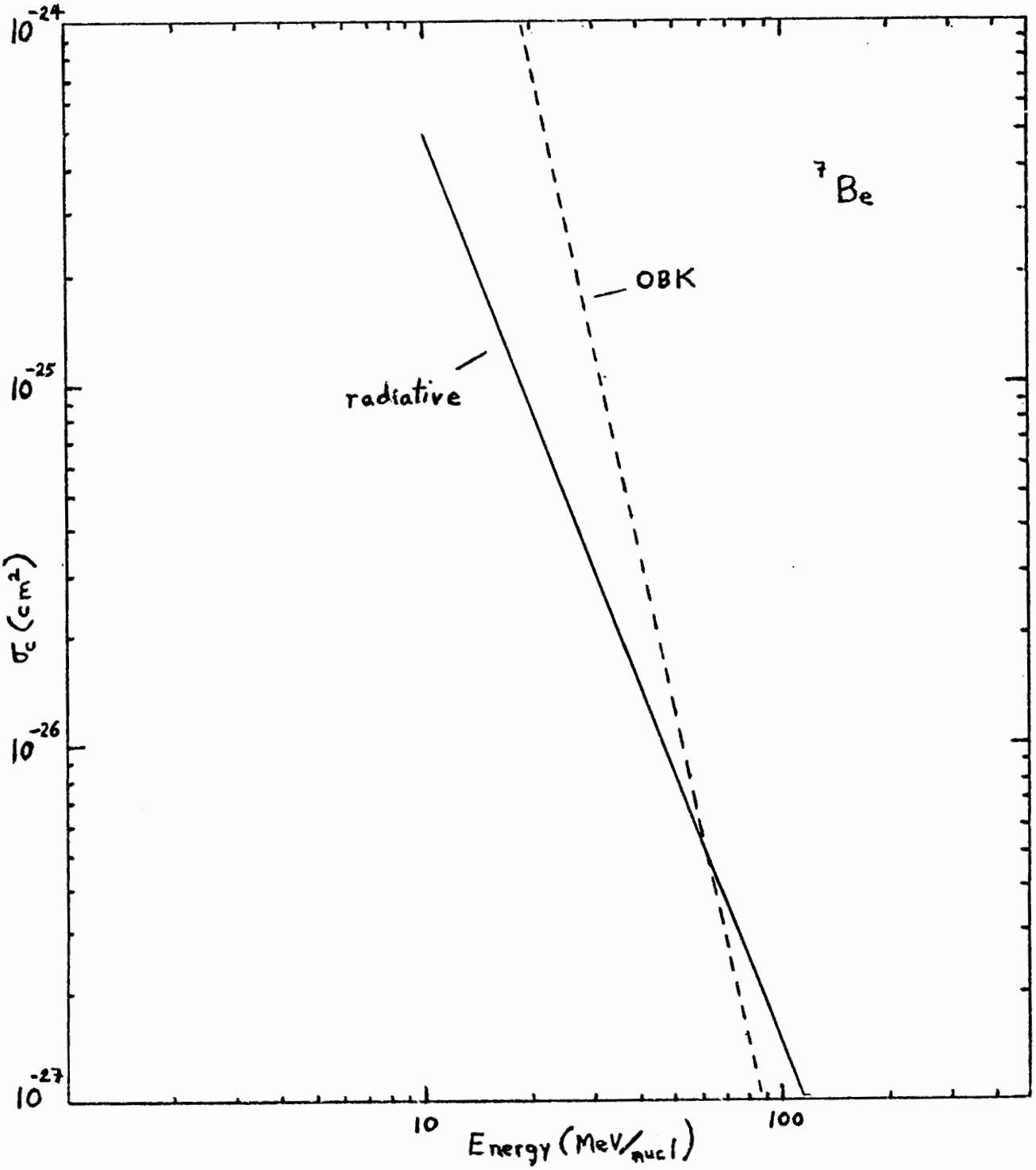

Fig. 3 Calculated electron capture cross section for ^{7}Be in interstellar medium.

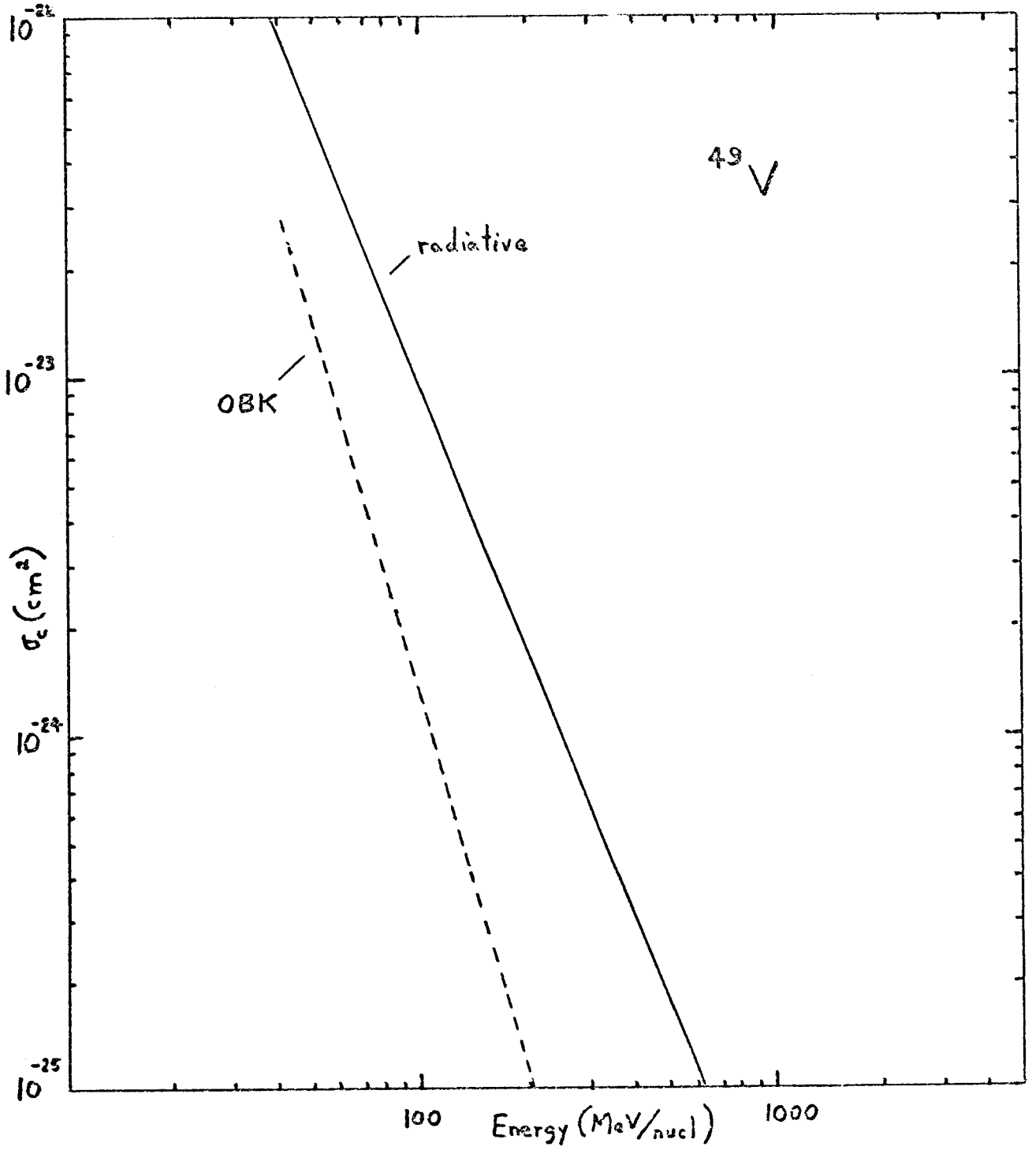

Fig. 4 Same as Fig. 3 for ^{49}V.

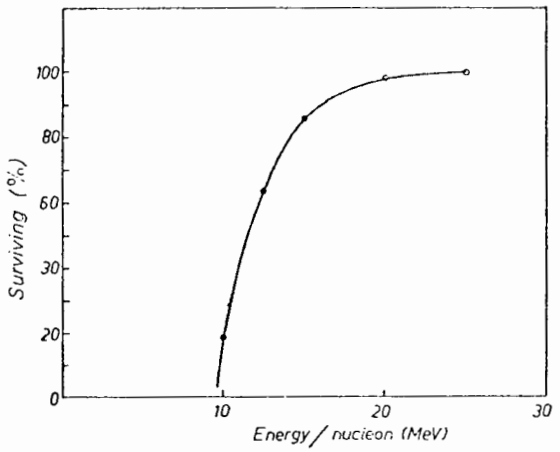

Fig. 5 Calculated survival of ^{7}Be in cosmic rays (From ref. 11).

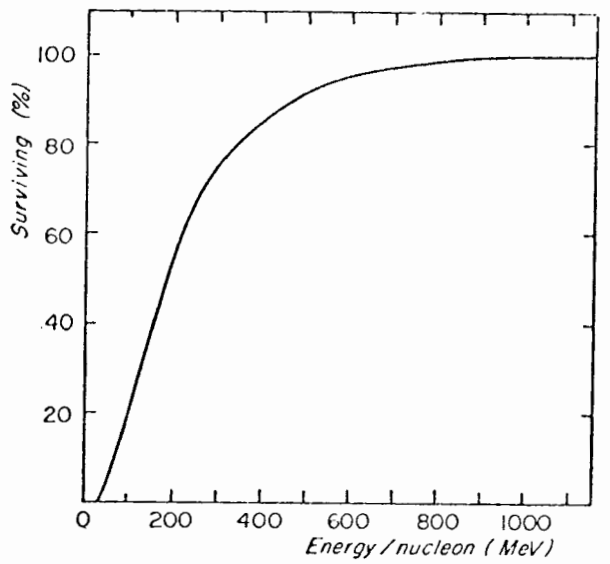

Fig. 6 Calculated survival of ^{49}V in cosmic rays (From Ref. 12).

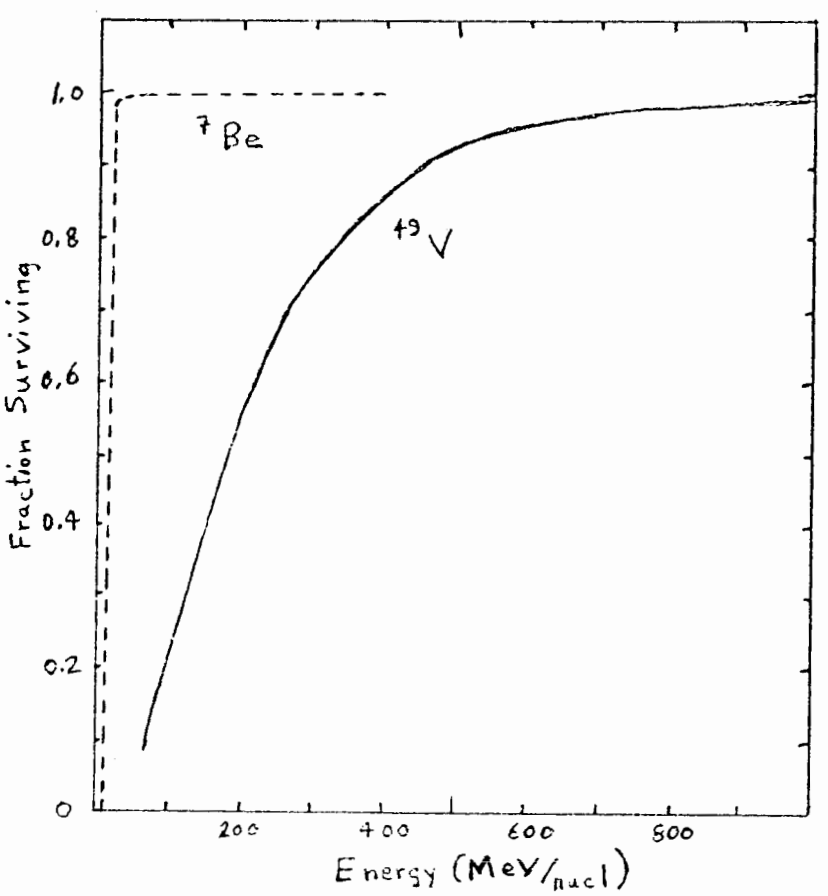

Fig. 7 Comparison of survival curves for ^{7}Be and ^{49}V in cosmic rays.

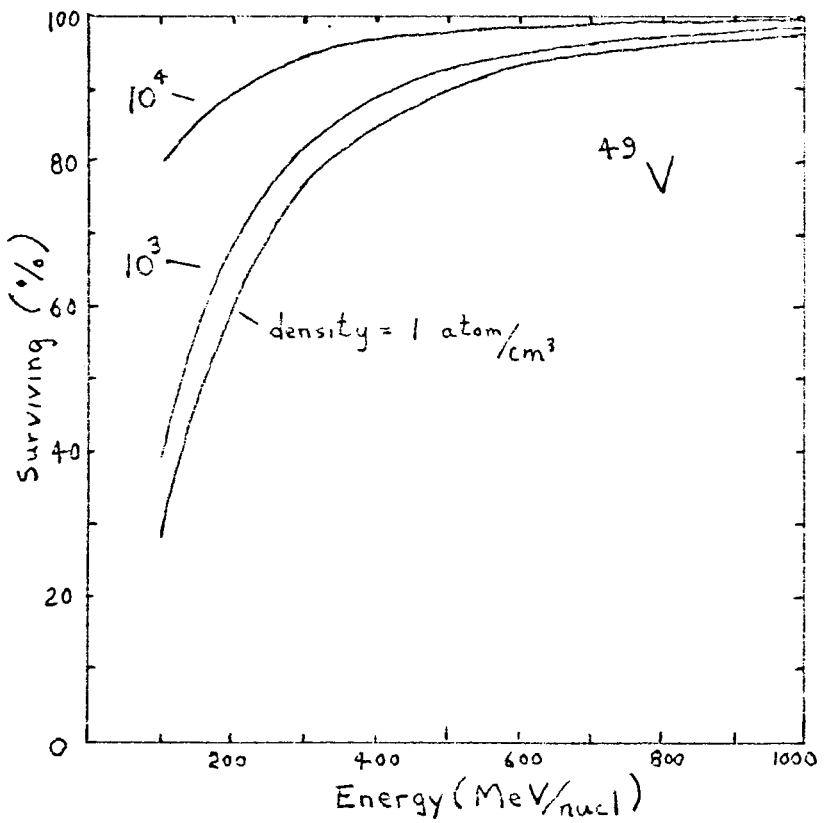

Fig. 8 Calculated survival of ^{49}V as a function of density of spallation medium (density = 1, 10^3 and 10^4 atoms/cm^3 and assumed exponential path length distribution of .5 gm/cm^2.)

SUMMARY SESSION, HIGH ENERGY SUMMER STUDY, LBL, JULY 15-26, 1974

Remarks by W. J. Swiatecki

I would like to make a few general remarks not directed specifically at any given paper presented during the past two weeks. Just some thoughts that come to mind as a result of the present summer study, last year's study, and the whole subject of high-energy heavy ions.

First Thought: We should distinguish between two aspects of the present situation:

1. Clearing the weeds,
2. Getting to the heart of the matter.

Clearing the weeds means isolating results that follow from standard theory and which are not expected to contain radically new features. The heart of the matter are phenomena about which standard (nuclear) theory has little or nothing to say--for example phenomena associated with nuclear density doubling, multiple meson production and relativity.

In clearing the weeds we should proceed in a level-headed way and with due respect for established knowledge. This is no place to expect spectacular results in rough experiments. At the level of 20% experiments one expects standard theory to give the main features. Accurate and detailed results might be more revealing, but let us be modest and regard part of our work as a necessary clearing of weeds before coming to the heart of the matter.

My Second Thought is that so far we haven't really gotten to the heart of the matter. The bulk of the reports we heard dealt with marginal aspects of the problem. Obviously experiments with deuterons and alpha particles are far from full-blooded density doubling situations, but even the fragmentation experiments with Oxygen and Carbon probably involve only peripheral collisions that don't bring out radically new features.

Let us make sure that our thinking doesn't get stuck in the weeds and let us keep clear in our minds that the real objective is to find out what happens when two large nuclei are piled up at high energy. (Improving the Bevatron vacuum so that one can go to at least medium weight nuclei is an important matter in this connection.)

My Third Thought is that I am not happy about how things are going either in clearing the weeds or getting to the heart of the matter. The frustrating delay in applying standard knowledge in nuclear theory to clearing the weeds has several reasons, and I would like to comment on two. One reason is that we are now paying the price of the overspecialization in our education as physicists. It is ridiculous that "high-energy physicists" should have so much difficulty in communicating with "low-energy physicists." I would like to see a return to conditions where no self-respecting scientist would even accept a label such as "low-energy" or "high-energy" physicist. (Was Maxwell a high-frequency or a low-frequency physicist?) Let us remember in our thinking, and especially in talking to other people, that there are only rather few basic principles in physics and that

they are the same in all fields. Let us stay closely in touch with the basic principles and cut out the horrendous specialized jargon that makes intelligent communication impossible.

A related thought is that the funding of physics on the basis of high, medium and low energy, or other ridiculous classifications, should be resisted as destructive of the unity of physics. There is only one physics and some of the difficulties we have in proceeding efficiently with the relativistic heavy-ion studies are there, I believe, because we have forgotten about this unity.

A second past sin which makes it difficult to apply existing nuclear theory to the heavy ion situation is the over-reliance on computers. Think of the Monte Carlo cascade calculations of the past 20 years that obviously should have been in the forefront of many discussions but have hardly been invoked in the past two weeks. I think a good part of the reason for this is that these calculations were done on computers, and a computer is a dumb machine which gives you only the answer you asked for. If some years later you want to ask a question about a related aspect of the problem--say the angular momentum deposited in a cascade--the chances are that you will find the original work useless. Compare that with a result worked out analytically and expressed by a formula. It can be looked at years later, turned around, played with and modified and used to answer new questions. This inflexibility of computer outputs as against analytical treatments should always be remembered when the temptation arises to dump a problem on the computer. A computer "solution"--in quotes--is

no real solution of a physical problem in the broader sense. If computers hadn't been available one would probably have worked out analytical cascade theories that would now be more useful.

I am also unhappy--but in a vaguer way--about our approach to the heart of the matter in high-energy heavy ion physics. I would like to have seen someone give a well thought-out assessment of the principal factors to bear in mind when approaching the novel domain of highly excited, relativistic matter in bulk. What are the relevant dimensionless parameters that subdivide the domain into various regions dominated by different considerations? What are the hypotheses and physical principles that are being tested? What is the best guess at the crucial experiments?

I am not qualified to make such an assessment, but let me give you a hint of what I have in mind. Yesterday I drew a diagram of various energy regions and of certain critical energies per particle around which the physics changes qualitatively. One might add a baryon number dimension to such a diagram (see figure) and try to clarify one's ideas on the basic physics to be expected in various regions, on the techniques and approximations to be used in those regions, and on the strategies to be adopted in building or modifying accelerators to explore the new domain.

I missed in our meetings the breadth of such an approach.

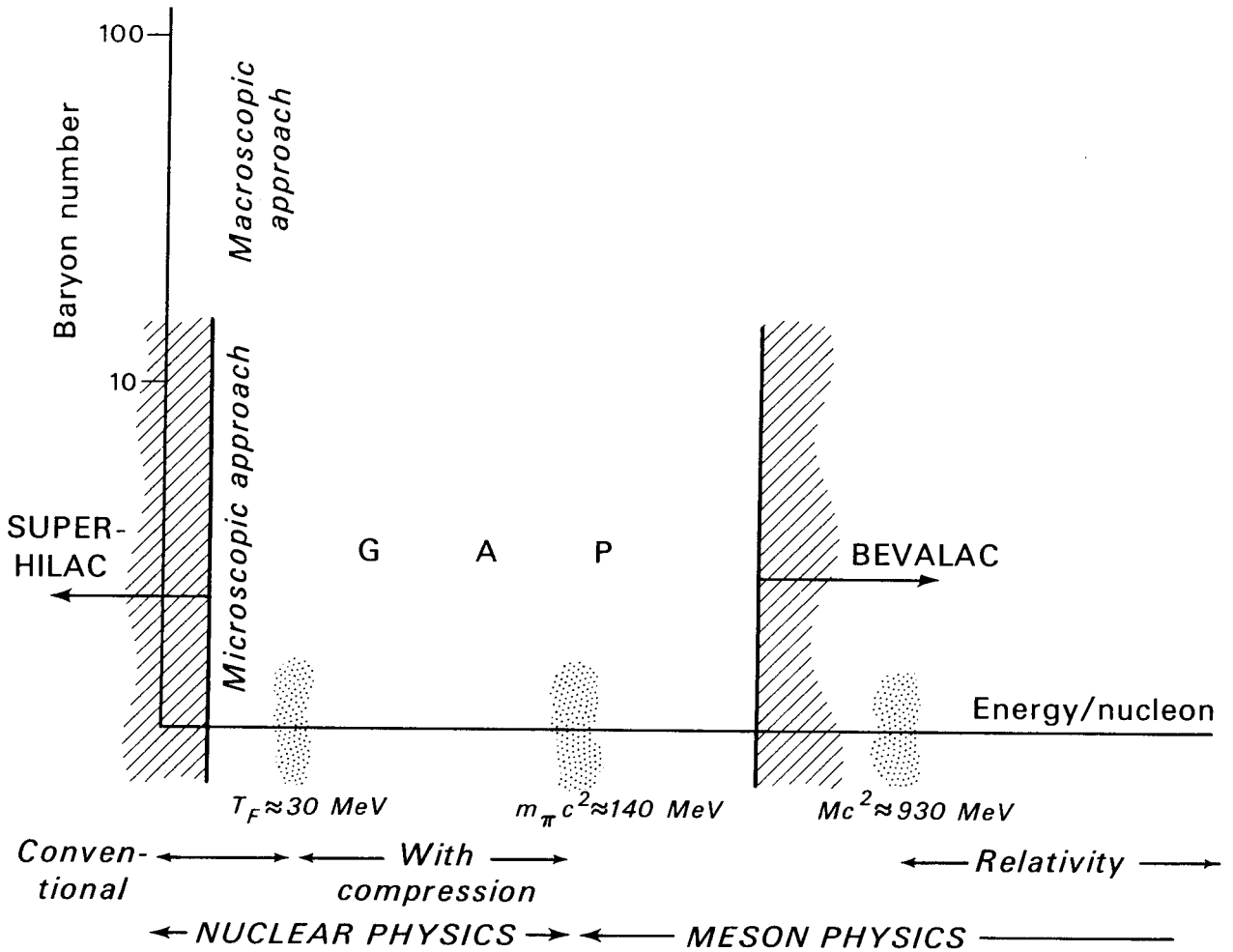

XBL 7410-8102

SUMMARY REMARKS*

James P. Vary†

Brookhaven National Laboratory, Upton, New York 11973

Certain aspects of new data and theory which have been presented at this conference are drawn together in order to gain new perspectives. Some microscopic nuclear structure and reaction highlights are reviewed and suggestions are presented.

I. INTRODUCTION

One cannot help but agree with the remarks of Dr. Swiatecki that someone should spend enough time to obtain and present a careful global overview of the domains of physical interest for heavy-ions over all energies presently available. I can only comment that he should not exclude himself from the class of physicists capable of such a task especially since the time and effort required is certainly more available to those of his class - i.e., the tenured class of physicists.

---

* Work performed under the auspices of the U.S. Atomic Energy Commission.

† Summary talk presented to the Second High Energy Heavy Ion Summer Study. Lawrence Berkeley Laboratory (July 15-26, 1974).

Naturally, I will take a somewhat different tack in these remarks. Let me focus on some of the underlying microscopic themes that have recurred often in the conference. Due to time limitations, I will mention only a few which, I believe, are of particular relevance to microscopic nuclear physics. Let me divide the remarks into the broad categories of nuclear structure and nuclear reactions.

II. NUCLEAR STRUCTURE

Let me just state that there was great interest in unusual structure and reaction phenomena that have been speculated might occur when massive ions collide at intermediate and high energies. Specifically, speculations about unusual Q.E.D. effects when the charge of the projectile plus target system exceeds 137 (W. Greiner), the analogous possibility of supercritical fields (Boson or vacuum quantum numbers) in superdense baryon matter (A. Kerman), how they may be stimulated by shock wave phenomena (G. Chapline, W. Greiner, E. Teller) and possibly even approach thermodynamic equilibrium (G. Chapline, E. Teller) have stirred much discussion. It may be suggested, however, that the Q.E.D. effects and shock wave phenomena may usefully be explored with beam energies in the region of 20 to 200 MeV/nucleon (MeV/n) to which one day of this conference was devoted. Three constraints coarsely define the lab kinetic energy per nucleon (E_L/n) region for these purposes. First, one must surmount the Coulomb barrier for a heavy projectile-target situation ($E_L/n > 10$ MeV/n); second, the collision processes must take place at times short compared to relaxation or rearrangement times ($E_L/n \gtrsim 60$ MeV/n); and third, allowing for energy loss due to particle creation and some rearrangement (friction) one maximizes the

interaction time consistent with the other two constraints ($E_L/n \lesssim$ 200 MeV/n). Friction and shock wave phenomena in this energy region would presumably occur with sufficient probability to make them easily observable. However, of course, one has fewer particles produced here so a true condensate may not be expected. As one increases energy, however, the third constraint becomes less satisfied and one must deal with decreasing probabilities. To increase interaction time more of the individual nucleon-nucleon collisions must be highly inelastic leading to the conjecture that only "head on" collisions at Bevalac energies have a reasonable chance of producing a condensate if it exists at all.

Let us now consider phenomena which may have additional relevance at Bevalac energies. Here the sense of the summer study is that we are at a very preliminary stage experimentally and theoretically. First attempts have been presented to reconcile preliminary data with the naive lowest order theory. The data of the Heckman group on projectile fragmentation has been studied within the framework of what might be called the Extreme Single Particle Shell Model by J. Lepore and R. Riddell. Their basic accomplishment to date has been to evaluate spectroscopic factors for inclusive cross section measurements in the impulse approximation. Additionally, they have studied the question of the c.m. fermi motion of the projectile fragments in order to compare with observed momenta distributions. This has been a noble analytic project within a harmonic oscillator framework dealing with projectiles up through ^{16}O.

There is a simple reaction analysis framework that comes to mind which would be appropriate to couple with their extensive structure efforts in order to compute absolute cross-sections and angular distributions for more detailed comparison with the data. Such an effort would

hopefully lead, eventually, to conclusions regarding clustering phenomena and other correlations in light nuclei.

The framework consists of a Plane Wave Impulse Approximation which can be corrected for distortion effects in the Glauber framework. This should be increasingly valid as one goes to higher energies. Certainly it would be useful as a first attempt for projectile fragmentation studies.

The general class of reactions is of the inclusive type

$$A+B \rightarrow C+X \tag{1}$$

where C is detected and X is everything else possible. The goal is to evaluate the transition amplitude

$$T_{if} = \sum_x \langle \psi_f^x | V | \psi_i \rangle \tag{2}$$

in a simple scheme and obtain the differential cross-section

$$d\sigma/d\Omega = |T_{if}|^2 \tag{3}$$

We approximate

$$\psi_i = \Phi_A \Phi_B \varphi_i$$

where Φ_A and Φ_B are the initial internal wave functions and φ_i is the wavefunction of relative motion. Antisymmetrization is neglected in this impulse treatment. Similarly

$$\psi_f^x = \Phi_C \Phi_x \varphi_f^x \tag{4}$$

where Φ_x is the internal wave function for the unobserved system and φ_f^x is the wave function of relative motion with respect to x. It is probably a reasonable approximation at high energies and consistent with an impulse

approximation to assume φ_f^x is independent of x

$$\varphi_f^x \sim \varphi_f \tag{5}$$

Thus we obtain, assuming a local effective relative operator for the perturbing interaction

$$T_{if} \sim \langle \varphi_f | V | \varphi_i \rangle \sum_x \langle \Phi_C \Phi_x | \Phi_A \Phi_B \rangle \tag{6}$$

We label the inclusive spectroscopic factor as

$$S_C^{AB} = \sum_x \langle \Phi_C \Phi_x | \Phi_A \Phi_B \rangle \tag{7}$$

and this is the quantity of the type evaluated by Lepore and Riddell. To achieve an absolute cross section prediction one may use the lowest order microscopic theory for V, φ_i and φ_f in an impact parameter scheme for which

$$V(b,z) = V(\vec{r}) = \int [\rho_A(\vec{r}\,') - \rho_C(\vec{r}\,')] \rho_B(\vec{r}\,' - \vec{r}) d^3r' \tag{8}$$

$$\varphi(b,z) = \varphi_0 \exp\left[-\tfrac{1}{2}\sigma(1-i\beta) \int_{-\infty}^{z} T(b,z')dz' \right] \tag{9}$$

$$T(b,z) = T(\vec{r}) = \int \rho_A(\vec{r}\,') \rho_B(\vec{r}\,' - \vec{r}) d^3r' \tag{10}$$

where φ_0 is an appropriate plane wave, ρ_ϵ signifies the ground state density (ϵ significes A,B or C), σ is the nucleon-nucleon total cross

section at the same lab energy as the E_L/n of the projectile and β is the ratio of real part to imaginary part of the nucleon-nucleon forward scattering amplitude at that energy. One may assume for convenience and consistent with the impulse approximation that φ_i and φ_f have the same analytic form.

One must attempt an analysis of the data to at least this level of sophistication in order to understand whether the data emerging from the projectile fragmentation studies (Heckman, Schroeder) and the target fragmentation studies (Poskanzer) contain nuclear structure information beyond that of the extreme single particle model.

This now leads to a question. Does the existing preliminary data show signs of containing structure information beyond the most naive level? Specifically one asks whether it may be possible to see correlation information in this data. A priori, most everyone would not have expected this, since correlations have proved elusive even in high energy particle-nucleus studies where, presumably, the tools have been extensively developed and some data has been analyzed [see, for example, E. Lambert and H. Feshbach, Ann. Phys. (N.Y.) 76, 80 (1973)]. I'm sure not many people came to this summer study, including myself, expecting to hear discussions of correlations in nuclei. However, the fragmentation studies of the very light projectiles such as deuterons and alphas (Schroeder) and of ^{16}O (Heckman) have found structure in the momenta profiles of the proton which may deviate from what is expected on the basis of fermi motion considerations alone. I call your attention to the momenta of particles advanced from the beam velocity especially in the ^{16}O data. Ordinarily, the fermi motion of a proton in a single particle orbital in a light nucleus would imply something of a Gaussian distribution for its momentum profile.

However, strong deviations from Gaussian are seen in this data. How much of this is due to multiple scattering effects and how much may be attributed to short range correlations deserves further study.

Let us recall briefly the nature and ramifications of short range correlations in nuclei. To the best of our current knwoledge we are asking how much does the correct relative wave function, ψ, between two nucleons in the nucleus differ from the uncorrelated wave function, φ, of the simple shell model. Based on present knowledge of the two nucleon interaction with its strong short range hard core of radius C we expect something like the following picture to be valid for a relative $\ell = 0$ state:

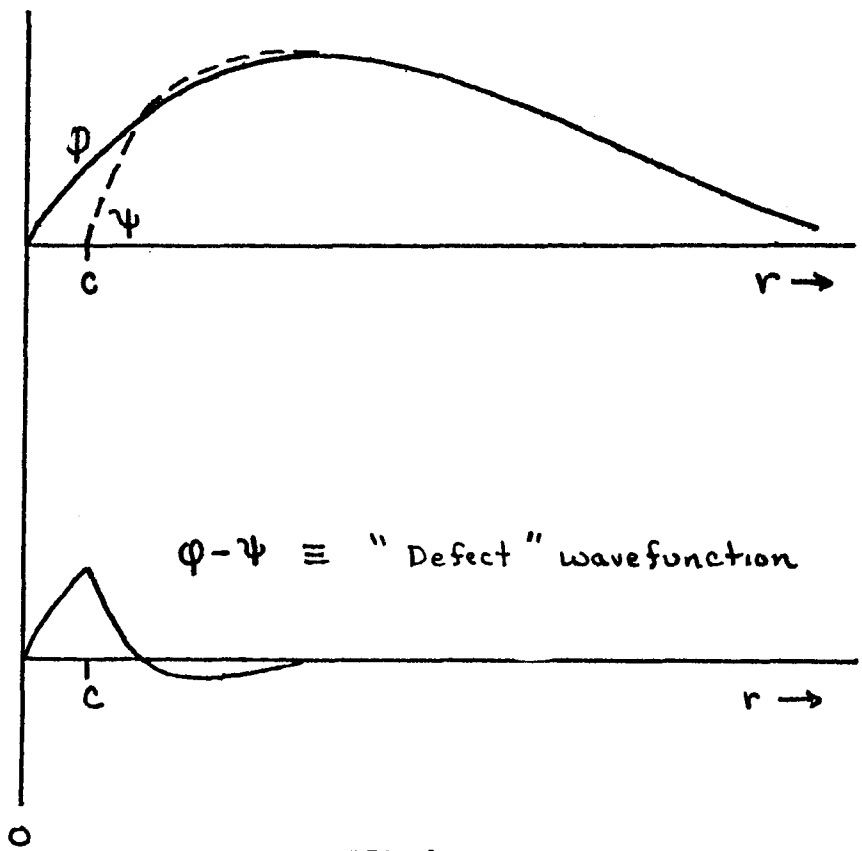

FIG. 1

However, the exact nature of ψ within about 2C or 3C of $r = 0$ is quite uncertain according to many recent theoretical studies. Figure 2 displays some candidates for s state relative motion in the deuteron and Fig. 3 demonstrates the resulting momentum space probability distribution

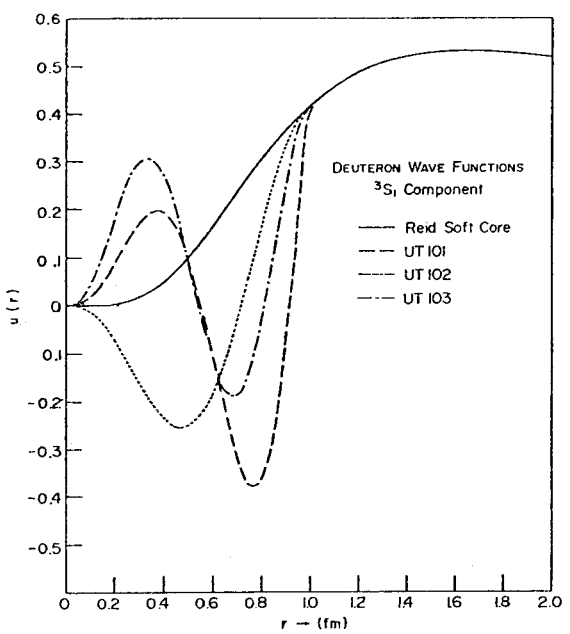

FIG. 2

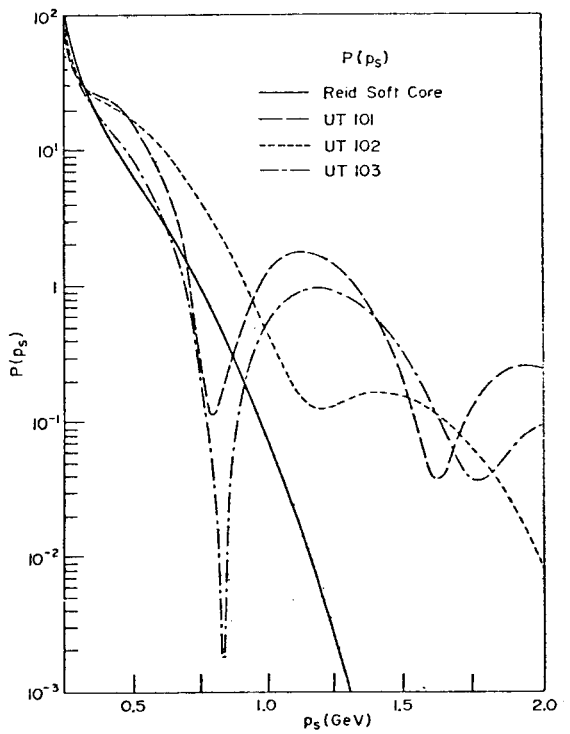

FIG. 3

J. Vary, Phys. Rev. C7, 521 (1973)

for a nucleon in the deuteron. The differences between these wave functions cannot be distinguished through available elastic electron scattering

data or through their implied deuteron ground state properties since these differences are restricted to small distances and high momenta. The data presented here showing protons advanced from the incident deuteron velocity by as much as 1.25 GeV/c may be usefully analyzed to attempt to unravel the as yet unknown high momentum components of the deuteron.

While we are on the subject of high momenta structure components in nuclei it is indeed interesting that baryon resonances in nuclei have recently been studied through nuclear reactions at high energies (R. Schaeffer). The fact that the Heckman data sees ^{15}C in the fragmentation studies with an ^{16}O beam is suggestive of a possible Δ^{++} transfer or knockout. The additional point made by Heckman that the ^{15}C momentum profile appeared shifted with respect to a simple fragmentation position would be consistent with the high momentum transfer accompanying the Δ^{++} mechanism. This is an area of much current debate in nuclear structure and it would be attractive to have further analysis of the ^{15}C results in this context.

Let me conclude the discussions on nuclear structure and momenta distributions with a simple rough sketch of what one expects the true momentum distribution to resemble. For reference purposes we indicate in Fig. 4, by a solid line, the momentum distribution of an infinite system of fermions at zero temperature whose density corresponds to the saturation density of finite nuclei.

Then a large nucleus like ^{208}Pb in the simple single particle shell model would look like the long dashed curve. Now, if we introduce short range correlations such as those generated by a realistic hard core nucleon-nucleon interaction one would expect to obtain a density profile

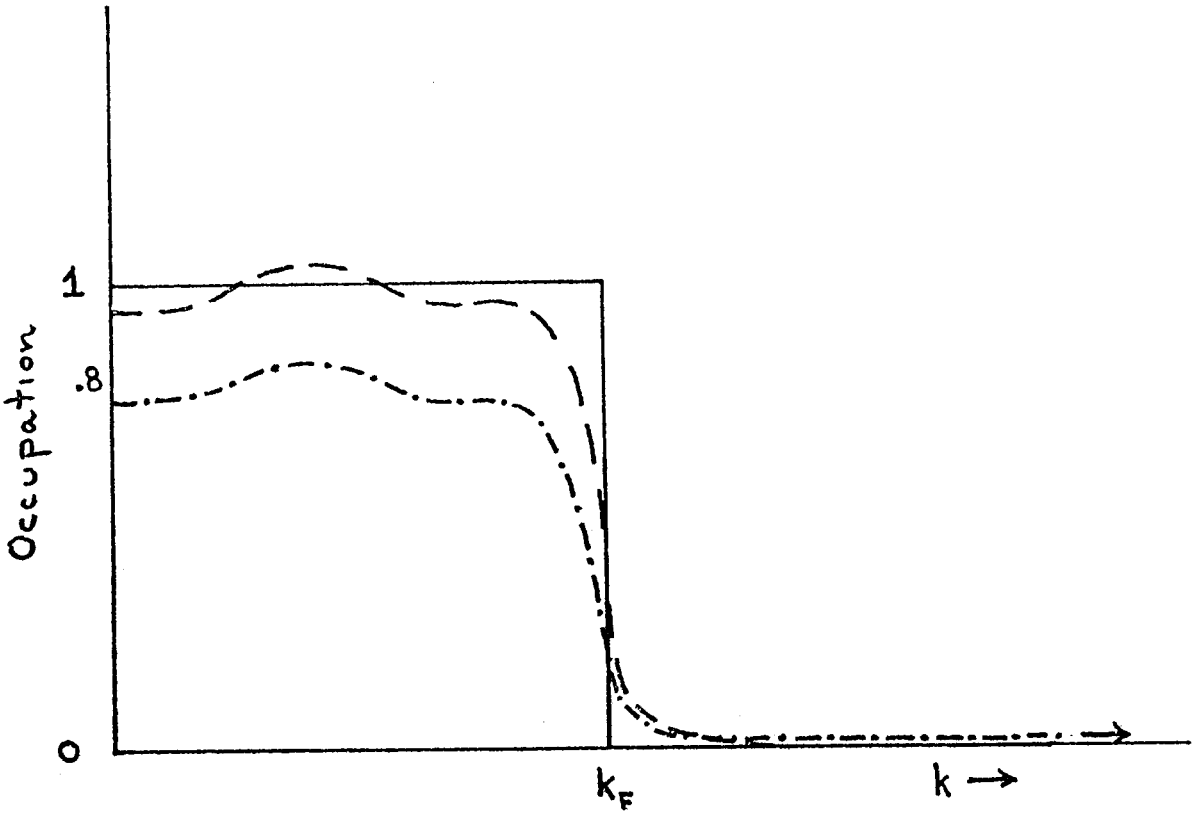

FIG. 4

something like the dashed-dot curve. The point is that one expects a long smooth tail extending to very high momenta. Probability is robbed from the low-momenta states in a rather democratic fashion (short range correlations are nearly state independent) and distributed smoothly over states of high momenta. It is precisely this smooth nature of the redistribution of momentum that renders the simple shell model valid for most purposes in low energy applications. Relative properties as measured by operators of low momentum components [B(E2), one nucleon stripping and pickup experiments, etc.] are nearly unaffected except, possibly, in absolute strength and this is accommodated within a renormalized or "effective" strength assigned to the operator.

Most of the above sketch remains a theoretical one since I am not

aware of any experimental information which conclusively demonstrates the presence of this high momentum tail. This, I believe, is an interesting possibility to explore in your fragmentation studies. Although the effects may be on the 1% level you may be well equipped to see them in the advanced momenta region. Recall the inclusive proton measurements with ^{16}O projectiles that demonstrated a high momentum component which was nearly flat and deviated by orders of magnitude from the single Gaussian shape fit to the low momentum region. There would seem to be plenty of room here for even qualitative analysis yet.

III. NUCLEAR REACTIONS

Within the constraints of the time remaining I would like to review a couple of the reaction topics that especially relate to the microscopic formalisms discussed.

The question of whether heavy ion cross sections factorize at high energies was initially discussed at length at this conference last year (Chew) and has now appeared in at least three articles in the current literature. The data is not yet available (Jaros) but some theoretical analyses in the Chew framework (Uchiyama) and in the Glauber approach (Vary) were presented here. Let us compare these analyses with each other and with some specific reaction data.

Let us first reconsider the Glauber results. The audience was reminded (Heckman) of some older cosmic ray results that suggested a parametrization of the nucleus-nucleus cross section that was based on geometrical properties modified by an "overlap factor", γ. This goes by the title Bradt-Peters parametrization, whereby:

$$\sigma^R = \alpha(A^{1/3} + B^{1/3} - \gamma)^2 \qquad (11)$$

where A and B are the number of nucleons in the projectile and target and γ is typically expected to be of order unity. This formula reproduces well the actual results of Galuber calculations displayed as points in Fig. 5. I thank Dr. Heckman for his analysis of the calculations presented in Fig. 5.

The conclusion from the microscopic approach remains unaltered: factorization breaks down by more than 20% when the radii of the colliding ions differ by more than 50%. This breakdown is easily understood since the cross sections follow the dictates of geometry.

Let us now compare the theoretical and experimental results presented here for some specific reactions. Figure 6 shows the inclusive $^{16}O \rightarrow N$ and $^{12}C \rightarrow B$ reaction data (Heckman) but now re-plotted according to a projectile plus target geometrical scale. One sees more clearly that except for the lowest and highest points the data nearly coincide with a straight line. The filled circles are the (shifted) Glauber results for the total reaction cross section for ^{14}N. When the results of a Chew type analysis (Uchiyama) are normalized by the ^{208}Pb microscopic result it is found, quite surprisingly, that they also follow a geometrical behavior. The question now arises whether this pattern persists for all reaction cross sections in the Chew analysis. Also, how sensitive is the pattern to the various assumptions input into the Uchiyama calculations? If the geometrical property is inherent to the analysis then we may expect factorization to be controlled by the dictates of geometry. The previously mentioned breakdown of factorization is then found.

An attempt was made to extol the virtues of a microscopic approach for providing a backdrop of theoretical results to compare with Bevalac

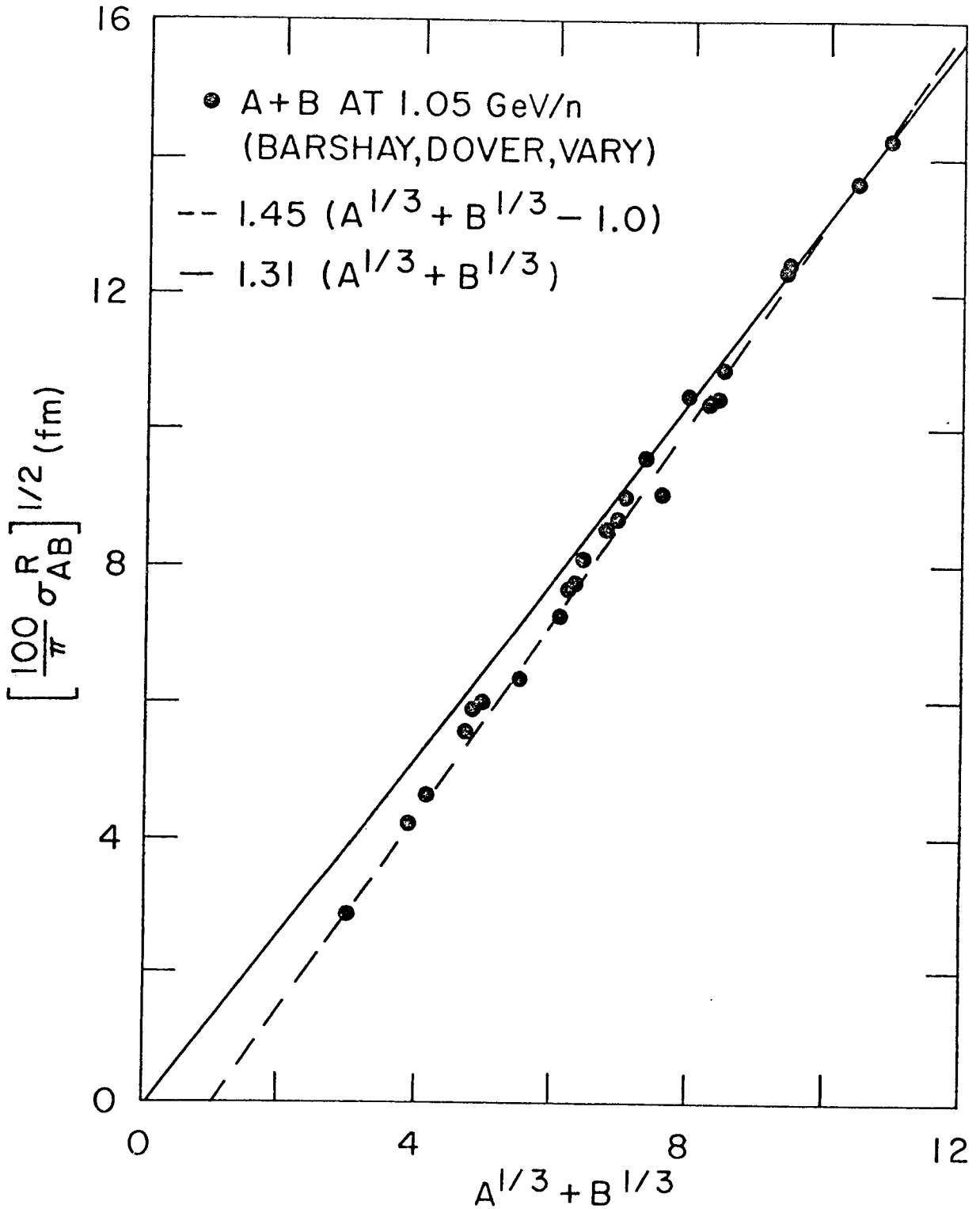
A+B AT 1.05 GeV/n
(BARSHAY, DOVER, VARY)
-- 1.45 (A^1/3 + B^1/3 − 1.0)
— 1.31 (A^1/3 + B^1/3)
[100/π σ^R_AB]^1/2 (fm)
A^1/3 + B^1/3
0
4
8
12
16

FIG. 5

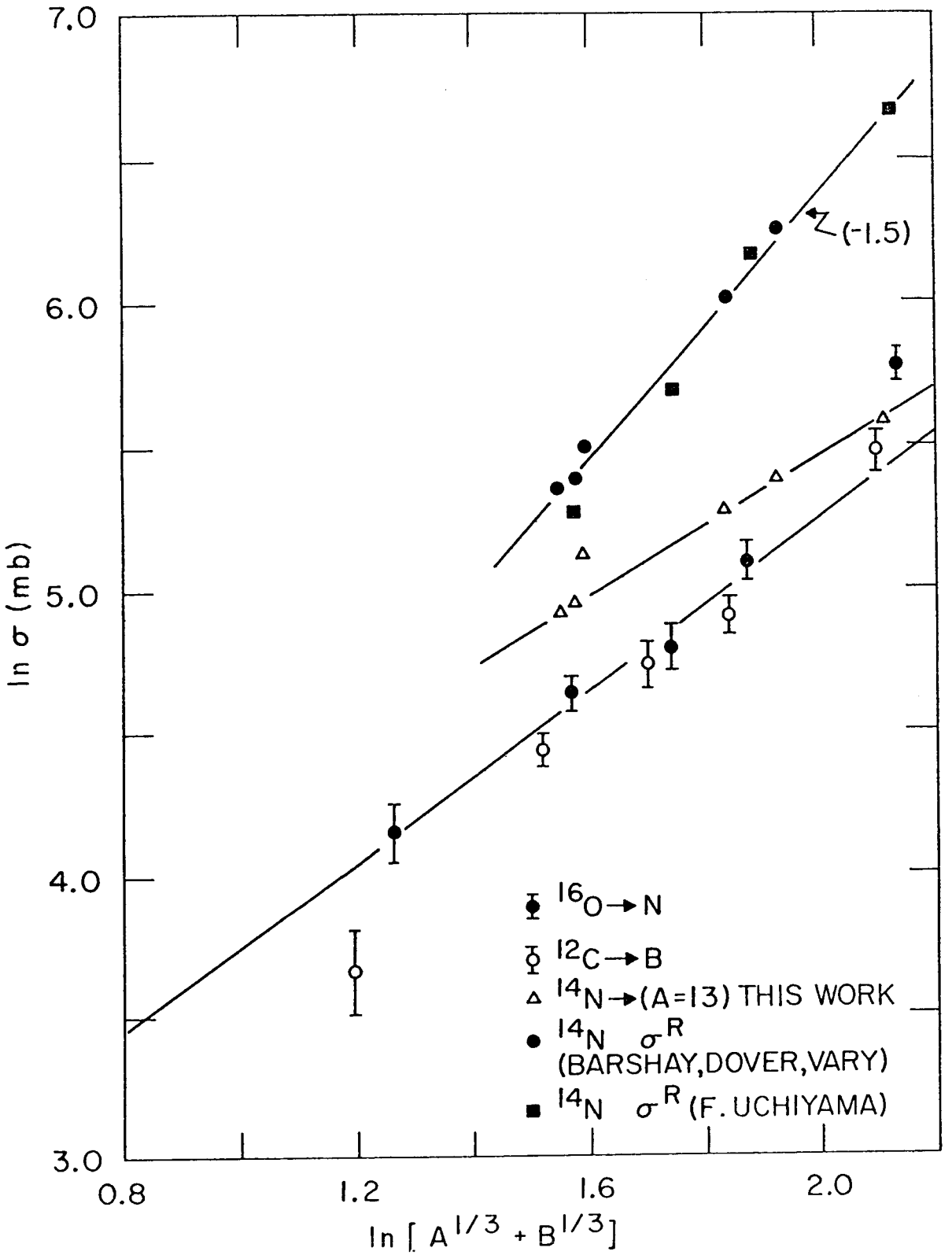
7.0
6.0
5.0
4.0
3.0
ln σ (mb)
0.8
1.2
1.6
2.0
ln [A^1/3 + B^1/3]
(-1.5)
16O→N
12C→B
14N→(A=13) THIS WORK
14N σR
(BARSHAY,DOVER,VARY)
14N σR (F. UCHIYAMA)

FIG. 6

experiments. Let me finish my remarks by showing an example of how straightforward such an analysis might be. I choose the projectile fragmentation case and for simplicity attempt to naively estimate the inclusive cross section for

$$A + B \rightarrow (A-1) + X \tag{12}$$

where the A-1 system is detected intact. We shall assume that a surface nucleon has been removed suddenly leaving the (A-1) system, most of the time, in the ground state or some low lying excited state so that it does not subsequently break up. Actually, if we only desire the behavior of the inclusive cross section as a function of the target nucleus it is only necessary to assume that the population of the states of the (A-1) system is independent of the target. This seems reasonable. On the other hand, the more restrictive assumption permits the assignment of an absolute cross section to the theoretical results. A simple semi-microscopic analysis with the additional assumption that β, the previously mentioned ratio of real to imaginary nucleon-nucleon amplitude, is negligibly small proceeds as follows: we define a mean free path function, $\lambda(b,Z)$, for two interacting heavy ions in the impact parameter scheme by

$$1/\lambda(b,z) = \sigma T(b,z) \tag{13}$$

where $T(b,Z)$ is given by Eq. (10). Thus the total number of nucleon-nucleon collisions when two heavy ions collide at impact parameter b is $N(b)$ given by

$$N(b) = \sigma T(b) = \int_{-\infty}^{\infty} \frac{1}{\lambda(b,z)}\, dz \tag{14}$$

Now let $b_1(b_2)$ represent that impact parameter for which there is, on the average, $\frac{1}{2}(\frac{3}{2})$ a nucleon-nucleon collision. Thus, in this region of impact parameters there will be in an average sense one nucleon-nucleon collision involving one nucleon of each the projectile and target. If the projectile is light enough ($A = 14$ in our case) it is assumed the struck projectile nucleon escapes without hitting any of the other projectile nucleons (sudden removal with no final state interactions involving the projectile). Next, recall that the Galuber expression for the reaction cross section as a function of b is

$$\sigma^R(b) = 2\pi(1-e^{-\sigma T(b)}) \tag{15}$$

Then the inclusive cross section we wish is approximated by

$$\sigma^R_{A \to (A-1)} \approx \int_{b_1}^{b_2} \sigma^R(b) b db \tag{16}$$

A set of results for ^{14}N incident on a few targets at 1 GeV/n is shown by the open triangles in Fig. 6. The slope of the results is probably their most interesting aspect. Taking the data and theory as a whole one concludes that proceeding from the specific $A \to (A-1)$ case to the experimental mix of isotopic fragments and then on to the total reaction cross section yields an increasing geometrical slope.

It should be remembered that an earlier description of projectile fragmentation in a macroscopic abrasion-ablation scheme had been proposed (Bowman, Swiatecki and Tsang, LBL-2908 preprint). The model outlined

above is simply a semi-microscopic analogy to their abrasion scheme.

To close my discussion of reactions I would like to offer an alternative cosmological case to the colliding neutron stars shown by W. Greiner, as an example of collisions of two very heavy ions at very high energies. His example emphasized the hydrodynamic shock wave phenomena. This one emphasizes the few particle nature and gas type behavior while at the same time exhibiting some collective effects. What attracts me to this example is the model employed in the analysis. It was a simple potential model involving gravitational forces folded over the mass density distributions. Figure 7 shows two equal mass galaxies colliding where one has some initial symmetric distribution with spin counter to the parabolic orbit of the incident galaxy. As

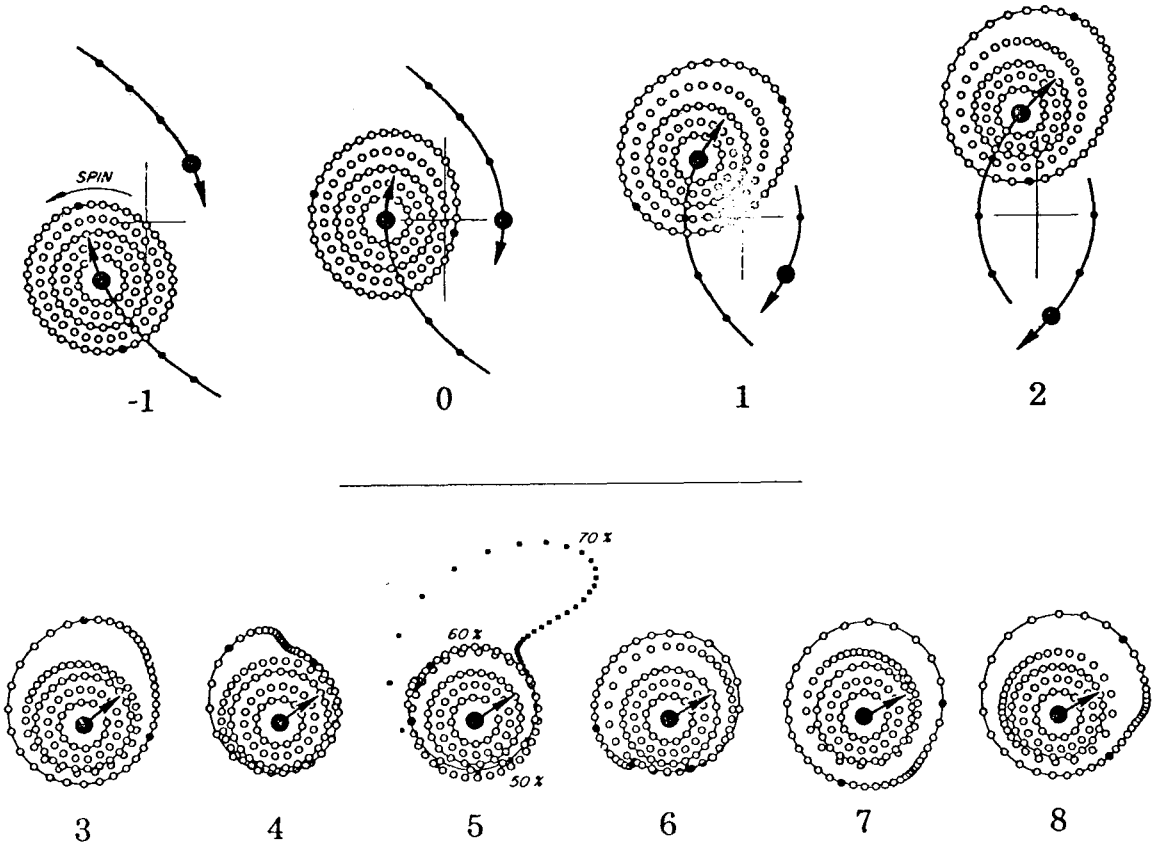

FIG. 7

A. Toomre and J. Toomre, Astroph. Jnl., 178, 623 (1972)

time proceeds from one frame to the next one witnesses the buildup of a tidal wave which eventually spews out mass in the "target fragmentation region" leaving some hot residual system which seeks some stable mode.

If nothing else, this demonstrates there is considerable interest throughout physics in the collisions of structured objects especially in so far as the phenomena may be explained in the context of the simplest microscopic approach.

IMPRESSIONS OF THE SECOND SUMMER STUDY ON RELATIVISTIC HEAVY IONS

Alfred S. Goldhaber

Institute for Theoretical Physics
State University of New York
Stony Brook, N. Y. 11794

July 31, 1974

In evaluating this year's gathering, we may ask three questions:

1. What points were made for the first time, or at least more vividly than last year?

2. What experimental and theoretical progress has taken place in the past year?

3. What are the important short and long term goals for the Bevalac project, which have emerged or been reinforced in this meeting?

Before dealing with these questions, we should remind ourselves of the ways in which Bevalac supplies the opportunity to investigate new physical situations, as well as the technical capacity to analyze phenomena which are not readily or accurately studied at previously available facilities. The intrinsically new physics at Bevalac comes in the collisions of energetic nuclei with nuclear targets. No other accelerator can provide this capacity at the moment. Obviously, the optimum chances for observing new phenomena will come if the heaviest projectiles impinge on the heaviest targets, but very heavy projectiles are at least two years off. On the other hand, much technically new physics can be studied when nuclear projectiles strike even the lightest

targets. In principle, these processes are completely equivalent to the inverse, in which a light projectile strikes a heavier target. However, it is much easier to observe reaction products which are slow in the projectile velocity frame than those which are slow in the target (laboratory) frame. Thus, the systematics and rates of heavy ion fragmentation or transmutation, a subject of great importance to cosmic ray physics, are best studied at Bevalac.

1. New things.

(a) Returning to our first question, the possible uses of projectile transmutation were expanded in presentations spelling out two attractive possibilities, the measurement of cross sections for electron pickup by energetic fully stripped ions, and the observation of fast hypernuclei. Both of these were mentioned last year, but this time in more detail, with experimental proposals being submitted by the speakers. Aside from testing atomic scattering theory, the electron pickup experiments are important for the case of ions which are stable when fully stripped, but can decay weakly by atomic electron capture. The amount of such ions in cosmic rays permits a refined analysis of the propagation of the rays, determining not only the total amount of matter traversed (in gms/cm^2) but also how much the density varied along the path, since this would affect the probability of electron capture and subsequent weak decay of these species. In the matter of hypernuclei, not only would lifetime measurements become practical, but also the identification of a hypernucleus becomes much easier, when its point of decay is geometrically displaced from its point of creation.

(b) A suggestion not even heard last year concerned the possibility that one or more distinct new phases of nuclear matter could be created under the conditions of high density (and perhaps temperature) produced in central collisions of heavy nuclei. There seemed to be a partial consensus that such phenomena would be most accessible in the several hundred MeV/A range, rather than the more typical 1-2 GeV/A of recent experiments, since the small momentum transfer in nucleon-nucleon collisions would inhibit formation of a nuclear fluid, at rest in the center of mass, for the highest Bevalac beam momenta. The essential point of such proposals is that a coherent coupling to mesonic degrees of freedom could create stable or metastable states with a density far higher than ordinary nuclear matter. It was pointed out that even if many or all of the postulates in these proposals are wrong, there may still exist density isomers of ordinary heavy nuclei, and Bevalac might be able to produce them, at least when operating in the lower part of its energy range. Little was said about how such states could be detected. If metastable, they might show peculiarities in secondary interactions. If quite unstable, they might be associated with bursts of pions exhibiting some striking momentum correlations.

(c) Something new for this meeting was the description of successful theoretical models for large angle elastic scattering and pickup reactions in nuclear collisions, based on inclusion of excited nucleons in the wavefunctions of the colliding nuclei. These models have been applied at rather low energies for Bevalac, but they raise the question whether Bevalac could generate some further tests of the

excited nucleon models. Indeed, the observed ^{15}C fragments of ^{16}O projectiles may have come from Δ^{++} knockout (or pickup) by the target.

(d) Another topic, only mentioned last year but developed at length this time, concerned the formation of shock waves in nuclear collisions, at energies below meson production threshold, perhaps 100 MeV/A. It was plausibly argued that such waves could be formed in central nucleus-nucleus collisions, provided the nuclei were fairly big, and the nucleon-nucleon scattering close to isotropic. Presumably, the evidence of a shock would be fragments "squirted out" at 90° in the center-of-velocity frame, accompanied by forward and backward going fragments with velocity approximating that of sound in the nuclear medium.

(e) Some remote possibilities for applying knowledge gained at Bevalac were pointed out, having to do with special processes of nucleosynthesis depending on collisions of relativistic heavy ions, perhaps in supernova explosions, perhaps in the very early universe. However, the considerable success of models not requiring relativistic energies leaves this type of application in limbo for the time being.

(f) One day of the meeting was devoted to exposing work at Berkeley and elsewhere with heavy ions of less than 20 MeV/A. Impressive and beautiful results have been obtained. For example, at these energies there are signs of two competing processes, either a quick collision followed by projectile and/or target breakup, or compound nucleus formation followed by nearly complete loss of memory of the initial state. Of the many experimental projects still open at

these energies, or slightly higher ones, two are the search for superheavy metastable elements of $Z \approx 114$, and the appearance of positrons coming from "breakdown of the vacuum" when a nucleus of instantaneous charge $Z_{eff} \gtrsim 170$ is formed momentarily during the close approach of two very heavy nuclei. Both these projects would benefit from acceleration of Pb or U or even Pu ions, which is hindered for the moment mostly by problems with manufacture of reliable and copious ion sources. Just as with the Bevalac, the lower energy Berkeley machines have proposed improvement programs, to increase energy, intensity and charge of the beams which can be produced.

(g) The main proposal for Bevalac improvement is the introduction of a new vacuum tube in the Bevatron, and new, faster pumps to go with it. This could bring the vacuum down from 10^{-8} to 10^{-9} Torr, permitting acceleration of highly stripped beams with useful flux at least up to Pb, and perhaps to U (though only for purposes requiring limited beam intensity). The projected cost is slightly over a million dollars, plus a negligible additional operating cost. After approval, it should take about one year to make this improvement.

2. Progress

(a) There has been some progress in the past year. The Bevalac itself is coming into operation, and within a few months should be accelerating Ar ions. However, without trying to place blame in any particular quarter, we may note that the ratio of expenditure for experiments to that for Bevalac development and operation seems disproportionately low. If more funding for experiments cannot be supplied, further progress will be slow indeed.

(b) Several experiments have been carried out, and are now in the stage of analysis. New results were reported on projectile and target fragmentation, with perhaps the biggest effort going into the study of low velocity transfer ^{12}C and ^{16}O projectile fragments for a variety of targets. For this second generation experiment, a nearly complete analysis gives more information and greater precision than available a year ago. The target fragmentation experiments can be compared with results obtained with proton beams, and some reasonable conclusions emerge, such as the statement that, the heavier the projectile, the more energy and momentum it can deposit in the target residue left over after the direct reaction between projectile and target. Detailed theoretical discussions of these results would be welcome.

(c) The theory of small velocity fragments in the projectile frame has made a definite advance, but it is still clear that a physically complete theoretical picture is not easy to produce. First, the advance: Already a year ago, the isotropy of fragment momenta, and the near-independence of target of the ratios of different fragment production rates, cried out for explanation in terms of the structure of the projectile before collision. However, the apparent independence on a fragment's mass of its momentum distribution was puzzling and disturbing. In the meantime it has been realized that a parabolic $\left(M_{FRAG}(M_{PROJ}-M_{FRAG})\right)$ dependence of mean square momentum on fragment mass arises from simple statistical assumptions and the hypothesis of negligible coherent momentum transfer to the projectile

in the collision. At the same time the second generation experiment shows good agreement with this result. While fuzzy thinking displayed in my summary last year has now been cleared away, the real work of computing fragmentation cross sections has yet to begin. Such work must describe a process which proceeds in two stages. A small number of projectile nucleons interact directly with the target (probably only the edge of the target). Then the nuclear residue spits out some single nucleons and some larger fragments. The hard questions are, how is sufficient energy transferred to the residue, and how is this energy distributed once received? Probably the first, and certainly the second question cannot be answered in terms of low energy nuclear structure; the time scale is too short, or the energies too large. The simple results on momentum distributions of approaches which ignore the space time structure of the collision-fragmentation process may be preserved by a complete theory, since they depend so little on details. Nevertheless, without more physical input and some perspicacious new approximations, there seems little hope of computing cross sections and fragmentation branching ratios. One mysterious result is the greater relative ease of producing fragments down by only one unit in Z when the target is Pb than when it is C. Could there be a coherent excitation process involved? As a general statement, we may argue that if different numbers of projectile nucleons interact with the target to produce residues emitting different fragments, then the ratios of these different fragments should depend on the target. Except for the $\Delta Z = -1$

transitions, there is no sign of such dependence beyond the 20% level. This is mysterious.

(d) One subject in which some useful, straightforward "microscopic" calculations have been made in the past year is that of nucleus-nucleus total cross sections. The main point of these efforts, beyond giving predictions to be compared with data, was to test theoretically, in the conventional picture of the nucleus, the factorization rules suggested by particle-particle cross sections. Not surprisingly, the studies showed that nuclei behave like black discs with cross sections nearly proportional to the square of the sum of the nuclear radii of projectile and target $\sim (A_P^{1/3} + A_T^{1/3})^2$. Obviously this form is not factorizable in principle, but it departs drastically from the factorization rule if, e.g., target is much heavier than projectile, giving $\sigma_{TT} << \sigma_{PT}^2/\sigma_{PP}$. While notions developed in high energy physics (many of which spring from nuclear physics!) may supply useful guides to classification of collision processes, it would be foolish to apply these notions blindly and expect them to work. The nuclear collision problem differs dramatically in geometric scale, excitation spectrum, and other properties, so that only with some intelligence and selectivity can experiences with particles and with nuclei fructify each other. Such efforts are well worthwhile if this caution is kept in mind.

(e) A final sign of progress is the development of the Bevalac User's Association, evidenced in the increasing numbers of experimental proposals, as well as the increased size and enthusiasm of this year's participation in the summer study.

3. Goals

(a) The Bevalac permits nearly bias free studies of projectile transmutation. It is important that such studies be accomplished in a precise, systematic way, to be of maximum value for applications, and to give the most stringent tests to theory. It is also important, as in most physics problems, that theorists examine carefully the actual data, rather than accept summary statements (such as this one!) which may be true but misleading. In the particular case of projectile fragmentation, the substantial improvement in experimental accuracy merits a substantial effort to develop a realistic theory.

(b) The possibility of exciting new phenomena in the collisions of very heavy nuclei makes it urgent to improve the Bevalac vacuum to accommodate the heaviest projectiles.

(c) The likelihood of qualitative changes in the results of collisions between energies of order 100 MeV and 1 GeV makes it important to plan and conduct experiments that cover the whole range. In fact, it seems quite possible that the lower energies will produce more dramatic effects!

(d) There may well be significant experiments to be done of a type not yet proposed. For example, it was suggested that channeling of heavy ions in crystals might occur, and lead to interesting effects. Whether or not this be so, it seems quite worthwhile to devote some time and imagination to the question, "What can be done with Bevalac that can't be done without it?" This meeting showed there are some positive answers. Are there more?

(e) Because of its special history, LBL is in an unusual position to give leadership in heavy ion experiments from MeV to GeV energies. In order to capitalize on this strength, it would be good physics as well as good politics to develop close, regular cooperation and communication among those working with the different facilities located here. Perhaps we should recall Benjamin Franklin's injunction to his colleagues, "Gentlemen, let us all hang together, or we may all hang separately." In other words, make out of necessity a golden opportunity to strike down artificial barriers in physics, providing better perspective on many aspects of nuclear dynamics.

G.P.O. 692-300/94